Hydraulics Research
Wallingford

MODELLING OF RIVER AND FLOOD PLAIN FLOW USING THE FINITE ELEMENT METHOD

Paul G Samuels MA PhD

Report No SR 61
November 1985

Registered Office: Hydraulics Research Limited,
Wallingford, Oxfordshire OX10 8BA.
Telephone: 0491 35381. Telex: 848552

FOREWORD

This report contains the text of the PhD thesis the author presented to the University of Reading in September 1985. Although the report is laid out in the style of the thesis, some minor errors that were discovered after the thesis was examined and accepted by the University of Reading have been corrected in this edition. The thesis covers work undertaken on a part time basis in the Department of Mathematics from 1977 to 1985.

ABSTRACT

This thesis examines both the mathematical formulation of the physics of river flows and the use of the finite element method on the resulting equations. The type and appropriate boundary data for three models of the flow are discussed; steady flow controlled by friction, and, steady and unsteady flow incorporating the convective accelerations. The means chosen to depth integrate the convective accelerations is shown to influence the type of the equations and the conditions for their solution to exhibit closed streamlines. An analytic solution is derived for the interaction between the flows in the channel and flood plain assuming a simple rectangular geometry. It indicates that the entire width of the channel may be affected by the drag of the slower flood plain flow.

Galerkin finite element approximations are applied to the stream function and potential formulations of the equations. The potential formulation is new and uses the water surface level as a non-linear velocity potential. It is shown to be superior to using a stream function for friction controlled flow. The velocity field is taken as piecewise constant in each triangular element and a new recovery technique is introduced to estimate its derivatives. The computation of the convective accelerations uses these derivatives. A successive substitution algorithm converges only for sufficiently slow steady flows. Analysis of this limit motivated the use of a time stepping method which proved stable for all velocities tested subject to a limit upon the time step.

The method produces acceptable results when judged against experimental observations from a laboratory flume. The performance of

the method is, however, unsatisfactory for data representing a practical problem, flow at a bridge site. Further work is recommended before the methods can be used in engineering practice.

CONTENTS Page

FIGURES:

ACKNOWLEDGEMENTS

I am indebted to my supervisor, Professor K W Morton, now at Oxford University, for his advice and stimulating criticism. Dr M J Baines was appointed as my supervisor at Reading University in October 1984 and I am grateful for his helpful comments upon a draft of this thesis. I also wish to thank my external supervisor at Hydraulics Research, Dr Roland Price, for his encouragement, many discussions and for introducing me to computational hydraulics.

The research described in this thesis was sponsored up to 31 March 1982 by the Department of the Environment as a part of the basic research programme of the Hydraulics Research Station. Since privatization of Hydraulics Research Limited, the work has been supported by the Ministry of Agriculture, Fisheries and Food under their strategic research commission A. The views expressed in this thesis, however, reflect neither the opinion nor the policy of MAFF or DoE.

I am grateful to the typists and illustrators at Hydraulics Research who produced this thesis from a somewhat untidy original draft.

NOTATION

The notation used for principal variables (water level, velocity, etc) is consistent throughout the thesis. However, other symbols can have different meanings as defined according to the context.

A	element area
a_1, a_2, a_3, a_4	constants
b	bed level
c	cos ($\frac{1}{2}k\Delta x$)
$\underline{c}$	convection term
c	constant
C	Chezy roughness coefficient
C	constant
Cr	Courant number $U\Delta t/\Delta x$
D	depth
$\underline{e}$	unit vector
E	error at a node
f	Darcy friction factor
$\underline{F}$	body force
F	friction function (or friction velocity)
F	streamwise component of ∇E
Fm	mesh Froude number
g	acceleration due to gravity
G	transverse (cross-stream/normal) component of ∇E
G	function
h	water surface level
H	finite element approximation to h
I	function

k	wave number in Fourier Analysis
k_s	roughness size
K	conveyance function
$\ell_n \ell_s$	metric functions
n	Manning's roughness coefficient
N	area coordinate basis function
ρ	exponent of depth in conveyance function
$\underline{q}$	unit flow vecotr (components q_x, q_y)
$\underline{Q}$	finite element approximation to $\underline{q}$
Q	total discharge
r	asymptotic convergence rate
r	radial polar coordinate
R	radius of curvature
s	sin ($\frac{1}{2}k\Delta x$)
s	streamline coordinate
s	surface slope
t	time
$\underline{T}$	turbulent stress term
$\underline{u}$	3d velocity vector (components u,v,w)
$\underline{u}$	2d velocity vector (components u,v)
u	plan velocity component
$\underline{U}$	2d depth averaged flow velocity vector (components U,V)
U	plan depth average velocity component
v	velocity deficit
v	plan velocity component
V	depth averaged plan velocity component
w	vertical velocity component

w	weighting coefficient in quadrature rule
x,y,z	coordinate axes
α	velocity distribution coefficient
α	constant
$\underline{\alpha}$	perturbation to surface slope
β	$\alpha - D\partial_h \alpha$
$\underline{\beta}$	perturbation to velocity
$\underline{\gamma}$	perturbation to convection term
γ	constant
Γ	boundary
δ	perturbation to water level
δ	distance
δ	shear layer width
Δ	twice the area of a triangle
ε	turbulent eddy viscosity
ε	convergence parameter
η	update vector to H
Θ	time weighting coordinate
Θ	polar (angular) coordinate
λ	relaxation parameter
μ	gradient parameter
μ	mesh ratio $\Delta t / \Delta x$
ε	update to Ψ
π	function
ρ	density
ρ	radius
σ	stress tensor
$\underline{\underline{\tau}}$	
τ_{xx}	stress components

ϕ	function
ϕ	basis function (linear)
Φ	function
χ	basis function (linear discontinuous or constant)
ψ	stream function
Ψ	finite element approximation to ψ
Ω	flow domain

Subscripts

e,i,j,k	node or element values
u,d	up and down stream
t	transverse (ie, normal to stream)
s	streamwise
x,y,z	in coordinate direction
D,N	Dirichlet and Neumann boundary data

Superscripts

e	element value
i	iteration index
m	iteration index
n	iteration index or time step

Operators, etc

M_C, M_L	averaging finite difference operators
∂_x, etc	partial derivative with respect to x

$\Delta_o, \Delta_-, \Delta_+$ difference operators (central, backwards, forwards)

$< ., . >$ inner product over flow domain

$\underline{\nabla}$ gradient

$\hat{}$ Fourier transform

CHAPTER 1

INTRODUCTION

1.1 Physical background

Rivers form a part of the natural environment and fulfil a variety of functions including water supply, drainage and recreation. The river usually comprises a well defined channel flanked by areas of land which are subject to occasional inundation; the flood plain. The plan form of the channel and flood plain system depends upon many geomorphological factors as does the time scale overwhich changes may occur, see for example Chorley, (1969). Whether the river is in flood or not the flow boundaries are geometrically irregular, being the edges of the river valley or main channel. On the flood plain human activity (residential and industrial development, agriculture, road construction etc.) sometimes conflicts with the natural function of the land to pass flood discharges. Engineers and others with the responsibility to manage river basins often use models to study proposed engineering works to ensure that the capital expenditure involved is a good long term investment.

Two types of model can be employed in design studies; analogue models and computational models. The most common type of analogue model is the scale physical hydraulic model. However, air-pressure models have been used, see Militeev and Shkolnikov (1981), and it is conceivable that analogue computer studies may have been done. Physical models may be constructed

to a natural or distorted scale and may be used to study extremely complicated flows. They have an immediate visual impact for engineer and layman alike and are a well established investigative method for example Novak and Cabelka, (1981). Physical models, however, are expensive to construct and operate, and they are limited by scale effects and the space available for their construction.

Over the past twenty-five years, a variety of computational river models have been developed, see Cunge, Holly and Verwey, (1980). In one-dimensional models the flow is averaged across a section normal to the typical velocity direction; this process gives the Saint-Venant equations of open channel flow. Some quasi two-dimensional models have been constructed in which the river flood plain is divided into a number of cells. The exchange of flow between contiguous cells is based upon the the physical properties of their common boundary and the difference in water level between the cells, see Section 1.3.2. One-dimensional models are a widely accepted method of simulating the flow in long reaches of rivers but they cannot resolve all the local detail that may be required. No model can represent any features of the flow at a scale finer than the grid size without additional assumptions nor can any one-dimensional model represent features which are produced by two or three dimensional effects. Empirical formulae and coefficients can be included to simulate, for example, the meandering of the main channel within the flood plain or the energy losses associated with a bridge (Samuels and Gray, 1982). However, when precise information is required on the

effects of such features it is usually necessary to construct a physical model.

1.2 Scope of Thesis

This thesis examines several models of flow in a river and over its flood plain. The investigation has been limited to two-dimensional models, in plan, rather like a birds eye view of the flow. The models are based upon standard principles of fluid dynamics incorporating a variety of physically realistic simplifications. In none of the models is the bed topography allowed to change in time since for British rivers, the time scale for geomorphological changes to the system is usually much greater than duration of a flood. The finite element method is used to generate numerical approximations to the solution of the resulting flow equations. The ultimate goal of the project was not the development of new numerical techniques for their own sake but the construction of computational models that can be used for solving problems of engineering importance. The conference paper, Samuels (1983a), included as Appendix 5 gives a summary of most of the main points of this thesis.

As various processes are included in the mathematical model the nature of the equations changes. This affects the most appropriate numerical method for solving the flow equations. The numerical methods considered in this research project were directed at choosing the lowest order of approximation possible for the flow equations. It was assumed that, since the typical

data available for commercial studies are quite coarse, it was not reasonable to use high order approximation schemes. A topographic survey of a river and its flood plain can be expensive particularly if the river cross sections are surveyed with a separation comparable with the main channel width or if many flood plain ground levels an accuracy better than ±0.1m are required. In any prototype investigation there is pressure to keep data needs to the minimum necessry for the accuracy required from the study. However, the complex relationship between the model accuracy and the density of prototype data is not considered further in this thesis.

At some stages in the course of this investigation several approaches were possible to solve particular problems. To have examined all these would have extended the duration of the project considerably. Usually the most simple approach was examined, in line with the overall philosophy discussed above. The properties of the methods adopted, however, are analsyed in detail.

1.3 Mathematical modelling of flow on river flood plains

1.3.1 Types of model

This section reviews the various approaches adopted for modelling river and flood plain flow. There appears to be no consensus of opinion on what equations are the best for constructing a two dimensional model of flood plain flow. This is in marked contrast to the near universal acceptance of the

Saint Venant equations for modelling one-dimensional flow in rivers, see Cunge, Holly and Verwey (1980). The section concentrates on models which produce quantitative predictions of the flow and not on qualitative models such as the one described by Lewin and Hughes (1980).

Two-dimensional models of flood plain flow vary widely in their complexity from the simplest statement of steady flow, with the surface slope equal to the friction slope, to those taking account of the variation of inundated area with time and including the effects of turbulent dissipation of energy. Models may be classified as:

(1) **cell type** in which the flow is computed from cell to cell on the flood plain according to certain laws,
(2) **differential equation type**, in which the bulk flow is described as a set of coupled partial differential equations derived from physical principles.

Models in the second class may employ the method of characteristics, a finite difference method (fdm) or the finite element method (fem) to generate approximate solutions of the differential equations. Some may be constructed to satisfy conservation laws for certain physical quantities. Such properties are important if hydraulic jumps or bores occur in the flow field and could be taken as the ultimate test of all models. Abbott (1979) and Cunge, Holly and Verwey (1980) point out the importance of proper treatment of conservation principles for one dimensional flows. In particular, Cunge et

al show how Preissmann's classic finite difference scheme is in fact a statement of the integral form of the conservation laws for one dimensional flow.

1.3.2 Cell type models

The distinctive feature of cell type models is that they are based on irregular computational grids which are defined according to the ground topography. Usually the boundaries of these cells are taken either along lines normal to the local direction of flow or along lines across which there will be no flow. The grid thus roughly follows the outline of the channel and flood plain in plan, see Fig 1.1. This constrasts with the regular, rectangular grids used in finite difference methods. Several cell models have been developed over the past 15 years, see Zanobetti et al (1968), Cunge (1971), Thirriot and Gaudu (1971), Cunge (1975), Weiss (1976), Price (1980) and Lesleighter (1983). These models vary in their complexity. Most neglect the effects on the momentum equation of the co-ordinate transformation that is involved in passing from the natural river topography to the idealized situation.
Typically, flow on the flood plain is controlled by equations such as:

$$Q_{ij} = K_{\ell}(h_i - h_j)^{0.5} \qquad (1.1)$$

for a river type link between cells i and j or for a weir type link:

$$Q_{ij} = c\, f(h_i,h_j)\, (h_i-h_w)^{1.5} \qquad (1.2)$$

where h_w is the height of the weir crest.
In a steady flow simulation the levels h_i and discharges Q_{ij}

are obtained by iteration and for unsteady flow the total volume V of water stored in each computational cell is also taken into account. The calibration of such models depends upon the correct choice for the links of the conveyance function K_ℓ and the weir discharge coefficients c and f in equations (1.1) and (1.2) respectively. The flood plain flow may be coupled to either steady or unsteady flow in the main river channel. Placing river or weir type links at cell boundaries or where to allow no flow at all is left to the judgement of the engineer responsible for investigation. These decisions can radically affect the model results, see Cunge (1971).

When the water level variation over the flood plain is controlled by features such as banks, hedges, fences etc and the cell boundaries are placed along these features, a cell model should produce satisfactory results. However, if the head losses occur more or less uniformly over the whole flow domain, such as when the bed stresses are dominant, a cell model may give misleading results. For friction controlled flow the dynamic equation becomes:

$$K^2 \underline{\nabla} h + \underline{q}|\underline{q}| = 0 \qquad (1.3)$$

where K is the conveyance function, h the stage (water surface level) and $\underline{q}$ the unit flow vector, see Section 2.5.1. In the direction of the unit vector $\underline{e}_s$ we have:

$$K^2 \partial_s h = - |\underline{q}|^2 \, \underline{e}_q \cdot \underline{e}_s \qquad (1.4)$$

where $\underline{e}_q$ is the unit vector in the direction of the flow

velocity. Comparing this with the equation (1.1) used for river links suggests that:

$$K_{\ell} = \ell K \left|\underline{e}_q \cdot \underline{e}_s\right|^{-\frac{1}{2}} \left|\underline{e}_s \cdot \underline{e}_n\right| / \left|\Delta s\right|^{\frac{1}{2}} \qquad (1.5)$$

where $\underline{e}_n$ is the unit vector normal to the common side between the two cells, ℓ is the length of the side and Δs and $\underline{e}_s$ are the distance and unit vector between the cell centres. The weakness of the cell type model lies in the dependence of the conveyance function for the link K_{ℓ} upon the local direction of the flow through the factor $\left|\underline{e}_q \cdot \underline{e}_s\right|^{-\frac{1}{2}}$. Thus the appropriate conveyance function for a link may change if the flow pattern of the flood plain changes significantly. This will limit the predictive abilites of such models when assessing the effects of works which alter the direction of flow across the flood plain.

Alternatively it is possible to include some of the dynamics of the flow on the flood plain by treating the channel and flood plain flow paths as separate one dimensional channels using the Saint Venant equations (see Grijsen and Meijer (1979) and Samuels (1979)). In such models there may be stability problems associated with the treatment of the flow over the river banks (see Samuels (1983b), Tagg and Samuels (1984) and Cunge, Holly and Verwey (1980)). However, this type of model can produce realistic results for the design of engineering works.

1.3.3 Models based on the method of characteristics

Kalkwijk and De Vriend (1980) used a scheme based on

characteristics to solve the equations describing primary and secondary flow in river bends. They transformed the flow equations into a coordinate system based upon the approximate streamlines of the primary flow. This method requires an a priori estimate of the streamlines of the flow and so may be difficult to apply to flows that are not contained by a well defined river channel. Schmitz, Seus and Czirwitzky (1983) have produced a method based upon a different transformation of the flow equations, and subsequent integration over the complete characteristic cone of these equations. Their method describes the topography of the river using a rectangular grid which is capable of local refinement. This method would appear to be a viable alternative to the finite element model described in this thesis. Schmitz et al, however, acknowledge that their model requires significant computational resources and cannot easily include situations where the lateral extent of flooding is not known in advance of the computation.

1.3.4 Models based on the finite difference method

Finite difference methods have been applied successfully to the shallow water equations in estuaries for many years. The principal problems emerge from the representation of the boundaries of the flow domain. It is possible to use curvilinear coordinates to improve the representation of the boundaries in simulations of tidal flow. This, however, leads to a more complicated set of equations to solve as the local stretching and distortion of the cartesian coordinate grid is included in the differential equations.

Recently Vreugdenhil and Wijbenga (1982) have applied a finite difference model from tidal engineering to a river channel and flood plain system and compared the results with those from a physical model. Their investigation showed the sensitivity of the results to various terms in the mathematical model equations. This is discussed further in chapter 2 below. Overall they report a good agreement between the physical and computational models, despite the relatively jagged appearance of the fitted difference net to the line of the main river channel. The model was based upon a 30m grid with a river width of about 150m and a flood plain width of up to 450m. The model time step was limited by the need for the anti-diffusive effects of the truncation error to be dominated by physical diffusion of the system. This forced the use of time steps of 10 seconds or less despite formal unconditional stability of the numerical scheme employed.

Zielke and Urban (1981) compare several models based on finite difference and finite element methods, including some based on coupling one and two-dimensional models together. Their example computations come from models developed initially for tidal flow. When using a finite difference based model with a grid size of 50m, the maximum that could resolve the river channel width, Zielke and Urban report that "it was not always easy to represent the characteristic features of the terrain" and the calculations were limited to time steps of 4 seconds. Militeev and Shkolnikov (1981) also describe the application of a finite difference based model of flood plain flow, comparing its results with an experimental study. Again, they comment on

difficulties caused by the relative coarseness of the grids employed.

There is not space here to describe the use of standard fdms for two dimensional fluid flow, including tidal flow. These are well covered by standard texts such as Roache (1972) and Abbott (1979).

1.3.5 Models based on the finite element method

Over the past 15 years there has been a great interest in applying the fem to problems of fluid flow. Several applications to tidal hydraulic problems have been made, see for example Brebbia and Connor (1976), Herrling (1978) and Holtz and Nitsche (1980). However, less has been published on the use of the fem to model flood plain flow. This is somewhat surprising since the irregular topography of a river flood plain lends itself naturally to description by finite elements.

Franques and Yannitell (1974) and Tseng (1975) have both developed finite element models for flow on river flood plains in the neighbourhood of a bridge. One conclusion drawn from these papers is that much of the head loss at the bridge they studied is accounted for by friction losses along correctly located streamlines. Niemeyer (1979) has presented an application of the finite element method to steady flow at the confluence of two main rivers. In their comparison paper Zielke and Urban (1981) describe an application of the estuary finite element model developed by Holtz and Nitsche (1980) to

flow on a river meandering in its flood plain. This model also takes account of the variation of the inundated area of the flood plain in time. Herrling (1982) also applied an estuary model to river flow. King and Norton (1978) and Lee (1980) both describe the application of Tseng's model to particular case studies. King and Norton draw attention to large errors within the model for the continuity equation (54% in the worse case). Lee points out the difficulties in representing the bottom topography and roughness variations and questions whether a new approach is needed. Tseng's model is based upon quite large finite elements with a quadratic variation of velocity in each.

Su, Wang and Alonso (1980) have developed a model for two dimensional flow within a river channel. They applied their model to investigate flow at channel junctions. The model contained a linearization of the flow equations, putting the convection term in particular at the old time or iteration. The approach was therefore similar to that adopted for the present investigation and some of the consequences of this representation of the convection term are described in chapter 5 below.

Some other finite element solutions of the flood plain flow equations have been published in which the tests reported were restricted to rectangular meshes over rectangular domains and thus geometric problems were avoided. Taylor (1976) looked at the runoff over a hill slope and for his tests the convection term in the dynamic equation was small in comparison with the

other terms. Thienpont and Berlamont (1980) compare the results of their model with experimental data for a flume with and without an obstacle in the centre of the flow field. These comparisons indicate the presence of a diffusive effect which is larger than in the prototype. Katapodes (1980) simulates the propagation of a dam break wave in a rectangular basin with regions of supercritical flow. Finally, Moult (1980) presents a model based upon using a stream function of lateral discharge into a channel.

These published results use a variety of element types and formulations of the flow equations as laid out in Table 1.1. Here ψ and ω represent stream function and vorticity, $\underline{q}$ and $\underline{U}$ represent the unit discharge and mean velocity vectors (see chapter 2) and h denotes either water surface level or depth.

It is clear from Table 1.1 that there is no consensus on what is the most appropriate fem to use for modelling river and flood plain flow. Some discontinuous velocity fields have been used, e.g. Franques and Yannitell (1974), whereas other workers use a velocity representation of higher order than that for water level, e.g. Tseng (1975). Even the most appropriate formulation of the flow equations is not clear. Some of the merits and disadvantages of these various approaches are discussed below. In fact in only two of the papers listed in Table 1.1, Lee (1980) and Zielke and Urban (1981) is the river channel resolved separately from the flood plain in any example computation.

TABLE 1.1 COMPARISON OF PUBLISHED FINITE ELEMENT RIVER MODELS

AUTHORS	VARIABLES	ELEMENT TYPE			COMMENTS
		Shape	number of nodes		
			ϕ, $\underline{q}$ or $\underline{U}$	ω or h	
Franques and Yannitell (1974)	ϕ, h	triangle	3	(3)	h from Bernoulli equation
Tseng (1975), King and Norton (1978), Lee (1980)	$\underline{q}$,h	triangle	6	3	
Taylor (1976)	$\underline{U}$, h	rectangle	4	4	Convection terms small compared with friction
		rectangle	8	8	
		rectangle	12	12	
Herrling (1978 and 1982)	$\underline{U}$, h	triangle	6	6	Approximation of $\underline{U}$ discontinuous as $\underline{U}$ calculated locally from h
Niemeyer (1979)	$\underline{U}$, h	triangle	6	6	mesh of mixed isoparametric
		quadrilateral	8	8	elements
Su, Wang and Alonso (1980)	$\underline{U}$, h	quadrilateral	4	4	
Thienpont and Berlamont (1980)	$\underline{q}$, h	quadrilateral	8	4	isoparametric
Katapodes (1980)	$\underline{U}$, h	rectangle	4	4	included supercritical flow
Moult (1980)	ϕ, ω	triangle	(3)	3	Calculations of ϕ and h subservient to ω
Zielke and Urban (1981)	$\underline{q}$, h	triangle	3	3	

CHAPTER 2

THE MATHEMATICAL MODEL

In this chapter we develop the two-dimensional depth integrated flow equations and analyse some of their properties. The integration of fluid flow equations through the flow depth is not new, see for example Dronkers (1964), Leendertse (1967) and Kuipers and Vreugdenhil (1973). However, the treatment of the convection term $(\underline{u}.\ \underline{\nabla})\underline{u}$ presented here differs from the approach usually adopted. This difference is not superficial since it can affect both the type of the set of partial differential equations and the conditions under which a steady flow model may exhibit closd streamlines (see Sections 2.2.3, 2.4.3 and 2.6 below). The equations are also derived in terms of the unit flow vector $\underline{q}$ rather than the depth mean velocity vector $\underline{U}$.

Having derived in detail the depth integrated flow equations in Section 2.2, the representation of turbulent stresses is discussed only briefly in Section 2.3 since in the computational studies these stresses were neglected. The practical significance of these stresses, however, is discussed in Section 2.4.2 where estimates are given of the typical widths of the shear layers at the edges of the flow field and at the boundary between the main channel and flood plain.

The three sets of model equations used as a basis of practical computations are then set out in Section 2.5, being steady

friction controlled flow and steady and unsteady flow with friction and convection. In Section 2.6 we examine the type of these equations and what are appropriate boundary data. Some aspects of these problems are not fully resolved. Finally, in Section 2.7 we present the steady flow equations in the curvilinear orthogonal co-ordinate system based upon the streamlines of the flow. This form of the equation is convenient for manual calculations of the magnitude of various terms.

2.1 Assumptions

There are at least four distinct phases in developing a deterministic computer based model of any prototype situation. They are:

1. determine the relevant physics of the real life situation;
2. express the physics in a convenient symbolic form - the mathematical model;
3. construct algorithms to approximate the mathematical model equations - the numerical model;
4. incorporate data which link the numerical model to the prototype.

This chapter is concerned with the first two of these steps; the other two steps are discussed in the remainder of the thesis.

At the outset the following assumptions will be made:

1. Newtonian mechanics are appropriate;
2. the flow is turbulent;
3. the fluid density is uniform;
4. the fluid is incompressible;
5. vertical accelerations are negligible;
6. there are no tangential stresses on the air/water free surface;
7. the effects of the earths rotation can be neglected;
8. the spatial variation of atmospheric pressure can be neglected;
9. the river bed does not change with time.

Other more detailed assumptions necessary to derive particular model equations are identified as appropriate. All the above assumptions are reasonable for the construction of a model of the bulk flow in a river and over its flood plain. Obviously some of the assumptions can be relaxed, giving different flow equations with a different range of applicability. Typical of the restrictions forced by these assumptions is the neglect of secondary flows (assumption 5). These flows occur at sharp changes in the river bed, see for example Knight et al (1983), and around river bends, see Henderson (1966) and Kalkwijk and de Vriend (1980). The latter authors show how the mathematical model can be augmented to include a certain class of secondary flows.

The starting point for producing the two dimensional mathematical model is the full three dimensional fluid flow

equations. These are derived from applying Newton's principles of mass and momentum conservation to the motion of a fluid element, see sections 2.2 and 3.2 of Batchelor (1967). In cartesian coordinates these equations are:

$$\partial_t \rho + \underline{\nabla}.(\rho \underline{u}) = 0 \qquad (2.1)$$

$$\rho \partial_t \underline{u} + \rho \underline{u}.\underline{\nabla u} = \rho \underline{F} + \underline{\nabla}.\underline{\underline{\sigma}} \quad . \qquad (2.2)$$

Here, $\underline{u}$ is the three dimensional velocity vector, ρ is the fluid density, $\rho \underline{F}$ represents the body forces and $\underline{\underline{\sigma}}$ is the tensor of internal stresses within the fluid. The gradient operator $\underline{\nabla}$ above has components in all three directions. However, unless explicitly stated to the contrary in the remainder of this thesis, the operator will be restricted to two plan dimensions, that is in cartesian coordinates

$$\underline{\nabla} \equiv \underline{e}_x \partial_x + \underline{e}_y \partial_y$$

2.2 Derivation of the two dimensional flow equations

2.2.1 The continuity equation

Assumptions 3 and 4 in section 2.1 implies that the three dimensional continuity equation (2.1) can be simplified to:

$$\partial_x u + \partial_y v + \partial_z w = 0 \quad . \qquad (2.3)$$

The continuity equation for 2D flow in plan is derived by integrating (2.3) over the depth of the flow and applying the appropriate boundary conditions at the bed and the free surface which are:

$$\partial_t z_0 + u \partial_x z_0 + v \partial_y z_0 - w = 0 \qquad (2.4)$$

where $z_0 = b$ for the river bed and $z_0 = h$ for the free surface, see Fig 2.1. Assumption 9 implies that $\partial_t b = 0$. This process

gives:

$$\partial_x \int_b^h u\,dz + \partial_y \int_b^h v\,dz + \partial_t h = 0 \ . \qquad (2.5)$$

Defining the unit flows q_x and q_y by:

$$q_x = \int_b^h u\,dz \ ; \ q_y = \int_b^h v\,dz \qquad (2.6)$$

we obtain the continuity equation used in the model

$$\underline{\nabla} \cdot \underline{q} + \partial_t h = 0 \qquad (2.7)$$

with $\underline{q} = (q_x \ q_y)^t$. The form of the continuity equation in terms of depth mean velocities used by some workers (see the literature review in section 1.3) is:

$$\underline{\nabla} \cdot (D \ \underline{U}) + \partial_t D = 0 \qquad (2.8)$$

where D is the flow depth (h - b) and the mean velocity vector $\underline{U}$ is defined as:

$$\underline{U} = \underline{q}/D \qquad (2.9)$$

Comparing equations (2.8) and (2.1) it is evident that, although the flow is incompressible, a form of compressibility has been reintroduced into the flow equations through the existence of a free surface. The depth D now plays the role of the density in (2.1). It will be seen that the solutions of the two-dimensional equations for river flow exhibit some of the same phenomena as compressible aerodynamic flows.

2.2.2 The dynamic equation

The dynamic equation is obtained by a depth integration of equation (2.2). However, the process is somewhat more complicated than the derivation of equation (2.7) described above. It is well known that the horizontal velocity

components u and v vary with depth. In order to incorporate this variation into the model we assume that we can define a vertical velocity profile which is common to u and v, thus:

$$u = U\,\Phi(z) \;;\; v = V\,\Phi(z) \qquad (2.10)$$

where U and V are the components of the depth mean velocity vector $\underline{U}$ in equation (2.9). This assumption restricts the model to where the flow is well mixed vertically and does not change direction in the vertical and is not stratified. Furthermore, the form of $\Phi(z)$ in (2.10) is assumed to be the same for steady and unsteady flow conditions.

The sole body force acting on the fluid is gravity. Thus the term $\underline{F}$ in equation (2.2) is given by:

$$\underline{F} = -g\underline{e}_z \qquad (2.11)$$

The internal stress tensor is separated into an isotropic part (the mechanical pressure, p) and deviatoric part $\underline{\underline{\tau}}$, whose existence is solely due to the fluid motion:

$$\underline{\underline{\sigma}} = p\,\underline{\underline{\delta}} + \underline{\underline{\tau}} \qquad (2.12)$$

where $\underline{\underline{\delta}}$ is the isotropic tensor and (in three dimensions)

$$\underline{\nabla} \cdot p\underline{\underline{\delta}} = \underline{\nabla}p \qquad (2.13)$$

First of all, consider motion in the vertical direction. The assumption that vertical accelerations are small implies that the corresponding deviatoric part of the stress tensor is also small. Integrating the appropriate component of the dynamic equation (2.2) over the depth we obtain:

$$\int (\partial_z p + \rho g)\, dz = \text{constant}$$

Hence:

$$p(z) + \rho g z = \text{constant}$$

On the free surface p = Pa, the atmospheric pressure, thus:

$$p = Pa + \rho g(h - z) \tag{2.14}$$

which is the hydrostatic pressure distribution.

Now consider one of the horizontal components of the dynamic equation, in the direction $\underline{e}_x$ say, and integrate this through depth.

$$\rho \int_b^h \partial_t u \, dz + \rho \int_b^h (u\partial_x u + v\partial_y u + w\partial_z u) \, dz + \int_b^h \partial_x \left[Pa + \rho g \, (h - z)\right] dz$$

$$= \int_b^h (\partial_x \tau_{xx} + \partial_y \tau_{xy} + \partial_z \tau_{xz}) dz \tag{2.15}$$

Examining the terms in (2.15) individually we have:

$$\int_b^h \partial_t u \, dz = \partial_t q_x + u\partial_t b - u\partial_t h \tag{2.16}$$

Using equation (2.3) the second term in (2.15) becomes:

$$\int_b^h (u\partial_x u + v\partial_y u + w\partial_z u) dz = \int_b^h (\partial_x u^2 + \partial_y uv + \partial_z uw) dz \tag{2.17}$$

$$\int_b^h (\partial_z uw) dz = uw\Big|_h - uw\Big|_b \tag{2.18}$$

$$\int_b^h (\partial_x u^2 + \partial_y uv) dz = \partial_x \int_b^h u^2 \, dz + \partial_y \int_b^h uv \, dz$$

$$u^2\partial_x h - uv\partial_y h + u^2\partial_x b + uv\partial_y b \, . \tag{2.19}$$

The third term in equation (2.15) becomes:

$$\int_b^h \partial_x \left(Pa + \rho g(h - z)\right) dz = \int_b^h (\rho g \partial_x h) dz = \rho g D \partial_x h \tag{2.20}$$

since from assumption 8 in section 2.1 $\partial_x Pa = 0$.

The stress terms on the RHS of equation 2.15 become:

$$\int_b^h (\partial_x \tau_{xx} + \partial_y \tau_{xy} + \partial_z \tau_{xz}) dz =$$

$$\partial_x \int_b^h (\tau_{xx}) \, dz + \partial_y \int_b^h (\tau_{xy}) \, dz + (\tau_{xz} - \tau_{xx} \, \partial_x z_0 - \tau_{xy} \, \partial_y z_0)\Big|_b^h \tag{2.21}$$

in which the final term is the difference of the stresses on the free surface and the bed.

Although the effective stresses on the air/water interface can be readily quantified, see for example Heaps (1969), they are excluded from this model of flood plain flow. Significant wind stresses only occur at high wind speeds in excess of about 20m/s (gale force 8 and stronger).

The bed stresses on the RHS of equation (2.21) may be calculated from one of several empirical formulae of the general form (at $z_0 = b$):

$$\tau_{xb} = \tau_{xz} - \tau_{xx}\,\partial_x z_0 - \tau_{xy}\,\partial_y z_0 = 0.125\,\rho f u\,(u^2 + v^2)^{\frac{1}{2}} \qquad (2.22)$$

where f is the Darcy friction factor and u and v are the components of the depth mean velocity vector $\underline{u}$ of equation (2.9). Henderson (1966) presents the following forms of the friction factor which are in common engineering use:

1. Chezy's law:

   $$f = 8gC^{-2} \qquad (2.23)$$

   where C is the Chezy coefficient which has dimensions $L^{\frac{1}{2}}T^{-1}$

2. Manning's equation:

   $$f = 8gn^2 D^{-1/3} \qquad (2.24)$$

   where n is Manning's roughness coefficient and D the depth of flow. Manning's n has dimensions $L^{-1/3}T$

3. Colebrook-White equation (rough-turbulent)

$$f = \left(2 \log_{10} (14.8\ D/k_s)\right)^{-2} \qquad (2.25)$$

where k_s is the roughness size, having dimensions of length. The constant 14.8 is not precisely defined, see Ackers (1958) and Reynolds (1974). Any changes to its value will merely alter the roughness size used in calibrating the model.

Ackers also shows that Manning's equation (2.24) is an approximation to the Colebrook-White equation (2.25) provided that:

$$n = 0.038\ k_s^{1/6}$$

and

$$7\ k_s < D < 140 k_s$$

Changing to natural logarithms equation (2.25) may be written as:

$$\frac{8}{f} = a_1 \left(\ln (14.8D/k_s)\right)^2 \qquad (2.26a)$$

where the constant a_1 has the value $32(\log_{10} e)^2$. This equation for f becomes singular as D tends to zero. Following Ackers (1958) we may replace the logarithm by a power law for small depths thus:

$$\frac{8}{f} = a_2 \left(\frac{D}{k_s}\right)^{a_3} \quad \text{for} \quad D < a_4 k_s \qquad (2.26b)$$

Once the exponent a_3 has been chosen, the cross over point between (2.26a) and (2.26b) and the constant a_2 are determined by the conditions for f to be continuous and to have a continuous derivative with respect to depth at $D = a_4 k_s$. In this

investigation, a_3 has been set to 1.0 and the numerical values of the other constants are:

$$a_1 = 6.035574304$$

$$a_2 = 48.35610855$$

$$a_4 = 0.499260542$$

The model program contains all three friction laws to facilitate comparison with other studies and experimental data. When trying to reproduce scale physical model results the Colebrook-White equation should be used since the parameter k_s may be readily related to the surface finish of the model. For calibrating a model against field data either the Colebrook-White or Manning's equation should be used. However, many European and American engineers use the Chezy equation because of its simplicity. Ackers (1958) shows how the Colebrook-White resistance law can be linked to the logarithmic velocity profile often assumed for the function $\Phi(z)$ in equation (2.10). The logarithmic profile cannot, however, be used near the bed where it becomes singular.

Reassembling the dynamic equation (2.15) from the expansions in equations (2.16) to (2.22) we have:

$$\partial_t q_x + \partial_x \int_b^h u^2 dz + \partial_y \int_b^h uv dz + gD\partial_x h + \frac{f}{8D^2} q_x |\underline{q}|$$

$$= \frac{1}{\rho} \partial_x \left(\int_b^h \tau_{xx} \, dz \right) + \frac{1}{\rho} \partial_y \left(\int_b^h \tau_{xy} \, dz \right) \qquad (2.27)$$

since the other terms on the free surface and the bed cancel exactly on application of the kinematic boundary condition (2.4). Using the velocity profile equation (2.10) the depth mean square velocities in (2.27) can be written as:

$$\int_b^h u^2 dz = \frac{\alpha}{D} q_x^2 \quad ; \quad \int_b^h uv dz = \frac{\alpha}{D} q_x q_y \qquad (2.28)$$

where the coefficient α is dimensionless and greater than or equal to 1, and is given by:

$$\alpha = D \int_b^h \Phi^2 \, dz \; / \; (\int_b^h \Phi \, dz)^2$$

$$= \int_b^h \Phi^2 \, dz \; / \; D$$

For convenience the function Φ can also be treated as a power law in depth that is:

$$\Phi(z) \propto (z - b)^p$$

with p lying in the range 1/6 to 1/10. Samuels and Gray (1982) show that for this form of Φ the corresponding value of α lies in the range 1.021 to 1.008, and α is independent of depth.

The treatment of the horizontal component of the dynamic equation in the direction $\underline{e}_y$ follows in a similar fashion. Defining the 2-D exchange vector $\underline{T} = (T_x, T_y)^t$ as:

$$T_x = \frac{1}{\rho g D} \partial_x \int_b^h \tau_{xx} \, dz + \frac{1}{\rho g D} \partial_y \int_b^h \tau_{xy} \, \partial z \qquad (2.29a)$$

$$T_y = \frac{1}{\rho g D} \partial_x \int_b^h \tau_{yx} \, dz + \frac{1}{\rho g D} \partial_y \int_b^h \tau_{yy} \, \partial_z \qquad (2.29b)$$

we may write the dynamic equation in vector form as:

$$\frac{1}{gD} \partial_t \, \underline{q} + \frac{1}{gD} \underline{\nabla} \cdot (\alpha \, \underline{q} \, \underline{q}/D) + \underline{q}|\underline{q}|/K^2 + \underline{\nabla} h = \underline{T} \qquad (2.30)$$

where $\underline{q} \, \underline{q}$ is a diadic tensor and K^2 is defined by:

$$K^2 = 8gD^3/f \qquad (2.31a)$$

The friction factor f depends upon depth accordng to equations (2.23), (2.24) and (2.25) and an equivalent formula for K^2 is

$$K^2 = CD^p \qquad (2.31b)$$

The power p is 3 for Chezy's equation, 10/3 for Manning's equation and lies between 3 and 4 for the Colebrook-White equation with the power law extension for small depths.

2.2.3 Alternative forms of the dynamic equation

Two different approaches are possible in deriving the dynamic equation. Firstly, instead of using the velocity distribution coefficient α of equation (2.28) the depth integrated convection term may be written as follows:

$$\partial_x \int_b^h u^2 dz = \partial_x \left(\frac{q_x q_x}{D}\right) + \partial_x \int_b^h (u - U)^2 dz \qquad (2.32a)$$

since $u^2 = \left(U - (U - u)\right)^2$ and $\int_b^h U\,(U - u)dz = 0$. Similarly:

$$\partial_y \int_b^h uv\, dz = \partial_y \left(\frac{q_x q_y}{D}\right) + \partial_y \int_b^h (u - U)(v - V)dz \qquad (2.32b)$$

Kuipers and Vreugdenhil (1973) and Falconer (1977) draw an analogy between the terms involving the departures from the mean velocities, (u - U) etc, and the Reynolds stress terms in turbulence modelling and suggest that they can be incorporated into the model in the same way as the turbulence stresses. The values of the departures, (u - U), are largest near the bed and the terms which involve these departures can be argued to introduce a form of dispersion into the model. Although plausible, treating these dispersive terms in the same way as

turbulent stresses implies that a model of steady flow with convection can exhibit closed streamlines in the absence of other effective stresses. This is shown in certain circumstances to be false in section 2.4.3 below. Also the equations (2.34) and (2.37) obtained below by including these dispersive terms with the turbulent stress terms when combined with the continuity equation form an incompletely parabolic system. The alternative formulation of the dynamic equation with the distribution coefficient α, however, gives a hyperbolic system, see section 2.6 below.

Nevertheless, defining $\tilde{T}_x$, analogous to T_x of equation (2.29a), as:

$$\tilde{T}_x = \frac{1}{\rho g D} \{\partial_x \int_b^h (\tau_{xx} + \rho(U-u)^2)dz + \partial_y \int_b^h (\tau_{xy} + \rho(U-u)(V-v))dz\} \quad . \qquad (2.33)$$

with a similar equation for $\tilde{T}_y$ we have the dynamic equation:

$$\frac{1}{gD} \partial_t \underline{q} + \frac{1}{gD} \underline{\nabla}.(\underline{q}\underline{q}/D) + \underline{q}|\underline{q}|/K^2 + \underline{\nabla}h = \underline{\tilde{T}} \quad . \qquad (2.34)$$

Here the exchange vector $\underline{\tilde{T}}$, $(\tilde{T}_x, \tilde{T}_y)^t$, includes the dispersive terms from the departure of the fluid velocity from its depth mean value.

The dynamic equation can also be written in terms of the depth mean velocity vector U.

$$\frac{1}{gD} \partial_t(\underline{U}D) + \frac{1}{gD} \underline{\nabla}.(\alpha \underline{U}\,\underline{U}\,D) + \underline{U}|\underline{U}|D^2/K^2 + \underline{\nabla}h = \underline{T} \qquad (2.36)$$

Or, if the velocity distribution coefficient α is set to 1 and

the exchange vector is modified as in (2.33) above:

$$\frac{1}{g}\,\partial_t \underline{U} + \frac{1}{g}\,(\underline{U}.\underline{\nabla})\underline{U} + \underline{U}|\underline{U}|D^2/K^2 + \underline{\nabla}h = \underline{\tilde{T}} \qquad (2.37)$$

which is the form of the dynamic equation used, for example, by Dronkers (1964), Leendertse (1967), Kuipers and Vreugdenhil (1973), Falconcer (1977) and Vreugdenhil and Wijbenga (1982).

2.3 The effects of turbulence

The derivation of the two-dimensional depth averaged equations (2.7) and (2.30) has not taken explicit account of the turbulence of the flow. The derivation of the Reynolds equations of turbulent flow involves an average over a time scale that is large compared with that of turbulent fluctuations but small compared with variations in the bulk flow, see for example Rouse (1959) or Reynolds (1974). This averaging process is conceptually similar to the continuum hypothesis, (Batchelor, 1967), which underlies fluid dynamics. When written in terms of the turbulent mean velocities, etc, the basic equations for mass and momentum conservation are the same as (2.1) and (2.2) with the stress tensor $\underline{\underline{\sigma}}$ containing the so called Reynolds stresses as well as the viscous stresses. The discussion in section 2.2.2 makes no assumption on the form of this stress tensor.

These Reynolds stresses affect the mean velocity profiles both in plan and in depth. The logarithmic velocity profile with depth discussed briefly in section 2.2.2 results from a simple

empirical relation between the Reynolds stresses in the vertical plane and the flow field, the mixing length hypothesis, see Appendix I of Ackers, (1958). In the horizontal plane the Reynolds stresses produce a lateral "diffusion" of momentum, the size of the effect being related in a complex manner to the bulk flow field. The inclusion of the Reynolds stresses in the flow equations requires some form of turbulence model. The simplest of these introduce no extra equations into the system, whereas others introduce one or more additional equations which describe the transport of characteristic features of the turbulence field. For a discussion of turbulence models see Rodi (1980). The simplest turbulence closures lead to equations for $\underline{T}$ or $\underline{\tilde{T}}$ like:

$$\underline{T} = \frac{\varepsilon_1}{g} \nabla^2 \underline{U} \qquad (2.38a)$$

or

$$\underline{T} = \frac{\varepsilon_2}{g} \nabla^2 \underline{q} \qquad (2.38b)$$

where ε_1 and ε_2 may be taken as constant or may be related to some parameters of the flow field such as depth and local velocity gradient. Falconer (1977) examined the use of turbulence models for modelling jet induced flows in harbours. He concluded that only the simplest form of turbulence model was justified for his particular case. Vreugdenhil and Wijbenga (1982) also used the representation of turbulent (or effective) stresses given by equation (2.38a).

2.4 The effects of various terms in the model equations

2.4.1 Physical parameters

Before further approximations to the flow equations are developed it is necessary to examine the relative importance of the various terms in the equations. Table 2.1 gives ranges of values for some of the parameters for British rivers. The general picture is that over moderate distances, say a few kilometres, the flow at the flood peak may be taken as approximately steady with the friction slope balancing the surface slope. Locally other effects may become important, depending upon the topographic features of the river valley.

2.4.2 The effective stresses

The simple turbulence closure model equation (2.38) gives rise to boundary or shear layers in the solution to the flow equations. Vreugdenhil and Wijbenga (1982) show how these boundary layers can alter the total conveyance of a cross section. The thickness of the boundary layers depends upon the effective diffusivity parameter ε of equation (2.38). Different values of ε produce different velocity distributions across the river and flood plain which in turn produce different total bed stress for the cross section. Approximate values for the boundary layer thickness are derived below.

Consider steady flow in the x direction at a section across the river and flood plain where the channel is straight and the flow depths for the channel and flood plain are constant but

TABLE 2.1

PARAMETER RANGES FOR UK RIVERS

Parameter	Channel		Flood plain	
	range	typical	range	typical
width (m)	5 to 200	30	0 to 2000	500
depth of flow (m)	1 to 10	5	0 to 4	1
velocity (m/s)	0.5 to 3	1	0 to 2	0.3
streamwise surface slope	10^{-2} to 10^{-5}	5×10^{-4}	10^{-2} to 10^{-5}	5×10^{-4}
transverse surface slope	up to 10^{-2} locally	-	up to 10^{-3} locally	-
radius of curvature of streamlines (m)	natural >30 near structures	-	> 100	-
	0 (1)	-	0 (1)	-
rate of change of surface elevation (m/s)	up to 10^{-3} (tidal)	-	0 (10^{-5})	10^{-5}
	10^{-4} (fluvial)	10^{-5}		
friction slope $\underline{q}\lvert\underline{q}\rvert/K^2$	10^{-2} to 10^{-5}	5×10^{-4}	10^{-2} to 10^{-5}	5×10^{-4}
temporal acceleration $\lvert\partial_t \underline{U}\rvert$ (m/s^2)	0 (10^{-5}) or less	-	0 (10^{-5}) or less	-

different, see Fig 2.2. The dynamic equation for the lateral distribution of the stream velocity U is:

$$fU^2/8D + g\partial_x h = \varepsilon\partial_{yy}U \qquad (2.39)$$

We may set the surface slope $\partial_x h$ to $-s$, a constant, where $s > 0$, and the dynamic equation becomes

$$fU^2/8D = gs + \varepsilon U'' \qquad (2.40)$$

in which the primes denote differentiation with respect to y.

Multiplying by U' we obtain the first integral

$$\frac{\beta}{2}(U')^2 = \frac{U^3}{3} - U_o^2 U + c$$

where c is a constant of integration, $U_o^2 = 8gDs/f$ and $\beta = 8D\varepsilon/f$. Now suppose that the cross section is semi-infinite laterally with the flow at the left hand wall $y = 0$ unaffected by the conditions to the right. From equation (2.40) we deduce that $U \to U_o$ as $y \to \infty$ and we use this condition to determine the constant of integration c as $2U_o^3/3$.

Defining the velocity deficit v as $U_o - U$ we find

$$(v')^2 = v^2\left[2U_o/\beta - 2v/3\beta\right] \qquad (2.41)$$

Equation (2.41) can be solved analytically for the current simple geometry by employing some further substitutions. Firstly, let η^2 denote $2U/\beta$ and μ denote $2v/3\beta$; equation (2.41) becomes

$$(\mu')^2 = \mu^2(\eta^2 - \mu)$$

Now set $\zeta^2 = \eta^2 - \mu$ and the differential equation becomes

$$4\zeta^2(\zeta')^2 = (\eta^2 - \zeta^2)^2\zeta^2$$

$$\text{or} \quad \frac{2d\zeta}{(\eta^2 - \zeta^2)} = \pm dy$$

The ambiguity in sign will be resolved by appealing to the physical characteristics of the flow. Integrating the above gives

$$2\ \text{arctanh}(\zeta/\eta) = \pm y\eta + 2c$$

where c is another constant of integration. Reverting to the original notation we have

$$U(y) = U_o \{3\ \tanh^2 [\pm(U_o/2\beta)^{\frac{1}{2}}\ y + c\ ] - 2\}.$$

The constant c is determined from the boundary condition $U = 0$ at $y =$ giving $c = \text{arctanh}[\pm\sqrt{(2/3)}\ ]$ that is

$$c = \pm\ln[(\sqrt{2}+\sqrt{3})/(\sqrt{3}-\sqrt{2})]^{\frac{1}{2}} = \pm 1.1462.$$

At the edge of the flow we require that $U > 0$ which allows us to resolve the ambiguity of signs to give

$$U(y) = U_o[3\ \tanh^2\{(U_o/2\beta)^{\frac{1}{2}}y + 1.1462\} - 2\ ]. \qquad (2.42)$$

The boundary layer thickness is commonly taken to be the distance over which the velocity deficit reduces to 0.01 of the free stream value. Putting $U(\delta) = 0.99U_o$ in equation (2.42) gives the boundary layer thickness δ as

$$\delta = 3.39\ (\beta/U_o)^{\frac{1}{2}} \quad .$$

Substituting the values of β and U_o gives

$$\delta = 5.70\ (\frac{D}{gsf})^{\frac{1}{4}} \varepsilon^{\frac{1}{2}} \quad . \qquad (2.43)$$

In order to calculate the size of the boundary layer we need to estimate the typical magnitude of the turbulent exchange parameter ε, which has so far been assumed constant. Vreugdenhil and Wijbenga (1982) give the following estimate based upon the experimental work of Lean and Weare (1979),

$$\varepsilon = 0.01\,\delta|\Delta U| \qquad (2.44)$$

Here $|\Delta U|$ is the velocity of difference across the shear layer which we may take to be U_o. Substituting these values in equation (2.43) and simplifying gives

$$\delta = 0.92\ D/f \qquad (2.45)$$

Vreugdenhil and Wijbenga also give some sample computations assuming $\varepsilon = 3.0 m^2 s^{-1}$ and $\varepsilon = 1.0 m^2 s^{-1}$.

A further estimate of ε is available from the text by Cunge, Holly and Verwey (1980). When discussing pollution modelling these authors suggest a cross stream exchange coefficient of the form

$$\varepsilon = \lambda U_* D \qquad (2.46)$$

where the constant λ lies in the range (0.25, 0.7) and the friction velocity U_* is related to the bed stress τ_b by

$$U_* = (\tau_b/\rho)^{\frac{1}{2}}$$

Using equation (2.22) for the bed stress we have

$$\varepsilon = \lambda DU\ (f/8)^{\frac{1}{2}} \qquad (2.47)$$

We note that the turbulent exchange parameter now depends upon the flow velocity U and thus equation (2.47) would give $\varepsilon = 0$ at the edge of the flow since $U = 0$ there. This of course is unacceptable and presumably results from the neglect of the usually insignificant viscous stresses in the derivation of (2.46). Taking a mean value of λ to be 0.4 and a mean value of U to be $0.5U_o$ and substituting into equation (2.43) gives

$$\delta = 2.5\ D/f^{\frac{1}{2}} \qquad (2.48)$$

Table 2.2 below gives typical values for the boundary layer width at the edge of the flood plain and the main channel based

upon the above estimates of the exchange parameter. The values are based upon the following physical parameters:

Surface slope	0.0004
Flood plain roughness size	3m
Channel roughness size	0.3m
Flood plain depth of flow	1.0m
Channel depth of flow	10.0m

Using the Colebrook-White equation (2.25) gives the friction factor f as 0.520 for the flood plain and 0.0344 for the channel and undisturbed flow velocities of 0.25m/s and 3.0m/s for the flood plain and channel respectively.

Table 2.2 Estimates of boundary layer width in metres

	Channel	Flood plain
Equation (2.43) $\varepsilon = 1.0 m^2 s^{-1}$	94	27
Equation (2.43) $\varepsilon = 3.0 m^2 s^{-1}$	160	46
Equation (2.45)	270	1.8
Equation (2.48)	58	2.9

Comparing these boundary layer sizes with the typical widths of the channel and flood plain quoted in Table 2.1 suggests that, whereas the boundary layer at the edge of the flood plain is localised, the flow over the entire width of the main channel is affected by the drag from the banks. The same conclusion can be drawn about the influence of the slow moving flood plain of on the flow in the main channel. The velocity may be affected across the entire width of the channel, see also Fig 4 from the paper by Vreugdenhil and Wijbenga (1982). To estimate the influence of the shear force from the faster channel flow on the velocity distribution on the flood plain, we may repeat the calculations of equations (2.44) to (2.48) using the channel velocity in equation (2.44) and a mean of half this value in equation (2.47). This gives estimates of the width of the shear layer on the flood plain to be 69m using equation (2.44) and 33m using equation (2.47). Again, given that the flood plain is of the order of 500m wide, we see that the shear layer should not influence the flow over its entire width. Clearly the current knowledge of the magnitude of the turbulent exchange parameter ε is unsatisfactory and the above conclusions are only tentative.

The models discussed in this thesis do not contain any representation of the effective stresses. There are two main consequences of this assumption. Firstly, the roughness values required to calibrate the model against prototype data will be different, possibly substantially so, from those for a model including the effective stresses. Secondly, the true solution

to the equations should not contain any closed stream lines for steady flow conditions except possible with grossly non uniform values of the velocity distribution coefficient α over the flow domain. The models, nevertheless, reproduce important features of the prototype such as the faster flow concentrated in the main channel.

2.4.3 Closed streamlines

Here we consider the conditions under which the solution to the mathematical model equations can exhibit closed streamlines. Suppose there is a closed streamline, c, within the flow domain, we may integrate the dynamic equation (2.36) around it to give:

$$\int_c \left(\partial_t \underline{U} + \frac{(1-\alpha)}{D}\underline{U}\partial_t D + \underline{U}.\underline{\nabla}(\alpha\underline{U}) + g\underline{U}|\underline{U}|D^2/K^2 + g\underline{\nabla}h\right).d\underline{s} = \int_c g\underline{T}.d\underline{s} \qquad (2.49)$$

Examining the lhs of (2.49) term by term we have:

$$\int_c \left(\partial_t \underline{U} + \frac{(1-\alpha)}{D}\underline{U}\partial_t D\right).d\underline{s} = \int_c \left(\partial_t|\underline{U}| + \frac{(1-\alpha)}{D}|\underline{U}|\partial_t D\right)ds \qquad (2.50)$$

$$\int_c g|\underline{U}|\underline{U}D^2/K^2.\, d\underline{s} = \int_c (g|\underline{U}|^2 D^2/K^2)ds \geq 0 \qquad (2.51)$$

$$\int_c \underline{\nabla}h.d\underline{s} = 0 \qquad (2.52)$$

and after some manipulation of vector identifies

$$\int_c \left(\underline{U}.\underline{\nabla}(\alpha\underline{U})\right).d\underline{s} = -\int_c \alpha\,\underline{\nabla}(\tfrac{1}{2}|\underline{U}|^2).d\underline{s} \qquad (2.53)$$

Sufficient conditions for the final integral in (2.53) to be zero are:

(a) α = constant on c, or;

(b) $|\underline{U}|^2$ = constant on c, or;

(c) $(\underline{\nabla}\alpha)\times\left(\underline{\nabla}(|\underline{U}|^2)\right) = 0$ within c.

Now consider some particular cases.

(1) $\alpha = 1$, $\underline{T} = \underline{0}$

Equation (2.49) reduces to:

$$\int_c \partial_t |\underline{U}| ds + \int_c g |\underline{U}| 2D^2/K^2 ds = 0 \quad . \quad (2.54)$$

Since the second term is non-negative the magnitude of the velocity around the closed streamline decreases as the energy of the flow is dissipated by friction. In the limit of steady flow we obtain the condition that $|\underline{U}| = 0$ on the closed streamline. Furthermore the steady flow continuity equation implies that, in the absence of any internal sources or sinks, $|\underline{q}| = 0$ over the entire flow field except at isolated points. Hence closed streamlines only exist in the trivial case of stationary flow.

(2) α constant ($\neq 1$), $\underline{T} = \underline{0}$

This situation occurs if a power law profile is assumed for the depth variation of the horizontal velocity components. The right hand side of equation (2.53) becomes identically zero and again we infer that there can only be closed streamlines in the trivial case $\underline{U} = \underline{0}$ if the flow is steady. A particular case result is $\alpha = 0$ when the convection term vanishes and we obtain the equation of friction controlled flow. Hence steady friction controlled flow should contain no closed streamlines.

(3) $\underline{T} = 0$, $\alpha > 1$, $|\underline{\nabla}\alpha| \neq 0$

This case is produced by a depthwise variation of the horizontal velocity components that is not a power law over the whole flow domain. For steady flow the line integral equation (2.49) becomes:

$$\int_c g|\underline{U}|^2 D^2/K^2 \, ds = \int_c \alpha \, \underline{\nabla}(\tfrac{1}{2}|\underline{U}|^2).ds \qquad (2.55)$$

and it is conceivable that some spatial variations of α may allow the existence of a closed streamline c for which the fluid velocity is non-zero.

(4) $\underline{T} \neq 0$

For steady flow the integral equation (2.49) becomes:

$$\int_c g|\underline{U}|^2 D^2/K^2 = \int_c g \, \underline{T}.ds + \int_c \alpha \, \underline{\nabla}(\tfrac{1}{2}|\underline{U}|^2).ds \, .$$

Again solutions to the steady flow equations may exhibit closed streamlines for all functions α.

Suppose that the velocity varies as some power of the depth then by case 2 the flow exhibits no closed streamlines when the turbulent stress terms are neglected. However, in the traditional formulation of the dynamic equation (2.37) the depth variation of the convection term leads to a non-zero effective stress vector $\underline{T}$. Hence we conclude by case 4 that the flow can contain closed streamlines in the absence of turbulent stresses. This anomaly is caused by the different methods and assumptions to depth integrate the convective accelerations.

2.5 Three mathematical models of flood plain flow

2.5.1 Steady friction controlled flow

The simplest mathematical model of flood plain flow considered in this thesis is that of steady friction controlled flow. The appropriate equations are:

continuity $$\underline{\nabla}.\underline{q} = 0 \qquad (2.56)$$

dynamic $$\underline{q}|\underline{q}|/K^2 + \underline{\nabla}h = 0 \qquad (2.57)$$

This pair of equations may be solved as they stand or be further manipulated to yield the stream function formulation or the potential formulation described below.

Defining the scalar stream function, ψ, by:

$$\underline{q} = \underline{\text{curl}}\ \psi = \partial_y \psi\, \underline{e}_x - \partial_x \psi \underline{e}_y$$

and taking the curl of the dynamic equation we have:

$$\underline{\nabla}.\left(|\underline{\nabla}\psi|K^{-2}\underline{\nabla}\psi\right) = 0 \qquad . \quad (2.58)$$

This is the stream function formulation of the problem and is the equation Franques and Yannitell (1974) used to define the streamlines of the flow field. Unfortunately the equation cannot be solved by itself since it depends implicitly on the water level through the conveyance K. Thus a numerical approximation to the solution of this equation will contain an iteration between the solution of this equation and one for determining the local water depths. Franques and Yannitell

produced the local depths by solving equation (2.37), with time derivatives and effective stresses set to zero, along the streamlines determined from an approximate solution of equation (2.58). This, however, is unsound since it includes the streamwise component of the convection term in the determination of water level but excludes the convection term entirely from the derivation of the flow field. The streamline integration should be based on equation (2.57) as discussed in chapter 3.

The potential formulation of the flow equations arises directly from a manipulation of equations (2.56) and (2.57). The dynamic equation can be rearranged to give the unit flow vector $\underline{q}$ explicitly thus:

$$\underline{q} = -K \underline{\nabla} h \left| \underline{\nabla} h \right|^{-\frac{1}{2}}$$

Substituting this in the continuity equation we obtain:

$$\underline{\nabla} \cdot (K \left| \underline{\nabla} h \right|^{-\frac{1}{2}} \underline{\nabla} h) = 0 \qquad (2.59)$$

This, the potential formulation of the flow equations, has not been used before to generate a model of flood plain flow. The water surface h acts as a form of (non-linear) velocity potential. It has the advantage over the stream function formulation that all terms in the equation depend solely upon h and are independent of the unit flow vector. Thus an approximation to the solution of equation (2.59) can be generated without recourse to the calculation of intermediate values of the unit flows in the iterative process.

2.5.2 Steady flow with convection and bed friction

In this case the continuity equation (2.56) is retained coupled with either of the dynamic equations:

$$\left(\frac{1}{gD}\right) \underline{\nabla}.(\alpha\, \underline{q}\, \underline{q}/D) + \underline{\nabla}h + \underline{q}|\underline{q}|/K^2 = 0 \qquad (2.60)$$

or

$$\frac{1}{g}\, \underline{U}.\underline{\nabla}(\alpha \underline{U}) + \underline{\nabla}h + \underline{q}|\underline{q}|/K^2 = 0 \qquad (2.61)$$

In either case writing the convection term $\frac{1}{g}\, \underline{U}.\underline{\nabla}\,(\alpha\, \underline{U})$ as $\underline{c}$ we may rearrange the dynamic equation as:

$$\underline{q} = -K\, (\underline{\nabla}h + \underline{c})\, |\underline{\nabla}h + \underline{c}|^{-\frac{1}{2}} \qquad (2.62)$$

and combining this with the continuity equation we obtain an equation similar to the potential formulation above but which now depends implicitly on the water velocities:

$$\underline{\nabla}.\ \left(K|\underline{\nabla}h+\underline{c}|^{-\frac{1}{2}}\ (\underline{\nabla}h+\underline{c})\right) = 0 \qquad (2.63)$$

2.5.3 Unsteady flow with convection and bed friction

The third mathematical model examined in this investigation was based upon adding the unsteady terms to the flow equations of section 2.5.2 above. The motivation for this was the development of an iteration method based upon time stepping to solve the steady flow equations including the convection term (see chapter 5). The continuity and dynamic equations are:

$$\underline{\nabla}.\underline{q} + \partial_t h = 0 \qquad (2.64)$$

$$\partial_t \underline{q} + \underline{\nabla}.(\underline{qq}/D) + gD\underline{\nabla}h + gD\underline{q}|\underline{q}|/K^2 = 0 \qquad (2.65)$$

In the dynamic equation the velocity distribution coefficient α has been set to 1.0 for all computations. Alternatively the dynamic equation may be written in terms of the depth mean

velocity $\underline{U}$:

$$\partial_t \underline{U} + (\underline{U}.\underline{\nabla})\underline{U} + g\underline{\nabla}h + gD^2\underline{U}|\underline{U}|/K^2 = 0 \quad . \qquad (2.66)$$

Note that from the discussion in section 2.4.3 any closed streamlines present in the initial data for the solution of these equations should decay when steady state boundary conditions are applied.

2.6 Classification of equations

2.6.1 Friction controlled flow

Both the stream function and potential formulations can be written in the form

$$\underline{\nabla}.\left[G\left|\underline{\nabla}\Phi\right|^P \underline{\nabla}\Phi\right] = 0 \qquad (2.67)$$

where the power P is 2 for the stream function formulation and P is $-\frac{1}{2}$ for the potential formulation. Denoting the derivatives by ∂_i where $x \equiv i = 1$ and $y \equiv i = 2$ and using summation convention we have

$$\partial_i\left[G(\partial_j\Phi\partial_j\Phi)^{\frac{1}{2}P}\ \partial_i\Phi\right] = 0 \quad . \qquad (2.68)$$

Expanding equation (2.68) we have:

$$\partial_i G\ \partial_i\Phi\,(\partial_j\Phi\partial_j\Phi)^{\frac{1}{2}P} + P\ \partial_{ij}\Phi\partial_j\Phi G(\partial_j\Phi\partial_j\Phi)^{\frac{1}{2}P-1}\partial_i\Phi$$
$$+ G\ (\partial_j\Phi\partial_j\Phi)^{\frac{1}{2}P}\ \partial_{ii}\Phi = 0 \qquad (2.69)$$

and if G is a function of Φ, x and y only we see that the coefficients of the second order derivatives are:

$$\partial_{xx}\Phi : G\left|\underline{\nabla}\Phi\right|^P\left[1 + P\left|\underline{\nabla}\Phi\right|^{-2}(\partial_x\Phi)^2\right] = a$$
$$\partial_{xy}\Phi : G\left|\underline{\nabla}\Phi\right|^P\left[2\ P\left|\underline{\nabla}\Phi\right|^{-2}\partial_x\Phi\ \partial_y\Phi\right] = 2b$$
$$\partial_{yy}\Phi : G\left|\underline{\nabla}\Phi\right|^P\left[1 + P\left|\underline{\nabla}\Phi\right|^{-2}\ (\partial_y\Phi)^2\right] = c$$

The condition for equation (2.67) to be elliptic is $b^2 < ac$ and using the definitions of a, b and c this becomes $1 + P > 0$ if $G|\nabla\Phi|^P$ is everywhere non zero. Hence both formulations of the steady friction controlled flow are elliptic. Since the flow can have no closed streamlines $|\underline{\nabla}h|$ and $|\underline{\nabla}\psi|$ can only vanish at isolated points. Also these gradients cannot become locally singular in the absence of sources and sinks of flow. These a-priori conditions, however, are not strong enough to meet the sufficient conditions for the existence of a unqiue solution to the non linear equations given by Froidevaux (1975). Existence and uniqueness of the solution have been proved by E E Süli (private communication) and this is reproduced in Appendix 4.

Suitable boundary conditions on the flow variable - ψ in (2.58) or h in (2.59) - are for the value of the variable itself, its normal derivative, or a combination of these two to be specified around the entire boundary of the flow domain. The conditions imposed on stream function and water level are complementary: when ψ is specified on a no-flow (solid) boundary in the stream function formulation, $\partial_n h$ is set to zero on the same boundary in the potential formulation. Similarly where $\partial_n \psi$ is set to zero in the stream function formulation, indicating normal flow across the boundary, h should be specified as constant in the potential formulation.

2.6.2 Steady flow with convection and bed friction

Writing the solution vector $\underset{\sim}{U} = (\underline{q}, h)^t$, we may represent the

equations (2.60) and 2.56) as a first order system thus:

$$A\,\partial_x \underset{\sim}{U} + B\,\partial_y \underset{\sim}{U} + \underset{\sim}{C}(\underset{\sim}{U}) = 0 \qquad (2.70)$$

where:

$$A = \begin{bmatrix} 2\alpha U & 0 & c^2 - \beta U^2 \\ \alpha V & \alpha U & -\beta UV \\ 1 & 0 & 0 \end{bmatrix} \qquad (2.71)$$

$$B = \begin{bmatrix} \alpha V & \alpha U & -\beta UV \\ 0 & 2\alpha V & c^2 - \beta V^2 \\ 0 & 1 & 0 \end{bmatrix} \qquad (2.72)$$

and $c = (gD)^{\frac{1}{2}}$, the speed of gravity waves; $\beta = (\alpha - D\partial_h \alpha)$ and $\underset{\sim}{C}(\underset{\sim}{U})$ contains the lower order terms from the bed friction and bed gradient. Following Garabedian (1964) p 98ff, the system has characteristic curves $\phi(x,y)$ = constant where:

$$\det (A\partial_x \phi + B\partial_y \phi) = 0$$

Setting $\partial_y \phi / \partial_x \phi = -\lambda$ and expanding the determinant we have:

$$(\alpha U - \lambda \alpha V)\left[\lambda^2(c^2 - \beta V^2) + 2\lambda\beta UV + (c^2 - \beta U^2)\right] = 0 \qquad (2.73)$$

Thus $$\lambda = U/V \qquad (2.74)$$

or $$\lambda = \frac{-\beta UV \pm c\left[\beta (U^2 + V^2) - c^2\right]}{(c^2 - \beta V^2)} \qquad (2.75)$$

The roots of this quadratic equation are real if:

$$\beta |\underline{U}|^2 \geq c^2$$

This is the condition for supercritical flow, with the parameter:

$$\nu^2 = \beta |\underline{U}|^2 / c^2 \qquad (2.76)$$

being the two dimensional equivalent of the critical flow number introduced by Price and Samuels (1980) for the one dimensional flow equations. When the velocity distribution coefficient α is set to 1:

$$\nu = |\underline{U}|/(gD)^{\frac{1}{2}} = Fr \qquad (2.77)$$

where Fr is the Froude number of the flow. For supercritical flow the system has three real characteristics one directed along the velocity vector $\underline{U}$ and the other two lying at equal angles Θ on either side of the flow direction where:

$$\Theta = \tan^{-1}\left((\nu^2 - 1)^{\frac{1}{2}}\right) \qquad (2.78)$$

Thus for supercritical flow all three characteristics enter the flow domain on an inflow boundary and none enter on an outflow boundary. Appropriate conditions therefore are to specify data on $\underline{q}$ and h on an inflow boundary and none on an outflow boundary. On the solid boundaries at the side of the flow domain we may specify $\underline{q}.\underline{n}$ to be zero, ie, one boundary condition only.

The case for subcritical flow in which there is only one real characteristic is not so clear cut. When considering compressible aerodynamic flow in which the flow equations are the same as (2.70) with $\alpha = \beta = 1$ and with $\underset{\sim}{C}(\underline{U})$ set to zero Garabedian (1964) reduces the subsonic (or subcritical) case to an elliptic problem by using the Bernoulli equation along streamlines. For this case the appropriate boundary conditions for the stream function are the same as those for friction controlled flow (section 2.6.1). The same approach, however, cannot be used for the more general equation (2.70) since the Bernoulli function now contains an integral of the frictional resistance, the term $\underset{\sim}{C}(\underline{U})$ along the streamline, see Franques

and Yannitell (1974). This, however, is only a technical difficulty as zero order terms should not affect the classification of the equations. The number and location of boundary conditions for these two cases are shown on Figure 2.3.

Although the boundary conditions which guarantee a well posed problem are not known, the numerical calculations were found to be stable with water level prescribed on the inflow and outflow boundaries and the convection term $(\underline{U}.\underline{\nabla})\underline{U}$ set to zero in the elements touching a flow boundary. When combined with a constant water level along each flow boundary this produced zero tangential velocities. Values of water level on the flow boundaries are an appropriate condition for both steady friction controlled flow (section 2.6.1) and for unsteady subcritical flow with convection and friction (section 2.6.3). In all cases specifying as zero the normal component of the depth mean velocity or unit flow vector is appropriate on boundaries across which there is no flow.

2.6.3 Unsteady flow with convection and bed friction

Employing the same solution vector $\underset{\sim}{U} \equiv (q,h)^t$ as in section 2.6.2, we may write the flow equations (2.30) and (2.7) as a first order system thus:

$$I\partial_t \underset{\sim}{U} + A(\underset{\sim}{U})\ \partial_x \underset{\sim}{U} + B(\underset{\sim}{U})\ \partial_y \underset{\sim}{U} + \underset{\sim}{C}(\underset{\sim}{U}) = 0 \qquad (2.79)$$

where I is the identity matrix, A and B are given by (2.65) and (2.66) respectively and $\underset{\sim}{C}$ contains the lower order terms from

the bed friction and bed gradient. Following Garabedian (1964) the system has characteristic surfaces defined by:

$\phi(\underline{x},t) = \text{constant}$

where ϕ is determined by the equation:

$$\det (I\partial_t \phi + A\partial_x \phi + B\partial_y \phi) = 0 \qquad (2.80)$$

The nature of the characteristics implied by the equation (2.80) is discussed in detail in Appendix 1 using methods similar to those of Daubert and Graffe (1967). They identified the characteristics of the shallow water equations, ie the limit in which the velocity distribution coefficient α is unity. The skewed circular bicharacteristic cone found by Daubert and Graffe appears as the appropriate special case ($\alpha = 1$) of the general system (2.79). In practice the distribution coefficient is likely to be close to unity and the shape of the bicharacteristic surface, in loose terms, is a skewed elliptical cone. (In some cases a true ellipse and in others an oval which is not a conic section). For values of α (and its depthwise variation) outside those of practical importance, the bicharacteristic surface has some unusual shapes which are topologically different from a circular cone.

For the near elliptical cases the condition for the bicharacteristic surface to lie wholly within the problem domain, ie for the flow to be supercritical, is identical to that found for steady flow in section 2.6.2. The condition is that the critical flow number of equation (2.76) satisfies $\nu^2 > 1$. The intimate link between the characteristics of the steady and unsteady flow equations can be further illustrated

in the case of supercritical flow and $\alpha = 1$ by considering the normal projection of the skew circular bi-characteristic cone of the unsteady flow equations onto the plane $t = 0$. The extreme generators of the cone, when projected, fall on lines at an angle either side of the x axis given by $\tan^{-1}\left((Fr^2 - 1)^{-\frac{1}{2}}\right)$.
These lines are precisely the characteristics of the steady flow equations, see Fig 2.4.

Daubert and Graffe (1967) discuss the number of boundary conditions that should be applied to the shallow water equations. They show that for subcritical flow two quantities must be specified on an inflow boundary and one on an outflow boundary. For supercritical flow three conditions should be given on an inflow boundary and none on an outflow boundary. Along a boundary across which there is no flow a single condition should be specified. The same arguments hold for the more general equations in this section since the bi-characteristic surface is topologically equivalent to the skew circular cone of Daubert and Graffe. The one condition that changes is the definition of when the flow is sub or supercritical, which in Daubert and Graffe's work depends upon the square of the Froude number equation (2.77), but here depends on the critical flow number v^2.

Having established the number of boundary conditions which must be applied we need to choose those conditions which give a well posed problem. The appropriate conditions for the shallow

water equations have been discussed by Oliger and Sundström (1978) and at greater length by Verboom, Stelling and Officier (1982). The identification of the characteristics of the non-linear system (2.79) ensures the existence of a unique solution to the equations for analytic Cauchy data by expanding the solution as a Taylor series. Considering the flow in a domain over the time $[0, T]$ the initial-boundary value problem for the hyperbolic system (2.79) produced by giving data on Ω at $t = 0$ and on $\partial\Omega \times (0, T)$ yields a Cauchy problem provided that the inflow and outflow boudaries are nowhere characteristic, that is the flow is not exactly critical on these boundaries.

Verboom et al (op.cit) apply the classical energy method to determine what boundary data gives a stable solution of the shallow water equations. They consider the flow equations with the depth mean velocity $\underline{U}$ as a dependent variable instead of the unit flow vector $\underline{q}$. This change of variables should not affect the choice of boundary conditions which provide a well posed problem, neither should the coefficient α for values sufficiently close to 1 (the shallow water case), since the topology of the bi-characteristic surfaces is unaffected. The energy method as applied by Verboom et al provides sufficient conditions for a well posed problem which may in fact not be necessary since the stabilising effect of the non-linear friction losses is ignored. In particular they show that for sub-critical flow the following boundary data are appropriate:

on inflow boundaries - water level and tangential velocity

on outflow boundaries - water level

on solid boundaries - normal velocity.

2.6.4 Higher order terms

Including the turbulent stresses in the model as a diffusive type term (see section 2.3) changes the type of the flow equations. The system represented by equations (2.7) and (2.30) is no longer hyperbolic. Gustafsson and Sundström (1978) describe such systems as incompletely parabolic and they analyse appropriate boundary data. In particular further conditions need to be imposed on the solid boundaries which may describe either no slip or free slip for the tangential component of velocity. The no slip condition gives rise to the formation of a boundary layer in which the tangential component velocity rises from zero at the edge of the flow region to the free stream value. The typical size of such a boundary layer has been discussed in section 2.4.2 above and it will require a mesh of comparable size to resolve it. Vreugdenhil and Wijbenga (1982) found this too restrictive for their practical computation.

2.7 Streamline coordinate system

When the flow is steady the appropriate continuity equation (2.56) implies the existence of a stream function. The flow equations may be written in the curvilinear coordinate system based upon lines of constant stream function and normals to them.

Let (s,n) be the streamwise and normal coordinates and x(s,n) and y(s,n) be the mapping functions from (s,n) to the common cartesian coordinates (x,y). The metric functions for the (s,n) system are:

$$\ell_s = \left[(\partial_s x)^2 + (\partial_s y)^2\right]^{\frac{1}{2}} \tag{2.81}$$

$$\ell_n = \left[(\partial_n x)^2 + (\partial_n y)^2\right]^{\frac{1}{2}} \tag{2.82}$$

Since the (s,n) system is orthogonal we have the relationship:

$$\partial_s x \; \partial_n x + \partial_s y \; \partial_n y = 0 \tag{2.83}$$

For the case of $\alpha = 1$ equations (2.56) and (2.60) become (Rouse 1959):

$$\partial_s(\ell_n q) = 0 \tag{2.84}$$

$$\partial_s(h + U^2/2g) + \ell_s D^2 U^2/k^2 = 0 \tag{2.85}$$

$$-\ell_s^{-1} \partial_n \ell_s (U^2/g) + \partial_n h = 0 \tag{2.86}$$

where $q = UD$ is now the magnitude of the two dimensional unit flow vector $\underline{q}$. The continuity equation (2.84) can be integrated immediately to give:

$\ell_n q$ = constant on a streamline

The components of the convection term are:

stream direction $\partial_s(U^2/2g)$

normal direction $-U^2/gR$.

The radius of curvature R of the streamlines is given by

$R = \ell_s(\partial_n \ell_s)^{-1}$

There does not appear to be any advantage in basing a computational algorithm on these equations since the metric functions (2.81) and (2.82) and the orthogonality condition (2.83) are part of the overall problem as is bed topography in the (s,n) system. However, the simple nature of the convection

term in this coordinate system may be used to check values obtained from actual computations, provided that the radius of curvature of the streamlines can be estimated.

A case where the use of streamline coordinates is helpful is flow round a bend which is an arc of a circle. Consider steady, uniform flow a channel with rectangular cross section forming a 180^0 bend (as represented by Mesh 8 of Appendix 2). If the streamlines around the bend are semi-circles following the channel geometry we may write the flow equations using polar coordinates (r, θ)

$$UD = q(r) \tag{2.88}$$

$$-r^{-1} \partial_\theta h + U^2 D^2 K^{-2} = 0 \tag{2.89}$$

$$\partial_r h - U^2 (gr)^{-1} = 0 \tag{2.90}$$

The depth mean velocity U is a function of r only and the assumption of uniform flow implies $\partial_\theta h$ is a constant. Suppose that the water depth is constant (to first order) across the flow; equation (2.89) reduces to

$$U = C_1 r^{-\frac{1}{2}} \tag{2.91}$$

where C_1 is $K (\partial_\theta h)^{\frac{1}{2}} D^{-1}$. The magnitude of the convection term in equation (2.90) is

$$\left| U^2 (gr)^{-1} \right| = C_2 r^{-2} \tag{2.92}$$

where C_2 is $K^2 \partial_\theta h (gD^2)^{-1}$. The water level difference across the flow is

$$\left[h \right]_{R_i}^{R_o} = C_2 \left[R_i^{-1} - R_o^{-1} \right] \tag{2.93}$$

where R_i is the radius of the inside of the bend and R_o is the

radius of the outside. A second order solution could be produced by including this variation of water level in equation (2.89) and (2.90).

CHAPTER 3

THE STREAM FUNCTION MODEL

3.1 Introduction

The stream function model is based upon the pair of equations:

$$\underline{\nabla} \cdot \{K^{-2} |\underline{\nabla}\psi| \underline{\nabla}\psi\} \tag{3.1}$$

$$\partial_s h + K^{-2} |\underline{\nabla}\psi|^2 \tag{3.2}$$

see section 2.5.1 above.

Equation (3.1) is formed by taking the curl of the steady two dimensional flow dynamic equation to remove the gradient of the water level. It determines the streamline geometry for the given mesh and boundary conditions. Equation (3.2) is merely the trace of the full dynamic equation (2.57) in the direction s of a streamline. Since the conveyance function K in equation (2.31a) depends upon the flow depth (and hence upon surface level) equations (3.1) and (3.2) are solved by successive iteration. The stream function ψ is determined from (3.1) given a water level function h, and h determined from (3.2) given a stream function ψ.

The method outlined above is essentially the same as that proposed by Franques and Yannitell (1974). The principal difference is that in contrast to the work of Franques and Yannitell the Bernoulli equation (3.2) contains no contribution from the convection term. The reason for this is that the equation (3.1) used to define the flow field also omits the

convection term. A consequence of this is that the water level should be constant on an outflow boundary which is normal to the flow direction. One test of the quality of the numerical results is that the water level calculated on each inflow boundary should also be constant.

The stream function formulation was tested for several different mesh geometries, see Table A2.1 in Appendix 2. Much of this chapter discusses the convergence of various iterative methods for generating approximate solutions to equation (3.1) and (3.2). Having obtained methods which converge using an acceptable amount of computation the quality of the numerical results and their physical significance are then discussed.

3.2 The finite element approximation

3.2.1 The basis functions

In the stream function formulation both the stream function itself and the water level are represented by piecewise linear continuous functions based upon the values at the nodes of the mesh. For example the stream function $\psi(x,y)$ is approximated by $\Psi(x,y)$ which is given by:

$$\Psi = \sum \Psi_j \, N_j^e \, (x,y) \qquad (3.3)$$

where the sum runs over all the elements e and $N_j^e\,(x,y)$ are the basis functions. In the computer code the basis functions for

a general triangle have been determined from the area coordinates, thus for the triangle in Fig 3.1,

$$N_i^e(p) = \text{area}(pjk)/\text{area}(ijk) \tag{3.4}$$

Defining the orthogonal unit vectors $(\underline{e}_1, \underline{e}_2, \underline{e}_3)$ with $\underline{e}_3$ pointing out of the plane of the triangle ijk we may define the basis function and its gradient by

$$N_i^e(\underline{x}) = \Delta^{-1}\{\underline{x}\times\underline{x}_j + \underline{x}_k\times\underline{x} + \underline{x}_j\times\underline{x}_k\}\cdot\underline{e}_3 \tag{3.5}$$

$$\underline{\nabla} N_i^e(\underline{x}) = \Delta^{-1}(\underline{x}_j - \underline{x}_k)\times\underline{e}_3 \tag{3.6}$$

$$\text{where } \Delta = (\underline{x}_i\times\underline{x}_j + \underline{x}_j\times\underline{x}_k + \underline{x}_k\times\underline{x}_i)\cdot\underline{e}_3 \tag{3.7}$$

is twice the area of the triangle ijk and $\underline{x}_i$ etc are position vectors from an arbitrary origin.

The use of linear triangles for the basis function has a further consequence of numerical importance: all the streamlines, ie contours of Ψ in a given element, are parallel lines. Thus except in the trivial case that Ψ is a constant in an element we may deduce the following simple observations.

Observation 1

In each triangle there exists a node, k, for which the streamline through that node is contained within the triangle and cuts the opposite side, s, of the triangle internally.

Observation 2

Except in the case that the streamline coincides with a side of the triangle the node in observation 1 is unique.

Observation 3

Each triangle in the mesh falls into one of the following categories, see Fig 3.2:

A : a side of the triangle coincides with a streamline,

B : the side s is downstream of node k,

C : the side s is upstream of node k.

These observations allow a particularly simple streamline integration procedure to be drawn up to approximate the solution of equation (3.2), see section 3.2.4 below.

3.2.2 The bed topography

The channel bed level and flood plain ground level in general slope gently in the downstream direction. At the river bank, however, there is a sharp change in bed level, and one of the early choices to be made in modelling the topography was how to include this characteristic feature. The options were either to model the ground level as continuous as in nature but with a much refined grid in the neighbourhood of the river banks, or to adopt a discontinuous representation of the bed.

The second option was chosen since the grid refinement required for the first option was not practical. The change between flood plain and channel bed levels occurs over a distance of

typically less than one twentieth of the main channel width.

Away from the essential discontinuities across the river banks the ground level may be treated as continuous or discontinuous. The early tests of the stream function model took the ground surface away from the banks to be piecewise linear continuous, using the same basis functions as for the stream function and water level. The only discontinuities lay at the river banks.

The final tests of the stream function model and all tests of the potential formulation used a lower order approximation for ground level: piecewise constant based notionally on the centroid of each triangular element. An advantage of this latter method was that no additional "book-keeping" was required in the course of the calculation since the discontinuity at a river bank was automatically included. The bed topography enters the computation only in the evaluation of the friction losses with a suitable quadrature rule.

3.2.3 Finite element equations for the stream function

The implementation of the stream function method has been based upon the standard (Bubnov -) Galerkin procedure of weighted residuals. This is done using the weak form of equation (3.1).

$$- < \underline{\nabla}.(C_f \underline{\nabla}\psi), \phi > = < C_f \underline{\nabla}\psi, \underline{\nabla}\phi > + \int C_f \phi \partial_n \psi d\Gamma = 0 \qquad (3.8)$$

where ϕ is any C^1 continuous test function, Γ is the boundary to the flow domain Ω, $C_f = K^{-2}|\underline{\nabla}\psi|$ and the inner product

notation $\langle \underline{a}, \underline{b} \rangle$ is defined by $\int\int \underline{a} \cdot \underline{b} \, d\Omega$. Thus given a water level approximation H and choosing ϕ to be one of the basis functions N_j we obtain the following equation for the approximation Ψ to the stream function:

$$< C_f \underline{\nabla}\Psi, \underline{\nabla} N_j > = - \int C_f N_j \partial_n \Psi d\Gamma \quad . \tag{3.9}$$

The boundary of the flow domain may be classified as either:

1. Γ_D on which Dirichlet data are specified for the stream function; the no flow boundaries.

2. Γ_N on which homogeneous Neumann data are specified for the stream function; the inflow and outflow boundaries.

The choice of test functions is restricted to those for which $N_j = 0$ for points on the boundary segments Γ_D, see Strang and Fix (1973) and Zienkiewicz (1977). On the boundary Γ_N we have $\partial_n \phi = 0$ since Γ_N is normal to the flow direction. Hence in all cases the boundary integral in equation (3.9) is identically zero and we have the finite element equations:

$$< C_f \underline{\nabla}\Psi, \underline{\nabla} N_j > = 0 \qquad 1 \leqslant j \leqslant N \qquad j \text{ not on } \Gamma_D \tag{3.10}$$

with the boundary conditions Ψ_k given for k on Γ_D. In the initial version of the stream function method, the coefficient C_f was evaluated from information at the preceding iteration. However, in the final version the value of $|\underline{\nabla}\Psi|$ in C_f was incorporated at the new iteration level.

Suppose the nodal values of stream function at the new

iterative level n+1 are written as:

$$\Psi_j^{n+1} = \Psi_j^n + \xi_j \tag{3.11}$$

and the finite element equations re-written in terms of ξ_j. A quasi-Newton form of equation (3.10) is obtained by expanding to first order in ξ_j thus:

$$\langle K^{-2} |\underline{\nabla}\Psi^n| \underline{\nabla}\xi, \underline{\nabla}N_j \rangle + \mu \langle K^{-2} |\underline{\nabla}\Psi^n|^{-1} \underline{\nabla}\Psi^n . \underline{\nabla}\xi \underline{\nabla}\Psi^n, \underline{\nabla}N_j \rangle$$
$$= - \langle K^{-2} |\underline{\nabla}\Psi^n| \underline{\nabla}N_j \rangle \tag{3.12}$$

The parameter μ controls how the influence of the variation ξ affects the magnitude of the gradient of the stream function. Taking $\mu = 0$ gives the successive substitution algorithm used by Franques and Yannitell (1974) and taking $\mu = 1$ gives a complete first order variation and produces a Newton scheme.

When forming the inner products in equation (3.12) numerical quadrature must be used. For the final version of the stream function model the centroid value was used since all the terms are piecewise constant in each element. The initial tests of the stream function and potential formulations included some trials of different quadrature rules.

The finite element equations are written in the form:

$$a_{ij}\, \xi_i = b_j \tag{3.13}$$

where $a_{ij} = \sum a_{ij}^e$ and $b_j = \sum b_j^e$ for $1 \leqslant e \leqslant$ number of elements. From equation (3.12) for element e we have, using centroid quadrature:

$$a_{ij}^e = A^e K^{-2} \left| \underline{\nabla}\Psi^n \right| \{ \underline{\nabla}N_i \cdot \underline{\nabla}N_j + \mu(\underline{\nabla}\Psi^n \cdot \underline{\nabla}N_i)(\underline{\nabla}\Psi^n \cdot \underline{\nabla}N_j) \left| \nabla\Psi^n \right|^{-2} \} \quad (3.14)$$

$$b_j^e = A^e K^{-2} \left| \nabla\Psi^n \right| \underline{\nabla}\Psi^n \cdot \underline{\nabla}N_j \quad (3.15)$$

In these equations A^e is the area of the element and all terms except K^{-2} are constants by definition. Thus the effect of numerical quadrature was restricted to the function K^{-2}.

The analysis in section 3.4.2 indicates that a more general updating procedure than equation (3.11) should be used to obtain Ψ_j^{n+1} thus:

$$\Psi_j^{n+1} = \Psi_j^n + \lambda\xi_j \quad (3.16)$$

where λ is a relaxation parameter

3.2.4 The stream line integration procedure

The Bernoulli equation (3.2) is used to define the water levels at each node appropriate to a given set of nodal values of stream function. The observations in section 3.2.1 on the streamline geometry allow the implementation of a particularly simple explicit marching procedure, as follows:

1 define water level at nodes on each outflow boundary,

2 examine all the elements connected to the outflow boundary, setting up a stack of integrable elements,

3 if stack is empty, halt,

4 calculate the water level at the upstream node of the integrable element at the top of the stack and remove that element from the stack,

5 examine each element containing the node where the water was defined in step 4 and add it to the stack if it is now integrable,

6 loop back to step 3.

The integrable elements of steps 2 and 5 are those of class B (see Fig 3.2), where the water level is known along the downstream side and unknown at the upstream node, together with those of class A, where the water level is known at the downstream node and at the node not on the streamline but is unknown at the upstream node. In step 4, if the water level is found to be known at all nodes of an element, then the next item on the stack is taken immediately.

We observe that

1 at the end of step 2 the stack must be non-empty if an outflow boundary contains more than one node,

2 the algorithm is finite,

3 the algorithm may not be unique and in that case the ordering of the elements may affect the calculated water levels.

The condition for the algorithm to be unique is that the elements in class A lie along the no flow boundaries of the mesh.

The calculation of water level at the upstream node is based upon a numerical approximation to equation (3.2). Thus:

$$h_u = h_d + \Delta s \left|\underline{\nabla}\Psi\right|^2 K^{-2} \qquad (3.17)$$

where h_u is the unknown water level at the upstream node, h_d is the water level at the point where the stream line intersects the downstream side, and Δs is the length of the segment of streamline within the triangle. The gradient of the stream function is evaluated from the most recent iteration. The conveyance function K is obtained at the centroid of the element and depends upon the unknown level h_u. Hence a Newton method was used on equation (3.17) with the derivative of K wrt h_u being obtained from the appropriate power law approximation, see section 2.2.2.

In the initial tests of the stream function model the Chezy friction law was used, which gives a quartic equation to solve from (3.17). In this case, since the bed topography was piecewise linear, the mean value of K was determined from the two ends of the streamline rather than by taking the element average value at the centroid.

Integrating against the stream direction ensures that the calculation is stable to growth of rounding error. Suppose that h_o is the solution of equation (3.2) and ζ is a perturbation from an error ζ_o at the downstream end s = d of the streamline. We have

$$\partial_s \zeta = (2p\zeta/D_o)\left|\underline{\nabla}\psi\right|^{2K-2} \quad . \tag{3.18}$$

where D_o is the undisturbed depth of flow $(h_o - z_b)$ and p is the power in the relationship

$$K = CD^p \tag{3.19}$$

This equation can be integrated as

$$\zeta(s) = \zeta_o \exp\{-\int_s^d (2pD_o |\underline{\nabla}\psi|^{2K-2})\, ds\} \tag{3.20}$$

We have $1.5 < p < 2$ (see section 2.2.2) and $d > s$ since we are considering s positive in the downstream direction. Hence we see that $\zeta(s) < \zeta_o$ and thus errors decay against the stream direction.

It is possible to interpret the streamline integration procedure as a Petrov-Galerkin finite element method based upon the full dynamic equation:

$$\underline{L}(h) = \underline{\nabla}h + |\underline{\nabla}\psi|^{K-2}\, \underline{\text{curl}}\ \psi = 0 \tag{3.21}$$

Define the weighting friction χ_k^e for an element as follows:

(a) $\chi_k^e = 1$ if e is in class A or class B and k is the upstream node,

(b) $\chi_k^e = 0$ otherwise.

This definition is appropriate to the case where algorithm is unique as defined above. Where this is not the case χ_k^e is taken as 1 in the <u>first</u> element encountered if e lies in class A and the streamline side is not along a mesh boundary. A possible but so far untested alternative is to take $\chi_k^e = \frac{1}{2}$ in the two elements concerned in such a case. The Petrov-Galerkin equivalent of the streamline integration procedure is then:

$$< \underline{L}(h).\ \underline{\text{curl}}\ \psi, \chi_k^e > = 0 \tag{3.22}$$

3.2.5 Numerical quadrature

Most of the computations used centroid quadrature, this being the simplest rule compatible with equation (3.1), see Strang and Fix (1973). However, two other formulae were tested. The 3 point degree 2 rule based upon the area coordinate values (2/3, 1/6, 1/6) with weight 1/3, and the 7 point degree 5 rule of Table 4.1 in Strang and Fix. The table of coefficients in Strang and Fix contains an error for this latter rule. The weight associated with the centroid should be 0.225 exactly, not 0.22503300033000 as indicated in the text: this correction ensures that

$$\sum w_i = 1 \qquad (3.23)$$

where w_i is the weighting value for quadrature point i.

3.3 Software techniques

3.3.1 Introduction

The initial software development and testing was carried out on an ICL 1904S computer. This had a usable storage capacity of about 85k words, equivalent to about 40k single precision real numbers. During the research this computer was replaced with an ICL 2972 which imposes no limitation on program size. The finite element codes have all been written in ANSI (1966)

standard Fortran and have operated successfully on both computers.

The choices made for internal data storage and manipulation were influenced by restricted core space of the ICL 1904S computer and as a result the software should fit easily on many of the current generation of 16 bit micro-computers.

3.3.2 Solution of linear equations

Practical problems in river engineering are likely to lead to meshes with several hundred nodes and variables. To fit this size problem on the 1904S computer, obviously an out of core method of solving the linear equations was required. The frontal technique developed for symmetric systems by Irons (1970) and adapted for non-symmetric systems by Hood (1976) was an obvious choice. Its operation is based upon the finite element philosophy of the gradual assembly of the system of linear equations and is particularly suited to 2D problems where the mesh has significantly more nodes in one direction than the other. This is typically the case for river models where the length of the reach of a river valley being studied is usually several times the width of the valley. Appendix 3 describes some modifications made to Hood's code.

3.3.3 Boundary data

In the final version of the code the mesh boundary is divided

into a number of segments where Dirichlet or Neumann data are imposed. The program examines the mesh in order to pick up the element edges along the boundaries. These elements do not share a common side with any other element. The user need only supply the nodes which divide the following different boundary types:

1. no flow - stream function specified
2. outflow - water level specified
3. inflow - no data given.

The code checks that all the boundary has been classified, warns if the mesh represents a multiply connected region, and checks that the boundary data are consistent. This last test includes a check on the values of the stream function at the limits of the flow boundaries to ensure that the data in fact gives inflow or outflow as appropriate.

3.3.4 Initialization

The iterative algorithm using equation (3.12) requires some initial values for $|\underline{\nabla}\Psi|$ and for the conveyance function K. The most important feature was found to be that of providing reasonable estimates for the conveyance K, since this has a significantly different value in the main channel from that typical for the flood plain. The value $|\underline{\nabla}\Psi|$ was set to unity in all elements for the initial iteration and the conveyance function calculated from the friction law together with an estimated depth at the centroid of each element. This depth was calculated from the water depths specified along the outflow

boundaries taking account of the various regions of the mesh defined riverbanks and the mesh boundary.

3.3.5 Convergence criteria

The convergence rate is of prime importance in determining whether the method is of use for practical calculations. As there are no known analytic solutions to the flow equations except for trivial geometries, the convergence criteria have been based on monitoring the relative change in properties of the solution as the iteration progresses. The measures of convergence adopted may be written in the form:

$$\varepsilon_f^n = \max_{1 \leq j \leq M} \{2|f_j^{n+1} - f_j^n| / |f_j^{n+1} + f_j^n|\} \qquad (3.25)$$

Here ε_f^n is the convergence parameter for the n-th iteration of the function f. The limit M of the range of j is the number of nodes if f is based at nodes (eg stream function) or the number of elements if f is based on elements (eg depth at centroid or velocity).

From the definition of ε_f^n we may deduce the following properties:

(a) if the sequence $\{f_j^n\}$ diverges at some value of j then $\varepsilon_f^n \to 2$,

(b) if the sequence $\{f_j^n\}$ oscillates between two values at some value of j then $\varepsilon_f^n = \varepsilon_f^{n-1}$,

(c) if the sequence $\{f_j^n\}$ converges to a limit $\{f_j^*\}$ at all

values of j then $\varepsilon_f^n \to 0$.

For the stream function formulation the convergence parameters were calculated for the values of stream function and depth at the nodes. The convergence parameter for depth was calculated only in the element used to define the water level at the node in question during the stream line integration procedure.

3.4 Performance and analysis of the iterative methods

3.4.1 Introduction

The tests described in this section were all based upon meshes derived from Sooky's (1964) flume geometry, see meshes 1 and 4 in Appendix 2. The analysis here concerns only the convergence rate of the iterative method for the finite element equations and not the convergence of the finite element solution to a solution of the differential equations as the element size is reduced. In engineering practice the mean element size is likely to be determined more by the topography of the prototype and the computing resources available than by the convergence properties of the method as the mesh size is reduced.

The initial use of the stream function formulation involved the successive substitution algorithm of Franques an Yannitell (1974) and the development of the two parameter updating algorithm. These tests were based upon the geometry of mesh 1

and a piecewise linear approximation to the ground level with discontinuities at the boundaries between the channel and the flood plain. The tests assumed Chezy's friction law and the first test included the convection term in the streamline integration.

The second phase of the work used the more general form of the finite element equations (3.12) to (3.15). The bed geometry for these tests was piecewise constant in each element with significantly larger discontinuities at the boundary between channel and flood plain than elsewhere. Tests of the potential formulation were also based on this description of the geometry see chapter 4.

3.4.2 Successive substitution algorithms

These algorithms are based upon taking the parameter μ in equation (3.12) as zero. They may be written as approximations to solutions of:

$$\underline{\nabla}\cdot\{(K(h^n))^{-2}|\underline{\nabla}\psi^n|\underline{\nabla}(\psi^n+\zeta)\} = 0 \qquad (3.26)$$

$$\psi^{n+1} = \psi^n + \lambda\zeta \qquad (3.27)$$

$$h^{n+1} = I(\psi^{n+1}) \qquad (3.28)$$

where the superscripts n, n+1 denote the iteration levels, λ is a relaxation parameter and I( ) represents the streamline integration procedure laid out in section 3.2.4. Taking λ as 1 we obtain the algorithm published by Franques and Yannitell. This had a poor convergence rate in all tests of the method.

TABLE 3.1

CONVERGENCE PARAMETERS FOR FRANQUES AND YANNITELL'S METHOD

	Test 1 With Initial Model		Test 2 With Final Model	
Iteration	Stream Function	Depth	Stream Function	Depth
1	0.182	0.0229	1.40	0.304
2	0.177	0.0217	1.29	0.257
3	0.171	0.0202	1.26	0.172
4	0.163	0.0179	1.13	0.126
5	0.156	0.0177	1.09	0.0963
6	0.149	0.0161	0.952	0.110
7	0.143	0.0158	0.907	0.0847
8	0.136	0.0142	0.787	0.0934
9	0.130	0.0148	0.714	0.0754
10	0.124	0.0141	-	-
average rate	0.96	0.95	0.92	0.84
asymptotic rate	0.96	0.97	0.90	0.94

Note: The average convergence rate shown has been calculated from all the iterations. The asymptotic rate is for the last four only.

The convergence parameter, ε, for stream function and depth at the nodes both satisfied the approximate relationship:

$$\varepsilon^{n+1} = r^n \varepsilon^1$$

The convergence rate r for stream function lay between 0.9 and 0.97 indicating that at least 20 interactions would be required to achieve each decimal digit of precision. The convergence parameter for the stream function was always an order of magnitude larger than that for the water depth, see Table 3.1.

That the convergence rate was near 1 suggested that the values of the solution were oscillating and this was confirmed by plotting the values of stream function at two nodes either side of a bank against one another, see Fig 3.3. Thus the flow was tipping between the channel and flood plain.

The performance of the iteration method can be analysed approximately assuming that the conveyance function K is constant. Hence we consider the model equation:

$$\underline{\nabla} \cdot \{ |\underline{\nabla}\psi| \underline{\nabla}\psi \} = 0 \qquad (3.29)$$

and suppose that the Galerkin equations have a solution $\{\Psi_j^*\}$ of nodal values. That is, for all test functions N_j,

$$\langle |\underline{\nabla} N_k \Psi_k^*| \underline{\nabla} N_i \Psi_i^*, \underline{\nabla} N_j \rangle = 0 \qquad (3.30)$$

where we have used summation convention on repeated suffices.

Now let the nth iterate Ψ_k^n for Ψ_k^* be:

$$\Psi_k^n = \Psi_k^* + E_k^n \tag{3.31}$$

where E_k^n is the nodal error. The weak form of equation (3.26) for the updating function ξ then becomes:

$$\langle | \underline{\nabla} N_k (\Psi_k^* + E_k^n) | \underline{\nabla} N_i (\Psi_i^* + E_i^n + \xi_i), \underline{\nabla} N_j \rangle = 0 \tag{3.32}$$

Expanding to first order only in terms of $\underline{E}_k^n$ and ξ_i we have:

$$\langle | \underline{\nabla} N_k \Psi_k^* | \underline{\nabla} N_i \xi_i, \underline{\nabla} N_j \rangle = - \langle | \underline{\nabla} N_k \Psi_k^* | \underline{\nabla} N_i E_i^n, \underline{\nabla} N_j \rangle \tag{3.33}$$
$$- \langle | \underline{\nabla} N_k \Psi_k^* |^{-1} (\underline{\nabla} N_k \Psi_k^* \cdot \underline{\nabla} N_i E_i^n) \underline{\nabla} N_k \Psi_k^*, \underline{\nabla} N_j \rangle + (\text{2nd order terms}) \quad .$$

To simplify equation (3.33) further we recall that $\underline{\nabla} N_k$ is constant in each element and that all the inner products are evaluated using centroid quadrature. In each element e we can write:

$$\underline{\nabla} E^n = F_e^n \, \underline{e}_s + G_e^n \, \underline{e}_t \tag{3.34}$$

where the orthogonal unit vectors $\underline{e}_s$ and $\underline{e}_t$ are in the directions of the approximate streamline and $\underline{\nabla} \Psi^*$ respectively. Thus the two inner products at the right hand side of (3.33) can be combined and written as:

$$- \sum_e \langle | \nabla \Psi_e^* | \{ 2G_e^n \, \underline{e}_t + F_e^n \, \underline{e}_s \}, \underline{\nabla} N_j \rangle \tag{3.35}$$

Using the updating procedure (3.27) we deduce that E^{n+1}

satisfies the following Galerkin equations (to first order).

$$\sum_e \langle | \nabla \Psi_e^* | \underline{\nabla} E^{n+1}, \underline{\nabla} N_j \rangle =$$

$$\sum_e \langle | \nabla \Psi_e^* | \{(1-2\lambda) G_e^n \underline{e}_t + (1-\lambda) F_e^n \underline{e}_s\}, \underline{\nabla} N_j \rangle \qquad (3.36)$$

By examining the form of equation (3.36) we see that the finite element equations for $\underline{\nabla} E^{n+1}$ will produce the weighted best fit for

$$(1-2\lambda) G_e^n \underline{e}_t + (1-\lambda) F_e^n \underline{e}_s \qquad (3.37)$$

However, the piecewise constant function represented by (3.37) does not in general lie in the image under grad of the piecewise linear approximation space used for the stream function.

Suppose the error E^n is such that $G_e^n >> F_e^n$ in a patch of elements, ie the stream direction is correct but the unit flows are inaccurate. In this case we would expect

$$G^{n+1} \simeq (1-2\lambda) G^n \qquad (3.38)$$

and hence if $\lambda = 1$, as suggested by Franques and Yannitell, we have $G^{n+1} \simeq - G^n$ and thus the successive iterates oscillate about the true solution. This explains the behaviour exhibited in the early tests and demonstrated by Fig 3.3. If, however, $G_e^n << F_e^n$ we might take $\lambda = 1$ and

$$F_e^{n+1} \simeq (1-\lambda) F_e^n, \qquad (3.39)$$

that is the error in the stream direction is eliminated.

Suppose now $\lambda = \frac{1}{2}$ then, from equation (3.38), we see that the error in the cross stream error is likely to be eliminated, should this dominate. However, from equation (3.39) the error in the stream direction is only halved where it is dominant. This suggests that for $\lambda = \frac{1}{2}$ the convergence rate r should be approximately 0.5.

The observation that the streamwise error is approximately eliminated by $\lambda = 1$ and the cross stream direction error eliminated by $\lambda = \frac{1}{2}$ suggests that an iterative method based upon taking the relaxation parameter as $\lambda = \frac{1}{2}$, $\lambda = 1$ in alternate iterations should out-perform the algorithm obtained by taking either of these values for all iterations.

Several tests were carried out which confirm the main points of the analysis above. These tests are summarized in Table 3.2 (along with others) and the convergence parameters given in Tables 3.3 and 3.4.

The convergence rates obtained in all these tests are a marked improvement upon the performance of the Franques-Yannitell iteration procedure (see Table 3.1). The asymptotic rates indicate the performance of the schemes after differences in the initialization have been removed, and lie mostly in the range 0.39 to 0.32. Thus approximately one digit of precision is obtained for every two iterations. The rates have been based upon the number of iterations for the stream function, since the calculation of water levels is explicit and does not require the solution of any sets of linear equations.

TABLE 3.2

TESTS OF THE STREAM FUNCTION FORMULATION

Test	Model	Mesh	Relaxation parameters λ		Gradient parameter μ	Iterations For Stream Function	Results Table
1	Initial	1	1.0	1.0	0.0	1	3.1
2	Final	4	1.0	1.0	0.0	1	3.1
3	Initial	1	0.5	0.5	0.0	1	3.3
4	Initial	1	0.5	1.0	0.0	1	3.3
5	Initial	1	0.5	1.0	0.0	2	3.3
6	Final	4	0.5	1.0	0.0	1	3.4
7	Final	4	0.5	1.0	0.0	2	3.4
8	Final	4	1.0	1.0	1.0	1	3.5
9	Final	4	1.0	1.0	1.0	2	3.5

Note: The differences between the initial and final models are described in section 3.4.1.

TABLE 3.3

CONVERGENCE PARAMETERS FOR TESTS 3, 4 AND 5 WITH THE INITIAL MODEL

Iterations for Stream Function	Test 3		Test 4		Test 5	
	Stream Function	Water Level	Stream Function	Water Level	Stream Function	Water Level
1	4.84(-1)	1.12(-1)	4.61(-1)	9.74(-1)	4.61(-1)	-
2	1.06(-1)	1.21(-2)	7.47(-2)	5.64(-3)	*8.51(-2)	9.41(-2)
3	1.53(-2)	3.47(-3)	2.46(-2)	2.16(-3)	8.77(-2)	-
4	3.84(-3)	1.36(-3)	5.73(-3)	3.56(-4)	*1.11(-2)	7.89(-3)
5	1.41(-3)	5.71(-4)	1.75(-3)	1.52(-4)	4.00(-3)	-
6	5.10(-4)	2.31(-4)	4.61(-4)	2.27(-5)	*4.19(-4)	4.18(-4)
7	1.90(-4)	9.16(-5)	1.47(-4)	1.02(-5)	3.81(-4)	-
8	7.27(-5)	3.60(-5)	4.58(-5)	1.86(-6)	*6.65(-5)	3.03(-5)
9	2.82(-5)	1.40(-5)	1.15(-5)	6.32(-7)	2.59(-5)	-
10	1.10(-5)	5.46(-6)	4.78(-6)	2.42(-7)	*6.86(-6)	1.40(-6)
11	4.34(-6)	2.12(-6)	1.30(-6)	6.40(-8)	3.27(-6)	-
12	1.72(-6)	8.62(-7)	4.68(-7)	2.91(-8)	*9.17(-7)	1.20(-7)
average rate	0.32	0.34	0.29	0.26	0.31	0.26
asymptotic rate	0.39	0.39	0.32	0.35	0.34	0.25

Notes: (a) $1.72(-6) = 1.72 \times 10^{-6}$

(b) the averate rates have all been based upon the number of iterations for stream function which is a measure of work involved

(c) * denotes change from previous iteration without a recalculation of water level.

TABLE 3.4

CONVERGENCE PARAMETERS FOR TESTS 6 AND 7 WITH THE FINAL MODEL

Iteration For Stream Function	Test 6 Stream Function	Test 6 Water Depth	Test 7 Stream Function	Test 7 Water Depth
1	2.15(0)	1.49(-1)	2.15(0)	-
2	2.44(-1)	3.16(-2)	*1.87(-1)	1.27(-1)
3	1.53(-1)	1.19(-2)	3.78(-1)	-
4	3.46(-2)	4.15(-3)	*1.57(-2)	3.38(-2)
5	2.42(-2)	1.65(-3)	6.10(-2)	-
6	3.77(-3)	3.96(-4)	*1.21(-3)	5.14(-3)
7	2.72(-3)	1.75(-4)	8.77(-3)	-
8	3.93(-4)	3.21(-5)	*4.28(-4)	7.29(-4)
9	2.96(-4)	1.73(-5)	1.08(-3)	-
10	-	-	*4.07(-5)	9.93(-5)
Average rate	0.33	0.32	0.41	0.41
Asymptotic rate	0.33	0.32	0.36	0.37

Notes: (a) all sites based upon numbers of iterations for stream function

(b) * denotes changes from the previous iteration of stream function without a recalculation of water levels.

Comparing the asymptotic rates achieved for tests 3 and 4 ($\lambda = \frac{1}{2}$ and $\lambda = \frac{1}{2}$, 1 alternately) the two parameter algorithm seems to offer a small advantage in its speed of convergence. In tests 5 and 7 two iterations of stream function were carried out for each iteration of water level, the reasoning behind this being that since the proportionate changes in water depth were in general somewhat smaller than the changes in stream function, the total effort might be reduced by obtaining these more accurate values of stream function. Although the convergence rates obtained in test 5 are comparable with those for test 4 with the initial model, the rates obtained in test 7 seem inferior to those of test 6 with the final model. These results indicate that the two parameter algorithms $\lambda = 0.5$, $\lambda = 1$, in alternate iterations, for the stream function is probably the best of the successive substitution methods. There is no clear advantage in not re-evaluating water levels each time the stream function is updated. The method takes about 12 or 13 iterations to achieve an accuracy of 1 part in 10^6. Having obtained a solution for the numerical model of the flow it is reasonable then to look at the relationship between the model results and what is observed in the prototype. This is done in section 3.4.4 below.

3.4.3 First order variation method

The idea of the first order variation method came from work on

the potential formulation discussed in chapters 4 and 5 below. The method includes to first order the change in $|\underline{\nabla}\Psi|$ at the new iteration level. The Galerkin equations for the method are given by equations (3.12) to (3.15) taking the gradient parameter μ as 1.0.

Tests were done with the final version of the model only on the geometry of mesh 4 with the ground (or bed) being a piecewise constant function. Table 3.5 gives the convergence parameters for two tests of the method. In the first of these tests, (number 8 of Table 3.3), the water level was recalculated after each iteration for the stream function. In the other test two iterations of stream function were done before the water levels were recalculated.

The results clearly show that, for the flume geometry used, the parameters for test 8 give the optimum performance in terms of convergence rate. Convergence to machine precision (6 decimal digits) occurred in about 6 to 7 iterations. The fact that the changes to water levels made for each invocation of the stream line integration procedure were nearly the same in tests 8 and 9 indicates that the extra iteration for stream function in test 9 produced no benefit. It is interesting to note that the additional (even) iteration for stream function in test 9 produced changes of the order of the square of the preceding (odd) iteration (of the starred and unstarred values in Table 3.6). This indicates that in the absence of changes to water level (and hence the conveyance function K) the first order variation method achieves an almost quadratic convergence.

TABLE 3.5

CONVERGENCE PARAMETERS FOR FIRST ORDER VARIATION METHOD

Iteration For Stream Function	Test 8 Stream Function	Test 8 Water Depth	Test 9 Stream Function	Test 9 Water Depth
1	1.07(0)	1.48(-1)	1.07(0)	-
2	1.38(-1)	1.63(-2)	*9.01(-2)	1.38(-1)
3	1.25(-2)	1.71(-3)	1.67(-1)	-
4	1.44(-3)	1.77(-4)	*5.53(-3)	2.50(-2)
5	2.14(-4)	2.34(-5)	2.35(-2)	-
6	2.73(-5)	2.89(-6)	*1.17(-4)	3.31(-3)
7	3.10(-6)	1.65(-6)	3.06(-3)	-
8	Converged to machine		*2.39(-6)	4.01(-4)
9	precision	-	3.66(-4)	-
10	-	-	*1.40(-6)	4.16(-5)
11	-	-	3.78(-5)	-
12	-	-	*7.03(-7)	4.12(-6)
Average rate for iterations	0.12 1 to 7	0.11 1 to 6	0.36 1 to 11	0.35 2 to 12

Notes: * denotes changes from the previous iteration of stream function without a recalculation of water levels.

3.4.4 Comparison with the prototype

In this section we consider the relationship between the numerical solution for meshes 1 and 4, with the stream function formulation, and Sooky's (1964) experimental results (Geometry 4) upon which the meshes were based. The meshes have an identical description of the geometry of a single meander wave, apart from the areas affected by making the mesh regular (see Appendix 2). No tests have been done to look at the convergence (in space) as the characteristic mesh dimension is reduced. In engineering practice the quality of the fit between the model and the prototype will depend upon the availability of calibration data, and the calibration process will result in roughness values (and possibly other physical parameters included in the model) which match the simulations to the prototype. The very process of calibration will implicitly include many phenomena such as:

1. physical processes not included in the mathematical model,
2. numerical errors such as:
   (a) truncation error
   (b) rounding error
   (c) quadrature error,
3. approximation to natural geometry.

The stream function formulation is based upon the assumption that in the dynamics of the flow the bed friction is dominant.

Hence certain aspects of Sooky's observations cannot be reproduced. These include:

1. the boundary layer at the edge of the flume,
2. secondary flow cells in the main channel,
3. water level variations due to the centripetal force around the meanders,
4. the shear layer between the channel and the flood plain.

Sooky's thesis (1964) contains detailed measurements of the flow structure with depth. However, in Table 11 he presents an integration throughout the depth giving the discharge in various sub-sections of the flume at various locations. Table 3.6 presents a comparison of Sooky's experimental results with the simulations in tests 4 and 8 (with the initial and final models respectively). No attempt was made to calibrate the computational model against the flume experiments. In test 4 the discharge was $0.00814 m^3/s$ (0.29cfs), the Chezy roughness coefficient C was set to 38.35 and the water level was horizontal on the outflow boundary. In test 8 the discharge was $0.01017 m^3/s$ (0.36cfs), a roughness size (k_s) of 3.6mm was used in the Colebrook-White equation and the water level was horizontal on the outlow boundary. (These discharge and roughness figures take account of the linear scaling factor of 100 applied to Mesh 4, see Appendix 2.) In Sooky's test the discharge was 0.28cfs and Sooky quotes a Manning value of 0.017 as being appropriate. The downstream depths in the computations were set to the mean value obtained by Sooky.

TABLE 3.6

COMPARISON OF DISCHARGE DISTRIBUTION

Value X/L from Sooky	Test	Position	Percentage of Flow Left	Main Channel	Right
0.5	Sooky	Meander crosses	27.2	44.9	27.9
	4	the centre	25.2	49.4	25.4
		line of			
	8	the flume	23.0	53.6	23.4
0.598	Sooky	Meander moving	22.1	43.8	34.2
	4	to left	22.2	49.5	28.3
	8	hand edge	20.5	53.6	25.9
0.75	Sooky	Meander at left hand edge	18.9	44.3	37.9
	4	Downstream end	19.6	47.7	32.7
	4	*Centre	19.5	48.0	32.5
	4	Upstream end	19.4	48.4	32.2
	8	Downstream end	18.2	52.7	29.1
	8	*Centre	17.8	52.2	30.0
	8	Upstream end	18.3	52.7	29.0
-	8	d/s limit	18.6	53.0	28.4
-	8	u/s limit	18.6	53.0	28.4

Note: * denotes left and right hand values transposed to facilitate comparison.

The computations and experiment agree in the overall picture; the flow is concentrated in the main channel and the main channel discharge remains more or less constant along the length of the meander. The calculations, however, do not give the same split of discharge between the channel and flood plain sub-sections as observed in Sooky's flume. In Sooky's experiment the channel accounted for 44 to 45% of the total flow, whereas in test 4 with the initial model it carried 48 to 50% and in test 8 this increased to 52 to 54%. The differences between tests 4 and 8 can be attributed to the difference in the roughness laws. For a constant value of k_s, the value of Chezy C should be higher in the deeper part of the flow. The differences between the calculation and experiment however are significant, as in test 8 the main channel carried 20% more discharge than observed, and the most likely cause of this difference is the inability of the mathematical model to represent the shear layers at the boundary between the main channel and flood plain and at the edge of the flood plain. This is discussed in section 2.4.2 above and by Vreugdenhil and Wijbenga (1982) who predict changes of this order of magnitude attributable to the treatment of the shear layer.

A second check on the quality of the model results is the water level variation predicted at the upstream boundary. The water level should be horizontal since this boundary is normal to the flow direction. In both tests 4 and 8 a variation of level was produced on the boundary. In test 4 the variation was approximately 0.07% of the depth of flow in the channel and in

test 8 it was 0.1% of the depth of flow in the main channel. Fig 3.4 shows the water level variation on the upstream boundary from test 8.

3.5 Tests with the Tallahala Creek data

Having concluded that the first order variation method provided a satisfactory solution procedure for the meandering river channel type of geometry, the final version of the model was tested on the Tallahala Creek data from Tseng (1975). This presents a different type of geometric irregularity in that the data contains no specific representation of a river channel but the lateral (solid) boundaries of the flow domain show a severe constriction at the embankment leading to a clear span road bridge, see Fig A2.6. Tseng's report includes values for the Chezy roughness coefficient, the ground level and the boundary conditions on water level and discharge.

The results of the computations were disappointing in that the convergence rate of the iterative method was poor and that the end solution was unacceptable. In all, three tests were done and the same general performance was obtained in each, see Table 3.7 and Fig 3.5. In test 1 the first order variation method was used, see section 3.4.3. Test 2 used the two parameter updating method with parameters 0.5 and 1.0 being used in alternate iterations, see section 3.4.2. In test 3 the first order variation method was again used but the streamline integration procedure was modified. Tests 1 and 2 achieved in

TABLE 3.7

CONVERGENCE PARAMETERS FOR TESTS WITH MESH FOR TALLAHALA CREEK

	Test 1		Test 2		Test 3	
Iteration Number	Stream Function	Water Level	Stream Function	Water Level	Stream Function	Water Level
1	3.50(-1)	1.20(-1)	6.29(-1)	1.23(-1)	3.17(-1)	1.32(-1)
2	9.21(-2)	8.61(-2)	1.86(-1)	1.79(-1)	6.68(-2)	5.69(-2)
3	4.40(-2)	4.48(-2)	6.83(-2)	1.33(-2)	2.01(-2)	2.56(-2)
4	2.29(-2)	1.83(-2)	1.79(-2)	1.46(-2)	7.91(-3)	9.79(-2)
5	1.34(-2)	6.70(-3)	2.10(-2)	2.82(-3)	3.77(-3)	3.76(-3)
6	5.43(-3)	2.60(-3)	6.98(-3)	1.24(-2)	2.52(-3)	1.52(-3)
7	2.31(-3)	1.32(-2)	1.08(-2)	1.21(-2)	1.40(-3)	6.49(-4)
8	3.27(-3)	1.25(-2)	5.12(-3)	1.19(-2)	6.83(-4)	2.95(-4)
9	3.63(-3)	1.25(-2)	9.99(-3)	1.19(-2)	3.05(-4)	1.27(-4)

practice the same convergence rate (see Table 3.7) and the water level profile on the upstream boundary was identical when plotted (see Fig 3.8). This suggested that the problem lay in the calculation algorithm for water level. The water level on the upstream boundary should of course be horizontal since the flow is assumed normal to the mesh boundary. Possible deficiencies of the streamline integration procedure of section 3.2.4 are that it is only based upon about half of the elements in the mesh (all those in class C, Fig 3.2, are excluded) and that it does not define the cross-stream gradient of water level. Test 3 included an allowance for the direction of the gradient of the water surface and was again based upon the first order variation method for stream function. The equation used for integration in each element was:

$$(1-\eta) < \underline{L}(h).\ \underline{\mathrm{curl}}\,\phi,\ \chi_k > + \eta < \underline{\nabla}h.\underline{\nabla}\phi,\ \chi_k > = 0 \qquad (3.40)$$

The first term in equation (3.40) is identical (except for the pre-multiplier) to the left hand side of equation (3.22) in section 3.2.4. The second term, with the penalty parameter η, expresses the condition that the surface gradient should be normal to the gradient of the stream function. The original algorithm corresponds to taking η as 0.0: in a test with $\eta \simeq 1$ the calculation procedure failed with negative water depths. In test 3 η was set to 0.1. The convergence rate improved from tests 1 and 2, see Table 3.7 and the distribution of water levels on the inflow boundary changed, see Fig 3.5. The transverse water surface slopes, however, were still of the

same order as the streamwise water surface slope which is not acceptable. The cause for this poor performance of the method has not been identified but is probably related to the large changes of gradient of stream function around the contracted and the selective nature of the stream line integration procedure discussed above.

3.6 Concluding remarks

This chapter has considered the application of the stream function formulation to two test problems. The first of these related to the experimental work of Sooky (1964) and the numerical method achieved a satisfactory performance. The second problem was based upon a field application from Tseng (1975) and here the stream function model performed badly. The area where the method needs to be improved most is probably in the streamline integration procedure. The model produces a water level variation on the upstream boundary which is normal to the stream direction, and hence a line on which water level should be horizontal. The inclusion of an orthogonality condition via a penalty parameter in the streamline integration procedure equation (3.40) did not solve the problem. Further work is required on this topic before the method can be used in engineering practice.

The stream function formulation tested was based upon the lowest order of approximation possible: piecewise linear basis functions. The use of higher order approximations should

improve the description of the flow field but at the cost of more computational effort and possibly more rigorous topographic data requirements. The stream function formulation cannot include the diffusion or convection terms in the flow equations without using C^1 inter-element continuity. The use of such elements is known to pose difficulties particularly where the material properties - in our case conveyance K - is discontinuous between elements, see Zienkiewicz (1977) chapter 10. The use of higher order elements for the stream function will complicate the streamline integration procedure. The division of these elements into the three classes of section 3.2.1 will not be possible, since the streamlines will not in general be straight lines and hence the streamline through a node may intersect one of the sides connected to that node. This will produce an algorithm that will link the water level at several nodes and so will not be solvable by the simple marching algorithm. This will be computationally more complex and expensive but so would any algorithm based upon the linear triangular elements which includes those elements in class C in determining the water levels.

CHAPTER 4

USING THE PRIMITIVE VARIABLES

4.1 Introduction

In this chapter we examine two possible formulations of the steady friction controlled flow equations in terms of the primitive variables. These are the unit flow vector $\underline{q}$ and the water surface level h. The flow equations themselves are discussed in Chapter 2 and some general material in Chapter 3 is pertinent, specifically the remarks on basis functions, bed approximations and numerical quadrature in Section 3.2 and the software techniques in Section 3.3.

The two methods both achieve a reduction of the order of the system of linear equations to be solved. First we discuss the use of approximately divergence free spaces for the trial functions, see Temam (1977) and Griffiths (1977). The second approach is to use the potential formulation in which the unit flow vector is eliminated from the model equations by formal manipulation.

4.2 Approximately Divergence Free Elements

4.2.1 Introduction

Here we demonstrate the failure of Temam's approximation APX5 for the flood plain flow equations, which produces satisfactory

results for the Navier Stokes (NS) equations. The approximation for the unit flow vector is non-conforming being spanned by piecewise linear discontinuous basis functions, see Fig 4.1. The use of the method is covered neither by the analysis of Temam (1977) for the NS equations nor by the work of Girault and Raviart (1979). Temam considers both the Stokes and the NS equations but in each case the physical dissipation is related to $\underline{\nabla}^2 \underline{u}$ whereas for flood plain flow the dissipation is of a lower order i.e. $\underline{q}|\underline{q}|$, and requires different boundary data. An appropriate linear model for the flood plain flow equations is a mixed method for the Laplace equation. Girault and Raviart discuss mixed methods for the Laplace equation but their analysis is restricted to conforming approximations. The approximation APX5 is the lowest order scheme that Temam shows can be applied to the NS equations. Including the convection and turbulent stress terms in the flood plain flow equations leads to a system similar to the NS equations and this motivated the study of Temam's approximation APX5 of the more simple case of friction controlled flow.

4.2.2 Approximation spaces

The key idea in this approach is that instead of searching for $\underline{q}$ in domain of over the whole product space $H_E^1(\Omega) \times H_E^1(\Omega)$ the choice is restricted to the divergence free subspace $D(\Omega)$ defined by

$$D(\Omega) = \{ \underline{q} \text{ in } H_E^1(\Omega) \times H_E^1(\Omega) \text{ with } \underline{\nabla}.\underline{q} = 0 \} \qquad (4.1)$$

Here the suffix E denotes functions which satisfy any Dirichlet

boundary data given. Following Griffiths (1977) we may characterise the approximation to $D(\Omega)$ by values of the tangential component at the mid-point of each element side, together with a stream function based upon the vertices to give the normal component at the mid side nodes. The basis function for a midside node χ_i and the area coordinate N_v for the opposite vertex are related by

$$\chi_i = 1 - 2N_v, \tag{4.2}$$

see Fig 5.1. The divergence free condition is satisfied weakly, in the sense that in each element we have

$$< \underline{\nabla}.\underline{Q}, \ \phi_e > = 0 \tag{4.3}$$

Here $\underline{Q}$ is described by the stream function and tangential components as above, and ϕ_e is the piecewise constant basis function used in the approximation for water level in the element.

4.2.3 Application to the Laplace equation

Taking the equations of friction controlled flow and setting $|\underline{q}|/K^2$ to 1 we have:

$$\underline{\nabla}.\underline{q} = 0 \tag{4.4}$$

$$\underline{q} + \underline{\nabla}h = 0 \tag{4.5}$$

which imply a Laplace equation for the water level h. Appropriate data are

$$\underline{q}.\underline{n} = 0 \tag{4.6a}$$

$$h = \text{constant} \tag{4.6b}$$

On no flow and normal flow boundaries respectively. We introduce a weak form of (4.4) and (4.5), thus

$$< \underline{\nabla}.\underline{q}, \ \phi > = 0 \tag{4.7}$$

$$< \underline{q},\ \underline{\psi} > + < \underline{\nabla} h,\ \underline{\psi} > = 0 \qquad (4.8)$$

Using Green's theorem for suitably smooth $\underline{\psi}$ equation (4.8) becomes

$$< \underline{q},\ \underline{\psi} > + \int_{\Gamma} (h\ \underline{\psi} \cdot \underline{n})\ d\Gamma = < \underline{\nabla} \cdot \underline{\psi},\ h > \qquad (4.9)$$

where Γ is the boundary of the domain. If now we restrict $\underline{q}$ and $\underline{\psi}$ to $D(\Omega)$, equation (4.7) is satisfied by definition and the right hand side of equation (4.9) is zero.

The Galerkin equations based upon (4.9) are therefore

$$< Q_k\ \underline{\chi}_k,\ \underline{\chi}_j > = - \int_{\Gamma} (H_e \phi_e\ \underline{\chi}_j \cdot \underline{n})\ d\Gamma \qquad (4.10)$$

Here $\underline{Q} = Q_k\ \underline{\chi}_k$ and $H = H_e \phi_e$ (with summation convention on k and e) and j ranges over the basis functions where Dirichlet data are not supplied. The direction of $\underline{\chi}_k$ is that of the unit vector associated with Q_k, ie the unit normal or tangent vectors at the mid-sides of the triangle. We note that if the $\underline{\chi}_j$ were to provide a conforming approximation, then the right hand side of equation (4.10) would be zero.

Now consider the mesh shown in Fig 4.2 with two right triangles joined to form a unit square. We apply boundary data consistent with $\underline{Q} = (1,0)$ to the Galerkin system (4.10);

Stream function	= 1 vertices 1 and 2
	= 0 vertices 3 and 4
Tangential velocity	= 1 mid-side nodes 5 and 7
	= 0 mid-side nodes 6 and 8

The sole variable not specified by this boundary data is the tangential velocity at the interior mid-side node 9 which should have magnitude $1/\sqrt{2}$. The sole Galerkin equation is

$$Q_9 \; < \underline{\chi}_9 \cdot \underline{\chi}_9 \; > \; = \int_\Gamma (H_e \, \phi_e \; \underline{\chi}_9 \cdot \underline{n}) \; d\Gamma \qquad (4.11)$$

Since the basis functions ϕ_e are constant in each element the right hand side of equation (4.11) is identically zero taking account of the definition of χ in equation (4.2). Hence we obtain:

$$1/3 \; Q_9 = 0, \qquad (4.12)$$

whereas the true solution is $Q_9 = 1/\sqrt{2}$. However, we can include the true solution for water level in the boundary integrals of equation (4.11). On inflow and outflow boundaries the water level is constant so the boundary integrals remain zero, but on the no flow boundaries the water surface has unit gradient. Calculating the integrals along the no flow boundaries gives:

$$1/3 \; Q_9 = \sqrt{2}/6, \qquad (4.13)$$

that is the exact solution.

The above example is a form of patch test for this particular mixed finite element method since the numerical values obtained are independent of the element size; see Zienkiewicz (1977). Since the failure of the patch test is related to the poor representation of integrals around the boundaries it is obvious

to consider raising the order of the element. This leads to more complex basis functions for the flow field $\underline{Q}$ to be approximately divergence-free, see Griffiths (1977). In fact the higher order elements all provide conforming approximations and so the problem calculating of the boundary integrals disappears.

This approach has not been pursued further since one aim of the research was to investigate the low orders of approximation that were assumed to be consistent the quality of data available for practical calculations. The compatibility conditions between the orders of approximation of the unit flow vector and the water level for these higher order methods may be examined using the theoretical framework of Girault and Raviart (1979). Since these methods are not tested here this analysis has not yet been done but should precede any further work on the approximately divergence-free formulations.

4.3 The potential formulation

4.3.1 Introduction

The discussion here concentrates on four features of the method:

1. the convergence rate of the successive substitution algorithms used,
2. the effects of numerical quadrature,
3. the representation of boundary flux,

4. a comparison with the results of the stream function formulation.

All the calculations were based upon a representation of Sooky's experimental geometry, see Mesh 1 in Appendix 2. The water level was approximated, as in the stream function formulation, by a piecewise linear continuous function using the basis functions set out in Section 3.2.1. The ground level was taken as piecewise constant within each element, as in the final tests of the stream function formulation. Two friction formulae were tested, Chezy's law and the Colebrook-White equation.

The calculations are based upon the mathematical model equations laid out in Section 2.5.1. The dynamic equation (2.56) is rearranged to give

$$\underline{q} = - K\left|\underline{\nabla} h\right|^{-\frac{1}{2}} \underline{\nabla} h \qquad (4.14)$$

and setting div $\underline{q}$ to zero we obtain

$$\underline{\nabla}\cdot(K\left|\underline{\nabla} h\right|^{-\frac{1}{2}} \underline{\nabla} h) = 0 \quad . \qquad (4.15)$$

With appropriate boundary data on the water level h this equation possesses a unique solution, see Section 2.6.1.

The finite element approximation to the solution of equation (4.15) may be generated using successive substitutions thus:

$$< c_f(H^n)\underline{\nabla}\,(H^n+\eta),\ \nabla N_i > + b_j^n \qquad (4.16)$$

Here H^n is the approximation to the water level at iteration

number n and b_j^n is determined by the boundary data. These Galerkin equations are solved for the updating vector η and the water level vector at the new iteration is defined by

$$H^{n+1} = H^n + \lambda\eta \tag{4.17}$$

where λ is a relaxation parameter. The unit flow vector in each element may be defined as

$$\underline{Q}^n = - \bar{K} \left| \underline{\nabla} H^n \right|^{-\frac{1}{2}} \underline{\nabla} H \tag{4.18}$$

Here $\bar{K}$ is the average value of the conveyance function defined by the quadrature rule thus,

$$\bar{K} = \sum w_i K(H^n(\underline{x}_i)) \tag{4.19}$$

where the sums runs over all the quadrature points i for the element. The friction parameter C_f in equation (4.16) may then be expressed as

$$C_f(H^n) = \bar{K}^2 \left| \underline{Q}^n \right|^{-1} \tag{4.20}$$

A key distinction between the stream function formulation and the potential formulation is the way the continuity equation is represented. By definition, a stream function satisfies the continuity equation locally and globally over the whole flow domain. In the potential formulation, however, the continuity equation is only satisfied as a weighted average, thus, from equation (4.16)

$$< \underline{Q}^*, \underline{\nabla} N_j > = 0 \tag{4.21}$$

where $\underline{Q}^*$ is limit of the sequence of values $\{\underline{Q}^n\}$ from equation (4.18) and j ranges over all the interior nodes of the finite element mesh.

4.3.2 Convergence of the iterative method

The convergence of the successive substitution algorithm defined by equations (4.16) to (4.20) may be studied in a similar way to the analysis in Section 3.4.2. Define as before H_k^* as the nodal values of the solution of the Galerkin equations and the error E_k^n at iteration n by

$$H_k^n = H_k^* + E_k^n \tag{4.22}$$

The approximations to the stream and normal vectors, $\underline{e}_s$ and $\underline{e}_t$, in each element are parallel and normal to $\underline{\nabla} H^*$ respectively. We define in each element streamwise and normal components of the gradient of E^n by

$$\underline{\nabla} E^n = F_e^n \underline{e}_s + G_e^n \underline{e}_t \tag{4.23}$$

Then we deduce that the error $\{E_k^{n+1}\}$ at the new iteration satisfies the following Galerkin equations to first order

$$\begin{aligned}&\textstyle\sum_e < \overline{K}_e^* |\underline{\nabla} H_e^*|^{-\frac{1}{2}} \underline{\nabla} E^{n+1}, \underline{\nabla} N_j > = \\ &\textstyle\sum_e < \overline{K}_e^* |\underline{\nabla} H_e^*|^{-\frac{1}{2}} \{\underline{e}_s [(1 - \tfrac{1}{2}\lambda) F_e^n - \lambda p |\underline{\nabla} H_e^*| \overline{E}_e^n / D] + \\ &\underline{e}_t [(1 - \lambda) G_e^n]\}, \underline{\nabla} N_j >\end{aligned} \tag{4.24}$$

On the right hand side of equation (4.24) the term $\lambda p |\underline{\nabla} H_e^*| E_e^n / D$ comes from the variation of the conveyance

function which is assumed to be of the form

$$K(D) = CD^p \qquad (4.25)$$

where D is the mean depth in the element defined by the quadrature rule.

Assuming that this term is small compared with F_n^e and G_n^e then we deduce that a two parameter updating algorithm will be effective in solving the non-linear finite element equations. The relaxation parameters should be 1 and 2 in alternate iterations giving the approximate elimination of the normal and streamwise components of $\underline{\nabla} E$ respectively. We may estimate when the term from the variation of the conveyance function is likely to be small. Let us examine the coefficient of $\underline{e}_s$ in the right hand side of equation (4.24). This is approximately

$$(1 - \tfrac{1}{2}\lambda) F_e^n - \lambda ps \bar{E}_e^n/D \qquad (4.25)$$

where s is the mean surface slope. Setting F_e^n as $\bar{E}_e^n/\Delta$ approximately where Δ is the mean length of the element in the stream direction, the expression (4.25) becomes

$$(1 - \tfrac{1}{2}\lambda - \lambda ps\Delta/D) F_e^n \qquad (4.26)$$

Hence the importance of the variation of conveyance depends upon the magnitude of $ps\Delta/D$. For the test geometry, Mesh 1, we have $D = 0.02m, s \simeq 0.002, p \simeq 1.8$ and $\Delta \simeq 0.08m$. Hence the expression (4.26) becomes approximately $(1 - \tfrac{1}{2}\lambda - 0.02\lambda) F_e^n$ and it should be appropriate to use parameter values 1 and 2 in alternate iterations for this geometry.

The value of the parameter $ps\Delta/D$ should, however, be examined for each application of the method. It is easy to forsee examples where the variation of the conveyance may not be negligible. Suppose we are calculating flow over a flood plain using a mesh with the following typical physical parameters: $s = 0.001$, $p = 1.7$, $\Delta = 100m$, $D = 1.0m$. The expression (4.26) now has the value $(1 - 0.67\lambda)F_e^n$ and relaxation parameters of 1 and 1.5 would be appropriate. These estimates assume of course that the nodal error E_k^n is essentially random rather than systematic.

Three pairs of relaxation parameters were tested and the convergence rates are shown in Table 4.1. (The convergence parameters are defined in Section 3.3.5). The results shown in Table 4.1 indicate that increasing the relaxation parameter to 1.5 or 2.0 in alternate iterations (tests 2 and 3) improves the convergence rate from using a value of 1.0 for all iterations. The convergence rate of 0.5 achieved in test 1 is the same as would be inferred from equation (4.24). The asymptotic rates for tests 2 and 3 are close to those found for the two parameter updating method applied to the stream function formulation, see Tables 3.3 and 3.4.

TABLE 4.1

CONVERGENCE PARAMETERS FOR THE POTENTIAL FORMULATION

	Test 1		Test 2		Test 3	
Iteration	Water Level	Discharge	Water Level	Discharge	Water Level	Discharge
1	1.42(-2)	1.72(0)	1.42(-2)	1.72(0)	1.44(-2)	1.72(0)
2	1.49(-2)	8.77(-1)	2.25(-2)	1.02(0)	3.07(-2)	1.10(0)
3	9.46(-3)	3.37(-1)	5.47(-3)	2.42(-1)	3.20(-3)	1.76(-1)
4	4.29(-3)	1.69(-1)	3.99(-3)	1.80(-1)	3.11(-3)	2.06(-1)
5	1.97(-3)	9.42(-2)	6.06(-4)	2.88(-2)	1.42(-4)	1.22(-2)
6	9.32(-4)	4.96(-2)	4.41(-4)	2.21(-2)	9.22(-5)	8.82(-3)
7	4.50(-4)	2.54(-2)	7.00(-5)	3.71(-3)	1.59(-5)	1.21(-3)
8	2.20(-4)	1.29(-2)	5.21(-5)	2.79(-3)	7.72(-6)	6.46(-4)
9	1.08(-4)	6.45(-3)	8.54(-6)	4.62(-4)	2.01(-6)	1.30(-4)
10	5.36(-5)	3.23(-3)	6.36(-6)	3.46(-4)	8.93(-7)	6.56(-5)
11	2.67(-5)	1.61(-3)	1.04(-6)	5.75(-5)	2.51(-7)	1.47(-5)
12	1.32(-5)	8.09(-4)	7.82(-7)	4.32(-5)	1.12(-7)	7.37(-6)
Average rate	0.53	0.50	0.39	0.36	0.33	0.31
Asymptotic rate	0.49	0.50	0.35	0.35	0.35	0.33
Relaxation parameters	odd 1.0 even 1.0		odd 1.0 even 1.5		odd 1.0 even 2.0	

The subsequent tests reported in this Chapter all used the relaxation parameters 1.0 and 2.0 alternately since this gave marginally the best rate of convergence in the first three tests.

4.3.3 Numerical Quadrature

The three quadrature rules of Section 3.2.5 were tested with the potential formulation. The convergence rates for the iteration and values of water level were found to be insensitive to the degree of the quadrature rule. The maximum difference in water level after 10 iterations between the rules was only 6×10^{-7}mm compared with a flood plain depth of 20mm. The variation in the magnitude of the unit flow vector calculated from equations (4.18) and (4.19) was somewhat larger. For example in element number 148 at the downstream end of the flow domain (see Fig 4.3) the following values were obtained.

Degree of quadrature	Unit flow magnitude (m^3/s)	Convergence parameters
1	5.2153760348(-3)	2.657(-5)
2	5.2154292675(-3)	2.653(-5)
5	5.2154292736(-3)	2.666(-5)

The convergence parameter indicates that changes of the order of 2 parts in 10^5 were occurring in the magnitude of the unit

flow and that the difference in the results obtained with the rules of degree 2 and 5 are not significant. The effect of using centroid quadrature rather than the higher degree rules is also barely significant in numerical terms. In practice the lowest degree of quadrature may be used since typical calibration criteria for models of flood flow rarely consider differences in velocity of the order of one percent significant.

4.3.4 Boundary flux

One of the measures of the quality of the solution for the stream function formulation was whether the water level was uniform along each inflow boundary, see Section 3.4.4. However this condition is imposed as data on the potential formulation and we use instead a complementary measure of the quality of the results of this method, namely whether the inflow and outflow to the region agree. In each element the program computed the magnitude of the approximation to the unit flow vector $|\underline{Q}|$ using equation (4.18). For elements lying on a flow boundary $\underline{Q}$ is normal to the element side on the boundary since the water level is specified as uniform there. Hence an estimate of the total discharge Q_T on a flow boundary could be built up as

$$Q_T = \sum |\underline{Q}_e| \delta_e \qquad (4.27)$$

where the sum runs over all the elements with a side on the flow boundary and δ_e is the length of the side on the flow boundary. Although the inflow and outflows were found to match to better than 1 part in 10^5 for a test based on Mesh 1 but with no channel, when the channel with its depth discontinuity

was reintroduced the discrepancy between inflow and outflow rose to about 3 percent.

The cause of this supposed error is simply that equation (4.27) is not a true statement of the Galerkin equations used to define the weak form of the continuity equation. The proper representation of the boundary flux is set out below. The continuity equation is

$$< \underline{\nabla}\cdot\underline{q},\ \pi > = - < \underline{q},\ \underline{\nabla}\pi > + \int \pi\, \underline{q}\cdot\underline{n}\, d\Gamma \qquad (4.28)$$

Hence for an inflow or outflow boundary Γ_f

$$Q_T = \int \pi\, \underline{q}\cdot\underline{n}\, d\Gamma_f = < \underline{q},\ \underline{\nabla}\pi > \qquad (4.29)$$

if π is defined such that it is zero on all other flow boundaries. One suitable definition for π is

$\pi = 1$ for all nodes on Γ_f

$\pi = 0$ at all other nodes.

With this definition for the test function π we have the following approximation to the boundary flux:

$$Q_T = \sum < \underline{Q}^e,\ \underline{\nabla}\pi^e >$$

where the sum runs over all the elements lying on or touching the flow boundary.

This definition of Q_T was included in the computer code and after ten iterations (using relaxation coefficients of 1.0 and 2.0 alternately) the inflow and outflow only differed by 3 parts in 10^7. The convergence parameter for the unit flow magnitude was 2.6(-5) after ten iterations indicating that the boundary flux converged faster than the interior solution. The convergence of the boundary flux was checked in subsequent

tests by evaluating the inflow and outflow for each iteration. Table 4.2 shows the boundary fluxes for a test based upon Mesh 1, which clearly shows a more rapid convergence for the flux compared to the solution as a whole.

This observation is of practical importance since it means that relatively few iterations need to be done to achieve a good estimate of the discharge in or out of the region. The total discharge will be a calibration parameter in the case where a roughness value is assumed and water levels are given on the flow boundaries. Hence the roughness can be adjusted (manually or automatically) after a few iterations of the algorithm. The same is the case in the typical design situation where the total flow and the roughnesses are known but the upstream water level is unknown. Only a few iterations need to be done for each trial water level.

TABLE 4.2

CONVERGENCE OF BOUNDARY FLUX

Iteration	Inflow (m^3/s)	Outflow (m^3/s)	ε_q
1	1.0626621705(-2)	9.3109511870(-3)	7.63(-1)
2	1.0151291473(-2)	1.0136650849(-2)	3.75(-1)
3	1.0169421465(-2)	1.0159376462(-2)	3.34(-2)
4	1.0181041130(-2)	1.0179807619(-2)	1.71(-2)
5	1.0179989047(-2)	1.0179846938(-2)	3.73(-3)
6	1.0179623826(-2)	1.0179808975(-2)	2.07(-3)
7	1.0179750718(-2)	1.0179785272(-2)	4.21(-4)
8	1.0179797728(-2)	1.0179776281(-2)	2.36(-4)
9	1.0179783408(-2)	1.0179779280(-2)	4.80(-5)
10	1.0179778296(-2)	1.0179779495(-2)	2.71(-5)

Results for a test of Mesh 1 using relaxation parameters of 1.0 and 2.0 alternately and a roughness size of k_s = 3.6mm in the Colebrook-White resistance equation. ε_q is the convergence parameter for the magnitude of the unit flow vector.

4.3.5 Comparison with prototype and stream function model

The results from the potential formulation may be compared with the flume data of Sooky (1964) in a similar fashion to the results in Section 3.4.4. The physical basis of the mathematical model of the flow is the same in each case, hence the limitations of the stream function model are pertinent

here. Table 4.3 gives a comparison of the flow division for the two formulations and the flume data. The discharges for each subsection in the potential formulation were calculated by hand using equation (4.27) and so may be subject to a small error.

The test of the potential formulation using Chezy's friction law had the upstream level set to the average water level on the upstream boundary from test 4 of the stream function model. The discharge was $8.13801(-3)m^3/s$ compared with $8.14109(-3)m^3/s$ for the stream function formulation. This difference although of numerical significance is of little practical importance. For the tests using the Colebrook-White roughness the upstream level was set to achieve a surface slope equal to the bed slope of the flume, ie 0.00160 compared with the surface slope of 0.00107 for the test using the Chezy law. The discharges for the potential and stream function for a roughness size of 3.6mm were both set to 1.017978(-2), and for a roughness value of 1.6mm the total discharge was $1.18256(-2)m^3/s$.

The results shown in Table 4.3 show that, for the same friction law, the two formulations agree more closely with each other in terms of the division of the flow between the channel and flood plains than they do with the flume data of Sooky (1964). The principal cause of the discrepancies is the omission of turbulents stresses from the mathematical model (see Section 3.4.4).

Further comparison of the two formulations, is possible, Table 4.4 gives the water levels across the centre of the mesh

TABLE 4.3

FLOW DIVISION. COMPARISON

Position	Formulation	Friction law	Percentage of flow		
			Left	Channel	Right
Left limit of meander	Sooky's experiments		18.9	44.3	37.9
Downstream end	SF inital	Chezy (38.35)	19.6	47.7	32.7
	Potential	Chezy (38.35)	19.3	48.9	31.8
	SF final	Colebrook (3.6)	18.2	52.7	29.1
	Potential	Colebrook (3.6)	17.5	53.6	28.9
	Potential	Colebrook (1.6)	17.8	52.9	29.3
Centre (Left and Right transposed)	SF initial	Chezy (38.35)	19.5	48.0	32.5
	Potential	Chezy (38.35)	20.0	47.3	32.7
	SF final	Colebrook (3.6)	17.8	52.2	30.0
	Potential	Colebrook (3.6)	18.2	51.7	30.1
	Potential	Colebrook (1.6)	18.5	51.0	30.5

TABLE 4.3

FLOW DIVISION. COMPARISON (CONT'D)

Upstream end	SF initial	Chezy (38.35)	19.4	48.4	32.2
	Potential	Chezy (38.35)	19.9	47.3	32.8
	SF final	Colebrook (3.6)	18.3	52.7	29.0
	Potential	Colebrook (3.6)	18.3	51.6	30.1
	Potential	Colebrook (3.6)	18.5	51.0	30.5

Notes

1 Results for stream function (SF) initial model are for test 4 in Table 3.6, and for the final model for test 8.

2 The value in ( ) after the name of the friction law denotes the coefficient value with units mm for Colebrook-White.

for the two tests using the Chezy friction law. Two features are apparent. Firstly, the water level on the left flood plain tends to be higher than on the right flood plain. It is not clear whether this difference is a feature of the solution of the flow equation, as no tests have been done on reduced mesh sizes. Secondly, there is considerably more variation in the transverse water surface profile from the stream function formulation, confirming the criticism of the streamline integration algorithm in Section 3.6.

TABLE 4.4

WATER LEVELS ACROSS CENTRE OF MESH 1

Node	Position	Stream function formulation (mm)	Potential formulation (mm)
42	R H edge of flow	21.616	21.673
43		21.595	21.673
44		21.592	21.674
45	edge of channel	21.613	21.674
46	edge of channel	21.593	21.675
47	edge of channel	21.607	21.675
48		21.618	21.675
49		21.602	21.674
50		21.620	21.674
51	LH edge of flow	21.619	21.675

4.4 Concluding Remarks

Of the two approaches discussed in this chapter the divergence free formulation has been shown to require a higher order approximation than the potential formulation. Hence in line with the philosophy outlined in chapter one concentration has been centred on the potential formulation. This method is in a sense complementary to the stream function formulation. The potential formulation performed satisfactorily on tests of a discretization of Sooky's experimental geometry. This method has been developed further by the introduction of the convection term into the mathematical model and by an improved iteration scheme similar to the first order variation method the stream function model.

These points form the subject of Chapter 5 which also includes a discussion of the application of the potential formulation for the Tallahala Greek data.

CHAPTER 5

MODELLING THE CONVECTION TERM

5.1 Introduction

This chapter considers the extension of the potential formulation to include the convection term which is defined in section 2.5.2. In the iterative sequence the convection term is always based upon known values of water level and unit flow rate. The convection term itself is recovered by estimating spatial derivatives of the representation of mean flow velocity implied by the approximations used for the principal flow variables and the ground topography. The algorithm used to calculate these derivatives is new. The iterative sequence is only conditionally convergent depending upon the magnitude of a mesh Froude number which is discussed in Sections 5.4 and 5.5. When the iteration method was changed to one motivated by time stepping to a steady state, stable calculations were obtained.

The initialisation of the iterative method requires the calculation of the flow field without convection and this is a straightforward application of the potential formulation of Section 4.3. The iterative method has been refined producing an improved method for the potential formulation based upon first order variations similar to that discussed in Section 3.4.3.

Some of the general discussion in Chapter 3 is relevant here, particularly the basis functions and topographic discretization in Section 3.2 and software techniques in Section 3.3. The method was applied to several of the mesh geometries described in Appendix 2.

The computations are based upon the following model equations.

Steady flow

$$\underline{\nabla}.\underline{q} = 0 \tag{5.1}$$

$$(\underline{U}.\underline{\nabla})\underline{U}/g + \underline{\nabla}h + \underline{q}|\underline{q}|/K^2 = 0 \tag{5.2}$$

Unsteady flow

$$\underline{\nabla}.\underline{q} + \partial_t h = 0 \tag{5.3}$$

$$(1/gD)\,\partial_t\underline{q} + (\underline{U}.\underline{\nabla})\underline{U}/g + \underline{\nabla}h + D^2\underline{U}|\underline{U}|/K^2 = 0 \tag{5.4}$$

The convection term $\underline{c}$ is the dimensionless vector quantity defined by

$$\underline{c} = (\underline{U}.\underline{\nabla})\underline{U}/g \tag{5.5}$$

5.2 Calculating the convection term

5.2.1 The basic method

The potential formulation of Chapter 4 used the following orders of approximation in each element:

Water level : piecewise linear

Bed level : piecewise constant

unit flow vector : piecewise constant

Formally then, the representation of the depth D is piecewise

linear discontinuous and the flow velocity is a discontinuous rational function. However, in the calculations the depth and discharge are only ever sampled at the element centroids when the one point integration rule is used. An approximation to the convection term $\underline{c}(\underline{U})$ of equation (5.5) may therefore be defined by the following steps:

1 calculate the mean velocity $\underline{U}_k = \underline{Q}_k/D_k$ in each element k with all values notionally at the centroid

2 For each element k define a set n_k of neighbouring elements, with at least two distinct elements in n_k. These will usually share a common side with element k but the definition of n_k is discussed at greater length in Section 5.2.2.

3 carry out a least squares best fit to the mean velocity vector assuming that it varies linearly and continuously over all the elements in n_k^+ defined as the union of n_k and k.

4 calculate the convection term from the velocity and its derivatives found in step 3.

The least squares fitting procedure in step 3 is as follows. For each ℓ in n_k^+ let

$$E_u^\ell = U_\ell - \tilde{U}_\ell - \alpha_\ell \partial_x \tilde{U}_k - \beta_\ell \partial_y \tilde{U}_k \qquad (5.6a)$$

$$E_v^\ell = V_\ell - \tilde{V}_k - \alpha_\ell \partial_x \tilde{V}_k - \beta_\ell \partial_x \tilde{V}_k \qquad (5.6b)$$

where $\underline{U}_\ell = (U_\ell, V_\ell)$ and the best fit velocity components and derivatives are $\tilde{U}_k$, $\partial_x \tilde{U}_k$, etc. The coefficients α_ℓ and β_ℓ are

the components of the position vector

$$(\alpha_\ell, \beta_\ell) = \underline{x}_\ell - \underline{x}_k \tag{5.7}$$

with $\underline{x}_\ell$ being the centroid of element ℓ. The parameters $\tilde{U}_k$, $\partial_x \tilde{U}_k$ etc are then obtained by minimisation of

$$E_u^2 = \sum (E_u^\ell)^2 \tag{5.8a}$$

$$E_v^2 = \sum (E_v^\ell)^2 \tag{5.8b}$$

with respect to these parameters where the sums run over the set n_k^+. By definition this set contains at least three distinct elements and the fitting procedure is only ill conditioned when the position vectors $(\alpha_\ell, \beta_\ell)$ are nearly collinear.

Having carried out the least squares fitting the approximate value of the convection term in element k is defined as

$$\underline{C}_k = (\tilde{U}_k \partial_x \tilde{U}_k + \tilde{V}_k \partial_y \tilde{U}_k \ , \ \tilde{U}_k \partial_x \tilde{V}_k + \tilde{V}_k \partial_y \tilde{V}_k) \tag{5.9}$$

Some tests of the method included a condition on accepting the approximation $\underline{C}_k$ based upon the size of the residual square error from the fitting procedure, relative to the residual based upon assuming the velocity is constant in n_k^+ at its mean value. Where the fitting procedure did not produce a significantly better result than using the mean velocity $\underline{C}_k$ was set to zero. This refinement, however, did not have much effect in practice except in the case where the calculations were diverging and the mean velocity was not coherently structured.

Where the set of elements n_k contains the three elements with

a common side with k, see Fig 5.1, the least squares fitting procedure gives what can be considered as a generalised central different approximation to the velocity gradients. The set n_k does not in this case take any account of the actual stream direction or an a priori estimate of it.

Consider the case where the actual flow velocity varies linearly with x and y. It is easy to show that the piecewise constant best fit to this velocity field is obtained by taking the actual flow velocity at the centroid of each triangular element. The least squares recovery procedure above returns the exact values of the velocity and its derivatives, and the convection term $\underline{C}_k$ defined by equation (5.9) is exact at the element centroid and also gives the exact integral over the element area when combined with one point quadrature. These are attractive properties of the recovery procedure. Finally we note that linear variation of velocity implies a quadratic variation of stream function and thus we recover in some cases the exact point values of convection term and its integral over an element for flows with curved streamlines. For example, inviscid, irrotational flow into the corner bounded by the x and y axes is given by the stream function xy, see Batchelor (1967), p411.

During the development of the model of steady flow with convection, several variants of the least squares recovery procedure for the convection term were tested. One variant fitted the values of the velocity derivations alone from data

in the patch of neighbouring elements. The convection term was evaluated from these derivatives and the approximation to the velocity calculated from the water surface in the target element. The numerical results quoted in Section 5.3 were obtained using this variant. The algorithm as described in steps (1) to (4) above, however, gave a better fit (measured by the sum of squares of the residual velocity error at each element centroid) and this forms the basis of the computations of Section 5.6.

5.2.2 Neighbouring element sets

The computations presented later in this chapter use four different definitions of the set of neighbouring elements n_k. These are the standard and upwind sets, each of which may recognise (or not) the presence of the edges of a main channel, across which there is a large variation in velocity. Some variation of the definitions was necessary for elements at the boundary of the flow domain.

1 The standard set

In this case the neighbour set n_k of an element k in the interior of the flow domain contains the three elements which share a common side with k, see Fig 5.1. This definition is also suitable for elements with only one node on the mesh boundary. Elements with one or two sides along the mesh boundary require special action since they have a reduced number of interior neighbours. Where the element k has only one side on the boundary, the basic neighbour set comprises the two elements which share a common side with element k.

A third element which shares a common node with k is added to the basic set. All elements sharing a common node are considered in order of distance, centroid to centroid, from k. The closest element is chosen which satisfies a test on the size of the determinant the coefficients of the equations in the least squares fitting procedure. This ensures the fitting procedure is well conditioned. For an element k with two sides on the boundary and hence only one neighbour n with a common side, the neighbour set for element k is taken as the neighbour set for element n. Fig 5.1 also shows typical cases at the boundary.

Using the definition of the coefficients α_ℓ and β_ℓ, equations (5.7), we set

$$S_1 = \sum\alpha_\ell^2 \; ; \; S_2 = \sum\beta_\ell^2 \; ; \; S_3 = \sum\alpha_\ell ; S_4 = \sum\beta_\ell \; ; \; S_5 = \sum\alpha_\ell\beta_\ell$$

with the sums running over the elements in the neighbour set. Now define

$$d_1 = 4S_1S_2 + 2S_3S_4S_5$$

$$d_2 = 4S_5S_5 + S_1S_4 + S_2S_3$$

and the determinant of the matrix from the least squares fitting procedure is

$$\text{Det} = d_1 - d_2$$

The test employed for elements near the boundary is that the ratio d_1/d_2 must not lie in the interval (0.95, 1.05). The choice of this interval was arbitrary and no adjustments were tested since the calculations were acceptable.

2 Standard set with banks

The definition is identical to the standard set with the exception of the strings of element sides along the depth discontinuities at the edges of the channel. These are treated in the same way as the exterior boundary of the flow domain.

3 A priori upwinding

The iterative procedure starts with a solution of the problem with zero convection. This solution can be used to define the velocity $\underline{U}_k$ in each element and hence introduce a degree of upwinding in the calculation of the convection term. In practice the set n_k in this case only contained two elements for every k and hence the least squares fitting procedure reduced to an exact fit for the velocity and its derivatives based on the three elements (ie, k and those in n_k). The set n_k was defined firstly from elements ℓ with a common side to k or a common node with k which satisfy the upwind condition

$$(\underline{x}_\ell - \underline{x}_k).\underline{U}_k < 0 \qquad (5.10)$$

where $\underline{x}_\ell$ and $\underline{x}_k$ are the position vectors of the centroids of elements ℓ and k respectively. From this set of elements the two closest to k (centroid to centroid) were retained in n_k. At the boundary of the mesh where no upwind neighbours could be found, a downwind approximation must be taken. Fig 5.2 shows typically neighbours for this case.

4 Upwinding with banks

The definition is the same as for the upwinded set of elements with the edges of the incised channel being treated in the same manner as the exterior boundary. The neighbour set n_k is not allowed to straddle the edge channel for any element.

5.3 Iteration for steady flow

5.3.1 The finite element equations

First of all we examine the following three stage iterative procedure

1 Calculate the water level approximation H^{n+1} given K^n, $|\underline{Q}^n|$ and $\underline{C}^n$, the approximations to conveyance, unit flow magnitude and convection term, from the Galerkin equations

$$\langle ((K^n)^2/|\underline{Q}^n|)(\underline{\nabla}H^{n+1} + \underline{C}^n), \underline{\nabla}N_j \rangle = 0 \qquad (5.11)$$

2 Calculate $\underline{Q}_k^{n+1}$ in each element k, given H^{n+1} and $\underline{C}^n$, from

$$\underline{Q}_k^{n+1} = -K^{n+1}(\underline{\nabla}H^{n+1} + \underline{C}^n)/|\underline{\nabla}H^{n+1} + \underline{C}^n|^{\frac{1}{2}} \qquad (5.12)$$

3 Calculate $\underline{C}_k^{n+1}$ in each element k from H^{n+1} and $\underline{Q}_k^{n+1}$ using the least squares fitting procedure.

At each stage of the iteration the Galerkin equations (5.11) for water level H^{n+1} represent an elliptic problem since the remaining coefficients are all evaluated at the previous iteration level and we may specify Dirichlet or Neumann data for H^{n+1} around the mesh boundary. For sufficiently slow flows the iteration sequence 1,2,3; 1,2,3.... was found to converge.

The nature of the limit on velocity for convergence is discussed in Section 5.4. The results described in this section are for flows which meet this condition, with the velocity being adjusted by altering the frictional resistance to the fluid motion. In an attempt to extend the limit for convergence the iteration sequence based upon 1,(2,3)(2,3),(2,3).....1,(2,3),(2,3).....1, etc, was tested but no advantage was obtained in iterating on equations (2,3) to convergence before re-calculating the water level. The overall rate of convergence was slower and so the original iteration sequence was retained for the comparative tests reported below. The comparison for these two iterative sequences was carried out on the geometry of Mesh 1 of Appendix 2.

5.3.2 Boundary conditions

At a "solid" boundary across which there is no flow we have the condition

$$\underline{q}\cdot\underline{n} = 0 \qquad (5.13)$$

From equation (5.2) we see that this is equivalent to

$$\{\nabla h + \underline{C}(\underline{u})\}\cdot\underline{n} = 0 \qquad (5.19)$$

which is the natural boundary condition on the Galerkin equations (5.11).

On the flow boundaries we impose the condition that

$$\underline{q}\cdot\underline{t} = 0 \qquad (5.20)$$

where $\underline{t}$ is the unit vector tangential to the boundary. Taking the dot product of equation (5.2) with $\underline{t}$ we obtain the ordinary differential equation for the boundary variation of water

level:

$$\nabla h \cdot \underline{t} + \underline{c} \cdot \underline{t} = 0 \qquad (5.21)$$

Hence given $\underline{C}$ we may calculate the tangential variation of water level across the boundary. This can be viewed as part of iterative process carried out before step 1 of the algorithm laid out in Section 5.3.1. The water levels at adjacent nodes i and j in element k along the boundary are related by

$$H_i^{n+1} - H_j^{n+1} = \Delta_k \underline{C}_k^n \qquad (5.22)$$

where Δ_k is the length of the boundary segment for element k.

As for the potential formulation of friction controlled flow, one measure of the quality of the numerical results is the agreement in the flux across the inflow and outflow boundaries. The boundary flux is calculated from equation (4.30) with the unit flow vector in each element given by equation (5.12) except that all terms are evaluated at the same iteration.

5.3.3 The U-shaped channel

Some tests were carried out using Mesh 8 (see Appendix 3) which represents a U-shaped rectangular channel without flood plain. The floor of the channel sloped longitudinally by 0.1m from the inflow to the outflow boundary and a constant depth of flow of 0.18m was applied at each end. These test conditions should generate a flow for which the first order analytic solution given in Section 2.7 is valid, since for sufficiently slow velocity the streamlines in the absence of secondary flows should form circular arcs around the 180^0 bend. The

approximate solution gives

$$U \propto r^{-\frac{1}{2}}$$

$$|\underline{C}| \propto r^{-2}$$

$$h \propto r^{-1}$$

where r is the radius of curvature of the streamline. The three stage iteration converged only for the lowest velocity condition tested. The mean velocity was approximately 0.043m/s, which corresponded to a roughness (k_s) size of 30.0m. The flow conditions are not of any physical consequence since the roughness is unrealistically large. However, the results merit some discussion as the approximate analytic form of the solution is known.

The convergence of the iterative sequence was quite slow, see Table 5.1. It appears that the initialisation of the solution was poor, since the relative changes in depth are 0.66 for the first iteration. The calculations stopped (intentionally) after 10 iterations; in the last iteration the changes in depth, inferred from the convergence parameter for depth, were of the order of 7×10^{-5}m. Hence the iteration has not been taken sufficiently far to give reliable values of water surface slope. In contrast to the potential formulation without convection the total discharge only converged at the same rate at the main solution.

We may check the quality of the results after 10 iterations by examining the solution at 90^0 and 120^0 from the upstream end of the bend.

TABLE 5.1

CONVERGENCE RATES FOR U-SHAPED CHANNEL

Iteration	Convergence parameters for		Outflow
	depth	unit flow	less inflow
1	6.64(-1)	1.64(0)	-1.56(-2)
2	1.24(-1)	9.85(-1)	-1.05(-3)
3	5.72(-2)	5.08(-1)	4.83(-4)
4	3.08(-2)	2.88(-1)	7.38(-4)
5	1.70(-2)	1.58(-1)	6.42(-4)
6	8.77(-3)	8.50(-2)	4.67(-4)
7	4.23(-3)	4.50(-2)	3.11(-4)
8	1.99(-3)	2.31(-2)	1.86(-4)
9	9.06(-4)	1.15(-2)	1.18(-4)
10	3.72(-4)	5.49(-3)	6.93(-5)
Asymptotic rate (last 4 iterations)	0.45	0.50	0.62

The mesh, which is predominantly composed of equilateral triangles, is aligned at convenient angles to the expected flow direction in each case, see Fig 5.3. The values of mean velocity and convection term in cartesian axes are given in Table 5.2. The streamwise velocity component and radial component of the convection term are summarised in Table 5.3. Some of the values in Table 5.3 are arithmetic averages for two or three contiguous elements (see Fig 5.3); these results are

TABLE 5.2

COMPUTED VELOCITY AND CONVECTION TERM COMPONENTS

	Velocity		Convection term	
Element	x component	y component	x component	y component
207	-3.44(-2)	-2.11(-2)	2.02(-5)	-2.56(-5)
209	-3.59(-2)	-2.24(-2)	2.31(-5)	-3.47(-5)
211	-3.76(-2)	-2.40(-2)	2.95(-5)	-3.96(-5)
216	-3.81(-2)	-2.42(-2)	3.25(-5)	-4.78(-5)
218	-3.62(-2)	-2.25(-2)	2.29(-5)	-3.47(-5)
220	-3.48(-2)	-2.12(-2)	1.56(-5)	-3.38(-5)
248	-4.72(-2)	-2.65(-3)	7.53(-7)	-6.94(-5)
259	-4.10(-2)	-7.25(-4)	9.89(-9)	-3.50(-5)
260	-4.10(-2)	-9.52(-4)	1.27(-7)	-3.64(-5)
264	-4.50(-2)	-8.57(-4)	5.54(-8)	-5.34(-5)
265	-4.50(-2)	-1.14(-3)	-4.66(-6)	-3.64(-5)
266	-4.68(-2)	7.99(-3)	6.12(-7)	-6.99(-5)

TABLE 5.3

SOLUTION VALUES AT 120° AND 90° AROUND THE BEND

Element numbers	Stream velocity	Radial convection term	Radius		
120°	U	C	r	$r^{-\frac{1}{2}}$	r^{-2}
207, 220	4.05(-2)	3.47(-5)	4.88	0.452	0.0420
209, 218	4.24(-2)	4.16(-5)	4.39	0.477	0.0519
211, 216	4.47(-2)	5.12(-5)	3.94	0.503	0.0644
90°					
259	4.10(-2)	3.50(-5)	4.84	0.454	0.0427
260	4.10(-2)	3.62(-5)	4.57	0.468	0.0479
264	4.50(-2)	5.34(-5)	4.01	0.499	0.0622
265	4.50(-2)	3.64(-5)	3.71	0.519	0.0727
259, 260	4.10(-2)	3.57(-5)	4.70	0.461	0.0453
264, 265	4.50(-2)	4.49(-5)	3.88	0.508	0.0664
246, 265, 266	4.63(-2)	5.85(-5)	3.64	0.524	0.0755

plotted on Figs 5.4 and 5.5. The figures also show the line for the first order analytical solution of equations (2.96) and (2.98) using the values of 0.18 for D; 0.0168 for $\partial_\theta h$; 0.1238 for K, giving 0.0891 for C_1 and 8.09(-4) for C_2.

Even though the numerical solution has not converged fully we see that it reproduces quite well the analytical velocity variation. Averaged velocity values over 2 or 3 elements are no more than 1% in error, individual element values are in error by up to 3%. The magnitude of the convection term shows more scatter, with the value in element 265 having an error of 40%; again the values averaged over 2 or 3 elements lie closer to the analytical solution. The tests used only four or five elements to span the width of the channel but no computations have been done with a finer grid. Thus it is not clear whether the errors in the convection term are due to insufficient convergence of the main flow field or to the coarse grid. Having obtained a method which is stable for all discharges (see Section 5.6) more tests should be carried out on this geometry, comparing the results with the first (and possibly higher) order analytic solution.

5.3.4 The meandering channel

This section describes tests using a series of meshes based upon flume geometry of Sooky (1964). The meshes represent a single meander wave (Mesh 1); a single meander wave with straight entry and exit reaches of three different equal lengths (Meshes 2, 5 and 6); and finally six repetitions of the

meander wave (Mesh 7). (The mesh numbers refer to Table A2.1 of Appendix 2). These tests were designed primarily to look at the effects of boundary data on the calculated flow conditions. In practice the variation of water level on a flow boundary will not be known precisely. It is important that the flow conditions in the area of interest is not unduly affected by errors in the boundary data.

The iteration only converged for the lowest velocity tested, and then the asymptotic state of convergence was similar in all tests, being about $(0.5)^n$ see Table 5.4. This rate agrees with the analysis in Section 5.4.2. At the end of 10 iterations the water depths were changing by about 1 part in 10^5 and the depth of flow in the main channel was about 60mm.

In some tests the water level across the flow boundaries was taken from equation (5.21) and for others the water level was specified as horizontal. This change did not affect the convergence of the iteration. The roughness size for the tests that converged was 36m, this being a factor of about 10^4 greater than the prototype value. The iteration diverged for tests with roughness sizes of 0.36m and 3.6mm. The water surface and bed slopes were set to 0.0016, with the intention that the flow rate should be similar for all tests.

For Mesh 1, the single meander wave, the transverse water surface profile across the centre of the mesh was markedly different from the boundary variation of water level from

TABLE 5.4

CONVERGENCE RATES FOR DIFFERENT MESHES

Mesh	Convergence parameter for water depth			Convergence parameter for unit flow		
	Iteration 6	Iteration 10	Asymptotic rate	Iteration 6	Iteration 10	Asymptotic rate
with variable water level on the flow boundaries						
1	1.37(-4)	8.43(-6)	0.498	7.68(-3)	4.36(-4)	0.488
2	1.49(-4)	8.67(-6)	0.491	8.72(-3)	4.62(-4)	0.480
5	5.59(-4)	4.15(-5)	0.522	6.25(-3)	3.94(-4)	0.501
6	9.69(-4)	7.26(-5)	0.523	6.96(-3)	4.98(-4)	0.517
7	7.06(-5)	3.78(-6)	0.481	3.18(-3)	2.11(-4)	0.508
with horizontal water level on the flow boundaries						
1	1.36(-4)	8.25(-6)	0.496	7.70(-3)	4.37(-6)	0.488
7	6.95(-5)	3.72(-6)	0.481	3.19(-3)	2.07(-4)	0.504

equation (5.21). Using a horizontal water level on the boundaries, however, did not affect the nature of the surface profile in the centre of the mesh except to shift it down vertically by the change in mean depth at the two boundaries, see Fig 5.6. This indicates that in the interior of the domain the transverse water surface slope is insensitive to the boundary water level.

The uniform straight extensions on either end of the single meander (Meshes 2, 5 and 6) also did not affect the transverse water surface slopes at the centre of the mesh, see Fig 5.7. The longest extension used, Mesh 6, showed the slowest convergence rate, Table 5.4. Plotting the transverse profiles for the two final iterations shows the surface slope is well established with the whole profile being lowered in the final iteration. The water levels at the upstream end of the meander show a similar variation to the levels for Mesh 1 with the boundary conditions from equation (5.21), see Fig 5.8. The water levels across the downstream end of the meander, however, are completely different with the surface slope across the channel being of the opposite sign, see Fig 5.9. These results were not affected by the length of the mesh extension and no simple explanation for this behaviour can be given. Again for the tests of Mesh 6 the results of the last two iterations show only a bulk movement of the water surface, maintaining the transverse slopes. The differences in water level at the same location in these three tests is explained by the changed length of the mesh. The absolute values of the river bed and the water level at the downstream end of the mesh were

identical in all tests.

The two tests of the repeated meander, Mesh 7, give conditions similar to Sooky's experiments which covered several meander waves. Figure 5.10 is taken from Figure 30 of Sooky's thesis (1964) and shows the experimental transverse water levels where the meander is at its closest to one wall of the flume. The difference in scale of the water level variations between the flume and the numerical tests was due to the large difference in discharge, $7.89(-3)m^3/s$ for the flume and $1.88(-4)m^3/s$ for the computations. The computed results for the centre of the meander wave Fig 5.11 show transverse water level variations which are similar for each meander, and are also similar to the results of the centre of the single meander, Figs 5.6 and 5.7. The transverse slopes at the full meander wave (ie where the channel is on the opposite side of the flume to the centre meander case) show transverse slopes which are consistently larger, see Fig 5.12, but are similar in shape to Sooky's experiments. Changing the water level variation on the inflow and outflow boundaries did not affect this, see Fig 5.13; it only produced a gross lowering of the surface profile as found in the tests of Mesh 1 (Fig 5.6). The numerical values of velocity and convection term were found to be identical to the iteration precision in these two cases, for successive meander waves. Table 5.5 provides a comparison for corresponding elements in the incised channel approximately one quarter of the distance along each meander. Scaling the water level rise across the channel from the computations [3(-6) to 6(-6)m] by

TABLE 5.5

RESULTS FOR SUCCESSIVE MEANDER WAVES (MESH 7)

	Element	Velocity Components		Convection term	
		x	y	x	y
	46	7.913(-3)	-2.651(-3)	-2.161(-7)	4.306(-6)
Water level	194	7.913(-3)	-2.643(-3)	-2.348(-7)	4.287(-6)
variable	342	7.912(-3)	-2.642(-3)	-2.355(-7)	4.287(-6)
on flow	490	7.913(-3)	-2.643(-3)	-2.292(-7)	4.285(-6)
boundaries	638	7.913(-3)	-2.643(-3)	-2.294(-7)	4.285(-6)
	786	7.912(-3)	-2.643(-3)	-2.266(-7)	4.281(-6)
	46	7.913(-3)	-2.647(-3)	-2.259(-7)	4.298(-6)
Water level	194	7.912(-3)	-2.643(-3)	-2.347(-7)	4.286(-6)
constant	342	7.912(-3)	-2.642(-3)	2.355(-7)	4.287(-6)
on flow	490	7.912(-3)	-2.643(-3)	2.292(-7)	4.284(-6)
boundaries	638	7.912(-3)	-2.643(-3)	2.294(-7)	4.284(-6)
	786	7.912(-3)	-2.643(-3)	2.270(-7)	4.282(-6)

the square of the discharge ratio between the computation and Sooky's experiments gives values, 5 to 10mm. These are larger than Sooky observed (approx 4mm) and this discrepancy may be explained by:

(i) changes in conveyence across the channel produced by the larger experimental variation of depth than computed $(0(10^{-1})$ rather than $0(10^{-4}))$

(ii) the different distribution of discharge between channel and flood plain caused by terms omitted from the mathematical model, principally the turbulent stresses.

Overall the results of the trial computations show consistent, albeit occasionally unexpected, behaviour. The results on the meandering channel, taken with the test on the U-shaped channel, show that the recovery procedure used to obtain the convection term produces acceptable results when the calculation converges.

5.3.5 The first order variation method

During the development of the time stepping approach, Section 5.6, an improvement was made to the iterative procedure for the steady flow. Equation (5.12) for the discharge in each element is explicit. Thus the term $\underline{Q}^n$ in equation (5.11) can be replaced by this relationship and a non-linear equation produced for water level at the new iteration n + 1. The water level may be expressed as $H_j^{n+1} = H_j^n + \Delta H_j$ and the first order variation equations are in fact merely a special case (the

limit as the time step becomes large) of the unsteady equations given in Section 5.6.1. When implemented, the steady flow version had the same limit on roughness size for convergence, but convergence was much more rapid than for the simple successive substitution method. Table 5.6 presents the converge rates for a test using mesh 2. The computed results, however, showed the same behaviour as that discussed in Section 5.3.4 and so are not described further.

Even when the overall iteration diverged, the inner iteration for water level, given bad values for the convection term, converged nearly quadratically. The divergence of the iteration was clearly linked to the number of times the recovery procedure was used to calculate the convection term.

TABLE 5.6

CONVERGENCE PARAMETERS OF FIRST ORDER VARIATION METHOD

Inner Iteration for water level	Outer iteration 1	2	3	4	5
1	1.40(-2)	3.68(-5)	3.10(-7)	5.25(-9)	1.38(-10)
2	5.05(-3)	9.61(-8)	1.52(-11)		
3	1.05(-3)	1.04(-11)			
4	1.80(-5)				
5	6.21(-9)				
Unit flow	7.26(-1)	1.78(-3)	2.90(-5)	1.10(-6)	4.64(-8)
Convection term components	1.0(0)	1.06(-1)	7.93(-3)	1.99(-4)	4.92(-6)

5.4 Convergence of the iterative sequence

5.4.1 Introduction

We examine here the conditions under which the iteration on the steady flow equations will converge to some limit. As in the discussion of Sections 3 and 4, we do not consider the convergence of the finite element approximation to the solution of the flow equations as the mesh size is reduced. However, in contrast to the previous work we do not express all the analysis in terms of the Galerkin equations satisfied to first

order by the error at successive iterations. Instead, we examine first order expansions of the flow equations on the assumption that a consistent finite element approximation will exhibit the same behaviour.

The computations already described indicated a practical limit on the prototype flows that could be simulated with the steady model incorporating convection. For geometries based upon Sooky's flume, Meshes 1 and 2, the calculations converged for a roughness size of 36m but diverged for roughness sizes of 0.36m and 0.0036m. The smallest roughness value produced a spectacular growth of velocity in successive iterations (see Fig 5.14).

Rather than being governed by some dimensionless parameter of the physical flow, such as Froude number, the condition for convergence of the iteration depends upon the mesh geometry and the conveyance function. This condition is derived first from an heuristic argument and is then shown to apply to the growth of an initially small pointwise error on the exact numerical solution for two regular mesh geometries. The same constraint applies to a one-dimensional analogue of the 2-D equations and the analysis of this simplified case in Section 5.5 suggests that an iterative method based upon time stepping should converge, conditional upon the time step. This provided the motivation for the algorithms based upon semi-implicit time stepping and is described in Section 5.6.

5.4.2 Approximate analysis of the three stage procedure

Consider the iteration to find surface slope $\underline{s}$, velocity $\underline{u}$ and convection term $\underline{c}$ with appropriate boundary data thus:

$$\underline{\nabla}.\{F^2(\underline{s}^{n+1} + \underline{c}^n)/|\underline{u}^n|\} = 0 \tag{5.23}$$

$$\underline{u}^{n+1} = -F(\underline{s}^{n+1} + \underline{c}^n)/|s^{n+1} + c^n|^{\frac{1}{2}} \tag{5.24}$$

$$\underline{c}^{n+1} = (\underline{u}^{n+1}.\underline{\nabla})\underline{u}^{n+1}/g \tag{5.25}$$

In the above the superscripts n etc denote the iteration level and we assume depth D and friction function F to be uniform with

$$F = K/D \tag{5.26}$$

F has dimension of velocity and may be interpreted as the velocity of friction controlled flow with unit surface slope. Assume that the iteration converges to a triple $(\underline{s}^*, \underline{u}^*, \underline{c}^*)$ and suppose that at each stage

$$\underline{s}^n = \underline{s}^* + \underline{\alpha}^n \tag{5.27a}$$

$$\underline{u}^n = \underline{u}^* + \underline{\beta}^n \tag{5.27b}$$

$$\underline{c}^n = \underline{c}^* + \underline{\gamma}^n \tag{5.27c}$$

where the variations $\underline{\alpha}^n$, $\underline{\beta}^n$ and $\underline{\gamma}^n$ are small. Substituting the relations (5.27) into equation (5.23) we have

$$\underline{\nabla}.\{F^2(\underline{\alpha}^{n+1} + \underline{\gamma}^n + \underline{s}^* + \underline{c}^*)/|\underline{u}^* + \underline{\beta}^n|\} = 0$$

which becomes to first order,

$$\underline{\nabla}.\{F^2(\underline{\alpha}^{n+1} + \underline{\gamma}^n)/|\underline{u}^*| - F^2\underline{\beta}^n.\underline{u}^*(\underline{s}^* + \underline{c}^*)/|\underline{u}^*|^3\} = 0 \qquad \text{(The}$$

equation for iteration on $\underline{u}^{n+1}$ is

$$\underline{\beta}^{n+1} + \underline{u}^* = -F(\underline{\alpha}^{n+1} + \underline{\gamma}^n + \underline{s}^* + \underline{c}^*)/|\underline{s}^* + \underline{c}^* + \underline{\alpha}^{n+1} + \underline{\gamma}^n|^{\frac{1}{2}} \tag{5.29}$$

Expanding this to first order and eliminating $\underline{\alpha}^{n+1}$ and $\underline{\gamma}^n$

between equations (5.28) and (5.29) we obtain

$$\underline{\beta}^{n+1} = \tfrac{1}{2}(\underline{\beta}^{u}.\underline{u}^{*})\underline{u}^{*}/\left|\underline{u}^{*}\right|^{2} \qquad (5.30)$$

In the elimination we have assumed that the expression in the curly brackets in equation (5.28) is itself zero to first order by application of the boundary conditions. Equation (5.30) implies that the velocity error is eliminated in the cross-stream direction and halved in the stream direction in each iteration. This behaviour is the same as deduced from the Galerkin equations for the case $\underline{c} = \underline{o}$ in Section 4.3.2 with the relaxation parameter set to 1.0 for each iteration.

Having established that the iteration for velocity should be stable we examine the convection term. Consider the simple case of the uniform flow in a straight sloping flume with no incised channel, with the velocity, convection and surface vectors given by:

$$\underline{u}^{*} = (u_{o},o) \ , \ \underline{c}^{*} = \underline{o} \ , \ \underline{s}^{*} = (s_{o},o)$$

Suppose that the computed velocity vector is

$$\underline{u}^{*} = \underline{u}^{*} + \underline{\beta}^{1} \qquad (5.31)$$

where $\underline{\beta}^{1}$ for example is generated by rounding error. The iteration will provide a convection term $\underline{c}^{1}$ given by

$$\underline{c}^{1} \approx (u_{o}/g)\ (\partial_{x}\ \beta_{x}^{1} \ , \ \partial_{x}\beta_{y}^{1}) \qquad (5.32)$$

where $\underline{\beta}^{1} = (\beta_{x}^{1} \ , \ \beta_{y}^{1})$.

If the magnitude of the rounding and other errors for this step is E^{1} and the grid size in the flow direction is Δ then

$$\partial_{x}\ \underline{\beta}^{1} \approx (E^{1}/\Delta)\ \underline{e}_{1} \qquad (5.33)$$

where $\underline{e}_1 = (\sin\Theta^1, \cos\Theta^1)$ is a unit vector. Suppose that, as observed in trial calculations, the surface slope vector $\underline{s}^*$ is unaffected to first order by the error in the velocity and convection vectors. We have for the second iteration

$$(\underline{u}^* + \underline{\beta}^2)|\underline{u}^* + \underline{\beta}^2| \approx - F^2(\underline{s}^* + \underline{c}^1) \qquad (5.34)$$

Expanding this to first order in $\underline{\beta}$ for each component we have:

$$2u_o\beta_x^2 = (F^2/g\Delta)\, E^1 \cos\Theta^1 + E_x^2 \qquad (5.35a)$$

$$u_o\beta_y^2 = (F^2/g\Delta)\, E^1 \sin\Theta^1 + E_y^2 \qquad (5.35b)$$

Hence we see that the original rounding error will be multiplied by a factor of approximately $(F^2/g\Delta)$, which clearly implies a limit on the convergence of iterative method.

Three tests were carried out to test this criterion for convergence. The topographic and boundary data were set up to give a uniform flow in the x direction which was exact (to rounding error) on the initilisation of the calculation. The depth of flow was 0.05m, the streamwise space step was 0.158m and three roughness sizes k_s were tested: 0.010001m, 0.2m and 2.0m. Using the Colebrook-White equation with power law extension as set out in Section 2.2.2 the values of the parameter $(F^2/g\Delta)$ may be calculated and are shown below with the growth (or otherwise) of y component of the velocity, u_y.

	Test 1	Test 2	Test 3
$F^2/g\Delta$	0.354	3.54	35.4
$\log_{10}(u_y)$ initial	O(-10)	O(-10)	O(-10)
$\log_{10}(u_y)$ final	O(-10)	O(-3)	O(-3)
number of iterations n	20	10	5
$n \log_{10}(F^2/g\Delta)$	-9	5.5	7.7

The predicted and observed growth rates of the numerical error are clearly consistent with one another.

5.4.3 The equilateral mesh

Consider the three step iteration procedure using equations (5.11) and (5.12) applied to uniform velocity u_o in a domain covered with equilateral triangles of altitude Δ. We take the flow direction to be along the x axis, which coincides with one of the element sides to simplify the algebra. Suppose that the initial estimate for the water level is exact, except with an error of ε at one node, A in Figure 5.15. We may calculate the flow velocities and values of the convection term for a patch of elements around node A. On the first iteration these have the values below:

Element	1	2	3	4	5	6
u	$-\sqrt{3}/4$	0	$\sqrt{3}/4$	$\sqrt{3}/4$	0	$-\sqrt{3}/4$
v	$\frac{1}{2}$	1	$-\frac{1}{2}$	$-\frac{1}{2}$	1	$-\frac{1}{2}$
c_x	0	$\sqrt{3}/2$	0	0	$\sqrt{3}/2$	0
c_y	1	0	-1	1	0	-1

where all the velocity values are multiples of $(\varepsilon F^2/u_o \Delta)$ and the convection term values are multiples of $(\sqrt{3}\ \varepsilon F^2/2g\Delta^2)$. Figure 5.16 shows the vectors with these components. The

velocity errors are obviously weakly irrotational in the patch since they are derived from the gradient of a scalar error, and a hand calculation shows that the convection term from the level error $\underline{c}$ to be weakly divergence free. We have

$$< \underline{\nabla}\cdot\underline{c},\ \phi_A > = < \underline{c}\ ,\ \underline{\nabla}\ \phi_A > = 0 \qquad (5.36)$$

where ϕ_A is the linear basis function with support over the patch around node A. However, we note that in general

$$< \underline{c}\ ,\ \underline{\nabla}\ \phi_j > \neq 0 \qquad (5.37)$$

when $j \neq A$ and j is connected to A. Therefore on the second iteration the field $\underline{c}$ will not affect the Galerkin equations for water level at node A but it will influence those for the surrounding nodes. Neglecting this influence on the periphery of the patch we may continue to calculate velocity and convection term vectors for the second iteration. The new velocity errors follow closely the pattern of the convection term from the first iteration, see Fig 5.17. Calculating the velocity derivatives and mean velocity in each element from the least squares fitting procedure of Section 5.2.2 gives the convection term pattern shown in the lower portion of Figure 5.17. The values of the components of these vectors are

Element	1	2	3	4	5	6
u	0	$\sqrt{3}/4$	0	0	$\sqrt{3}/4$	0
v	-1	0	1	-1	0	1
c_x	$-\sqrt{3}/16$	0	$\sqrt{3}/16$	$\sqrt{3}/16$	0	$-\sqrt{3}/16$
c_y	0	1	0	0	-1	0

where the velocity component values are multiples of $(\sqrt{3}\,\epsilon F^4/4g\Delta^2 u_o)$ and the convection term components are multiples

of $(3\varepsilon F^4/8g^2\Delta^3)$. The second iterate $\underline{c}_2$ for the convection term is no longer weakly divergence free, a hand calculation gives

$$\langle \underline{c}_2 , \underline{\nabla}\phi_A \rangle = (19\sqrt{3}\ \varepsilon\Delta/4)\ (F^2/g\Delta)^2 \qquad (5.38)$$

The consequent change in water level at node A ε_3 for the third iteration is therefore

$$\varepsilon_3 = (57\sqrt{3}/192)\ \varepsilon\ (F^2/g\Delta)^2 \qquad (5.39)$$

on the assumption that the water level remains fixed around the periphery of the patch. The vector $\underline{\nabla}\varepsilon_3$ does not coincide with $-\underline{c}_2$ in each element and hence the velocity field in the third iteration will have a slightly different character from that in the first, see Fig 5.18. The velocity component values are

Element	1	2	3	4	5	6
u	$13\sqrt{3}/58$	0	$-13\sqrt{3}/58$	$-13\sqrt{3}/58$	0	$13\sqrt{3}/58$
v	$-19/58$	1	$-19/58$	$19/58$	-1	$19/58$

and are multiples of $(87\varepsilon F^6/192g^2\Delta^3u_o)$. Hand calculation of the various components of the error for more steps of the iteration becomes tedious and does not further clarify the situation. Setting the square of the mesh Froude number Fm as

$$Fm^2 = F^2/g\Delta s \qquad (5.40)$$

where Δs is the length of the triangle sides $(2\Delta/\sqrt{3})$, we may summarise the results as follows

Maximum Error	Level	Velocity	Convection term
	ε	$\varepsilon F^2/u_o\Delta$	ε/Δ
Iteration 1	1	1	Fm^2
Iteration 2	0	$0.5\ Fm^2$	$0.5\ Fm^4$
Iteration 3	$0.68\ Fm^4$	$0.6\ Fm^4$	$0(Fm^6)$

For the iteration to converge clearly a limit on the magnitude of Fm is implied. Each calculation of the convection term

introduces a factor of Fm^2, and numerical experiments showed that it was the number of iterations for the convection term that determined the growth in error for two variants of the successive substitution algorithm. These were firstly to iterate for velocity and water level to convergence for a given convection term, and secondly to iterate to convergence (or divergence) for velocity and convection term for each iterate of water level.

The above analysis of the evolution of error with iteration can be repeated for other simple mesh geometries such as the rectangular mesh divided along parallel diagonals. The same pattern emerges with an irrotational velocity error and a weakly divergence-free convection term error entering the second stage of iteration, see Figure 5.18.

5.5 The equivalent one dimensional case

5.5.1 Introduction

In order to justify the use of the time stepping method of Section 5.6 we examine the procedure applied to the Saint-Venant equations. For a uniform channel of width B, depth D, with mean velocity U, and water level h, these equations are:

$$\partial_t h + \partial_x DU = 0 \qquad (5.41)$$

$$\partial_t U + U \partial_x h + g\,(\partial_x h + s_f) = 0 \quad . \qquad (5.42)$$

These equations are discussed, for example, by Cunge Holly and Verwey (1980) and have formed the basis for many practical

models. The friction slope s_f is quantified as

$$s_f = U|U|/F^2 \tag{5.43}$$

where the friction function F is the mean value over a cross section of the function F in equation (5.26).

The least squares recovery algorithm for the convection term requires the velocity field to be known. For simplicity, when setting up the time stepping method the convection term was always calculated at the old time level. This enabled velocity to be eliminated from the system of Galerkin equations and hence reduce the computational effort in each time step. In order to assess the likely stability properties of this procedure we consider Fourier analysis for two simplified cases.

5.2.2 Frictionless flow

Let h be perturbed by δ and U by ε and set s_f to zero in equation (5.42). This gives the following perturbation equations for an initially steady flow:

$$\partial_t \delta + D\partial_x \varepsilon + U\partial_x \delta = 0 \tag{5.44}$$

$$\partial_t \varepsilon + U\partial_x \varepsilon + g\partial_x \delta = 0 \quad . \tag{5.45}$$

These equations are a linear hyperbolic system with characteristic speeds $U \pm (gD)^{\frac{1}{2}}$ and thus have the same characteristics locally as the full St Venant equations. The equivalent one-dimensional scheme involves taking δ to be piecewise linear in each element, ε piecewise constant, and weighting (5.44) with the linear basis functions and (5.45) with constant basis functions. In equation (5.45), to

calculate $\partial_x \varepsilon$ in any element we take the difference over the two adjacent elements. For an infinite spatial grid $j\Delta x$ and between times $n\Delta t$ and $(n+1)\Delta t$ we have

$$M_L\ \delta_j^{n+1} - \tfrac{1}{2}\mu U\ \Delta_o \delta_j^{n+1} + D\,\mu\Delta_+ \varepsilon_{j-\frac{1}{2}}^{n+1} = M_L\ \delta_j^n \qquad (5.46)$$

$$M_c\ \varepsilon_{j-\frac{1}{2}}^{n+1} + \mu g\ \Delta_- \delta_j^{n+1} = M_c\ \varepsilon_{j-\frac{1}{2}}^{n+1} - \tfrac{1}{2}\mu U\ \Delta_o \omega_{j-\frac{1}{2}}^n \quad . \qquad (5.47)$$

The mesh ratio μ is $\Delta t/\Delta x$ and the operators M_L, M_c, etc are defined with their transforms below. Take the Fourier transforms of the discrete equations with wave number k, defining c and s to the cosine and sine of $\frac{1}{2}k\Delta x$ respectively. We have

Operator	Origin	Transform
M_L	averaging for linear function with linear weighting	$1-(2/3)s^2$
M_c	averaging for constant function with constant weighting	1
Δ_o	central difference spanning two elements	4ics
Δ_+	forwards difference over one element	2is(c+is)
Δ_-	backward difference over one element	2is(c-is)

Summing over all grid points s and defining

$$\hat{\delta}(k) = \sum \delta_j \exp\ (ikj\Delta x)$$

$$\hat{\varepsilon}(k) = \sum \varepsilon_{j-\frac{1}{2}} \exp\ \left(ik(j+\tfrac{1}{2})\Delta x\right)$$

the transform equations are:

$$A\ (\hat{\delta}^{n+1},\ \hat{\varepsilon}^{n+1})^t = B\ (\hat{\delta}^n, \hat{\varepsilon}^n)^t \qquad (5.48)$$

The coefficient matrices A and B are

$$A = \begin{bmatrix} (1-2/3s^2) + 2i\mu cs & 2iD\mu s \\ 2i\mu gs & 1 \end{bmatrix} \qquad (5.49)$$

$$B = \begin{bmatrix} (1-2/3s^2) & 0 \\ 0 & 1-2i\mu cs \end{bmatrix} . \qquad (5.50)$$

Suppose at each step for some complex λ

$$(\hat{\delta}^{n+1}, \hat{\varepsilon}^{n+1})^t = \lambda(\hat{\delta}^n, \hat{\varepsilon}^n)^t \qquad (5.51)$$

Then the eigenvalues λ are determined by the condition

$$\text{Det } [B - \lambda A] = 0 \qquad (5.52)$$

This gives a quadratic equation in λ with the following coefficients

$$\lambda^2 : (\alpha + \beta^2) + i\gamma = a \qquad (5.53a)$$

$$\lambda^1 : -[2\alpha + \gamma^2 + i\gamma(1-\alpha)] = b \qquad (5.53b)$$

$$\lambda^0 : \alpha(1-i\gamma) = c \qquad (5.53c)$$

$$\alpha = 1-2/3s^2 \qquad (5.54a)$$

$$\beta^2 = 4gD\mu^2 s^2 \qquad (5.54b)$$

$$\gamma = 2U\mu sc \qquad . \qquad (5.54c)$$

The conditions for the quadratic equations to have roots lying in the unit disc, from Miller (1971), are:

Condition A $\quad |a| > |c|$

Condition B $\quad (b\bar{a} - \bar{b}c) \leq |a|^2 - |c|^2$

Expand first of all condition A, which implies

$$(\alpha + \beta^2)^2 + \gamma^2 \geq \alpha^2 + \alpha^2\gamma^2$$

or $2\alpha\beta^2 + \beta^4 + \gamma^2 \geq \alpha^2\gamma^2$.

By definition α lies in the interval $[1/3, 1]$ and β^2 is non-negative, hence condition A is satisfied without restriction on μ or the flow velocity. Condition B leads to some tedious algebra; we may square each side and rearrange the condition as

$$\beta^8 + 4\alpha\beta^6 + \beta^4\gamma^2 (2-2\alpha^2 - 4\alpha - \gamma^2) + \beta^2\gamma^2 (6\alpha - 4\alpha^3 - \alpha^2 - 1)$$
$$+ \gamma^4 (1 - \alpha^2) \geq 0 \quad . \tag{5.55}$$

Looking back to the definitions of α, β and γ (5.54) we see that condition (5.55) involves terms of even powers up to 12 in s, 8 in μ and 4 in U and gD.

Firstly we observe that, in the limit of stationary flow, λ is zero and the condition is satisfied without restriction on the time step. That is, the scheme is unconditionally stable for the one-dimensional wave equation. Secondly the condition is satisfied at the limits of 0 and 1 for s^2 since γ^2 is zero for these values. Thirdly, examining the coefficient of $\beta^2\gamma^2$, we see that the cubic is α positive for the lower limit 1/3 of α, zero for the upper limit of α and has a single turning point in the interval (1/3, 1). Hence the coefficient of $\beta^2\gamma^2$ is non-negative for all relevant values of s^2. The coefficients of β^8, β^6 and β^0 in condition (5.55) are all non-negative by definition.

The remaining term is of indeterminate sign and may be written as

$$\beta^4\gamma^2 (2 - 2\alpha^2 - 4\alpha - \gamma^2) =$$
$$1024\ Cr^6\ Fr^{-4}\ s^6\ (1-s^2)\ [(Cr^2 + 4/3)s^2 - 1 - (2/9 + Cr^2)\ s^4] \ . \tag{5.56}$$

where the Courant number Cr is μU and the Froude number Fr is $U/(gD)^{\frac{1}{2}}$. Obviously the magnitude of this term depends upon the values of the Courant and Froude numbers of the case in question and by adjustment of these parameters the condition B may not be met.

However we may derive sufficient (but not necessary conditions) for the scheme to be stable by ignoring some terms in (5.55) shown to be positive. For example, retaining only the terms in β^6 and β^4 we deduce the following sufficient condition:

$$256\, s^6 Cr^6 Fr^{-6} (1-2/3\, s^2) +$$

$$1024 Cr^6 Fr^{-4} s^6 (1-s^2)\left[(Cr^2 + 4/3)s^2 - 1 - (2/9 + Cr^2)s^4\right] \geqslant 0$$

which, taking out a common factor of $256\, s^6 Cr^6 Fr^{-6}$, reduces to

$$(1-2/3s^2) + 4Fr^2(1-s^2)\left[(Cr^2+4/3)s^2 - 1 - (2/9+Cr^2)s^4\right] \geqslant 0 \quad . \quad (5.58)$$

Setting $(1-2/3s^2)$ to $1/3$ and $(1-s^2)$ to 1 in order to minimise the positive term and maximise the negative term in (5.58) we deduce that a sufficient condition for (5.58) to hold is

$$Fr < (1/12)^{\frac{1}{2}} \approx 0.29$$

without restriction on the Courant number. Hence, a fortiori, the condition B is met with this limit on Froude number for all Courant numbers. Of course the true stability region may not be so restrictive.

5.5.3 The rigid lid approximation

In this Section we consider the scheme applied to the dynamic equation alone. This is analysed since we assume that the depth D is uniform in space and time. In physical terms we have suppressed the natural "compressibility" of the shallow water equations. In general terms, no error in the calculation can be transformed into potential energy by raising the surface level but is restricted to altering the kinetic energy of the flow. The stability constraints which this forces are thus

likely to be more severe than for the method applied to the full system of equations. Again we examine stability using Fourier analysis. The model equation is

$$\partial_x U + U\partial_x U + gU|U|/F^2 = gs \qquad (5.59)$$

where s is the surface slope. Introducing a perturbation ε to the steady solution U we obtain

$$\partial_x \varepsilon + U\partial_x \varepsilon + 2g\varepsilon s_f/U = 0 \quad . \qquad (5.60)$$

The finite difference form of this equation is

$$M_C \varepsilon^{n+1}_{j-\frac{1}{2}} + \Delta t(2g\ s_f/U)\ M_C \varepsilon^{n+1}_{j-\frac{1}{2}} = M_C \varepsilon^{n}_{j-\frac{1}{2}} - \tfrac{1}{2}\mu U \Delta_o \varepsilon^{n}_{j-\frac{1}{2}} \quad . \qquad (5.61)$$

Hence using the transforms of the operators given above we have, assuming $\hat{\varepsilon}^{n+1} = \lambda\hat{\varepsilon}^{n}$,

$$(1+2g\Delta t s_f/U)\ \lambda = 1 - 2ics\mu U$$

ie, $$\lambda = (1-2ics\mu U)/(1+2g\Delta t\ s_f/U) \quad . \qquad (5.62)$$

For stability we require $|\lambda|$ not to exceed unity that is

$$1 + 4s^2(1-s^2)\mu^2U^2 < 1 + 4g\Delta t\ s_f/U + 4g^2\Delta t^2 s_f^{\ 2}/U^2 \qquad (5.63)$$

for s^2 in the interval (0, 1). Defining the mesh Froude number Fm by

$$Fm = F/(g\Delta x)^{\frac{1}{2}} \qquad (5.64)$$

the condition (5.63) may be rearranged as

$$Cr\ (1-4/Fm^4) \lesssim 4/Fm^2 \quad . \qquad (5.65)$$

We have two cases, firstly if $Fm \lesssim \sqrt{2}$ then there is no restriction on Courant number. This condition ties up with the analysis of the successive substitution scheme in Section 5.4.2. For larger values of Fm we require

$$Cr \lesssim 4Fm^2/(Fm^4 - 4) \quad . \qquad (5.66)$$

Thus for any value of the mesh Froude number we may obtain a

stable calculation by chosing sufficiently small Courant number (or time step).

5.5.4 Concluding remarks

The stability analysis of the one dimensional analogue is reassuring in that the explosive growth of error in the rigid lid approximation for the steady flow equations can be controlled by choosing a suitable time step. The analysis of frictionless flow which has the same pattern of characteristics as the St-Venant equations leads to the sufficient condition that the Froude number is less than 0.29, but this is likely to be conservative. The full perturbation equations with friction could be examined but the algebra would be extremely tedious. The full St-Venant equations also contain the physical instability of the formation of roll waves which can induce unstable numerical calculation for some schemes, See Samuels (1985).

5.6 Semi implicit time stepping

5.6.1 The Galerkin equations

The approximation is based upon the following mathematical model equations

$$\partial_t h + \underline{\nabla}.\underline{q} = 0 \qquad (5.67)$$

$$\partial_t \underline{u} + \underline{u}.\underline{\nabla}\,\underline{u} + g(\underline{\nabla} h + \underline{q}|\underline{q}|/K^2) = 0 \qquad (5.68)$$

The water level approximation H is piecewise linear in each element and the unit flow vector $\underline{Q}$ ($D\underline{U}$) is piecewise constant. We use a θ-weighting method in time and a Galerkin method

in space. Suppose that Θ_c and Θ_d are the time weighting coefficients for the continuity and dynamic equations respectively. The Galerkin equations are

$$< H^{n+1} - H^n, \phi_j > -$$
$$\Delta t \{\Theta_c < \underline{Q}^{n+1}, \underline{\nabla} \phi_j > + (1-\Theta_c) < \underline{Q}^n, \underline{\nabla} \phi_j >\} = 0 \qquad (5.69)$$

$$(1/g\Delta t) < \underline{Q}^{n+1}/D^{n+1} - \underline{Q}^n/D^n, \chi_k > + < \underline{c}^n, \chi_k > +$$
$$\Theta_d [< \underline{\nabla} H^{n+1}, \chi_k > + < Q^{n+1}|\underline{Q}^{n+1}|/(K^{n+1})^2, \chi_k >]$$
$$+ (1-\Theta_d) [< \underline{\nabla} H^n, \chi_k > + < Q^n|\underline{Q}^n|/(K^n)^2, \chi_k >] = 0 \qquad (5.70)$$

where ϕ_j is a piecewise linear basis function and χ_k is piecewise constant. The convection term $\underline{c}$ is evaluated at the old time level and is a constant in each element. This, together with the local support of χ_k, allows equation (5.70) to be written as a vector equation in each element, thus

$$\alpha \underline{Q}^{n+1} + \beta \underline{Q}^{n+1}|\underline{Q}^{n+1}| + \underline{\gamma} = 0 \qquad (5.71)$$

where

$$\alpha = 1/(g\Delta t\, D^{n+1})$$
$$\beta = \Theta_d/(K^{n+1})^2$$
$$\underline{\gamma} = \Theta_d \underline{\nabla} H^{n+1} + \underline{T}^n$$
$$\underline{T}^n = \underline{c}^n + (1-\Theta_d) \{\underline{\nabla} H^n + Q^n|\underline{Q}^n|/(K^n)^2\} - \underline{Q}^n/(g\Delta t D^n) \quad .$$

In the computations the term $\underline{T}^n$ is calcuated and stored at the beginning of each time step. From equation (5.71) we deduce the quadratic for $|\underline{Q}^{n+1}|$:

$$\beta |\underline{Q}^{n+1}|^2 + K|\underline{Q}^{n+1}| - |\underline{\gamma}| = 0 \quad . \qquad (5.73)$$

This has two roots and we take the positive one to give

$$\underline{Q}^{n+1} = -\underline{\gamma}/(\tfrac{1}{2}\alpha + [(\tfrac{1}{2}\alpha)^2 + |\underline{\gamma}|\beta]^{\frac{1}{2}}) \quad . \qquad (5.74)$$

Thus in each element we have the value of $\underline{Q}^{n+1}$ in terms of the unknown water levels H^{n+1} and the known conditions at the start of the time step. We may substititue this value of $\underline{Q}^{n+1}$ into the continuity equation (5.69) to give an equation in terms of water level alone, thus achieving a reduction of the number of simultaneous equations that need be solved each time step. Defining $\Phi(H^{n+1})$ by

$$\Phi = \tfrac{1}{2}\alpha + \left[(\tfrac{1}{2}\alpha)^2 + \beta|\gamma|\right]^{\frac{1}{2}} \qquad (5.75)$$

$$= 1/(2g\Delta t D^{n+1}) + \left[1/(2g\Delta t D^{n+1})^2 + \Theta_d|\Theta_d \underline{\nabla} H^{n+1} + \underline{T}^n|/(K^{n+1})^2\right]^{\frac{1}{2}}$$

we may write the Galerkin equations for H^{n+1} as

$$< H^{n+1} , \phi_j > + \Theta_c \Delta t <(\Theta_d \underline{\nabla} H^{n+1} + \underline{T}^n)/\Phi , \nabla\phi_j > = R_j^n \qquad (5.76)$$

where the right hand side R_j^n is

$$R_j^n = <H^n , \phi_j > + \Delta t (1-\Theta_c) < \underline{Q}^n , \underline{\nabla}\phi_j > \quad . \qquad (5.77)$$

Like the coefficient $\underline{T}^n$ in the definition (5.72), R_j^n need only be computed at the start of each time step. Equation (5.76) is non-linear in H^{n+1} and may be solved iteratively by setting at each node i

$$H_i^{n+1(m+1)} = H_i^{n+1(m)} + \Delta H_i$$

where the index in parentheses (m) denotes iteration number. We expand all functions of H^{n+1} to first order ΔH_i to get a system of equations of the form:

$$\textstyle\sum_i A_{ij} \Delta H_i = b_j \quad . \qquad (5.78)$$

The coefficient matrix is in general non-symmetric and is composed of the sum of element matrices A_{ij}^e. The right hand side b_j is also formed by a sum of the elements thus

$$b_j = - \textstyle\sum_e b_j^e + R_j^n \qquad (5.79)$$

R_j^n is given by equation (5.77) and b_j^e by

$$b_j^e = \langle H^{n+1} , \phi_j \rangle + [\theta_c \Delta t / \Phi(H^{n+1})] \; [\theta_d \langle \underline{\nabla} H^{n+1} , \underline{\nabla}\phi_j \rangle + \langle \underline{T}^n , \nabla\phi_j \rangle] \quad . \tag{5.80}$$

The element matrices are defined by

$$A_{ij}^e = \langle \phi_i, \phi_j \rangle + [\theta_c \Delta t / \Phi] \{[\theta_d \langle \underline{\nabla} H^{n+1} , \underline{\nabla}\phi_j \rangle + \langle \underline{T}^n , \underline{\nabla}\phi_j \rangle] [-(\sigma^e + \tau_i^e)/\Phi] + \theta_d \langle \underline{\nabla}\phi_i, \underline{\nabla}\phi_j \rangle\} \tag{5.81}$$

with the parameters σ^e and τ_i^e determined in each element by

$$\sigma^e = -\{1/3\bar{D}\} \{1/(2g\bar{D}\Delta t) + [\tfrac{1}{2}\theta_d | \theta_d \underline{\nabla} H^{n+1} + \underline{T}^n | p/(K^{n+1})^2 + 1/(2g\Delta t\bar{D})^2] / [1/(2g\bar{D}\Delta t)^2 + | \theta_d \underline{\nabla} H^{n+1} + \underline{T}^n | \theta_d / (K^{n+1})^2]^{\frac{1}{2}}\} \tag{5.82}$$

$$\tau_i^e = \theta_d [(\theta_d \underline{\nabla} H^{n+1} + \underline{T}^n) . \underline{\nabla}\phi_i] / \{2(K^{n+1})^2 | \theta_d \underline{\nabla} H^{n+1} + \underline{T}^n | [1/(2g\Delta t\bar{D})^2 + | \theta_d \underline{\nabla} H^{n+1} + \underline{T}^n | \theta_d / (K^{n+1})^2]^{\frac{1}{2}}\} \quad . \tag{5.83}$$

In equation (5.82) the coefficient p is the power of the conveyence depth relation as in Section 2.2.2.

The first order variation equations for steady flow with convection are obtained by taking Δt arbitrarily large in equations (5.78) to (5.83) and setting θ_c and θ_d to one. The time index n now denotes the outer iteration on the convection term and the index m denotes inner iterations to solve for the water level for a given value of the convection term. The equations for the potential formulation for steady flow without convection are obtained with the additional simplification that $\underline{c}^n$ is zero which, in turn, leads to $\underline{T}^n = 0$.

Although the Galerkin equations have been written in terms of arbitrary values of the weighting coefficients Θ_c and Θ_d, the actual computations discussed later in this section used the value 1.0 for both. This gives the two-dimensional version of the situation discussed in Section 5.5. For all the computations steady water levels were given on the inflow and outflow boundaries. No attempt was made to devise non-reflecting boundary conditions which allow free passage of errors out of the flow domain.

5.6.2 The meandering channel

The time stepping approach was tested using the single meander geometry with short straight reaches to the inflow and outflow boundaries (see Meshes 2, 3 and 4 in Appendix 2). Firstly the roughness size was set to 36m, the value that produced stable calculation for the steady flow iteration. Since the method should be unconditionally stable, the time step was set to 10^5 seconds, ie, a Courant number, Cr, of about 8×10^3. The computation converged to machine accuracy in five time steps, mirroring the performance of the first order variation method of Section 5.3.5, and producing the same solution.

The next set of tests established the limit on the time step required for stability for higher velocities. The convergence parameter for unit flow rate for tests with roughness size of 0.36m is shown in Figure 5.20. With a time step of 10 seconds, Cr $\approx$ 8, the calculations diverged quite rapidly. For a time step of 2 seconds Cr $\approx$ 1.6 the calculations diverge more

slowly. For a time step of 1 second the calculations appeared at first stable but, after falling for the first 10 iterations, the convergence parameters began to rise slowly. Finally after setting the time step to 0.5 seconds the model was stable, with the convergence parameter for unit flow falling to a value of 0.01 (ie a 1% change each time step) at step 13 and remaining around that value till the computation was halted at step 30.

These first tests all used the standard set with banks to define the neighbouring elements in the convection term calculation, see Section 5.2.2. The definition was changed to the standard set alone (allowing the neighbour set to straddle the depth discontinuity) and the calculations repeated for the 1.0 and 0.5 second time steps. The calculations still began to diverge for the 1.0 second step but at a lower rate, see Figure 5.20. The transverse water surface profiles for the two runs with a 0.5 second time step are shown on Figure 5.21. The profiles are similar in shape but the calculations without banks show a general raising of water level and a shallower surface slope. This method of calculating the convection term can be expected to introduce a larger numerical diffusion into the computations, and the comparison in the results supports this, taking account of the effect of a diffusion term modelling the turbulent stresses discussed in Section 2.4.2. The use of the upwind neighbour set (with banks) was also tested; the results plotted for the centre of the meander in Figure 5.2.2 are clearly different from the standard set and Sooky's experiments (Fig 5.10). The algorithm used to provide an upwind approximation was therefore not tested further.

At this point in the research the computer at HR Ltd was changed and the new ICL 2972 machine had a lower precision of single length arithmetic. This change from 11 digits to 7 digits precision had little effect on the calculations except that the convergence parameters would not decrease below $0(10^{-7})$. Thus the numerical approximations are in practice reasonably well conditioned.

The work of Levine (1985) shows that the error in sampling the gradient of a piecewise linear function over a triangular mesh is related to the topology of the mesh connections see Appendix 2. The topology of Mesh 2 is irregular with 5, 6 or 7 nodes being connected to each interior node. The triangulation was adjusted giving Mesh 3 which was regular, having 6 connections to each interior node. This revision, however, produced no significant changes in the computed water levels, with differences being of the order of a few parts in 10^5.

A roughness size of 0.36m as used in the tests above is still, however, much greater than the physical roughness of an experimental flume. The computations therefore were repeated with a roughness of 0.0036m, which is about the prototype value, and a time step of 0.1 seconds. The flow velocities were about 0.41m/s in the channel and 0.21m/s on the flood plain, with a total discharge of $0.101m^3/s$. These values are about 20% higher than Sooky's experiments on his Geometry 4 on

which the calculations are loosely based. No attempt has been made to calibrate the computational model, the key point being that the computations are no longer explosively unstable. The time step of 0.1 second did, however, appear to be too large as the convergence parameter for discharge was increasing slowly whilst the parameter for depth (on the first inner iteration) was falling slowly during the test, see Table 5.7.

TABLE 5.7

CONVERGENCE PARAMETERS (ROUGHNESS 3.6 MM TIME STEP 0.1s)

Time	Depth at inner iteration			Unit
step	1	2	3	flow
1	2.68(-2)	9.76(-5)	1.32(-6)	2.92(-2)
2	2.85(-2)	8.48(-5)	1.89(-6)	3.39(-2)
3	1.95(-2)	3.10(-5)	1.45(-6)	4.13(-2)
4	1.40(-2)	2.59(-5)	1.46(-6)	3.56(-2)
5	1.15(-2)	1.55(-5)	1.26(-6)	3.59(-2)
6	8.82(-3)	9.45(-6)	1.36(-6)	3.85(-2)
7	1.03(-2)	7.95(-6)	1.52(-6)	4.61(-2)
8	1.12(-2)	1.15(-5)	1.44(-6)	5.00(-2)
9	1.077(-2)	1.19(-5)	1.33(-6)	5.14(-2)
10	8.86(-3)	1.03(-5)	1.37(-6)	5.14(-2)

The linear dimensions of the mesh were all scaled by a factor 100 (Mesh 4), which implies a scaling of 10 for velocity and time to maintain Froudian similarity, see Henderson (1966), and a discharge scale of 10^5. The flow was calculated with a

roughness size of 0.36m which should produce results similar to the flume geometry with roughness 0.0036m. For a time step of 10 seconds the computations diverged. For a time step of 1 second the results were similar to those obtained in the corresponding test of Mesh 3 with a step of 0.1 seconds. Variations of a few parts in 10^6 for water level, 10^5 for velocity and 10^4 for the convection term, were apparent and the convergence parameters for each time step and inner iteration were nearly identical.

Finally a time step of 0.5 seconds was tested for the scaled mesh. This was stable with the convergence parameters shown on Figure 5.23 and the variation of water level across the centre of the mesh shown on Figure 5.24. The difference in water level across the channel (0.5m) is consistent with Sooky's experiments, allowing for the appropriate scale factors. Some of the principal parameters of the flow are:

	Flood Plain	Channel
depth	2.0m	6.1m
velocity	2.1m/s	4.1m/s
Froude number	0.47	0.53
Total width	97m	21m

The total discharge was $1010m^3/s$; the streamwise surface slope was 0.0016 and the transverse slope up to 0.02 locally. These flow conditions are possibly more severe than those in many UK rivers in flood. It should be noted that in some parts of the flow the convection term dominated the friction slope by a factor of about 15.

5.6.3 Tallahala Creek data

The time stepping method was applied to Mesh 9 which represents Tallahala Creek with Chezy roughness coefficients taken from Tseng (1975). The initilisation of the calculations involved a solution of the steady flow equations without convection using the first order variation method. In contrast to the flume based tests this converged only slowly with the asymptotic rate being $(0.783)^n$. Computations were carried out for 5 two second steps at which time the water depth changed by a maximum of 0.8% and the unit flow magnitude by 20%. In all time steps the maximum changes occurred in the throat of the contraction between the two embankments leading to the bridge. Figure 5.25 shows contours of water level at the end of the initialisation with zero convection. At the end of five time steps the only water levels which changed by more than 0.05m were in the throat of the contraction where decreases up to 0.15m occurred. The results for Tseng (1975) and Franques and Yannitell (1974) are shown on Figures 5.26 and 5.27 respectively. The contours of Figure 5.25 are closer to Tseng's results then those of Franques and Yannitell. An important feature is that, without the convection term, the water level difference through the contraction is nearly the same as the observations in Tseng (1975). This indicates that the head loss is probably due to frictional resistance on the increased length of streamlines.

A modification to the updating of water level was tried to improve the convergence of the level iterations. A relaxation

parameter of 0.5 was used for all nodes where the update was of opposite signs to the previous one at the node. This was invoked at up to 15% of the nodes on the mesh at any one iteration, but not consistently at any location. However it only marginally improved the convergence rate and did not significantly change the calculated water levels.

5.7 Concluding remarks

The least squares recovery method for obtaining the convection term has not produced acceptable results in all cases despite having some attractive properties. For iteration on the steady flow equations the method converged only for unrealistically low velocities. The method based upon time stepping stabilised the computations, dependent upon time step. It produced results for a scaled up version of the Sooky's (1964) flume data which had physical parameters that are comparable to intended engineering applications. The calculations did not give a steady state for steady water levels on the flow boundaries but depths and velocities varied between about 0.1 and 10% depending upon the time step. An interpretation of this behaviour is that evaluating the convection term introduces errors at each time step which are propagated out of the computational domain.

Further work on the method is required before it can be applied in earnest to practical problems. The accuracy of the computed convection term should be investigated as should be the poor performance of the iteration for water level for the Tallahala Creek data. It is not clear whether higher order of

approximation for the velocity or unit flow field may in fact be required for practical applications.

CHAPTER 6

CONCLUSIONS AND RECOMMENDATIONS

6.1 The mathematical model

6.1.1 Depth integration

The integration of the convective accelerations through the depth of the flow requires particular care. The velocity variation with depth may be considered either before or after (the usual approach) the depth integration. Treating the vertical structure before the depth integration gives equation (2.30). Solutions of this equation can have significantly different character from those of the usual approach, equation (2.37). The usual formulation can predict flows which have recirculation when the alternative formulation can have no closed streamlines. In the usual formulation it is argued that the depth variation of plan velocity produces terms analogous to the turbulent stress terms. However, it is known that they are of an order or more greater in magnitude than typical values of the turbulent stress. The use of dynamic equation (2.30) gives a hyperbolic set of equations in the absence of turbulent stresses whereas the use of equation (2.37) gives an incompletely parabolic system requiring different boundary data. These points are of practical importance outside the area of river flow modelling.

6.1.2 Turbulent stress terms

The effect of these terms on the lateral velocity distribution has been quantified through a new analytic solution for rectangular geometry, equation (2.42). This leads to estimates of shear layer width at the boundary between the flood plain and an incised river channel. It indicates that the shear layers from the banks interact in the main channel with the velocity not achieving the free stream value. This is consistent with the difference between computed results which ignore the turbulent stresses and Sooky's (1964) experiments. The form of the transverse velocity profile should be examined experimentally in more detail to confirm whether the simple mixing length hypothesis which underlies equation (2.42) is in fact valid for these flows.

6.2 The stream function formulation

The published iteration of Franques and Yannitell (1974) converged extremely slowly. The first order variation method, Section 3.4.3, has a much superior performance and produced good results for tests based upon Sooky's flume data. The method however produced poor results, both in terms of convergence rate and predicted water levels on the inflow boundary, for the Tallahala Creek data. Further work is required to identify why the iteration converged slowly on this geometry. The streamline integration algorithm needs to be improved to include in some manner the property that contours of the water level and stream function should be mutually orthogonal.

6.3 Primitive variable formulation

The first order variation form of the potential formulation converged rapidly when applied to the flume geometry when the convection term was excluded. When the convection term was incorporated into the model again the method converged but only for sufficiently slow flows. This limit has been explained by an analysis of the iterative method.

The algorithm used to calculate the convection term is new. It recovers the first derivatives of a piecewise constant velocity field by least squares fitting. The algorithm produces results which are consistent with a first order analytical solution of flow in a bend and with observations in an experimental flume. The method, however, has its limitations. Although the use of a time stepping method allowed stable computations for all flow velocities tested for the flume geometry, the time step required was small. A true steady state was not achieved despite the application of steady water levels at the flow boundaries. Further work is necessary before the method can be applied in practice. Attention should be directed to:

1 the comparison of the computed and first order analytic solution for flow in a bend at higher velocities;
2 widening the limit on time step for the method to be stable;
3 improving the performance of the inner iteration for water level for the Tallahala Creek data.

Improving the limit on time step will probably require a revision of the calculation of the convection term, weighting

the term towards the forward time level. This will lead to a larger set of linear equations to solve, as the elimination of the unit flow variables as in Section 5.6.1 will no longer be possible.

An alternative procedure could be to use a higher order approximation for the unit flow vector in the form of an approximately divergence-free element. This will have the advantage of readily being able to represent a diffusion type model of the turbulent stress terms, since then the flow equations are similar to the Navier-Stokes equations. However, there is a relationship between the orders of approximation that can used for the primitive variables and this will need to be examined along the lines of the work of Girault and Raviart (1979).

The model of flow without turbulent stress terms will incorporate some of the effects of these terms through its calibrated roughness values. If the turbulent stress terms are included and the roughness is unchanged, the distribution of flow between the channel and flood plain will change. As with the stream function formulation the proportion of the flow in the main channel was higher in the computations of the potential formulation then in Sooky's experiments.

6.4 Remarks on practical applications

For the low velocities used for the initial tests of the potential formulation with convection, the flow in the channel and flood plain geometry appeared insensitive to variations in

boundary data. The water surface slope was determined by the local bed geometry. This suggests that the boundaries in a practical application need not be removed too far from the area of interest provided that a line normal to the flow direction can be assessed. No tests, however, have been done on changing the alignment of the inflow or outflow boundary. Such sensitivity tests should be part of a practical application.

The potential formulation is complementary to the stream function formulation in the nature of the boundary conditions. When water levels are known at either end of the flow domain, as is usual in the case of calibration, the roughness will be adjusted to achieve the correct discharge (and interior water levels etc, where known). In the stream function formulation the roughness will be adjusted to achieve the correct water level on the upstream flow boundary. Such adjustments may be manual or done automatically in an outer iteration around the methods discussed in this thesis. Since friction losses are dominant for river flow, calibration should initially proceed on the assumption that the convection is zero. Final refinements may be made by including the convection term if an analysis of the velocities and curvature of the flow without convection suggest that this term may be significant.

In the design situation typically the water level is given at the downstream end of the flow domain and the total discharge is known. These are precisely the boundary data for the stream function formulation. In the potential formulation the total discharge will be obtained by adjusting the water level on the inflow boundary.

A difficulty in using the common cell-type flood plain model has been demonstrated in Section 1.4. For a river type link the conveyence function for a link between cells depends upon the velocity direction. This implies that a calibrated value may not be appropriate for design purposes where the flow direction changes. This feature is not reported in any of the references to cell type models cited in Chapter 1, and represents a serious limitation of the method.

6.5 Extensions to the mathematical model

The obvious extensions of the model equations from the computations presented in this thesis are:

1 to include the velocity distribution coefficient α in the convection term

2 to include the turbulent stress terms

The analysis of Chapter 2 and Appendix 1 indicates there should be no fundamental problem in the first of these extensions. Any model of the turbulent stress terms will change the boundary data requirements and possibly increase the number of equations to be solved.

A third extension of the model is to allow free boundaries at the edges of the flood plain. Currently these no flow boundaries are assumed fixed during the computation. This will probably require an additional level of iteration to determine the location of the edge of the flow. Finally some means must be found to incorporate structures such as weirs, sluices, flumes and raised embankments in the model. At these sites the

vertical accelerations and curvature of the water surface are not small and one of the assumptions behind the two dimensional equations is invalid. A penalty function approach could be used to replace the standard dynamic equation with the head-discharge relationship for the appropriate structure.

REFERENCES

ABBOTT M B (1979) : Computational Hydraulics; Elements of the Theory of Free Surface Flows, Pitman, London.

ACKERS P (1958) : Resistance of fluids flowing in channels and pipes, Hydraulics Research Paper No. 1, HMSO, London.

BATCHELOR G K (1967) : Introduction to fluid dynamics. Cambridge University Press.

CHORLEY R (1969) : Introduction to Fluvial Processes, University Paperbacks, Methuen, London.

CONNOR J J and BREBBIA C A (1976) : Finite Element Techniques for fluid flow, Newnes-Butterworth, London.

CUNGE J A (1971) : Schematisation des champs d'inondation dans les modeles mathematiques fluviaux, Proc. IAHR XIV Congress, Paris, Vol 5.

CUNGE J A (1975) : Two dimensional modelling of flood plains. Chap 17 of Unsteady flow in open channels. Ed. Mahmood & Yevjevich, Water Resources Publications, Colorado.

CUNGE J A, HOLLY F M and VERWEY A (1980) : Practical aspects of computational river hydraulics, Pitman.

DAUBERT A and GRAFFE O (1967) : Quelques aspects des ecoulements presque horizontaux a deux dimensions en plan et non permanents application aux estuaries. (Some aspects of near horizontal two-dimensional flow and their application to estuaries), Houille Blanche, pp 847-860 (in French).

DRONKERS J J (1964) : Tidal computations in rivers and coastal waters, North-Holland Publishing Company, Amsterdam.

FALCONER R (1977) : Mathematical modelling of jet-forced circulation in reservoirs and harbours, PhD Thesis, Department of Civil Engineering, Imperial College, London.

FRANQUES J T and YANNITELL D W (1974) : Two dimensional analysis of backwater at bridges., J. Hydr. Div. ASCE, vol 100 no HY3, pp 379-392.

FROIDEVAUX H (1975) : A finite element method for solving non-linear boundary value problems, Mathematics of finite elements and its applications (MAFELAP) II, ed J R Whiteman, Academic Press, London, pp 217-224.

GARABEDIAN P (1964) : Partial Differential Equations, John Wiley.

GIRAULT V and RAVIART P A (1979) : Finite element approximation of the Navier-Stokes equations, Lecture Notes in Mathematics No 749, Springer-Verlag, Berlin.

GRIFFITHS D F (1977) : Finite elements for incompressible flow, Report NA/23, Department of Mathematics, University of Dundee.

GRIJSEN J G and MEIJER Th. J G P (1979) : On the modelling of flood flow in large river systems with flood plain. Proc. 18th Congress of IAHR paper Dd 8.

GUSTAFSSON B and SUNDSTROM A (1978) : Incompletely parabolic problems in fluid dynamics. Soc. Ind. Appl. Math. J. Appl. Math, Vol 35, No. 2, September, pp343-357.

HEAPS N S (1969) : A two dimensional numerical sea model, Phil Trans Roy Soc, Vol 265, pp93-137.

HENDERSON F M (1966) : Open Channel Flow, McMillan Company, New York.

HERRLING B (1978) : Computation of shallow water waves with hybrid finite elements. Adv in water resources, Vol 1, December, pp313-320.

HERRLING B (1982) : Coupling one and two dimensional finite elements for the computation of tidal flow in estuaries, Adv. in water resources, Vol 5, December, pp227-232.

HOLTZ P and NITSCHE G (1980) : Tidal wave analysis for estuaries with inter-tidal flat. Proc. 3rd. Int. Conf. on Finite Elements for Water Resources. pp5113-5126.

HOOD P (1976) : Frontal solution program for unsymmetric matrices, Int. J. for Nun Meth Engng Vol 10 pp 379 to 399.

HOOD P (1977) : Note on Frontal Solution Program for Unsymmetric Matrices. Int. J. For Num. Meth, in Engng, Vol 11, p1055.

IRONS B M (1970) : A frontal solution program for finite element analysis, Int. J. Num. Meth. Engng, Vol 2, p5-32.

KALKWIJK J G, Th. and De Vriend H J (1980) : Computation of flow in shallow river bends. J. Hydr. Res. Vol 18 no 4.

KATOPODES N D (1980) : Finite element model for open channel flow near critical conditions, Proc. 3rd International Conference on Finite Elements in Water Resources, The University of Mississippi, Mississippi, USA.

KING I P and NORTON W R (1978) : Recent applications of RMA's finite element models for two dimensional hydrodynamics and water quality, Proc. 2nd International Conference on Finite Elements in Water Resources, Imperial College, London.

KNIGHT D W, DEMETRIOU J D and HAMED M E (1983) : Hydraulic analysis of channels with flood plains, Paper E1, pp129-144, Proc. International Conference on the Hydraulic Aspects of Floods and Flood Control (London, UK), September 13-15, Cranfield UK, BHRA Fluid Engineering.

KUIPERS J and VREUGDENHIL C B (1973) : Calculations of two-dimensional horizontal flow, Report S163-I, Delft Hydraulics Laboratory, Delft, The Netherlands.

LEAN G H and WEARE T J (1979) : Modelling two-dimensional circulating flow, Jnl Hydraulics Div ASCE, Vol. 105, HY1, pp17-26.

LEE J K (1980) : Two-dimensional finite element analysis of the hydraulic effect of highway bridge fills in a complex flood plain, Proc. 3rd International Conference on Finite Elements in Water Resources, The University of Mississippi, Mississippi, USA.

LEENDERTSE J J (1967) : Aspects of a computational model for long period water wave propagation, Memorandum RM-5294-PR, RAND Corporation, Santa Monica, California.

LESLEIGHTER E J (1983) : Flood plain flow using a two-dimensional numerical solution, Paper G2, pp207-215, Proc. International Conference on the Hydraulic Aspects of Floods and Flood Control (London, UK), September 13-15, Cranfield UK, BHRA Fluid Engineering.

LEVINE N (1985) : Superconvergent estimation of the gradient from linear finite element approximations on triangular elements, Numerical Analysis Report No. 3/85, Dept. of Mathematics, University of Reading.

LEWIN J and HUGHES D (1980) : Welsh flood plain studies II, application of a qualitative inundation model. Jnl. Hydrology. Vol 46 no 1/2 pp35-50.

MILITEEV A N and SHKOLNIKOV S Y (1981) : Numerical modelling of two-dimensional river flows in plan during floods. Preprints from IAHR conference on numerical modelling of river channel and overland flow, etc., Bratislava, May 4-8.

MILLER J J A (1971) : On the location of zeroes of certain classes of polynominals with applications to numerical analysis, Jnl. Inst. Math. Applics. Vol 8, pp397-406.

MOULT A (1980) : An upwind finite element formulation for convection or buoyancy dominated flows in rivers, bays and estuaries. Proc, 3rd International Conference on Finite Elements in Water Resources, The University of Mississippi, Mississippi, USA.

NIEMEYER G (1979) : Efficient simulation of non-linear steady flow, Jnl. Hydr. Div. ASCE. Vol 105 no HY3 pp185-195.

NOVAK P and CABELKA J (1981) : Models in Hydraulic Engineering - Physical Principles and Design Applications, Pitman, London.

OLIGER J and SUNDSTROM A (1978) : Theoretical and practical aspects of some boundary value problems in fluid dynamics. SIAM. Jnl. on Appl. Math. Vol 35 no 3 pp419-446.

PRICE R K (1980) : River Soar - study of flood alleviation HRS Report Ex 940.

PRICE R K and SAMUELS P G (1980) : A computational hydraulic model for rivers. Proc. Instn. Civ Engrs. Part 2, Vol 69, March, pp87-96.

REYNOLDS A J (1974) : Turbulent Flows in Engineering, John Wiley & Sons, London.

RICHTMYER R D and MORTON K W (1967) : Difference methods for initial-value problems, Interscience Publishers.

ROACHE P J (1972) : Computational Fluid Dynamics, Hermosa Publishers.

RODI W (1980) : Turbulence models and their application in hydraulics. IAHR state of the art paper, Delft, The Netherlands, IAHR Secretariat.

ROUSE H (1959) : Advanced mechanics of fluids, Wiley, New York.

SAMUELS P G (1979) : EMBER a numerical model of flow in an embanked river, Report IT183, Hydraulics Research, Wallingford.

SAMUELS P G (1983a) : Two-dimensional modelling of flood flows using the finite element method, Paper G4, pp229-240, Proc. International Conference on the Hydraulic Aspects of Floods and Flood Control (London, UK), September 13-15, Cranfield UK, BHRA Fluid Engineering.

SAMUELS P G (1983b) : Computational modelling of flood flows in embanked rivers, Paper H1, pp257-270, Proc. International Conference on the Hydraulic Aspects of Floods and Flood Control (London, UK), September 13-15, Cranfield UK, BHRA Fluid Engineering.

SAMUELS P G (1985) : Modelling open channel flow using Preissmann's scheme, Proc. 2nd International Conference on the Hydraulics of Floods and Flood Control (Cambridge, UK, 24-26 September), Cranfield UK, BHRA Fluid Engineering.

SAMUELS P G and GRAY M P (1982) : The FLUCOMP river model package : an engineer's guide, Report Ex 999, Hydraulics Research, Wallingford.

SCHMITZ G, SEUS G J and CZIRWITZKY H J (1983) : Simulating two-dimensional flood flow, Paper G1, pp195-206, Proc. International Conference on the Hydraulic Aspects of Floods and Flood Control (London, UK), September 13-15, Cranfield UK, BHRA Fluid Engineering.

SOOKY A A (1964) : The flow through a meander flood plain geometry. PhD Thesis, Purdue University, (65-2647, University Microfilms Inc, Ann Arbor, Michigan).

STRANG G and FIX G J (1973) : An analysis of the finite element method Prentice Hall Inc, New Jersey.

SU T Y, WANG S Y and ALONSO C V (1980) : Depth-averaging models of river flows, Proc. 3rd International Conference on Finite Elements in Water Resources, The University of Mississippi, Mississippi, USA.

TAGG A F and SAMUELS P G (1984) : Numerical modelling of embanked rivers, Report IT 274, Hydraulics Research, Wallingford.

TAYLOR C (1976) : A computer simulation of direct run-off, Proc. 1st Conference on Finite Elements in Water Resources, Princeton University, USA.

TEMAM R (1977) : Navier-Stokes equations. North Holland, Amsterdam.

THIENPONT M and BERLAMONT J (1980) : A finite element solution for depth-averaged two-dimensional Navier-Stokes equations for flows in rivers and channels, Proc. 3rd International Conference on Finite Elements in Water Resources, The University of Mississippi, Mississippi, USA.

THIRRIOT C and GAUDU R (1971) : Du reseau maille de conduites aux ecoulements d'innodation dans les plaines, Proc. 14th Conf. IAHR, Vol 5, p213.

TSENG M T (1975) : Evaluation of flood risk factors in the design of highway stream crossing. Vol III. Finite element model for bridge backwater computation, Report No FHWA-RD-75-53, Offices of Research & Development, Federal Highway Administration, Washington, D.C, USA.

VERBOOM G K, STELLING G S and OFFICIER M J (1982) : Boundary conditions for the shallow water equations, chapter 11 in Engineering Applications of Computational Hydraulics - Vol 1, ed by Abbott M B and Cunge J A, Pitman, London.

VREUGDENHIL C B and WIJBENGA J H A (1982) : Computation of flow patterns in rivers, Proc. ASCE, Journal of the Hydraulic Division, Vol 108 (HY11).

WEISS H W (1976) : An integrated approach to mathematical flood plain modelling, Report no 5/76 Hydrological Research Unit, University of Witwatersrand, Johannesburg, S.A.

ZANOBETTI D, LORGERE H, PREISSMANN A and CUNGE J A (1968) : Le modele mathematique due delta du Mekong, La Houille Blanche, No 1, 4 and 5.

ZIELKE W and URBAN W (1981) : Two-dimensional modelling of rivers with flood plains. Pre-prints of IAHR Conference on numerical modelling of river channel and overland flow. Bratislava May 4-8.

ZIENKIEWICZ O C (1977) : The finite element method, McGraw-Hill, London, (3rd Edn).

APPENDIX 1

The Characteristics of the Unsteady Flow Equations

We examine here the unsteady flow equations including the convective accelerations:

$$\partial_t h + \underline{\nabla} \cdot \underline{q} = 0 \qquad \text{A1.1}$$

$$\partial_t \underline{q} + \underline{\nabla}.(\alpha \underline{q}\underline{q}/D) + gD\underline{\nabla}h + gD\underline{q}|\underline{q}|/K^2 = 0 \qquad \text{A1.2}$$

This pair of equations may be written as a first order system thus:

$$I\ \partial_t \underset{\sim}{U} + A(\underset{\sim}{U})\ \partial_x \underset{\sim}{U} + B(\underset{\sim}{U})\ \partial_y \underset{\sim}{U} + \underset{\sim}{C}(\underset{\sim}{U}) = 0 \qquad \text{A1.3}$$

Here $\underset{\sim}{U}$ represents the solution variables $(\underline{q}, h)^t$, I is the identity matrix, $\underset{\sim}{C}$ embodies the low order terms (bed friction and bed gradient) and A and B are given below.

$$A = \begin{bmatrix} 2\alpha U & 0 & c^2 - \beta U^2 \\ \alpha V & \alpha U & -\beta UV \\ 1 & 0 & 0 \end{bmatrix} \qquad \text{A1.4}$$

$$B = \begin{bmatrix} \alpha V & \alpha U & -\beta UV \\ 0 & 2\alpha V & c^2 - \beta V^2 \\ 0 & 1 & 0 \end{bmatrix} \qquad \text{A1.5}$$

In equations (A1.4) and (A1.5), $c = (gD)^{\frac{1}{2}}$, the gravity wave speed, and $\beta = \alpha - D\partial_h \alpha$.

We determine the geometry of the characteristics by arguments

that follow quite closely Daubert and Graffe (1967) who established the characteristics of the shallow water equations. We will find that the general equations (A1.1) and (A1.2) do indeed have characteristics identified by Daubert and Graffe in the special case $\alpha = 1$, but other values of α can give rise to bicharacteristic surfaces of a different topological nature.

Following Garabedian (1964) the system has characteristic surfaces defined by:

$\phi(\underline{x}, t) = \text{constant}$

where ϕ is determined by the equation:

$$\det(I\,\partial_t \phi + A\,\partial_x \phi + B\,\partial_y \phi) = 0. \qquad \text{A1.6}$$

Substituting for A and B and carrying out some elementary row operations on the determinant reduces it to:

$$\begin{vmatrix} T(\phi) & 0 & -G_u(\phi) \\ 0 & T(\phi) & -G_v(\phi) \\ \partial_x \phi & \partial_y \phi & \partial_t \phi \end{vmatrix} = 0 \qquad \text{A1.7}$$

where:

$$T(\phi) = \partial_t \phi + \alpha U \partial_x \phi + \alpha V \partial_y \phi$$

$$G_u(\phi) = -(c^2 - \beta U^2)\partial_x \phi + \beta UV \partial_y \phi - \alpha U \partial_t \phi$$

$$G_v(\phi) = \beta UV \partial_x \phi - (c^2 - \beta V^2)\partial_y \phi - \alpha V \partial_t \phi.$$

Thus the characteristic surfaces are given by:

$$T\,(T\partial_t \phi + G_u \partial_x \phi + G_v \partial_y \phi) = 0. \qquad \text{A1.8}$$

The roots of this equation are:

$$\partial_t \phi + \alpha U \partial_x \phi + \alpha V \partial_y \phi = 0 \qquad \text{A1.9}$$

and

$$(\partial_t \phi)^2 + 2UV\beta\, \partial_x \phi \partial_y \phi + 2\alpha U \partial_t \phi \partial_x \phi + 2\alpha V \partial_t \phi \partial_y \phi$$
$$+ \beta U^2 (\partial_x \phi)^2 + \beta V^2 (\partial_y \phi)^2 - c^2 \left[(\partial_x \phi)^2 + (\partial_y \phi)^2 \right] = 0$$

which may be written as:

$$(\partial_t \phi + \alpha U \partial_x \phi + \alpha V \partial_y \phi)^2 - c^2 \left[(\partial_x \phi)^2 + (\partial_y \phi)^2 \right]$$
$$- (\alpha^2 - \beta)\, (U \partial_x \phi + V \partial_y \phi)^2 = 0. \qquad \text{A1.10}$$

We may determine the local form of the characteristic surfaces by considering the envelope of the planes tangent to them. Without loss of generality we may take the x axis to be aligned with the local flow direction and examine the characteristic surfaces that pass through the origin. Furthermore we assume the quantities U, V, c, α and β are constants with their values taken at the origin. The general equation of a plane $\phi(x,y,t)$ through the origin is:

$$\phi = x\phi_x + y\phi_y + t\phi_t = 0. \qquad \text{A1.11}$$

For the first family of characteristics we combine (A1.11) and (A1.8) to give:

$$\phi_x (x - \alpha U t) + y\phi_y = 0 \qquad \text{A1.12}$$

which is the equation of all planes containing the line

$$x = aUt; \quad y = 0 \qquad \text{A1.13}$$

For the second family of characteristics we combine (A1.11) and (A1.10) to give:

$$(x - \alpha U t)\phi_x + y\phi_y = \pm t \left[c^2 (\phi_x^2 + \phi_y^2) + (\alpha^2 - \beta U^2 \phi_x \right]^{\frac{1}{2}} \qquad \text{A1.14}$$

To identify the shape of the envelope of these planes consider

the intersection with the plane $t = t_0$ and move the origin to the point $(\alpha U t_0, 0, t_0)$. Also let $\phi_x = r\cos\theta$ and $\phi_y = r\sin\theta$ with $0 < \theta < 2\pi$ to account for the choice of sign in equation (A1.14), then:

$$x'r\cos\theta + y'r\sin\theta = ct_0 r\,(1 + k\cos^2\theta)^{\frac{1}{2}} \qquad \text{A1.15}$$

where $k = (\alpha^2 - \beta)\,U^2/c^2$, and x' and y' are co-ordinates with respect to the new origin.

Changing to polar co-ordinates (ρ, ζ) we have:

$$\rho\cos\zeta\cos\theta + \sin\zeta\sin\theta = ct_0\,(1 + k\cos^2\theta)^{\frac{1}{2}}. \qquad \text{A1.16}$$

Differentiating with respect to θ we have:

$$-\rho\cos\zeta\sin\theta + \rho\sin\zeta\cos\theta = ct_0 k\cos\theta\sin\theta(1+k\cos^2\theta)^{-\frac{1}{2}}. \qquad \text{A1.17}$$

Squaring and adding (A1.16) and (A1.17):

$$\rho^2\left(\cos^2(\zeta-\theta) + \sin^2(\zeta-\theta)\right) =$$

$$c^2t_0^2\left[(1+k\cos^2\theta)^2 + k^2\cos^2\theta\sin^2\theta\right](1+k\cos^2\theta)^{-1}$$

$$\text{or}\quad \rho(\theta) = \rho_0\left(1+(2k+k^2)\cos^2\theta\right)^{\frac{1}{2}}(1+k\cos^2\theta)^{-\frac{1}{2}} \qquad \text{A1.18}$$

where $\rho_0 = ct_0$.

Combining (A1.16) and (A1.18) we have:

$$\cos(\zeta-\theta) = (1 + k\cos^2\theta)\left(1 + (2k + k^2)\cos^2\theta\right)^{-\frac{1}{2}}. \qquad \text{A1.19}$$

The locus of the points given by the polar co-ordinates (ρ, ζ) may be plotted to give the intersection of the characteristic surfaces in the plane $t = t_0$. Firstly, in the case $k = 0$ (eg. $\alpha = \beta = 1$), the intersection is seen to be $\rho = \rho_0$, $\zeta = 0$ for

$0 < \theta < 2\pi$. This is the circle found by Daubert and Graffe (1967). From equation (A1.19) $\zeta = \pi/2$ if $\theta = \pi/2$ or if:

$\sin\theta = (1 + k\cos^2\theta)\ (1 + (2k + k^2)\cos^2\theta)^{-\frac{1}{2}}$.

This latter condition is satisfied when

$(1 + (2k + k^2)\cos^2\theta)(1 - \cos^2\theta) = 1 + 2\cos^2\theta + k^2\cos^4\theta$,

ie. $(k^2 - 1)\cos^2\theta = 2(k^2 + 1)\cos^4\theta$

ie. $\cos^2\theta = (k^2 - 1)/2(k^2 + 1)$ A1.20

This equation has real roots for θ provided that k lies outside the interval (-1, 1). Fig A1.1 shows the different curves that the point (ρ, ζ) traces out from equations (A1.18) and (A1.19) as θ varies. There are seven different cases depending upon the value of the parameter k which is related to the velocity distribution coefficient α by

$k = \alpha^2 - \alpha + D\partial_n\alpha$ A1.21

(a) $k < -1$ The locus is a hyperbola.

(b) $k = -1$ The locus is degenerate consisting of the two points $\rho = \rho_0$, $\zeta = \pm \pi/2$.

(c) $-1 < k < 0$ The locus is an ellipse with the minor axis on the line $\zeta = 0$.

(d) $k = 0$ The locus is a circle radius ρ_0.

(e) $0 < k < 1$ The locus lies between the circles $\rho = \rho_0$ and $\rho = (1+k)^{\frac{1}{2}}\rho_0$, but it is not an ellipse. The curve touches the inner circle at $\zeta = \pm\pi/2$.

(f) $k = 1$ The locus is similar to case (e) but a

cusp forms at the point of contact with the inner circle.

(g) $k > 1$ The locus still lies between the two circles $\rho = \rho_0$ and $\rho = (1+k)^{\frac{1}{2}}\rho_0$ but it now has loops centred on the line $\zeta = \pm\pi/2$.

Flows of practical interest will give values of k in the range (-1, 1). For example, at a Froude number of 1, $U = (gD)^{\frac{1}{2}}$ and then k is only greater than one if the exponent p of equation (2.31a) is greater than $(\sqrt{5} + 1)/2$; much larger than the typical values observed. Also κ can only be negative if $\partial_n \alpha$ is large and negative; again this is unlikely to occur in practice.

The envelope of the tangent planes of the second family of characteristics may now be seen to be a skewed cone for $-1 < k < 1$ with its axis along the same line as the common line, equation (A1.13) of the first family of characteristics. For k = 0 the intersection of this cone with the plane t = constant is a circle; for k negative it is an ellipse and for k positive it is the more complicated figure described above. The entire cone will lie on one side of the plane x = 0 for $t > 0$ if:

$$\alpha U t > \rho_0 (1 + k)^{\frac{1}{2}}. \qquad \text{A1.22}$$

Substituting for ρ_0 and k we obtain the condition:

$$\alpha Fr > \left((\alpha Fr)^2 + 1 - \nu^2\right)^{\frac{1}{2}} \qquad \text{A1.23}$$

where ν^2 is defined by equation (2.76). This condition is satisfied if $\nu^2 > 1$ which is identical to the condition for the steady flow equations to have three real characteristics, see section 2.6.2.

APPENDIX 2

The Mesh Geometries

The calculations in this thesis have been based upon nine geometries in all. The meshes come from three different sources with seven of them being based upon the experimental flume of Sooky (1964). Each mesh is described below and Table A2.1 gives the mesh dimensions and indicates the simulations performed with each one.

Mesh 1

This mesh represents a single meander wave of Sooky's flume. It is based upon his fourth geometry and has a longitudinal slope of 0.0016. The incised channel lies approximately 39mm below the level of the "flood plain" on either side. The channel is 210mm wide and has a sinuosity of about 1.07 (ratio of centre of channel length to shortest distance over one meander wave). The mesh was laid out manually and is shown on Fig A2.1. The mesh is not regular in that some nodes are joined by element sides to 5 or 7 other nodes as well as the standard 6 connections of a deformed equilateral mesh.

Meshes 2, 5 and 6

These meshes form a nested set; 6 contains 5 which contains 2 which contains 1. Fig A2.3 illustrates the nesting for Mesh 5.

The idea behind this set of meshes was to investigate what influence the proximity of the inflow and outflow boundaries had on the conditions in he centre of the meander wave. Mesh 6, which is not illustrated, was generated by doubling the straight extension on either end of the mesh that was used to generate Mesh 5 from Mesh 2. The elements used for these two extensions had a different aspect ratio from those used in the first extension from Mesh 1 to Mesh 2. The predicted water surface profiles were checked against one another at three locations; at the upstream and downstream limits of the meander and at the centre of the meander as indicated on Fig A2.3.

In all tests the mean bed slope was 0.0016 with an incised channel, 210mm wide, 39mm below the flood plain. The extension of the meshes was performed automatically and the flood plain level at the downstream end of each mesh was set to 0.0m. Thus the bed level for the elements in the common central portion of the mesh were raised in each extension.

Meshes 3 and 4

These meshes were derived from Mesh 2. Mesh 3 uses the same node co-ordinates as in a Mesh 2 but the connections between nodes was altered to make the geometry regular (that is it could be mapped onto an equilateral mesh). This was done because Levine (1985) has shown that the mesh topology affects the accuracy with which derivatives are recovered from the finite element approximation. Levine considers values of

derivatives at the mid-point of element sides, as these can be recovered more accurately than by taking the centroid value as done in this thesis. The piecewise constant approximation to the bed geometry implies that formally there are velocity discontinuities across the element edges. Hence the mid-side gradients of water level are not convenient for defining the unit flow or velocity vectors. A comparison of Fig A2.2 with either Fig A2.1 or Fig A2.3 will show the area affected by the re-ordering of the triangles. This may also be recognised by the chevron patterns on one side of Fig A2.2. Mesh 4 was generated from Mesh 2 by scaling all linear dimensions (horizontal and vertical) by a factor of 100. This produced a "life sized" version of the experimental flume with a channel width of 21m and a total width of 118m.

Mesh 7

This mesh was formed automatically by replicating Mesh 1 six times. It represents something like the whole of Sooky's experimental flume which had several channel meanders along it. Fig A2.4 shows the upstream third of this mesh (ie two meanders only). The elements (as for Meshes 1 to 6) were numbered across the flow, which is efficient for Hood's (1976) frontal solution method used to solve the liner equations. Mesh 7 was used to assess how repeatable were the calculated flow parameters from one meander to the next. Fig A2.4 shows the centre and full meander positions used for the water surface

profile plots of Figs 5.11 to 5.13. The flood plain level at the downstream limit of the mesh was again set to 0.0m.

Mesh 8

This mesh represents a hypothetical U shaped channel as may be constructed as an experimental facility. The channel has a semi-circular bend with inside radius 3.4m and outside radius 5.1m see Fig A2.5. There are 6m long straight reaches on either end of the bend. The channel has a rectangular cross section of width 1.7m and the centre of the channel falls by 0.1m in level over its length. The mesh is equilateral except for distortions adjacent to the boundaries and was produced by a commercial mesh generator. The elements, however, were numbered by hand across the flow to minimize the front size in Hood's (op cit) solution algorithm. For low velocity flows the first order analytical solution given in Section 2.7 should be appropriate around the bend.

Mesh 9

This mesh represents a highway crossing of Tallahala Creek and was adapted from data taken from the report by Tseng (1975). Both Tseng and Franques and Yannitell (1974) provide flow simulations for this site. Mesh 9, however, differs from the meshes used in either of these earlier studies. Tseng represented velocity by quadratic basis functions and his mesh was comprised of larger elements with mid-side velocity nodes.

Mesh 9 was generated by dividing each of Tseng's triangles into four by joining the mid-side nodes. Tseng's mesh included several triangles with very small ($<10°$) angles at one of their vertices. These lay around the solid boundaries and were removed when mesh was set up to give the geometry shown on Fig A2.6. All the mesh dimensions were converted to metric units and the datum adjusted by 100m to give an average bed level on the downstream end of the mesh of about 0.0m. This enables the water surface gradients to be calculated with the maximum precision for a given length of real numbers on the computer. In contrast to Meshes 1 and 7 there is no incised river channel represented in Tseng's data. However, there is a severe constriction in the width of the flow path which forces large curvature on the streamlines. The calculations were all based upon the Chezy roughness values from Tseng's report with a discharge of $630m^3/s$. The water levels used on the flow boundaries were set, where appropriate, to the mean value found by Tseng. These roughness and boundary data differ from those that Franques and Yannitell (1974) used.

TABLE A2.1

MESH PROPERTIES

Mesh number	Number of nodes	Number of elements	Dimensions (m)	Stream function formulation	Potential formulation	Figure number
1	92	148	1.28x1.18	initial	✓	A2.1
2	172	292	2.54x1½18	-	✓	A2.3
3	172	292	2.54x1.18	-	✓	A2.2
4	172	292	254 x 118	final	✓	A2.2
5	252	436	5.06x1.18	-	✓	A2.3
6	332	580	7.58x1.18	-	✓	-
7	502	888	7.68x1.18	-	✓	A2.4
8	343	542	1.7 wide x 10.2 dia	-	✓	A2.5
9	163	272	1600x844	final	✓	A2.6

APPENDIX 3

Solution of Linear Equations

The code published by Hood (1976) was modified when it was included in the model programs. Firstly, two corrections were made; one of these was published by Hood (1977) and the second only affected the case where the pivotal searching procedure produced an off-diagonal pivot. The substance of this correction is as follows. For off-diagonal pivoting the back-substitution phase may be written:

$$x_{\ell} = b_k - \sum_m a_{km}\, x_m \qquad \text{(A3.1)}$$

Here k is the pivotal row number, ℓ is the pivotal column number and a_{km} is non-zero only where the solution vector element x_m is already known. The value of x_m may have been set either by the boundary conditions or by the back substitution. In Hood's (1976) code the variable x_k appears on the right hand side in place of x_m in equation (A3.1). The correction requires the pivotal column number LCO to be written out of store on lines 261 and 306 and then read back into store on line 449. This column number is used as an index into the solution array SK at line 462.

Three modifications were also made to the code which were designed to increase the speed of execution.

1. The front size NCRIT was reduced after each elimination and only increased again when necessary. Thus the front size expands and contracts to match the number of active equations rather expanding to the maximum size required and then remaining at this value.

2. Wherever Dirichlet boundary data are supplied for a variable all entries in the corresponding matrix equation are set to zero except for the leading diagonal. There is no need to search for a pivot under these circumstances; diagonal pivoting is used as soon as the boundary data is recognised.

3. The ANSI (1966) standard for FORTRAN specifies the storage organization for 2D arrays. A one-dimensional array may be "equivalenced" to the 2D stiffness matrix and the 1D array used to access entries where the address can be computed more efficiently than using the 2D addressing.

Hood (1977) suggests further improvements to the code which affect its performance when searching for pivots. The principal one is to restrict the number of equations for the search, but to guarantee that at least 5 are available. This has not been implemented. The code in the model, however, allows the user to specify diagonal pivoting and not carry out any search. This procedure is stable for symmetric, definite matrices. An inspection of detailed diagnostic dumps of the operation of elimination algorithm revealed that Hood's

pivoting strategy produced diagonal pivoting for the Galerkin equations for both the stream function and potential formulations. Hence diagonal pivoting was selected at the outset of each run. Even where the Galerkin equations were non-symmetric in the first order variation algorithms no problems were encountered. Cutting out the search for pivots typically reduced the program run time by a factor of four.

The internal application of the boundary conditions differs from that proposed by Hood. Hood allowed space for a boundary value to be given to each variable but most of this storage was not used. In the code implemented therefore the boundary conditions and an index (equation) number are packed in ascending order of the index into smaller arrays. A simple binary search routine extracts the appropriate data whenever required.

APPENDIX 4

Existence and uniqueness for the friction controlled flow equations.

The material in this appendix was supplied by Endre E Süli of the University of Belgrade when visiting the Department of Mathematics at the University of Reading.

Consider the equation:

$$- \underline{\nabla} \cdot (K|\underline{\nabla} u|^{p-2} \underline{\nabla} u) = F \qquad \text{(A4.1)}$$

with the exponent $p > 1$. The restriction on p ensures that (A4.1) is elliptic, see Section 2.6.1.

The stream function formulation is the special case $p = 4$ and the potential formulation corresponds to $p = 3/2$. Take q as the conjugate of p, that is:

$$p^{-1} + q^{-1} = 1 \qquad \text{(A4.2)}$$

We now set up the problem with Dirichlet data

Problem P

Given positive K in $L_\infty(\Omega)$ bounded away from zero by c_0 and from above by c_1 almost everywhere in the domain Ω and given F in $W^{-1,q}(\Omega)$; find u in $W_0^{1,p}(\Omega)$ satisfying equation (A4.1) in Ω.

From here onwards the qualification (Ω) applies to all function

spaces. Define the operator A on u in $W_0^{1,p}$ by

$$Au = - \underline{\nabla}.(K|\underline{\nabla}u|^{p-2}\ \underline{\nabla}u)$$

We observe that for all u, v in $W_o^{1,p}$

1 A is monotone:

$$< Au - Av,\ u - v > \ \geqslant 0$$

2 A is coercive:

$$< Au,\ u > \ \geqslant c_0\ ||\underline{\nabla}u||_{Lp}^{p}$$

3 A is bounded:

$$< Au,\ v > \ \leqslant c_1\ ||\underline{\nabla}u||_{Lp}^{p-1}||\underline{\nabla}v||_{Lp}$$

$$||Au||_{W^{-1,q}}^{q} \leqslant c_1^{q}||u||_{W_o^{1,p}}^{p}$$

These three conditions imply that, by the Minty-Browder theorem, the problem P has at least one solution. However, since the condition 1 is not of strong monotonicity, the solution may not be unique.

Uniqueness of the solution may be proved by an alternative method. Introduce the following function Φ on u in $W_0^{1,p}$

$$\Phi(u) = p^{-1} \int K \sum_i |D_i u|^p \, d\Omega - <F,u> \qquad (A4.3)$$

We observe that by Poincare's inequality Φ is coercive over $W_0^{1,p}$. Also, since $1 < p < \infty$, the function $|x|^p$ is strictly convex and it follows that Φ is also strictly convex over the Sobolev space $W_0^{1,p}$. These two properties imply that the following minimization, problem Q, has exactly one solution u in $W_o^{1,p}$.

Problem Q

Find inf $\Phi(u)$ over $W_o^{1,P}$

However, the differential equation (A4.1) is the Euler equation for the minimization problem Q. Hence the solution u to Q is at the same time the unique solution to problem P. For further material consult Ciarlet (1978) and Ekeland and Temam (1976).

References

Ciarlet Ph (1978) : The finite element method for elliptic problems, North Holland.

Ekeland P and Teman R (1976) : Convex analysis and variational problems, North Holland.

Appendix 5

International Conference on the
Hydraulic Aspects of Floods & Flood Control
London, England: September 13-15, 1983

Two dimensional modelling of flood flows using the finite element method

P G Samuels

Summary

This paper examines two dimensional (in plan) models of flow over a flood plain. Three different sets of model equations are introduced and their mathematical type and appropriate boundary conditions are discussed. The solution of the flow equations by finite element methods is discussed for friction controlled flow and for flows including the convection of momentum. The numerical tests relate to a laboratory flume with a meandering channel and the discussion focusses on the rates of convergence of the numerical methods employed.

Organised and sponsored by

bhra fluid engineering

With the support of the British National Committee of I.C.I.D.

Nomenclature

Symbol	Description	Units
$\underline{C}$	the convection term $(\underline{u} \cdot \underline{\nabla})\underline{u}/g$	—
D	flow depth	m
E	turbulent eddy viscosity	$m^{-1}s^{-1}$
f	a flow variable (defined in text)	—
f_m	mesh Froude number	—
Fr	Froude number	—
g	acceleration due to gravity	ms^{-2}
h	water level	m
K	friction factor	m^2s^{-1}
$\underline{n}$	outward unit vector normal to the boundary	m
$\underline{q}(q_x, q_y)$	unit discharge (and components)	m^2s^{-1}
s	distance along a streamline	m
t	time	s
$\underline{T}$	turbulent stress term	—
$\underline{u}(u_x, u_y)$	depth mean velocity (= $\underline{q}/D$)	ms^{-1}
α	velocity distribution coefficient	—
ϵ	convergence parameter (defined in Section 3.1)	—
λ	iteration updating parameter	—
Ψ	stream function	m^3s^{-1}
$\underline{\nabla}$	gradient operator	m^{-1}
prefix Δ	increment	—
subscript j	value for node or element j	—
superscript (i)	value for iteration i	—
superscript n	value at time $n\Delta t$	—

1 Introduction

Although one dimensional models of river flow (Ref 1) are an established tool for simulating long reaches of river they cannot always provide all the local detail that is required. Such models cannot resolve any features of the flow either at a scale finer than the grid size used in the model or which are produced by two or three dimensional effects. For example, an embankment across a flood plain leading to a bridge may have a profound impact on the flow direction and water levels on the flood plain. Variations of the flow across the width of the river as well as along the length can be studied by using a two-dimensional (in plan) model. The use of standard finite difference techniques, based on a regular grid, are complicated by the highly irregular geometry of natural river valleys, but this is readily included by models based on the finite element method (Ref 2). The finite element method has been applied successfully to many types of fluid flow including tidal hydraulics (Refs 3, 4, 5). Relatively little work, however, has been published on using the finite element method for modelling flow in a river and over its flood plain.

This paper examines the formulation of two dimensional models of flood flow. As various processes are included in the mathematical model the nature of the equations change. This has an affect on the most appropriate numerical method for solving the flow equations. The numerical methods discussed in this paper are all directed at choosing the lowest order of approximation possible for the flow which is consistent with the quality of data available for commercial studies. A topographic survey of a river and its flood plain can be expensive, particularly if closely spaced river cross sections -at a spacing of the width of the main channel or less - or if many flood plain ground levels - with accuracy better than $\pm$ 0.1m - are required. In any prototype investigation there is pressure to keep the data needs to the minimum compatible with the accuracy required from the study. The relationship between the model accuracy and the density of prototype data, however, is not considered further in this paper.

2 The model equations

Assumptions 2.1 The starting point for producing the two dimensional flow equations is the fully three dimensional equations, see Sections 2.2 and 3.2 of Batchelor (Ref 6). Making amongst others the following assumptions these equations may be integrated through the depth of the flow giving equations (1) and (2) in Section 2.2:

1) Flow is incompressible and density constant.

2) Vertical velocity and acceleration are small.

3) There is no stress on the air/water surface.

4) The earths rotation can be neglected.

5) The river bed does not change with time.

This paper considers features characteristic of bulk flow in the river and flood plain system and the above assumptions are all reasonable. Obviously these assumptions can be altered giving different flow equations with a different range of applicability.

Typical of the restrictions forced by these assumptions is the neglect of secondary flow in river bends (assumption 2). This can be relaxed as shown by Kalkwijk and de Vriend (Ref 7).

Two dimensional flow equations 2.2

Using the notation at the front of the paper the flow equations are:

$$\text{Continuity: } \frac{\partial h}{\partial t} + \underline{\nabla} \cdot \underline{q} = 0 \tag{1}$$

$$\text{Dynamic: } \frac{1}{gD}\frac{\partial \underline{q}}{\partial t} + \frac{1}{gD}\underline{\nabla} \cdot \left(\alpha \frac{\underline{q}\,\underline{q}}{D}\right) + \underline{\nabla} h + \frac{\underline{q}|\underline{q}|}{K^2} = \underline{T} \tag{2}$$

In the rest of the paper the velocity distribution coefficient α will be set to 1.0 which is not unreasonable if the vertical velocity profile is approximately logarithmic. The stress term $\underline{T}$ will also be neglected. This term includes the turbulent stresses in the fluid and study its relation to the properties of the bulk flow has produced a variety of turbulence models (Ref 8). Ignoring the turbulent stresses may restrict the use of the model to regions without high rates of shear.

Simplifying equations (1) and (2) further we have the three following approximations to describe the flow.

(a) Steady friction controlled flow:

$$\underline{\nabla} \cdot \underline{q} = 0 \tag{3}$$

$$\underline{\nabla} h + \frac{\underline{q}|\underline{q}|}{K^2} = 0 \tag{4}$$

(b) Steady flow with convection and bottom friction:

$$\underline{\nabla} \cdot \underline{q} = 0 \tag{5}$$

$$-\underline{\nabla} h + \frac{\underline{q}|\underline{q}|}{K^2} + \frac{1}{gD}\underline{\nabla} \cdot \left(\frac{\underline{q}|\underline{q}|}{D}\right) = 0 \tag{6}$$

(c) Unsteady flow with convection and bottom friction:

$$\underline{\nabla} \cdot \underline{q} + \frac{\partial h}{\partial t} = 0 \tag{7}$$

$$\frac{1}{gD}\frac{\partial \underline{q}}{\partial t} + \underline{\nabla} h + \frac{\underline{q}|\underline{q}|}{K^2} + \frac{1}{gD}\underline{\nabla} \cdot \left(\frac{\underline{q}\,\underline{q}}{D}\right) = 0 \tag{8}$$

Defining the depth mean velocity by $\underline{u} = \underline{q}/D$ equations (6) and (8) may be rewritten as:

$$\underline{\nabla} h + \frac{\underline{u}|\underline{u}|D^2}{K^2} + \frac{1}{g}(\underline{u} \cdot \underline{\nabla})\underline{u} = 0 \tag{6a}$$

$$\frac{1}{g}\frac{\partial \underline{u}}{\partial t} + \underline{\nabla} h + \frac{\underline{u}|\underline{u}|D^2}{K^2} + \frac{1}{g}(\underline{u} \cdot \underline{\nabla})\underline{u} = 0 \tag{8a}$$

Equations (1) to (8) are all written in terms of the primitive variables, the velocities and water levels. The continuity equation for steady flow (3) and (5), however, allows the flow to be described in terms of a stream function Ψ by defining:

$$q_x = \frac{\partial \Psi}{\partial y}; \quad q_y = -\frac{\partial \Psi}{\partial x} \tag{9}$$

Substituting this in the dynamic equation (4) and taking its curl gives:

$$\underline{\nabla} \cdot [(|\underline{\nabla} \Psi| K^{-2}) \underline{\nabla} \Psi] = 0 \tag{10}$$

Franques and Yannitell (Ref 9) used this equation to define the stream lines of the flow. They rewrote equation (6a) in a co-ordinate system orientated with the flow and integrated it along the stream lines to give water levels, thus:

$$h_2 - h_1 + \frac{U_2^2}{2g} - \frac{U_1^2}{2g} + \int_1^2 (|\underline{\nabla \Psi}|^2 K^2) ds = 0 \tag{11}$$

where the points 1 and 2 lie on the same streamline.

An alternative simplification of equations (3) and (4) is to eliminate q between them assuming that the water level h performs the role of a velocity potential. The resulting equation will be termed the potential formulation and is:

$$\underline{\nabla} \cdot [(K |\underline{\nabla} h|^{-0.5}) \underline{\nabla} h] = 0 \tag{12}$$

To the author's knowledge the potential formulation above has not been used before to solve steady two-dimensional friction controlled flow over a river flood plain.

Classification of equations 2.3

The field equations for steady flow controlled by friction (10) and (12) are elliptic. They are also each degenerate in the case of $|\nabla \Psi|$ or $|\nabla h|$ vanishing anywhere in the flow field, this occurs when the flow becomes stationary. Suitable boundary conditions on the appropriate flow variable - stream function for equation (10) or water level for equation (12) - are for the variable, its normal derivative, or a combination of these two to be specified around the entire boundary of the region. The conditions imposed on the stream function and water level are complementary. Equations (3, (4), and (9) imply that when Ψ is specified as constant on a no-flow (solid) boundary in the stream function formulation, $\partial h/\partial n$ is set to zero on the same boundary in the potential formulation and that where $\partial \Psi/\partial n$ is set to zero in the stream function formulation indicating flow normal to the boundary, h is specified as constant in the potential formulation.

When the convection term is included in the model to give the dynamic equation (6) as opposed to (4), the nature of the flow equations changes. The equations form a quasi-linear system which may be classified according to the roots of the corresponding characteristic equation, see Garabedian, pp 94-99 (Ref 10). The system has three real characteristics and so is hyperbolic where the flow is supercritical but the characteristic equation has one real and two imaginary roots for subcritical flow. The flow is subcritical or supercritical according to whether the local value of the Froude number F_r defined by:

$$F_r = |\underline{u}|(gD)^{-0.5} \quad (13)$$

is less than or greater than unity. The same classification of the equations holds if the velocity distribution coefficient α is retained in the definition of the convection term of equation (2). In this case the discriminant for critical flow is the two dimensional analogue of the critical flow number introduced by Price and Samuels (Ref 1). For all flow regimes the appropriate condition on a no flow (or solid) boundary is to specify:

$$\underline{q} \cdot \underline{n} = 0 \quad (14)$$

The situation on the flow boundaries, however, is not so clear cut. For a domain where the flow is entirely supercritical the geometry of the characteristics indicates that data should only be specified on an inflow boundary, where information is transferred into the domain. When the flow is entirely subcritical the equations cannot be classified as simply elliptic, parabolic or hyperbolic. In this case the equations are similar to those for two dimensional compressible aerodynamic flow discussed by Garabedian (Ref 10) p 519ff. Garabedian shows the aerodynamic equations to be essentially elliptic for subsonic flow by eliminating the flow variable along the one real characteristic using the Bernoulli equation. Finally, under certain conditions the flow may be supercritical in some parts of the domain and subcritical in others. The location of the transition zones between the flow regimes depends upon the local ground topography, probably at a finer scale than it is possible to resolve economically with a model designed to look at a large area. This problem is not discussed further in this paper. It is interesting to note that, in contrast to steady constant flow governed by friction, the water level is not constant along a boundary which is normal everywhere to the flow across it. The water levels along such a boundary depend upon the curvature of the streamlines as they cross the boundary.

Following the discussion on pp 94 to 99 of Garabedian (Ref 10) the unsteady flow equations (7) and (8) may be shown to be always hyperbolic. The flow regimes may again be identified subcritical and supercritical according to the local value of the Froude number given in equation (13). On no flow boundaries equation (14) may be applied. On flow boundaries the conditions which may be applied depend upon the Froude number. For supercritical flow all three flow variables must be determined on an inflow boundary and none on an outflow boundary, see Oliger and Sundström (Ref 11) and Daubert and Graffe (Ref 12). The situation for subcritical flow, however, is more complicated. Two conditions must be imposed on an inflow boundary and one on an outflow boundary but not all choices of boundary conditions produce a well posed set of equations. Oliger and Sundström (Ref 11) give some conditions suitable for friction-less flows. These conditions may not be necessary for flows with a significant friction term as is the case of flood plain flow, they will however be sufficient. The water level may be given along an outflow boundary and both velocity components on an inflow boundary. Other more complicated conditions are admissable on the inflow boundary.

The turbulent stress terms are often introduced into the equations by setting:

$$\underline{T} = E \nabla^2 \underline{u} \qquad (15)$$

where E is some turbulent eddy viscosity. With this representation of T the unsteady flow equations are incompletely parabolic (Refs 11 and 13) and require different boundary conditions from the equations without the turbulent stress terms. These problems will not be considered further in this paper.

3 Numerical models of friction controlled flow

The test problem 3.1

All the numerical tests described in the remainder of the paper have been carried out on representations of part of the experimental flume used by Sooky (Ref 14). This flume had a regular sinusoidal channel let into its gently sloping floor; the slope of the flume and channel geometry were adjustable. The numerical model simulated Sooky's fourth geometry with bed slope of 0.0016; meander wave length 1.28m, meander amplitude 0.126m, channel depth 0.0381m, channel width 0.209m and total width 1.184m.

A single meander wave was covered by an irregular triangular mesh containing 92 nodes and 148 elements, see Fig 1. Most tests have been done on a single meander wave, some having a section of straight channel added on to either end. Some tests investigated the effect of the location of the boundaries on the flow in the central portion of the mesh, this was done by lengthening the straight portion at each end of the meander wave and in one case by repeating the meander wave six times. The main features of the flow in the central meander were not affected much by the location of the boundaries, nor was the convergence behaviour of the numerical methods tested. The rest of this paper is principally concerned with the numerical properties of the various methods investigated rather than a detailed comparison of their results with the flume data.

The systems of linear equations from the finite element method were solved using a corrected version of Hood's Frontal solution technique (Ref 15). This technique is particularly suitable for two dimensional regions where one dimension is much longer than the other as is usually the case of a model of part of a river valley. No analytical solutions exist for the flow equations in the test geometry. The rates of convergence of the iterative methods used were therefore measured in terms of the magnitude of the change in the flow variables at each iteration thus:

$$\epsilon^{(i)} = \max_j \left[2|f_j^{(i)} - f_j^{(i-1)}|/|f_j^{(i)} + f_j^{(i-1)}|\right]$$

where $\epsilon^{(i)}$ is the value of the convergance parameter for the variable f at iteration i and $f_j^{(i)}$ is the value of the variable f at a node or element j (as appropriate) for iteration i. The following three limits of ϵ are of interest.

(1) convergence of the sequence $[f_j^{(i)}]$ for all j is marked by either $\epsilon_j^{(i)} \rightarrow 0$ or $\epsilon_j^{(i)}/\epsilon_j^{(i-1)} \rightarrow c < 1$

(2) oscillation of the sequence $[f_j^{(i)}]$ at some j is marked by $\epsilon^{(i+1)} \approx \epsilon_j^{(i)}$

(3) divergence of the sequence $[f_j^{(i)}]$ at some j is marked by $\epsilon_j^{(i)} \rightarrow 2$.

The stream function formulation 3.2

The first test of the stream function formulation used the iterative method suggested by Franques and Yannitell (Ref 9). Given an initial guess for the solution each iteration consisted of determining the stream function from equation (10) with the non-linear coefficient $|\nabla\Psi|K^{-2}$ evaluated at the old iteration. The water levels were then determined from equation (11) using the most recent values of the stream function to calculate the velocities. The stream function and water level were represented by piecewise linear functions over the triangular mesh. This method was found to have a poor rate of convergence with $\epsilon^{(i+1)}/\epsilon^{(i)} \rightarrow 0.96$. This means that about 150 iterations would be required to achieve three decimal digits of precision. The first order behaviour of the iteration algorithm was analysed on the basis that at each iteration only a proportion of the predicted change in the flow variable Δf_j is taken, that is

$$f_j^{(i+1)} = f_j^{(i)} + \lambda \Delta f_j \qquad (16)$$

The analysis showed that setting $\lambda = 1$ give oscillatory results, as was found, setting $\lambda = 0.5$ would give convergence like $(0.5)^i$ which was again found and finally the optimum choice was to set $\lambda = 1$ and 0.5 in alternate iterations. This final choice was found to converge as $(0.38)^i$ giving 3 decimal digits of precision in 7 iterations. Franques and Yannitell suggest that the variation of the water level can be specified along the whole of the downstream flow boundary on which they set $\partial\Psi/\partial n$ to zero. As discussed in section 2.3 this is not consistent with using equation (10) to determine the flow field. The iteration method, however, converged with consistent and inconsistent water level data on the downstream flow boundary. No further work has been done on this formulation of the flow equations. The next step which is to include the convection term in the dynamic equation would require the stream function to be represented as having continuous derivatives across element boundaries. This requires a high order element and greatly increases the computational cost, see section 3.6 of Connor and Brebbia (Ref 3).

Potential formulation 3.3

Two iteration methods for the potential formulation were tested. The first method was similar to the successive substitution algorithm used to solve the stream function formulation. Equations (12) and (14) were iterated as a pair, using equation (12) to calculate a new set of water levels and equation (4) to calculate the discharge in each element. The non-linear coefficient $K|\nabla h|^{-0.5}$ in equation (12) was evaluated at the old iteration. This method was found to converge at about the same rate as the optimum method for the stream function formulation.

The second iteration method used equation (12) alone and was based on setting

$$h_j^{(i+1)} = h_j^{(i)} + \Delta h_j$$

at each node, expanding all terms in the Galerkin finite element equations to first order in Δh_j. The coefficients of the linear equations for the Δh_j were more complicated and expensive to compute than those for the first method tried. The iteration however converged nearly quadratically with $\epsilon_k^{(i+1)} \approx (\epsilon_k^{(i)})^2$ and machine precision, 11 significant digits, was achieved in about 4 iterations. On convergence the total inflow matched the total outflow exactly. With the potential formulation the normal discharge across each flow boundary is not constrained whereas in the stream function formulation it is fixed by the boundary data.

This second iteration method for the potential formulation is a basis for constructing practical models of friction controlled flood plain flow. The computational resources for a mesh with about 200 nodes and 400 elements were 40 K words of store and 30 seconds CPU time per iteration on the ICL 2960 computer at HRS running under the DME operating system.

4 Models including convection

Orders of approximation 4.1

The choice of approximations for water level and velocity in this case is not clear cut. It is well known that for solving the Navier Stokes equations of fluid flow there is a relationship between the orders of approximation that can be used for the various flow variables, see Temam (Ref 16). Papers published on solving the flood plain flow equations have used orders of approximation as shown below.

Authors	Reference	Water level	Velocity
Zielke & Urban	2	linear	linear
Herrling	17	linear	(discontinuous) linear
Tseng	18	linear	quadratic

In the limit as the friction term dominates the convection term the flow equations tend to those discussed in Section 3 above where the natural choice of order of approximation is a piecewise linear for water level or stream function. This is the lowest order possible and both the stream function and potential formulations can be argued to represent the velocity (or discharge) vector as piecewise constant within each triangular element. The difficulty in using this description of the flow once the convection term $(u \cdot \nabla)u$ has been included in the dynamic equation is that velocity gradients need to be determined from the piecewise constant values of velocity.

Calculating the convection term 4.2

Choosing the same description of the flow variables as described in section 3.3 above, the convection term may be calculated as follows.

1) For each element locate its neighbours which share a common side, see Fig 2.

2) Calculate the depth mean velocity $\underline{u}$ at the centroid of each element.

3) Calculate the least squares best fit velocity and its plan derivatives from the values in the centre of the element and its three neighbours.

4) Calculate the convection term from the best fit velocity and derivatives found in (3).

This process is in some sense analogous to taking a 'central difference' approximation to calculate the convection term since it is independent of the direction of the velocities. This fitting procedure uses known values of velocity and was always applied to estimate the convection term for the velocities calculated at the end of an iteration (for steady flow) or a time step (for unsteady flow).

Numerical experiments 4.3

First of all the convection term was included in the steady flow equations by modifying the algorithm used to solve the friction controlled flow. Since q is piecewise constant within each element it may be calculated from equation (6) as

$$\underline{q} = K(\underline{\nabla h} + \underline{C})\,|\underline{\nabla h} + \underline{C}|^{-0.5} \qquad (18)$$

where $\underline{C}$ is the convection term, $(\underline{u} \cdot \nabla)\underline{u}/g$. Equation (18) was substituted into the continuity equation (5) to give a single equation to solve for the water level h.

The method was found to converge in some cases and not in others. The flow overall velocity was adjusted by altering the value of the friction factor K. A first order analysis of the iteration method implied a stability limit dependent on the mesh Froude number defined by:

$$f_m = (K/D)\,(g\Delta s)^{-0.5}$$

where Δs is the space step size in the stream direction. The calculation was stable for $f_m < 1$ and unstable for $f_m > 1$ with the values of the solution variables growing exponentially at a rate proportional to f_m in the latter case. The growth rates predicted by the linearised analysis matched closely those found in the numerical experiments. This stability limit is too restrictive for practical computations since it forces a minimum size on the mesh size. Using typical values for the size of the friction factor it corresponds to about 10m for flood plain flow but to 300m for flow in the adjacent river channel.

Returning to the unsteady flow equations (7) and (8) these may be solved using a semi-implicit method based upon the steady flow solution method discussed above. This is done by setting:

$$\frac{\partial h}{\partial t} = \frac{h^{n+1} - h^n}{\Delta t}$$
$$\frac{\partial u}{\partial t} = \frac{u^{n+1} - u^n}{\Delta t}$$

and calculating all other terms in the equations except the convection term at the forward time level $(n+1)\Delta t$. The convection term is calculated at the time $n\Delta t$ as described in Section 4.2 above. Assuming the velocity to be piecewise constant it may again be eliminated by solving the dynamic equation locally in each element.

This method was applied to one of the flow cases found to be unstable for the steady flow equations. The computations were stable for steady flow boundary conditions provided that the time step was chosen to restrict the Courant number $|u|\Delta t/\Delta s$ to a value somewhat less than unity. The model results, however, did not converge to steady values for the test problem but rather changed by a small amount in each time step. The variations in the flow velocity were of the order 1 or 2% in each time step and the probable source of these changes is the error introduced by the least square fitting procedure used to calculate the convection term. Obviously a more thorough understanding of the properties of this method is required before it can be used in practice.

5 Concluding remarks

Several sets of model equations for flood plain flow have been discussed and the appropriate boundary conditions indicated. For steady friction controlled flow the implementation of the potential formulation described in section 3.3 appears to be the basis of a practical computational model. The best means of modelling flows where the convection term is important is still not clear. The stability restrictions are too severe on the steady flow equations using the least squares fitting procedure introduced in section 4.2. It is possible that a working model will be based on the unsteady flow equations using this fitting procedure but more work is required to establish this. Alternative solutions are to use another method for calculating the convection term based on the piecewise constant description of the flow velocity or to use a higher order of approximation for the velocity.

6 Acknowledgements

The work described in this paper formed a part of the basic research programme of Hydraulics Research and was funded by the Department of the Environment and the Ministry of Agriculture, Fisheries and Food. It also partly fulfills the requirements of Doctor of Philosophy at Reading University.

The author wishes to thank Prof K W Morton of Reading University and Dr R K Price of Hydraulics Research for their stimulating discussion and helpful criticism.

The opinions expressed in this paper are entirely those of the author and do not reflect the policy of either of the organisations who sponsored the work.

7 References

1. PRICE R K and SAMUELS P G. A computational hydraulic model for rivers. Proc Instn Civ Engrs, Part 2, vol **69**, March 1980, pp 87- 96.
2. ZIELKE W and URBAN K. Two-dimensional modelling of rivers with flood plains. Preprints from IAHR international conference on numerical modelling of river, channel and overland flow for water resources and environmental applications, (Bratislava, May 4-8, 1981), Proceedings in preparation by IAHR, Delft, Netherlands.
3. CONNOR J J and BREBBIA C A. Finite element techniques for fluid flow, London. Newnes-Butterworths, 1977.
4. HOLTZ K P and NITSCHE G. Tidal wave analysis for estuaries with intertidal flats. Proc Third international conference on finite elements in water resources (University of Mississippi, USA, May 19-23, 1980) pp 5113-5126.
5. HERRLING B. Computation of shallow water waves with hybrid finite elements. Adv in water resources, **Vol 1**, December 1978, pp 313- 320.
6. BATCHELOR G K. Introduction to fluid dynamics. Cambridge University Press, 1967.
7. KALKWIJK J P Th and deVRIEND H J. Computation of the flow in shallow river bends, Journal of Hydraulic Research, 1980, **Vol 18**, No. 4, pp 327-342.
8. RODI W. Turbulence models and their application in hydraulics. IAHR state of the art paper, Delft, The Netherlands, IAHR Secretariat, June 1980.
9. FRANQUES J T and YANNITELL D W. Two-dimensional analysis of backwater at bridges. J. Hydraul. Div. Am. Soc. Civ Engrs, **Vol 100**, No. HY3, March 1974, pp 379-392.
10. GARBEDIAN P. Partial differential equations, New York, John Wiley and Sons, 1964.
11. OLIGER J and SUNDSTRÖM A. Theoretical and practical aspects of some initial boundary value problems in fluid dynamics. Soc, Ind. Appl. Math, J. Appl. Math, **Vol 35**, No. 3, November 1978, pp 419- 446.
12. DAUBERT A and GRAFFE O. Quelques aspects des écoulements presque horizontaux a deux dimensions en plan et non permanents application aux estuaires. (Some aspects of near horizontal two-dimensional flow and their application to estuaries), Houille Blanche, 1967, pp 847-860 (in French).
13. GUSTAFSSON B and SUNDSTRÖM A. Incompletely parabolic problems in fluid dynamics. Soc. Ind. Appl. Math. J. Appl. Math, **Vol 35**, No. 2, September 1978, pp 343-357.

14. SOOKY A A. The flow through a meander flood plain geometry. PhD Thesis, Purdue University, 1964. (65-2647, University Microfilms Inc, Ann Arbor, Michigan).

15. HOOD P. Frontal solution program for unsymmetric matrices. Int. J. For Num. Meth, in Engng, **Vol 10**, pp 379-399, 1976.

16. TEMAM R. Navier Stokes equations. Amsterdam, North Holland, 1977.

17. HERRLING B. Coupling one and two dimensional finite elements for the computation of tidal flow in estuaries, Adv. in water resources, **Vol 5**, December 1980, pp 227-232.

18. TSENG M T. Finite element model for backwater computation. Proc. Am. Soc, Civ. Engrs. Symposium MODELLING 75, Vol II, pp 1448- 1466, 1975.

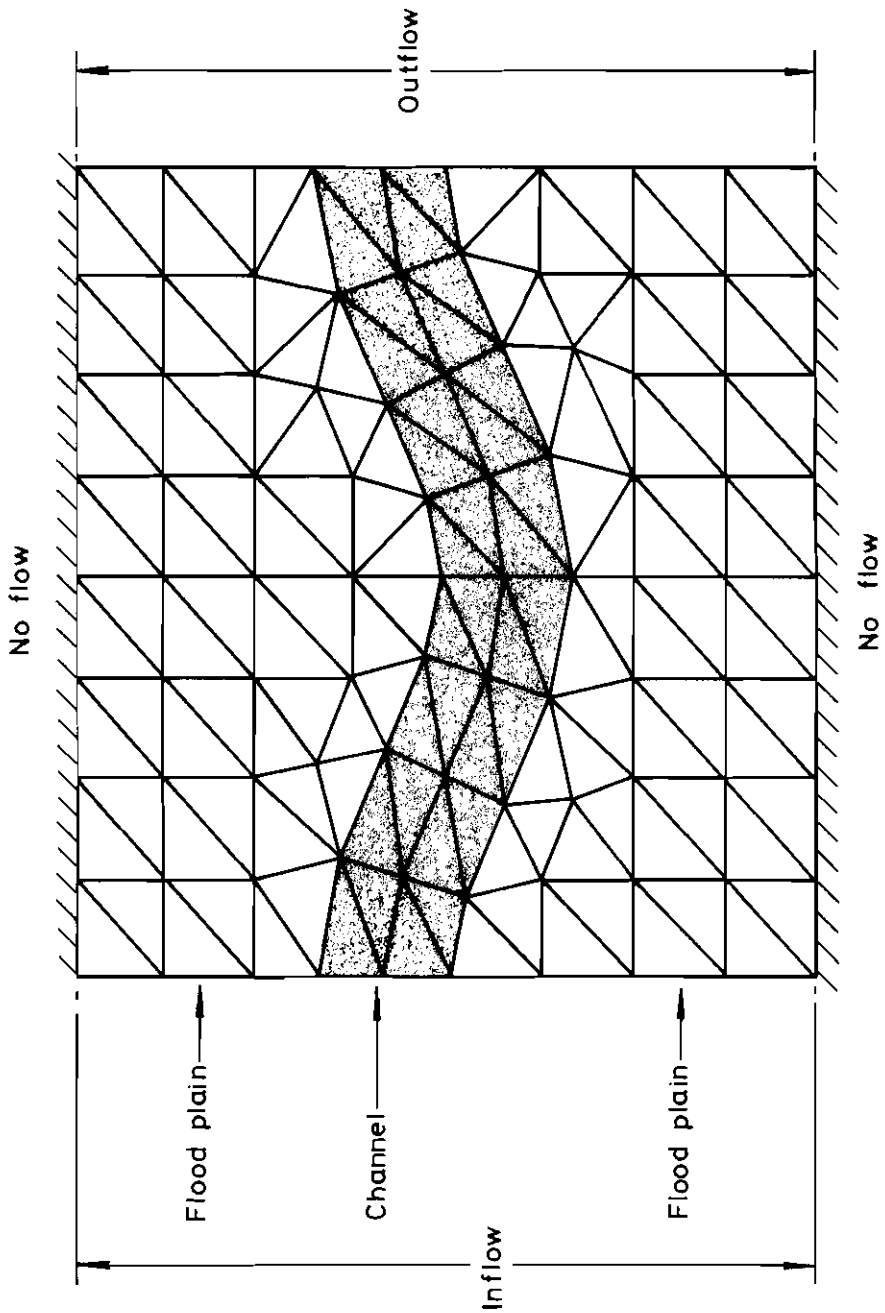

Fig 1 Finite element mesh over one meander wave

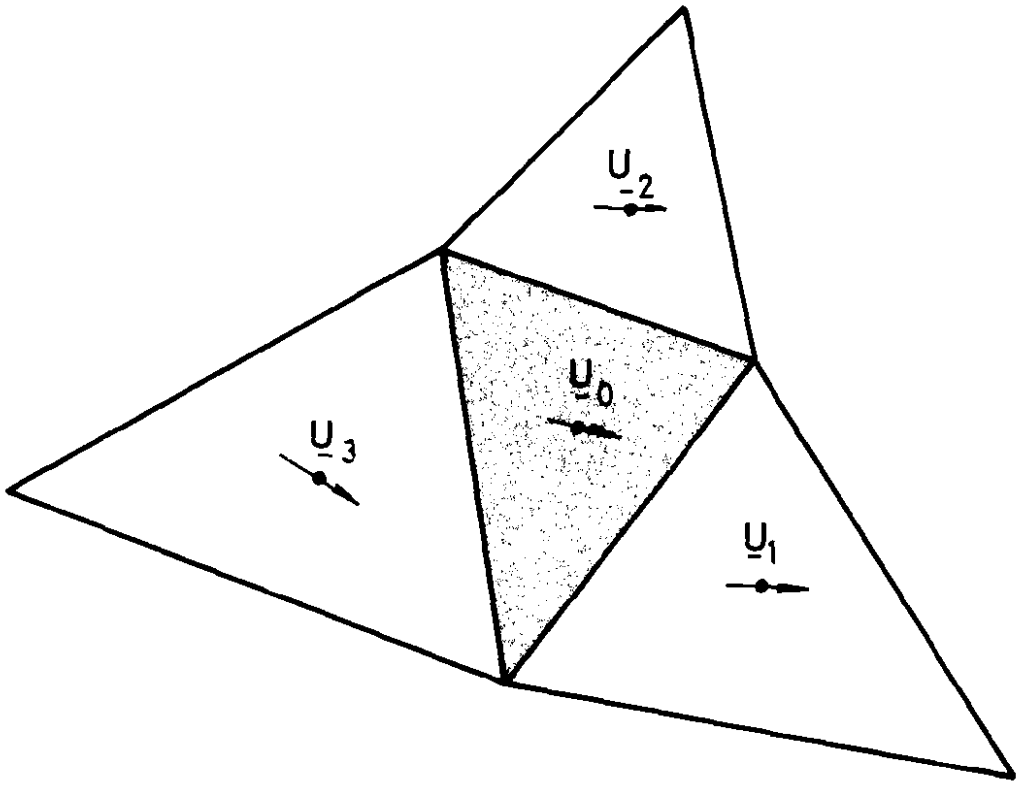

Fig 2 An element and its neighbours for calculation of convection term

Figures

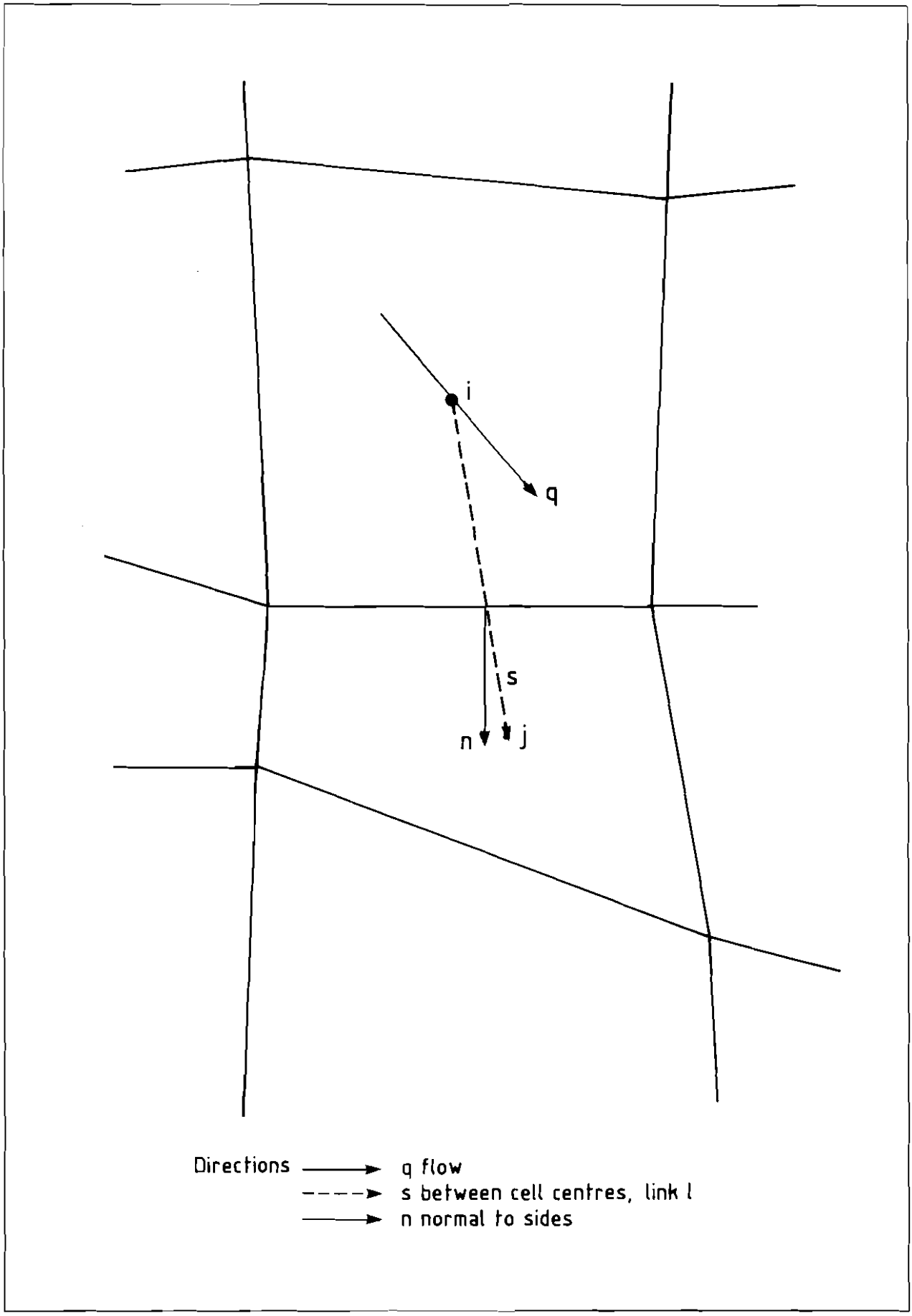

Fig 1.1 Part of grid for cell-type model

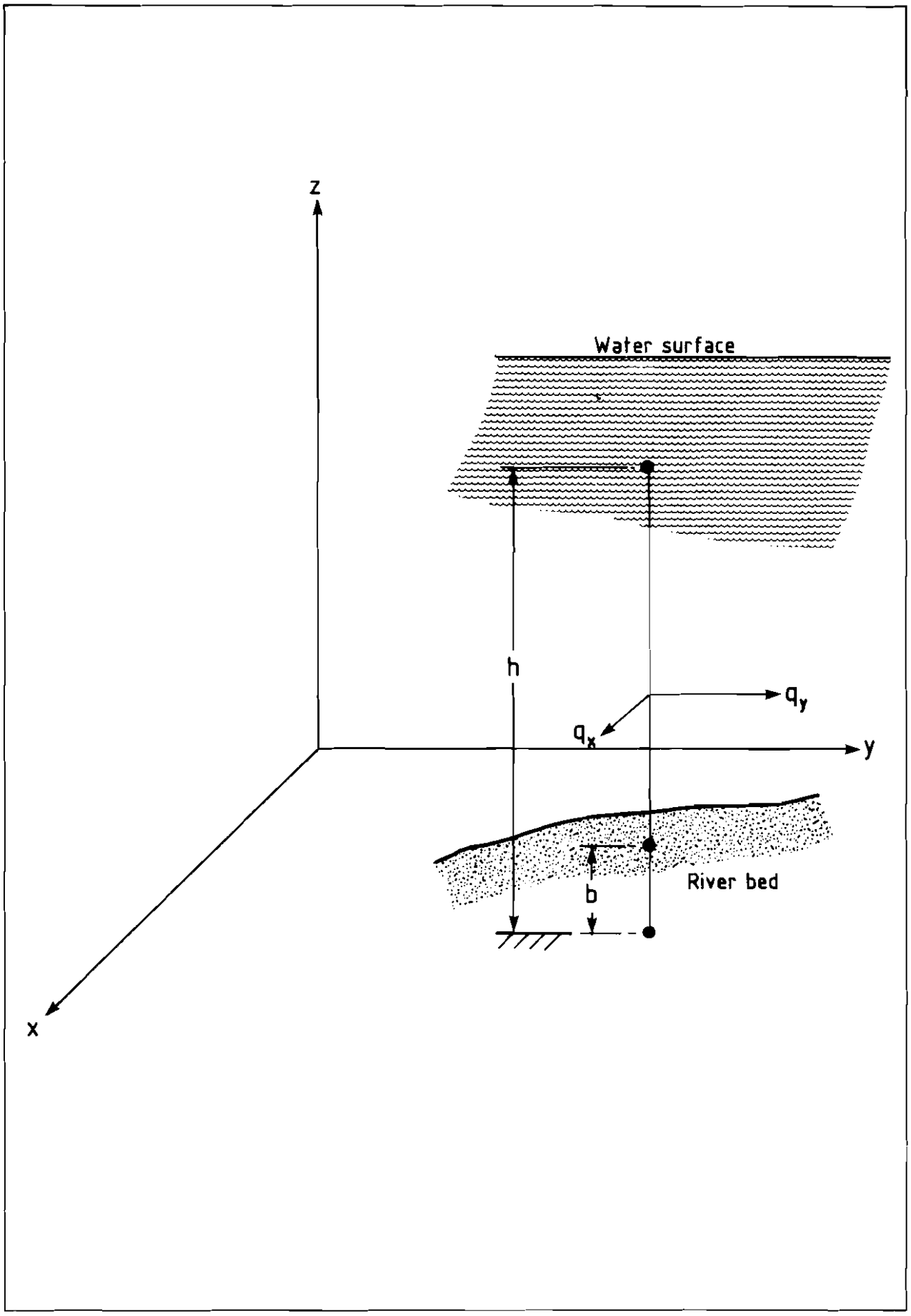

Fig 2.1 Definition of axes

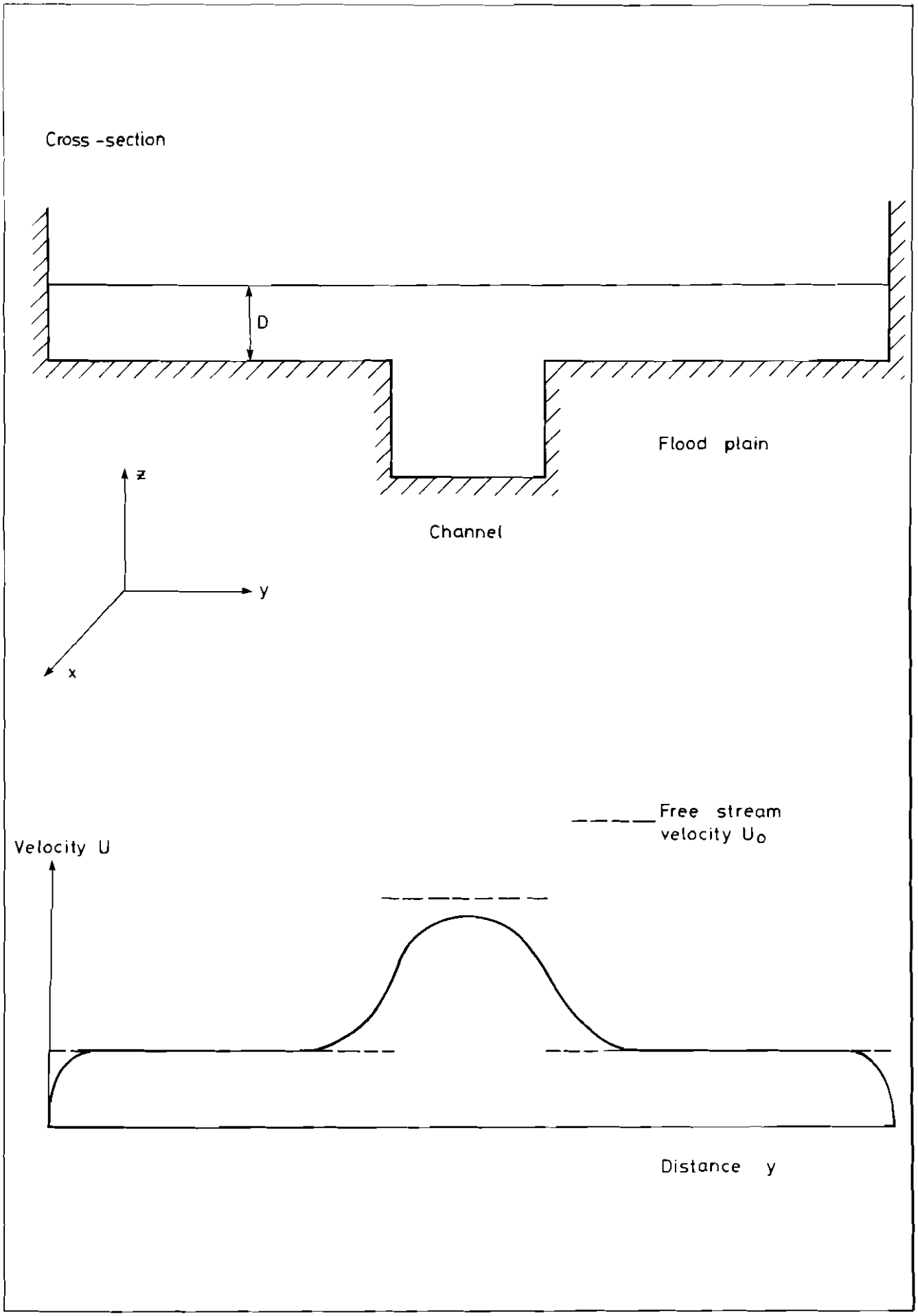

Fig 2-2 Definition sketch of lateral velocity variation

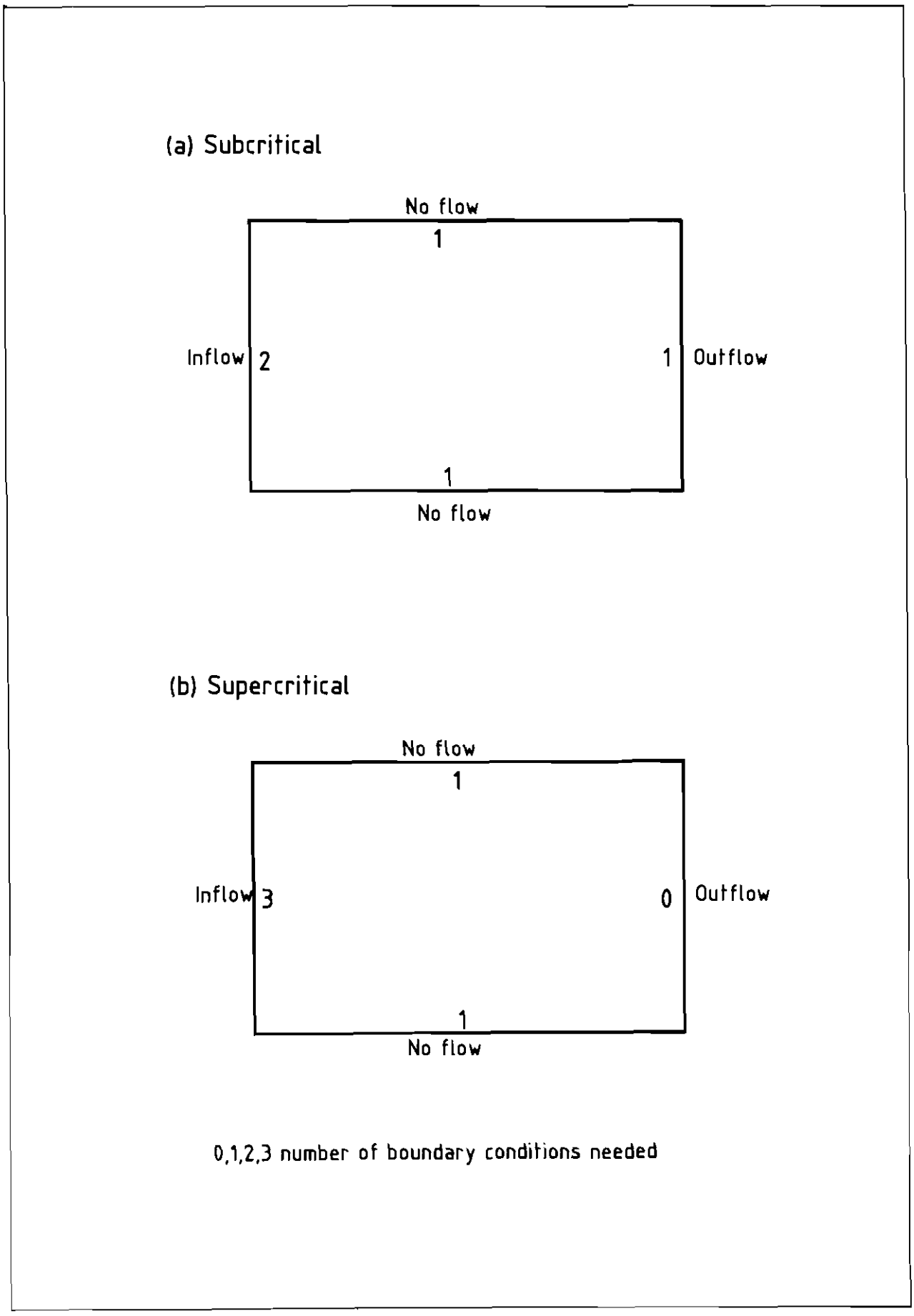

Fig 2.3 Boundary conditions for steady and unsteady flow (including convection term)

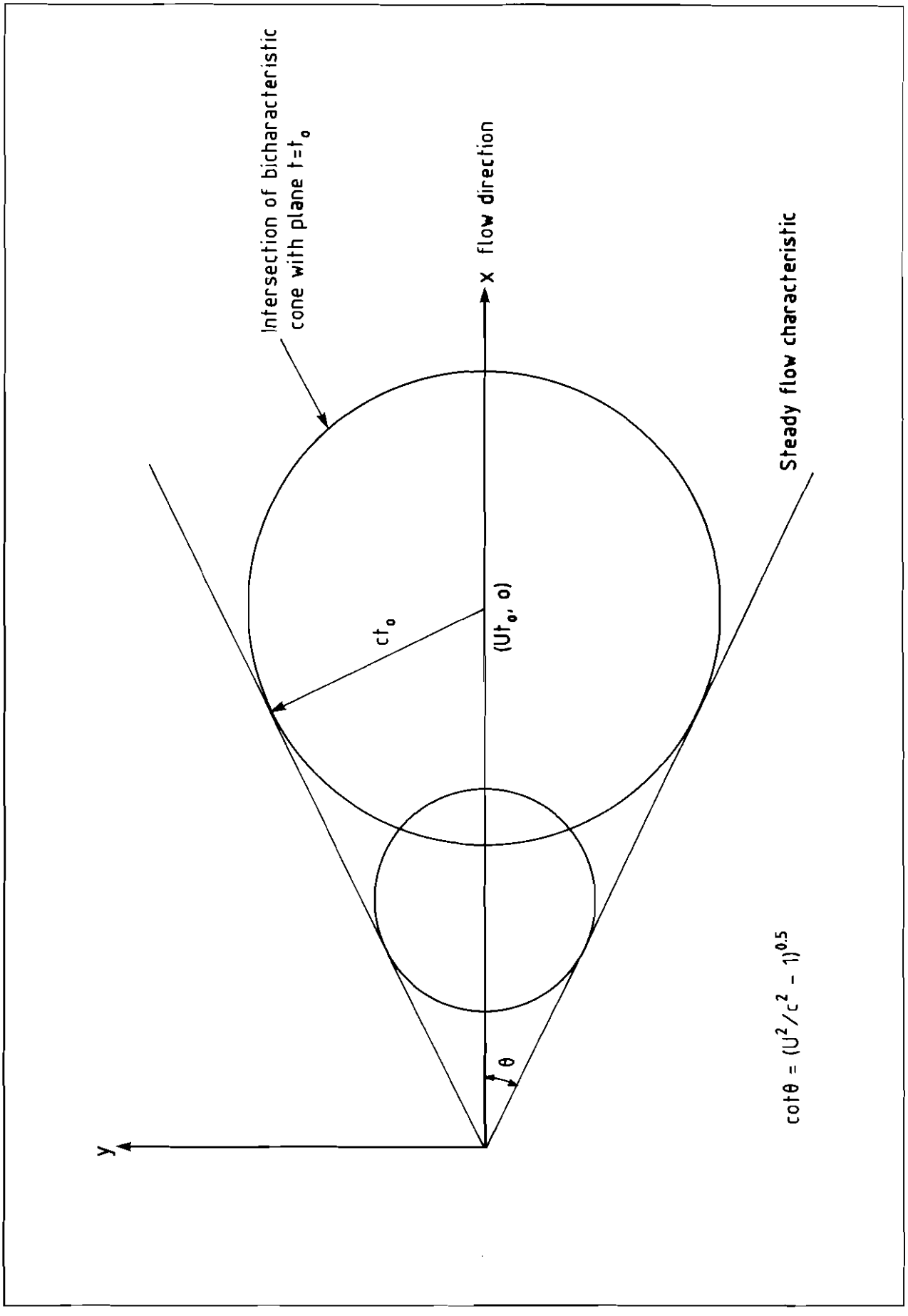

Fig 2.4 Characteristics for steady and unsteady supercritical flow (α = 1)

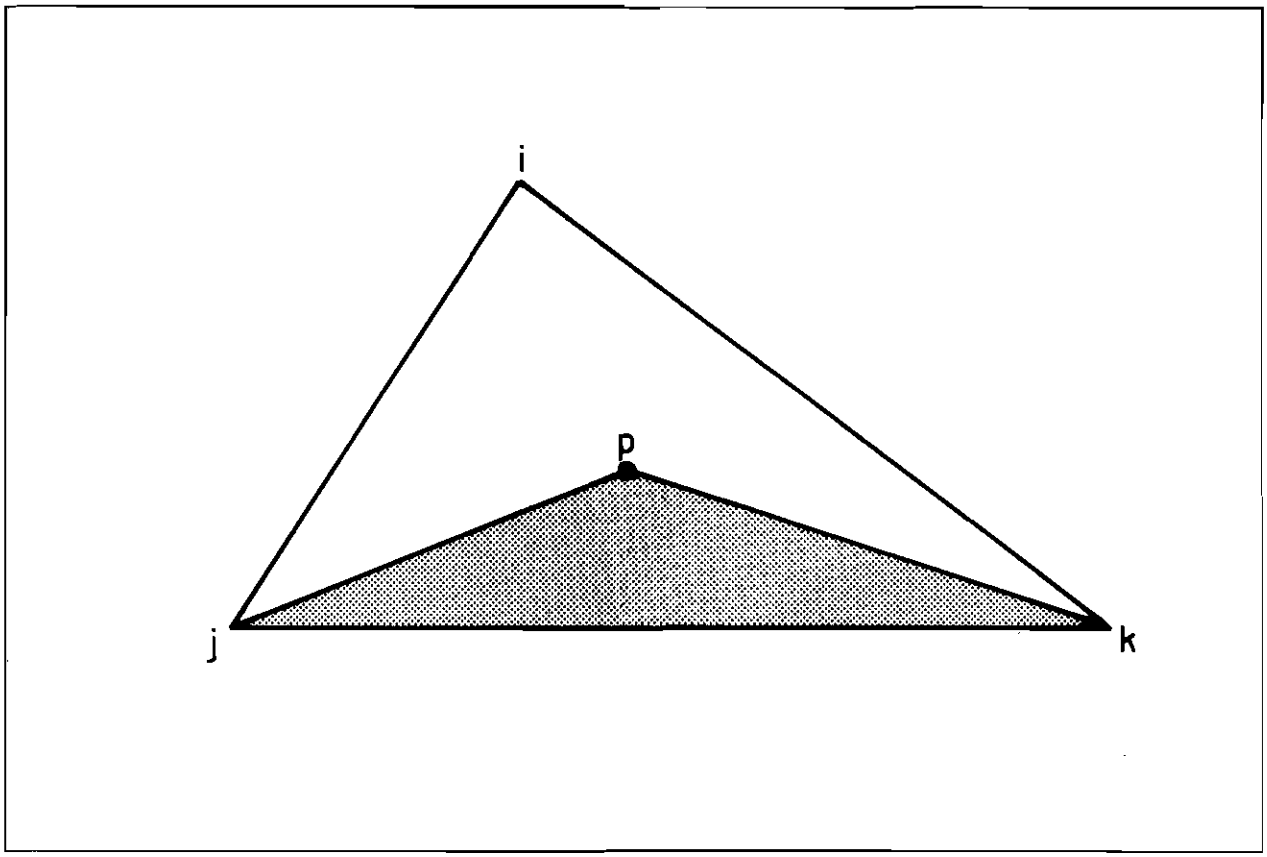

Fig 3.1 Definition of area coordinate

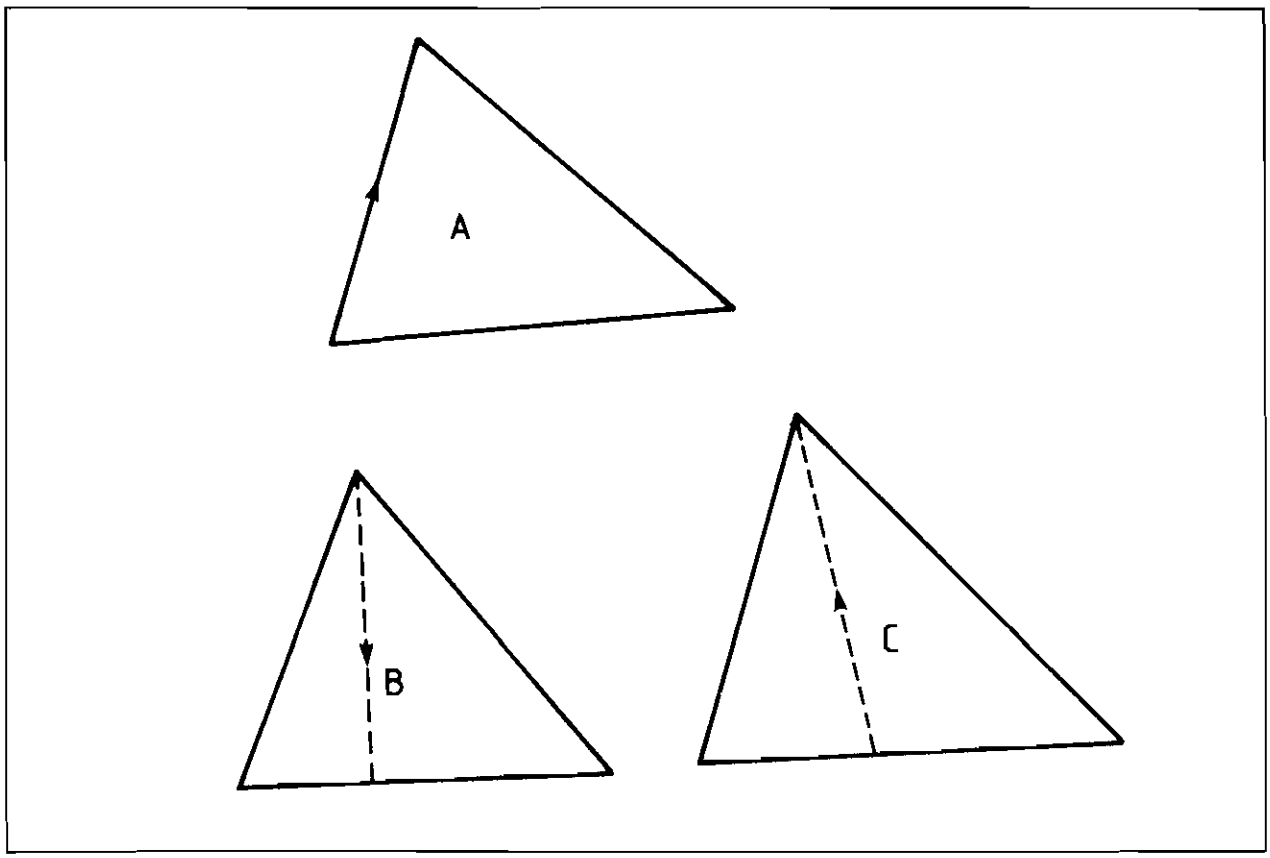

Fig 3.2 Element categories

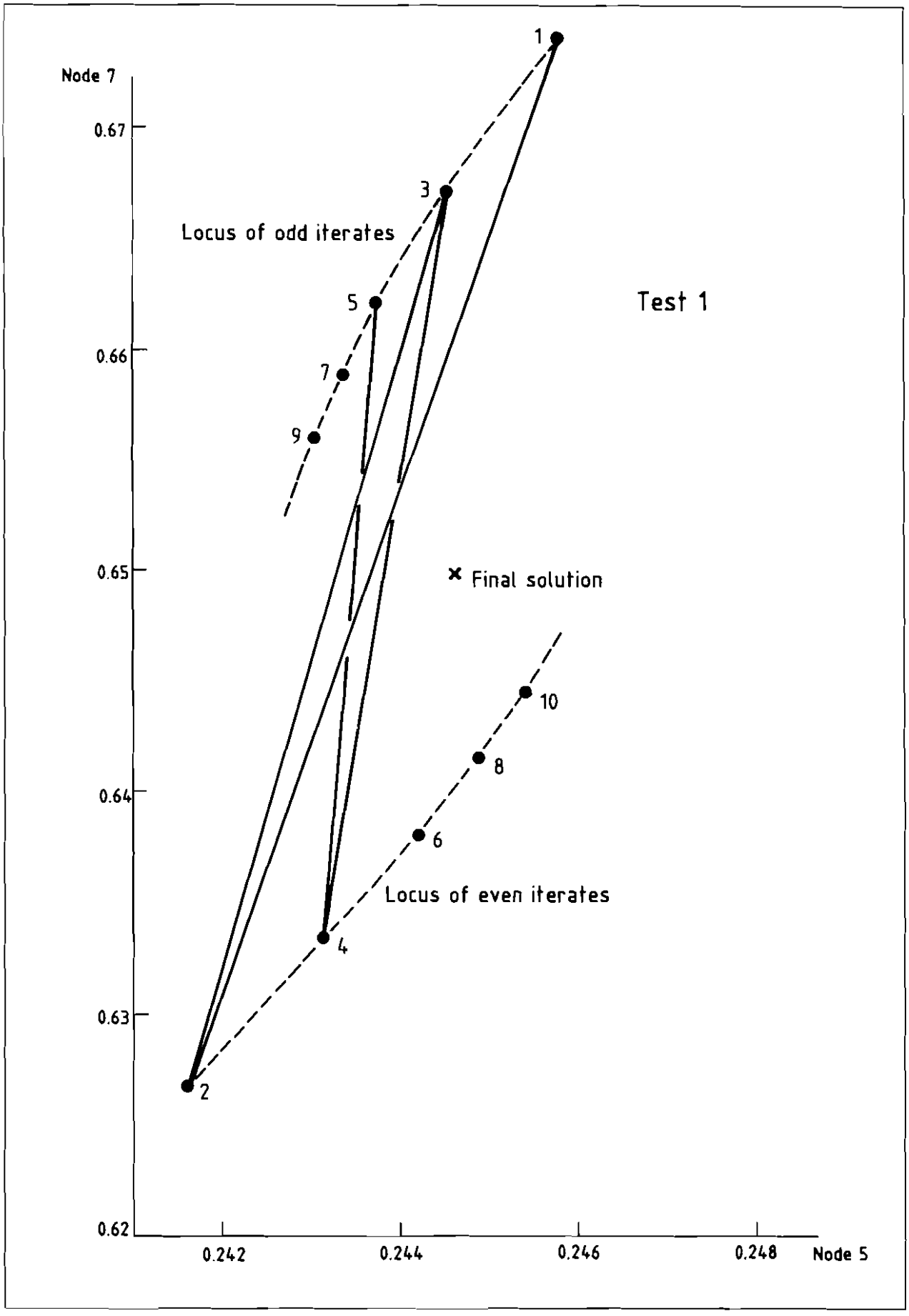

Fig 3.3 Convergence of stream function (Mesh 1)

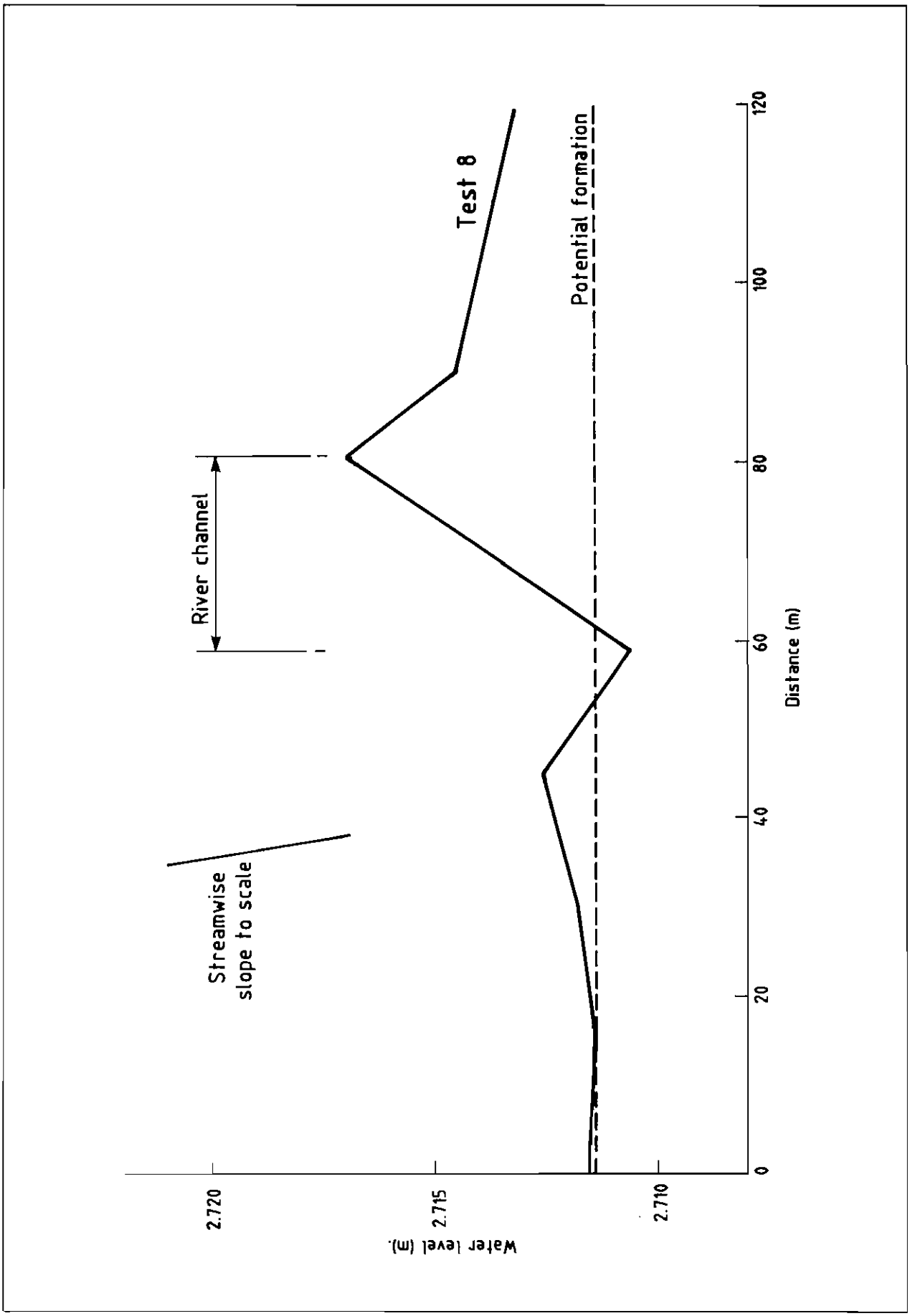

Fig 3.4 Water levels on upstream boundary (Mesh 4)

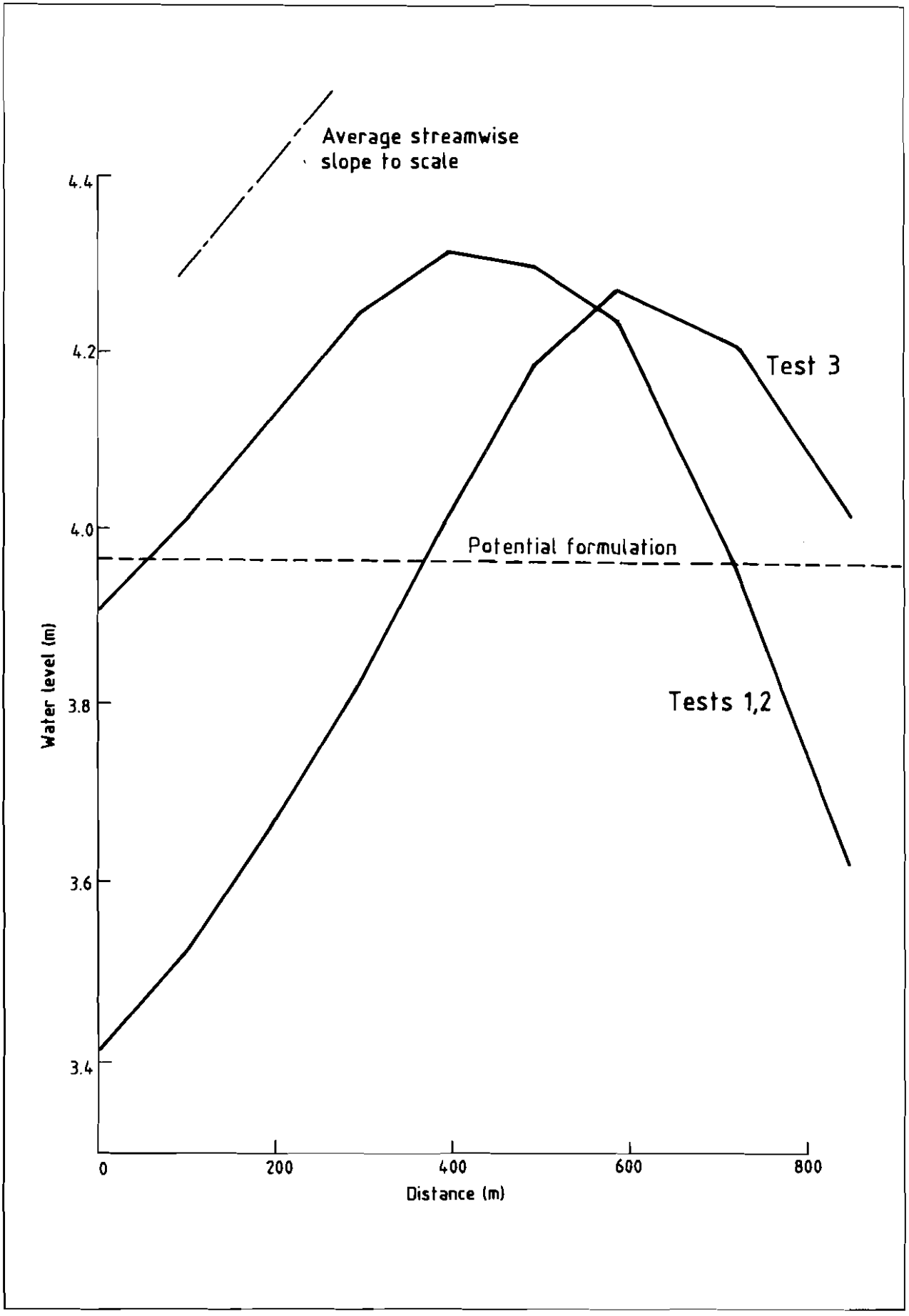

Fig 3.5 Water levels on upstream boundary (Mesh 9)

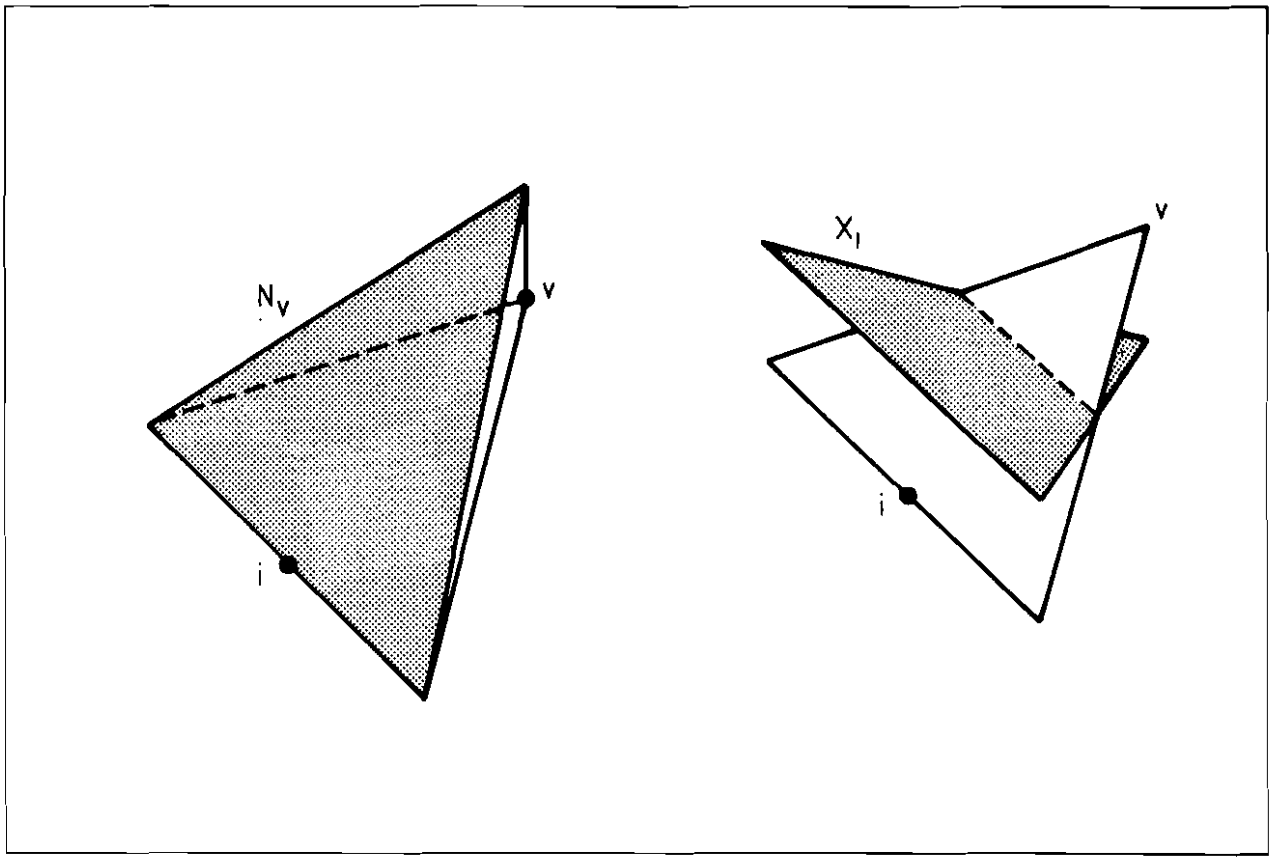

Fig 4.1 Definition of non-conforming basis function

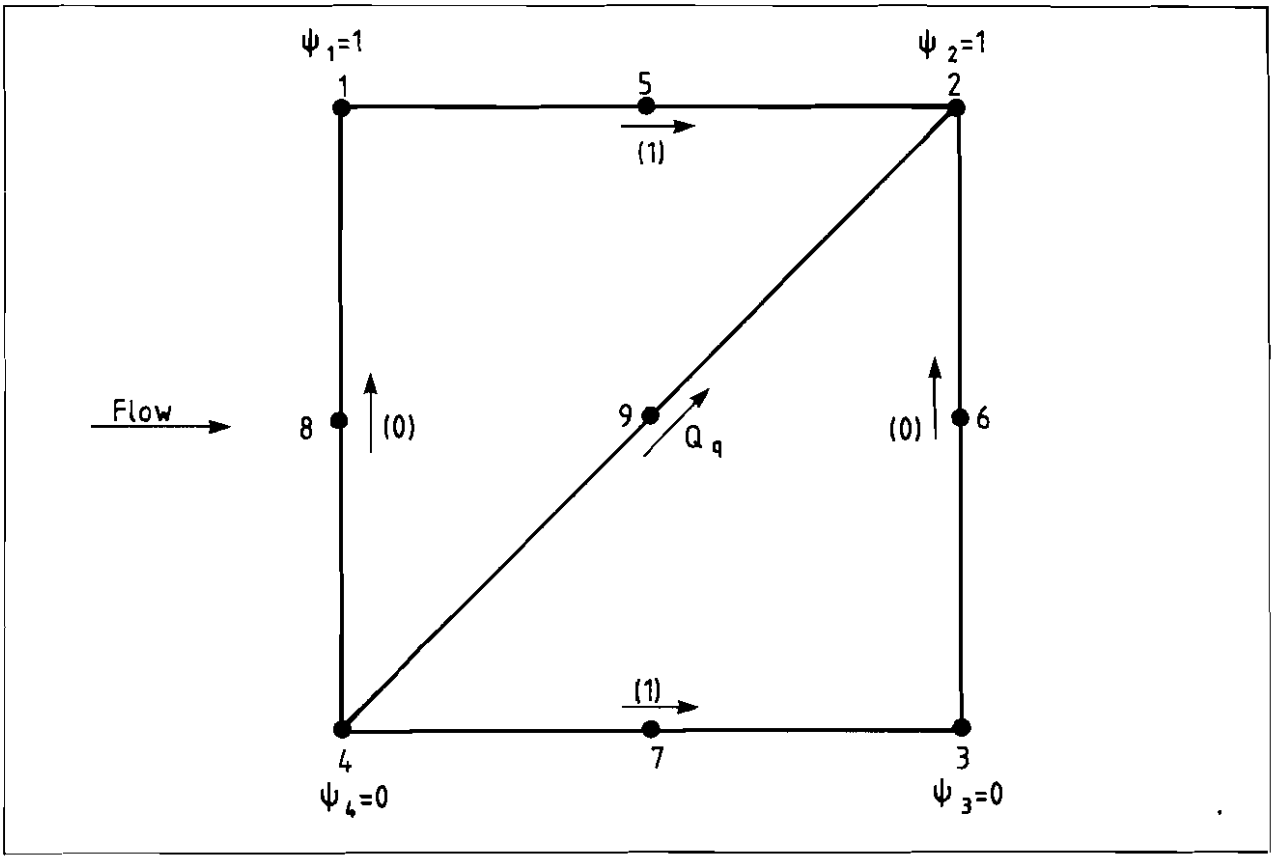

Fig 4.2 A two element patch

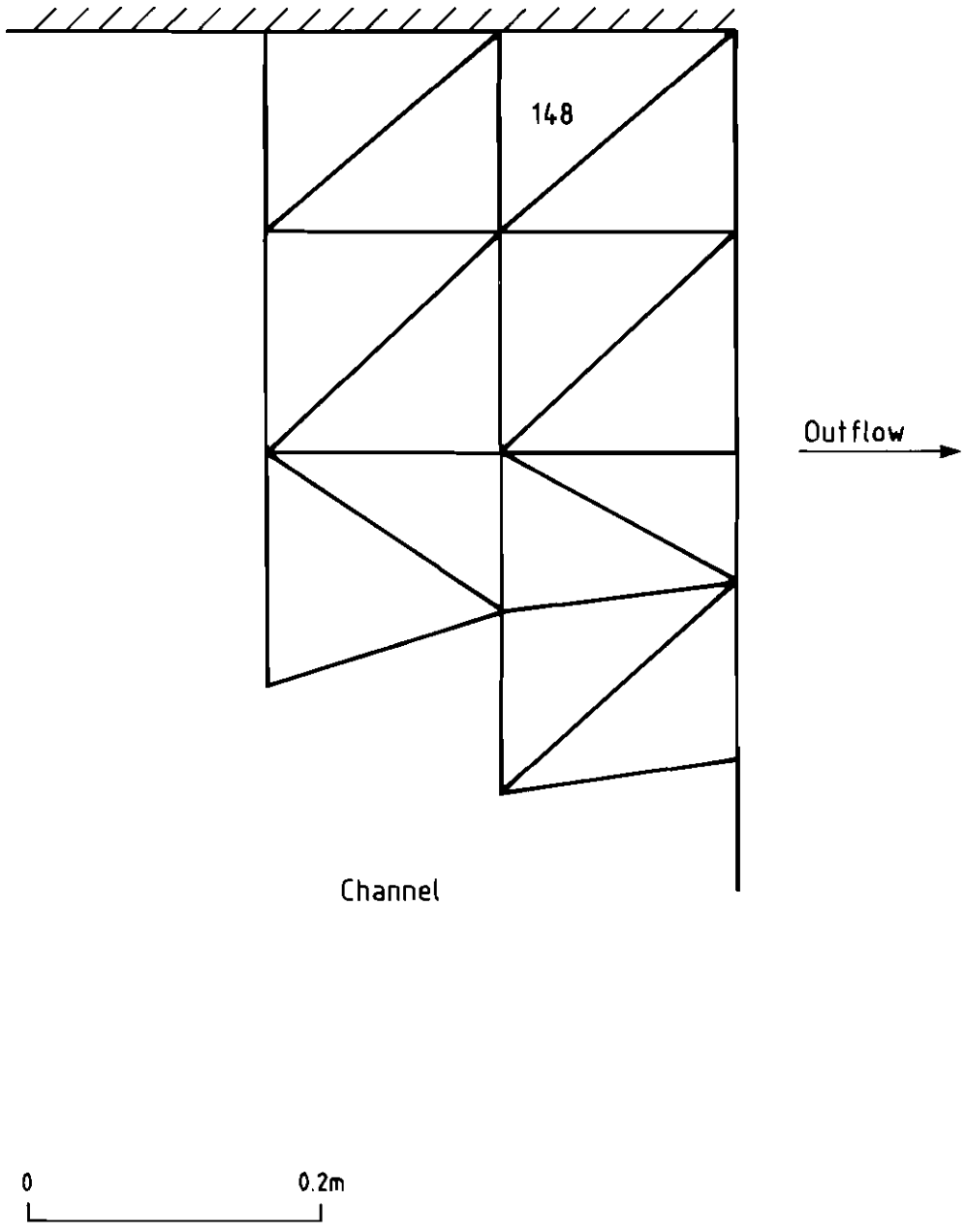

Fig 4.3 Location of element 148 on Mesh 1

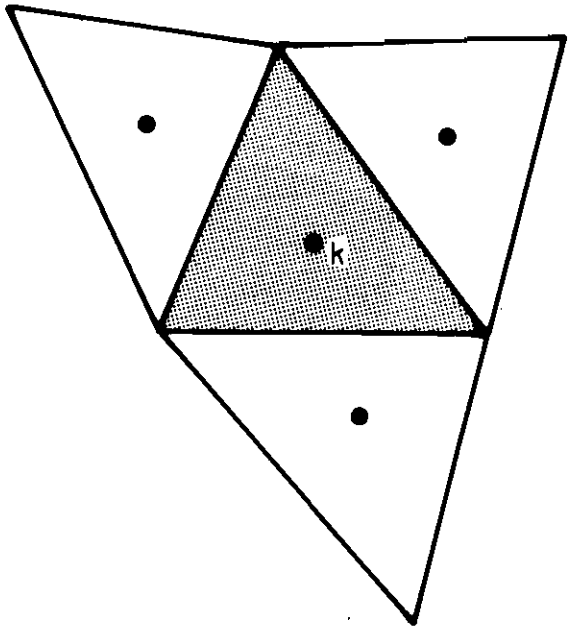

(a) Interior

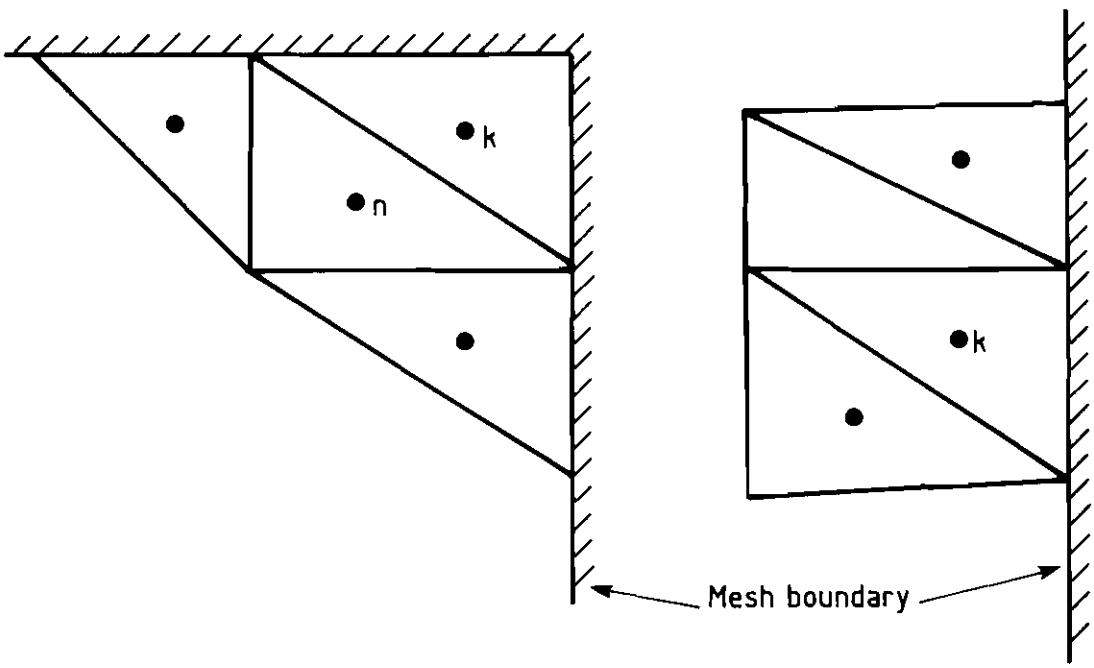

(b) Boundary cases

Fig 5.1 The standard element set

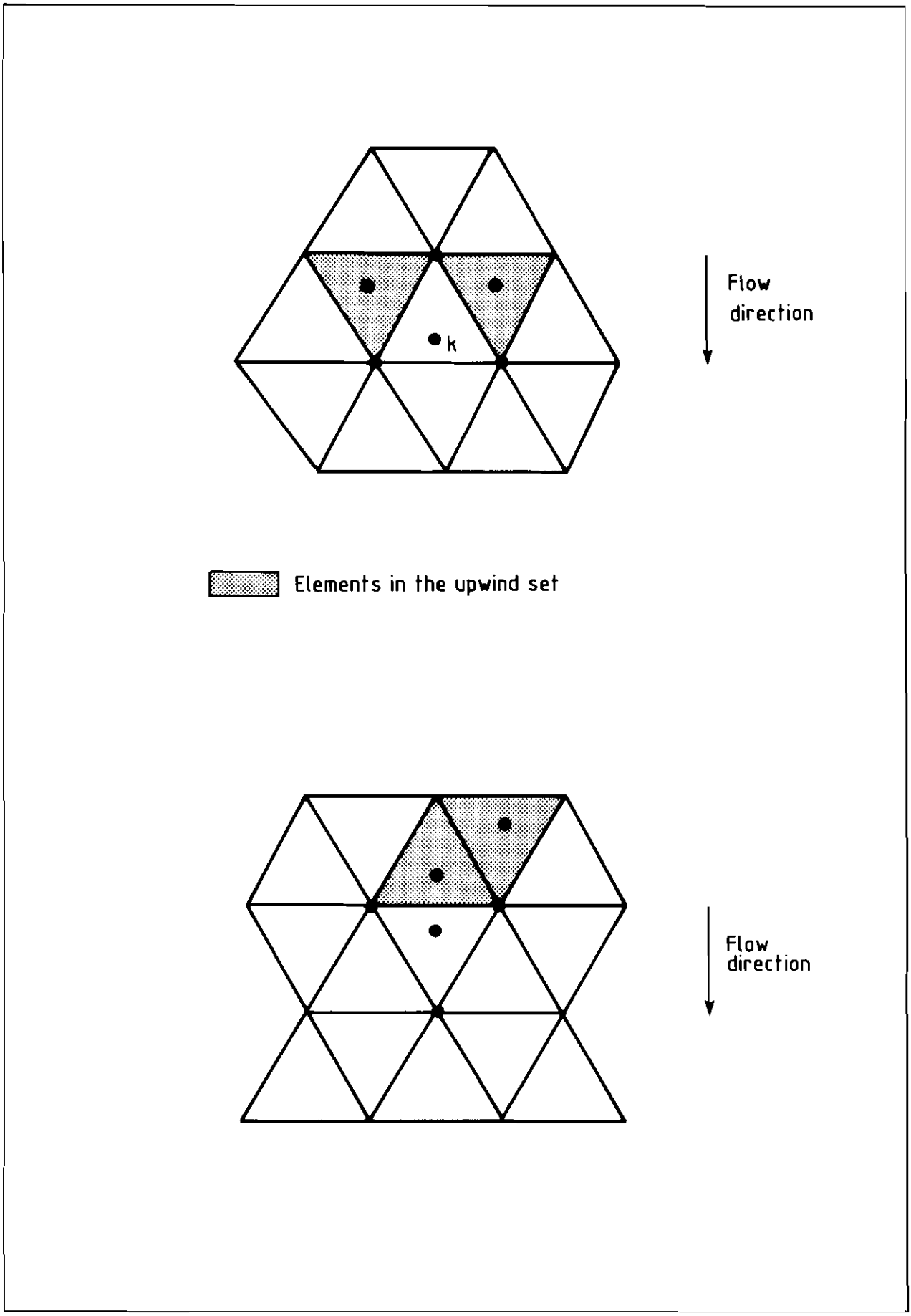

Fig 5.2 Typical upwind neighbour sets for element k

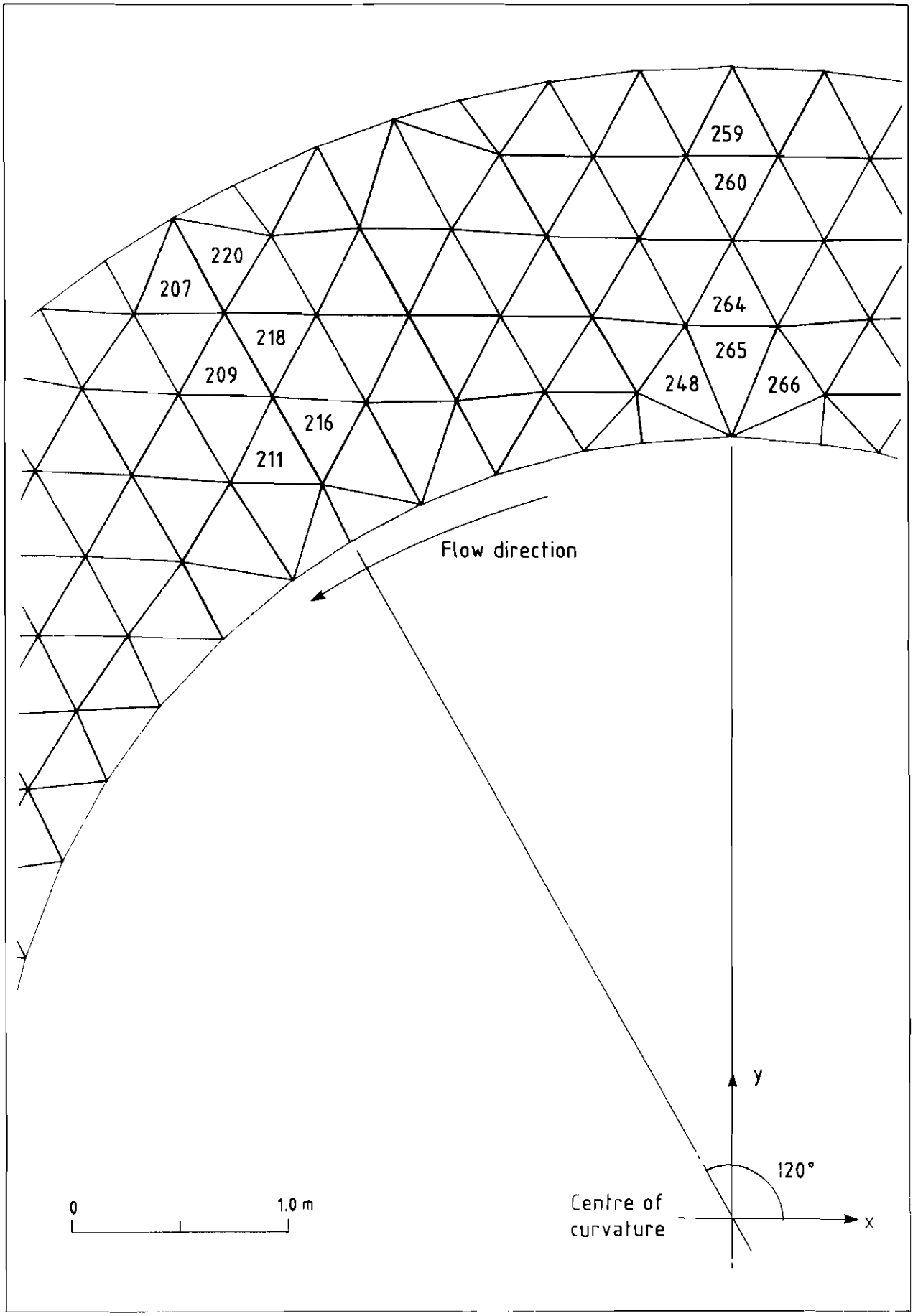

Fig 5.3 Mesh detail at centre of bend

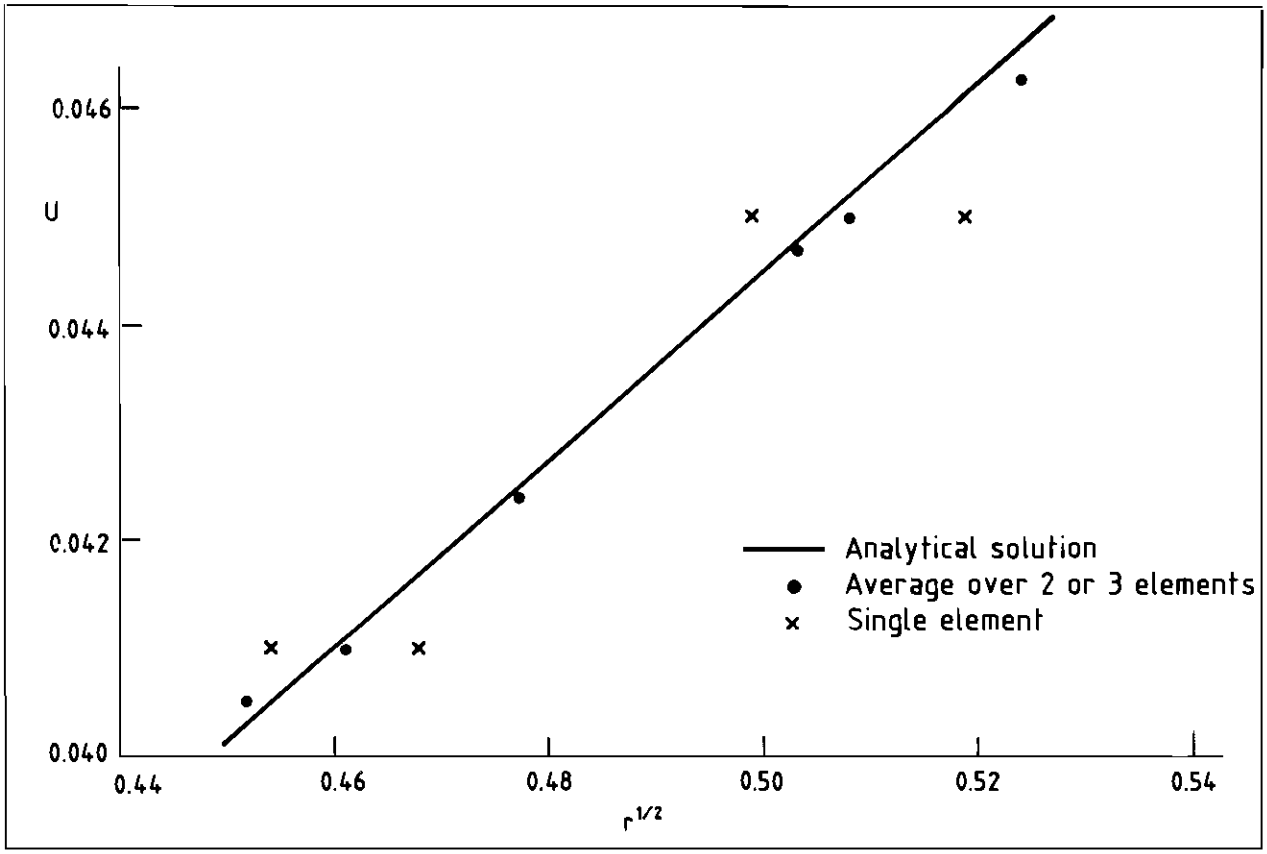

Fig 5.4 Computed and analytical variation of stream velocity

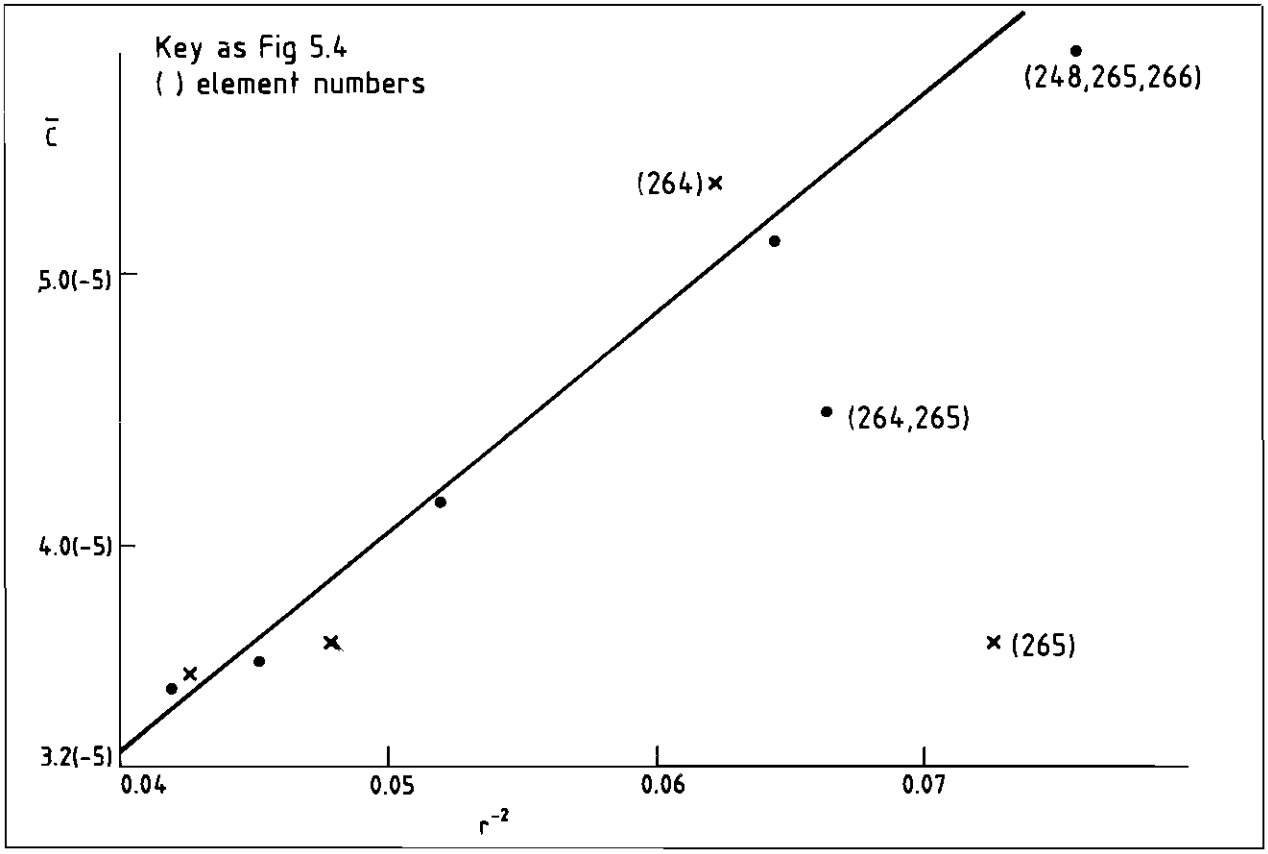

Fig 5.5 Computed and analytical variation of convection term

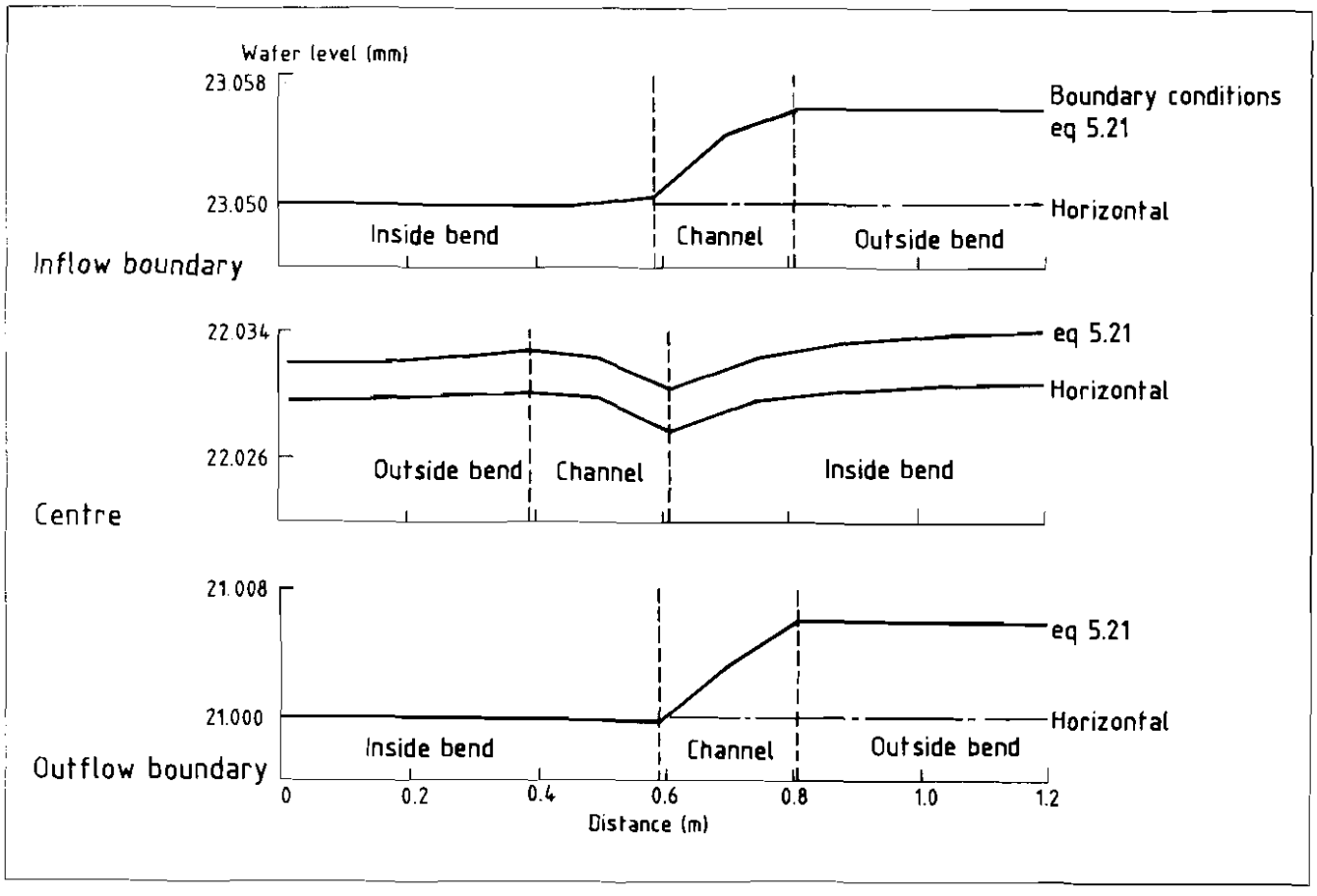

Fig 5.6 Transverse surface profiles (Mesh 1)

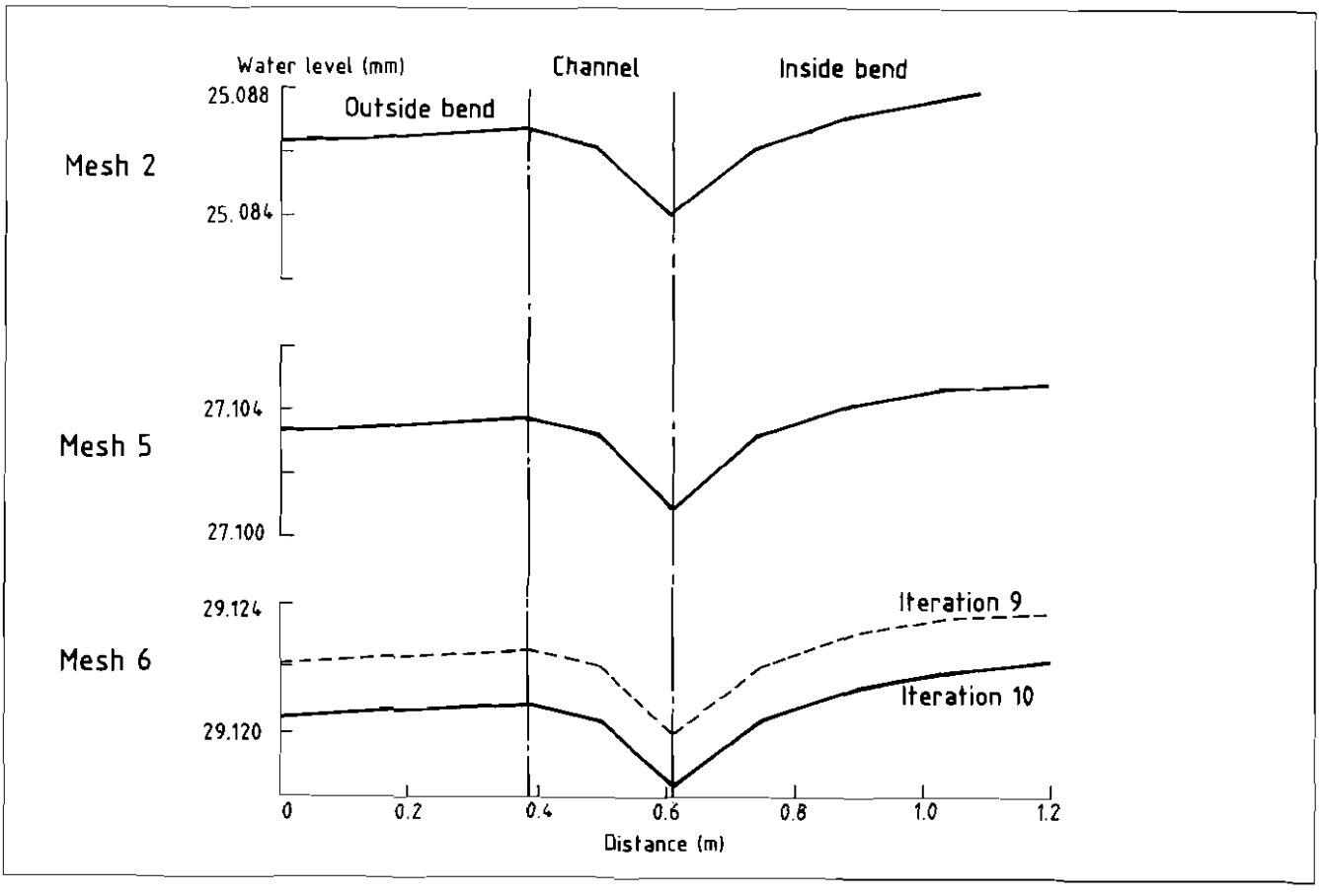

Fig 5.7 Transverse surface profiles - centre of meander (Meshes 2,5,6)

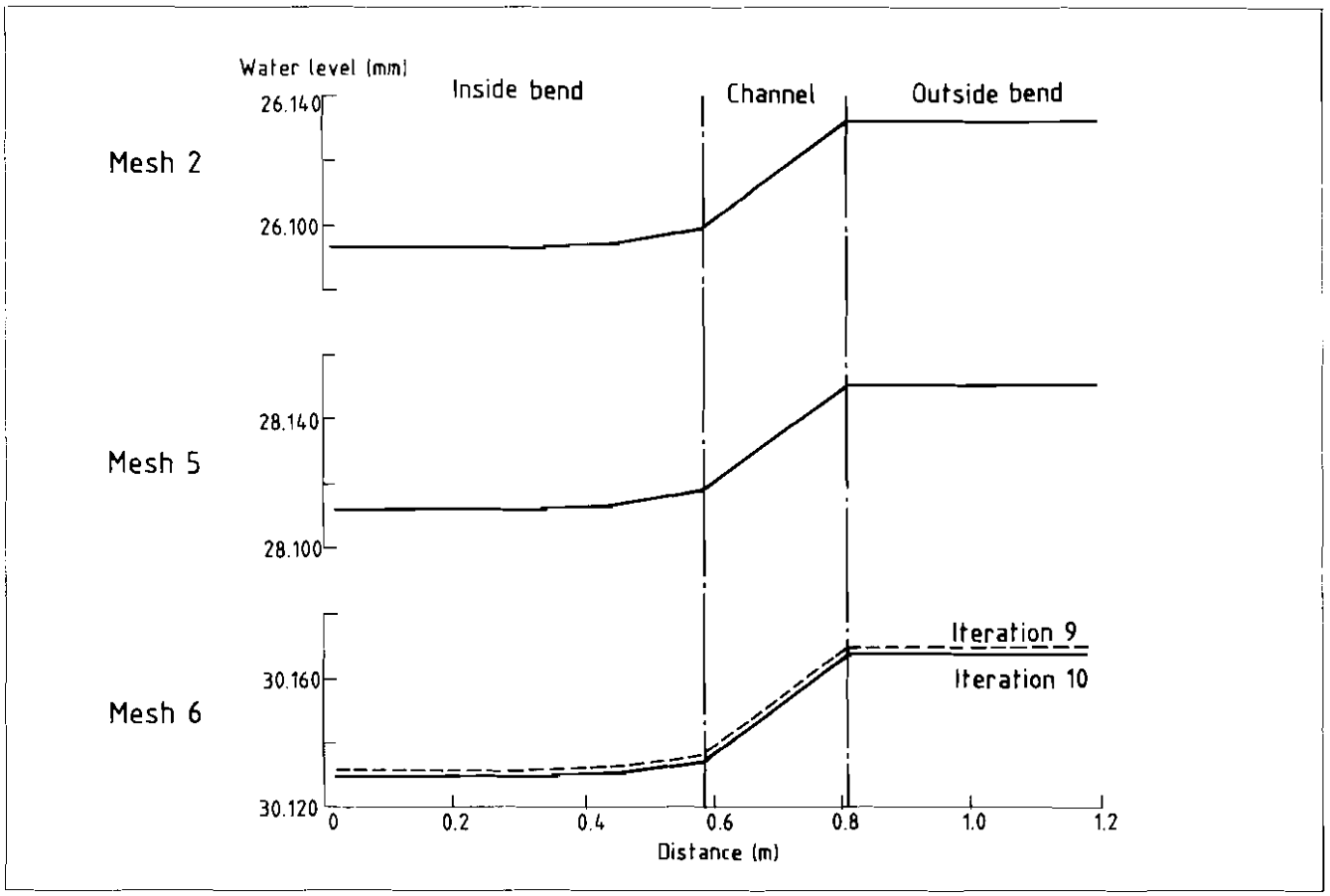

Fig 5.8 Transverse surface profiles - upstream end of meander (Meshes 2, 5,6)

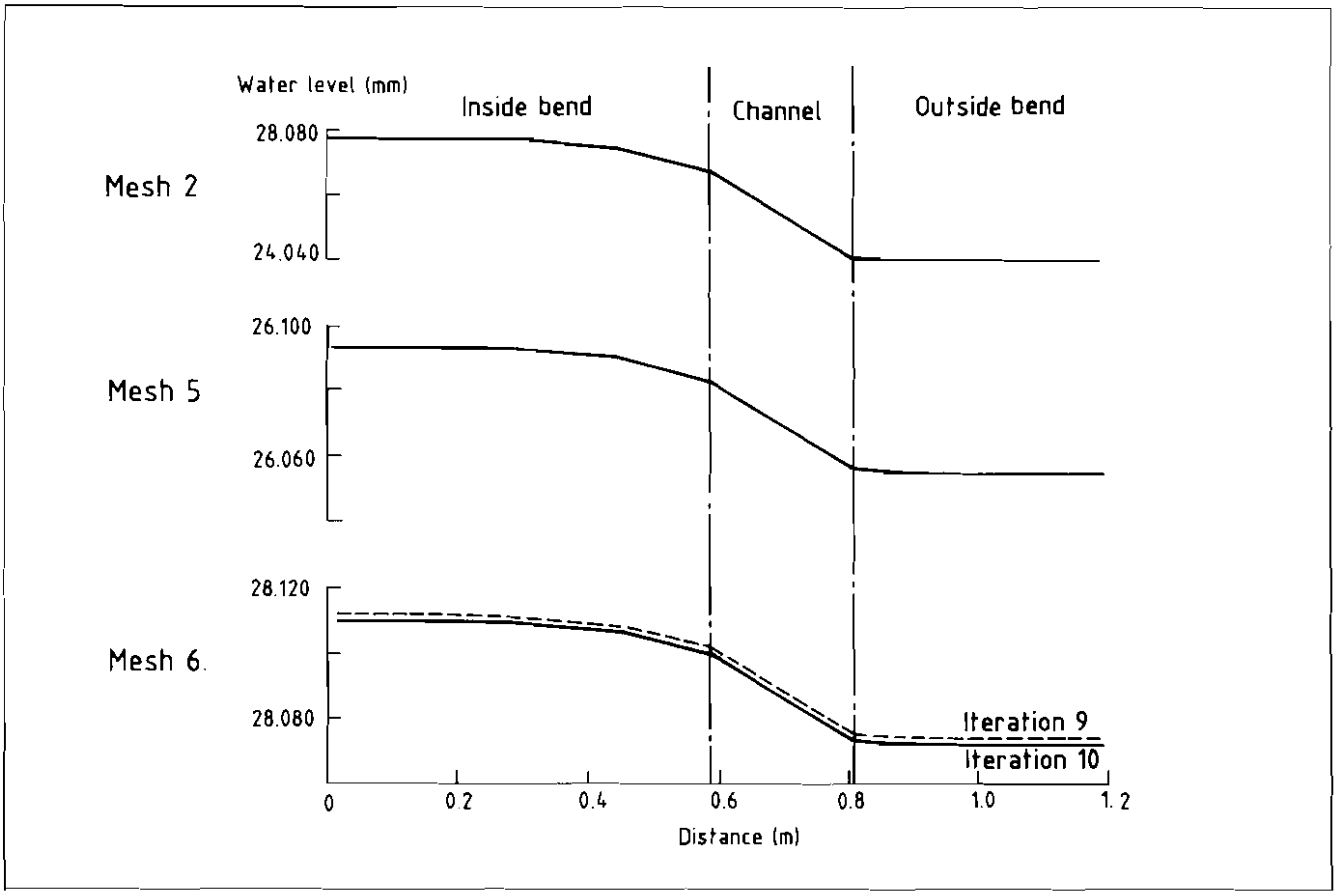

Fig 5.9 Transverse surface profiles -downstream end of meander (Meshes 2,5,6)

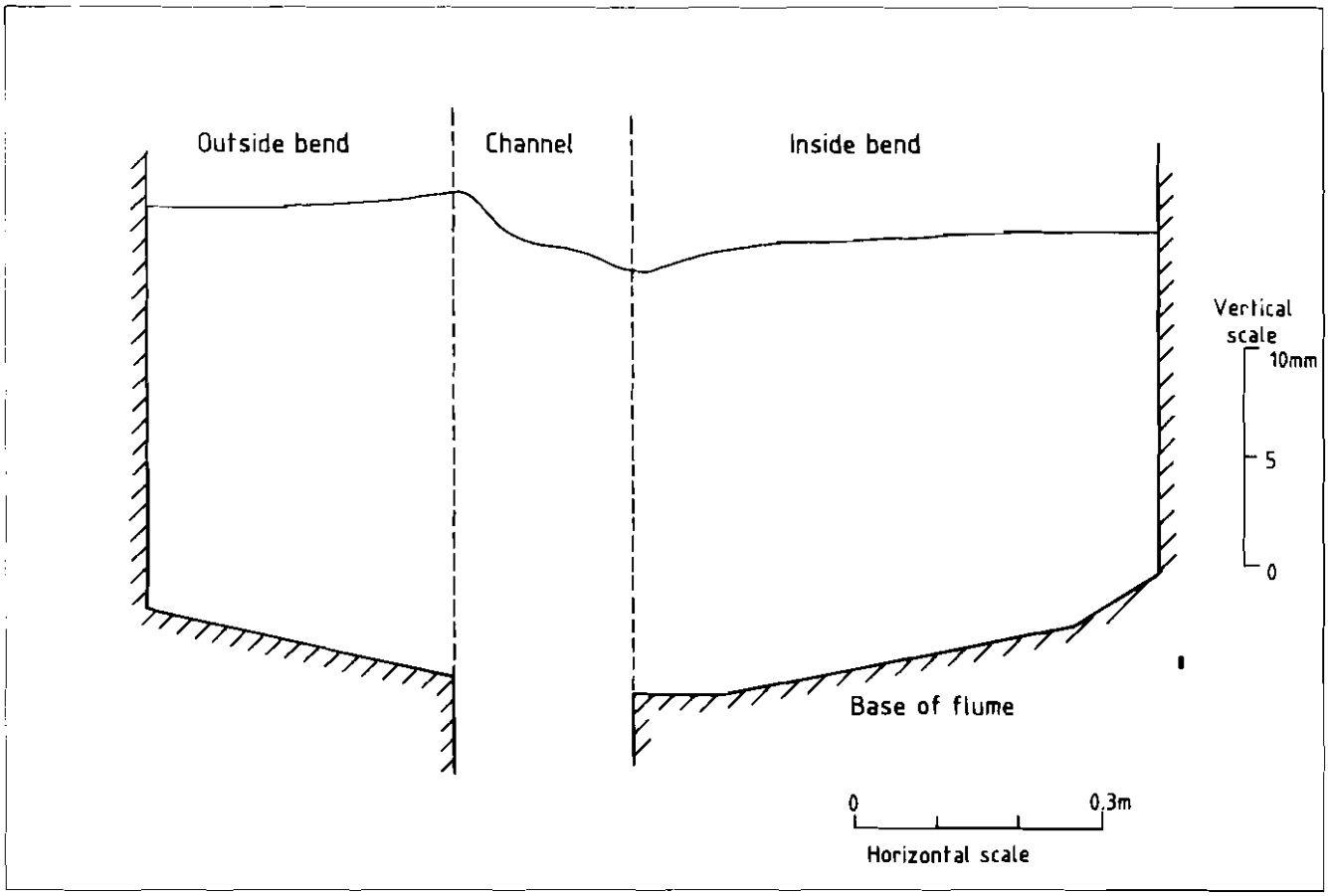

Fig 5.10 Cross-section of experimental flume from Sooky (1964)

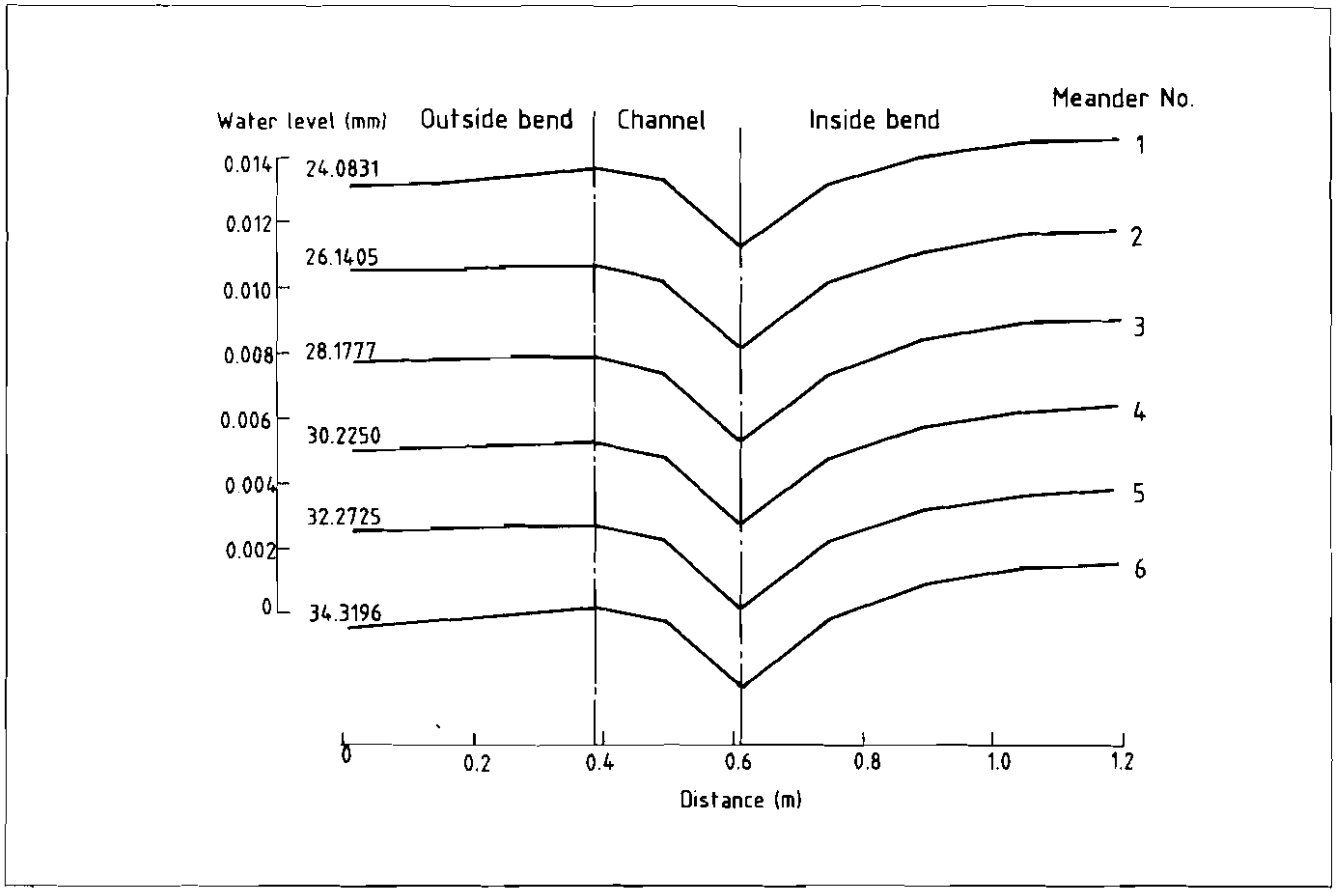

Fig 5.11 Transverse surface profiles at centre of meander (Mesh 7)

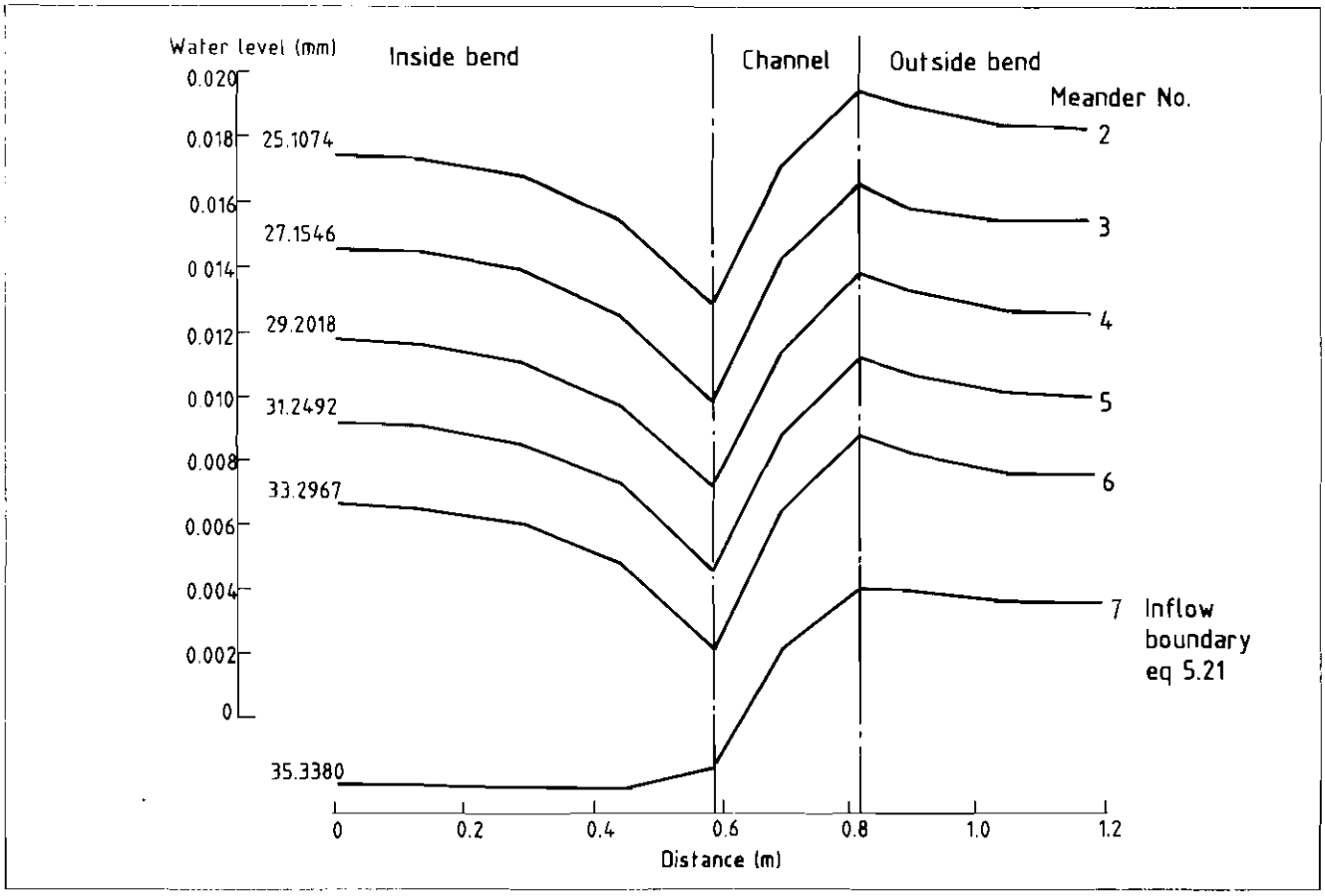

Fig 5.12 Transverse water surface profiles at full meander wave (Mesh 7)

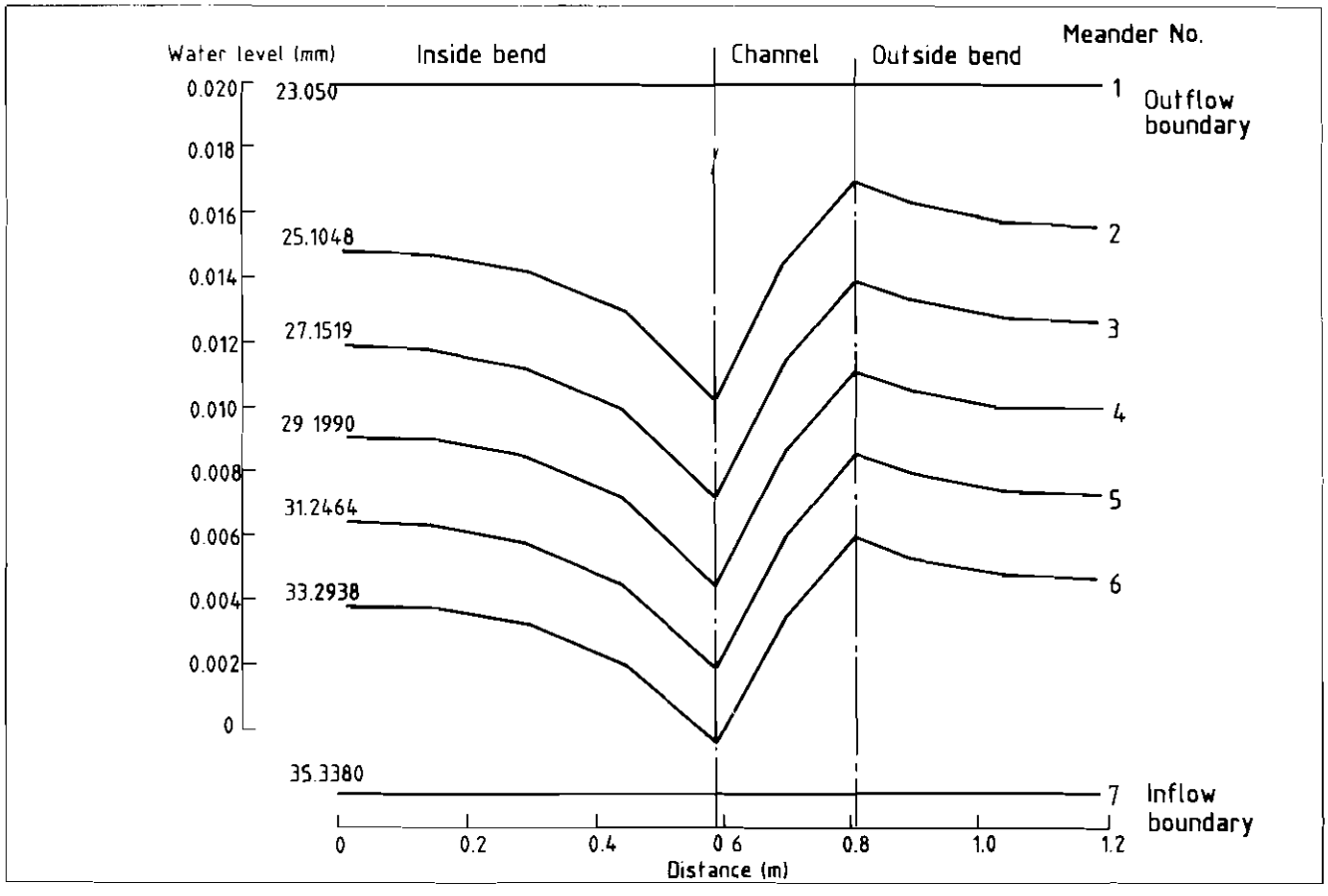

Fig 5.13 Transverse surface profiles at full meander wave for horizontal boundary conditions (Mesh 7)

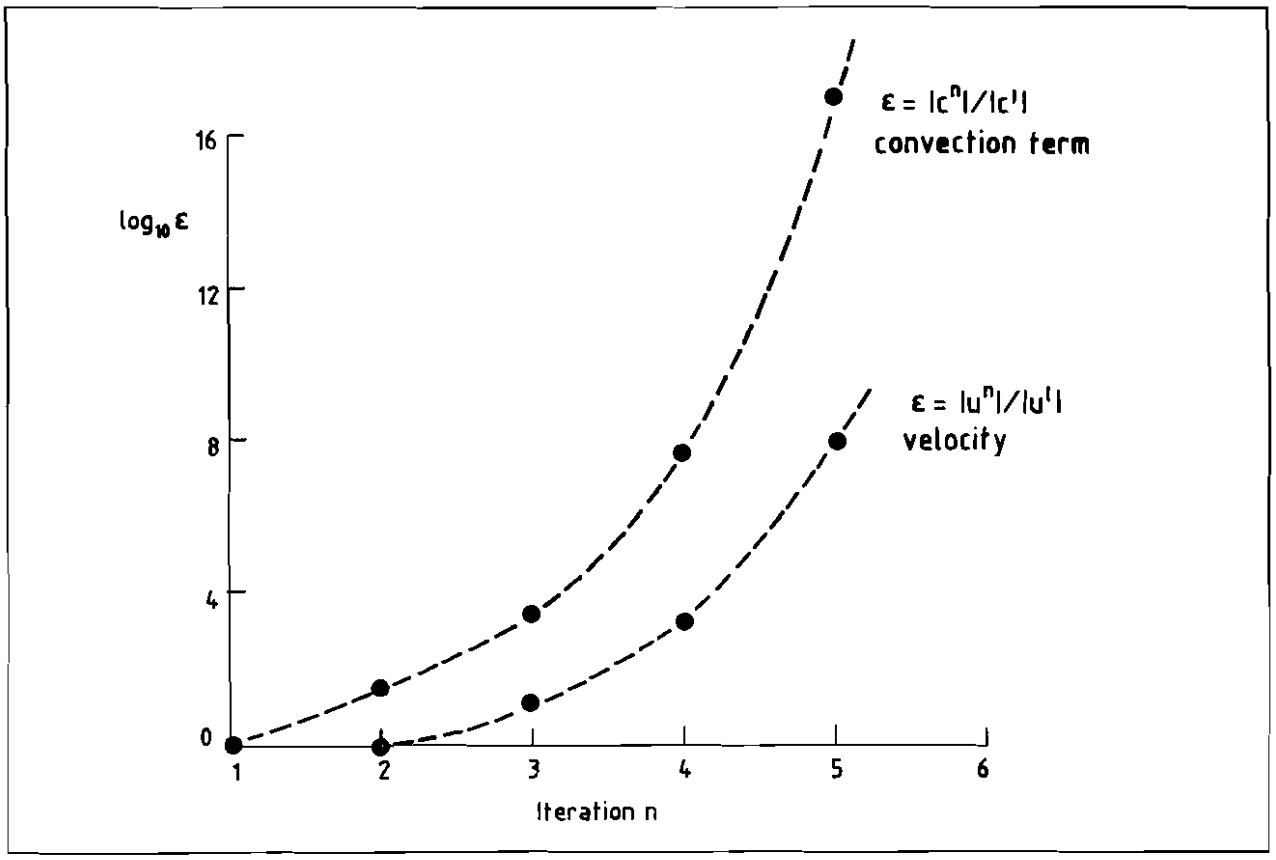

Fig 5.14 Growth of solution for roughness 3.6mm

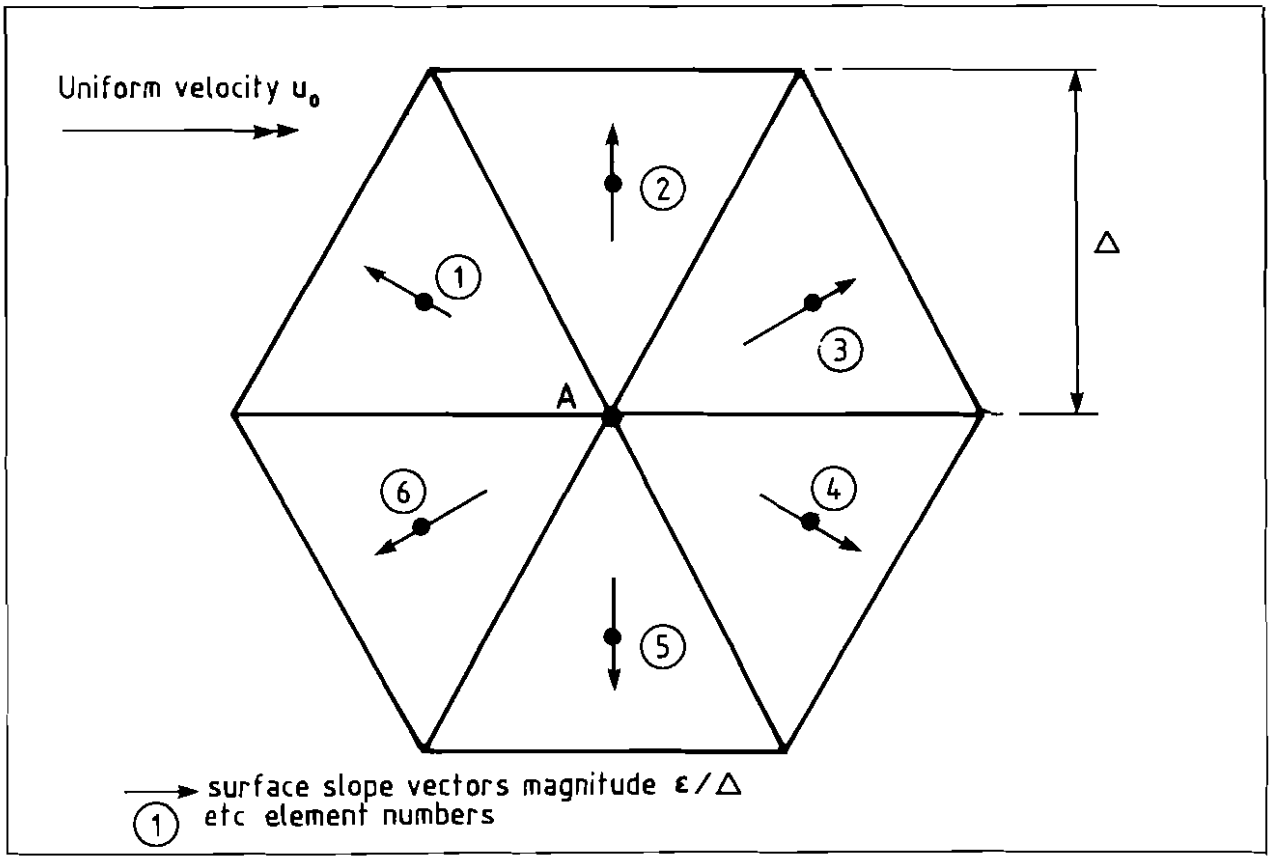

Fig 5.15 A patch around the node A

Velocity magnitude $\frac{\varepsilon F^2}{u_o \Delta}$

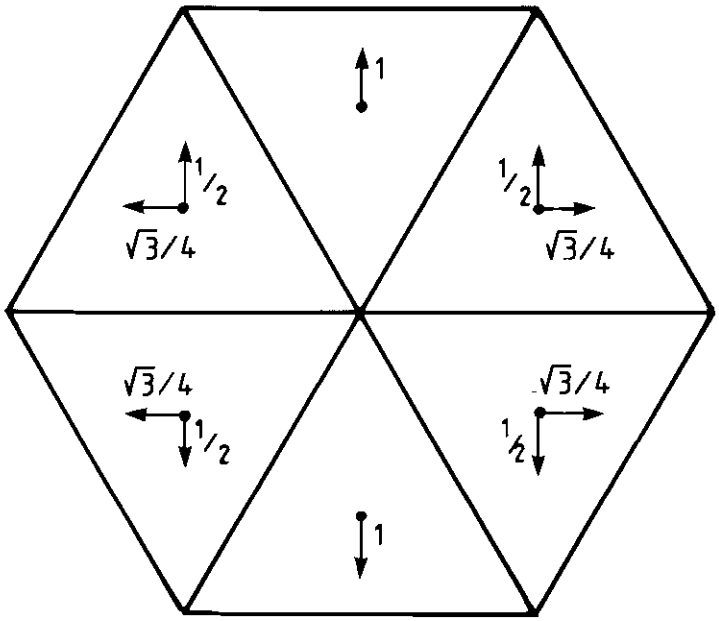

Convection term magnitude

$\frac{\sqrt{3}\varepsilon}{2}\left(\frac{F^2}{g\Delta}\right)$

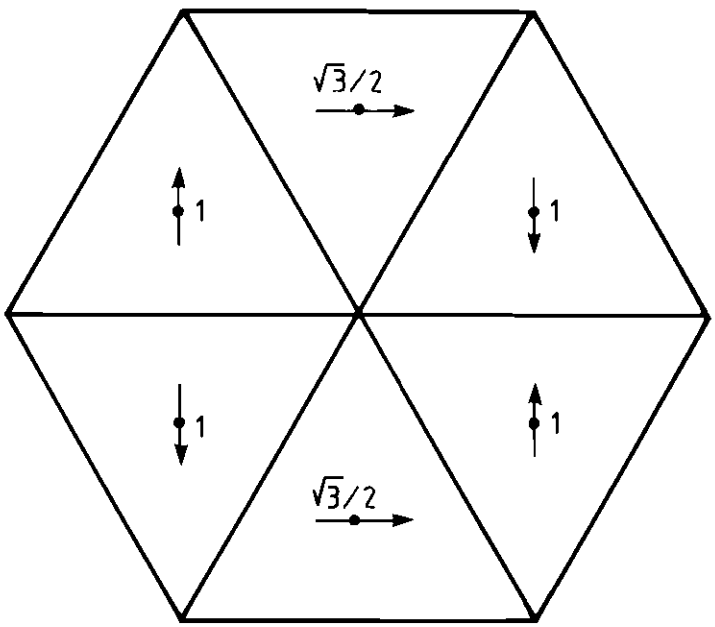

Fig 5.16 Error components for first iteration

Velocity magnitude

$$\frac{\sqrt{3}\varepsilon F^2}{4\,\Delta u_o}\left(\frac{E^2}{g\Delta}\right)$$

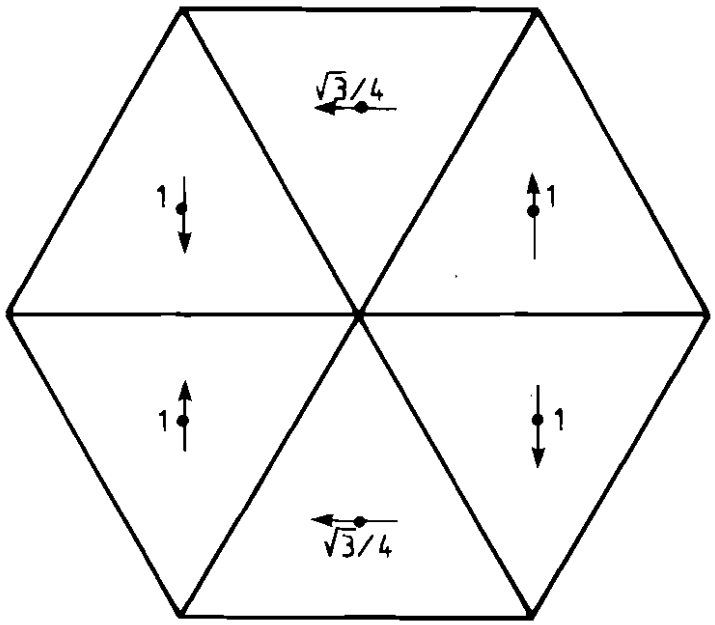

Convection term magnitude

$$\frac{3\varepsilon}{8}\left(\frac{F^2}{g\Delta}\right)^2$$

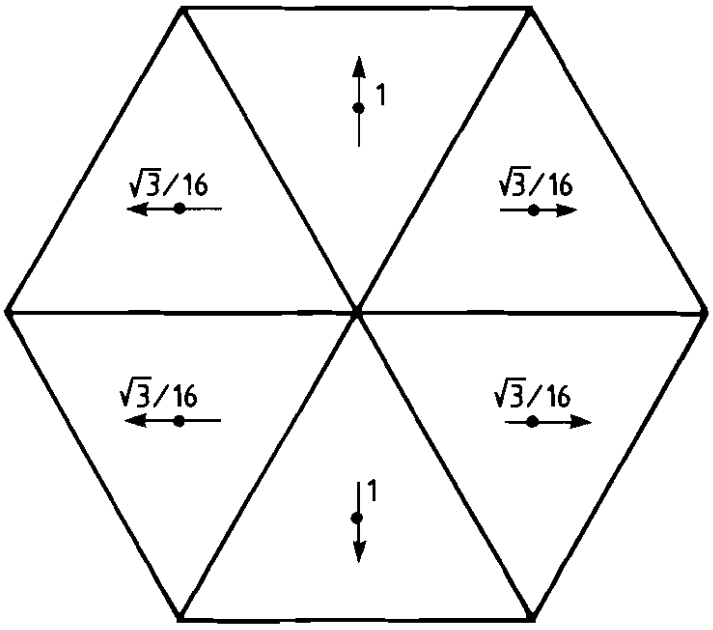

Fig 5.17 Error components for second iteration

Velocity magnitude

$$\frac{87\varepsilon F^2}{192\Delta U_0}\left(\frac{F^2}{g\Delta}\right)^2$$

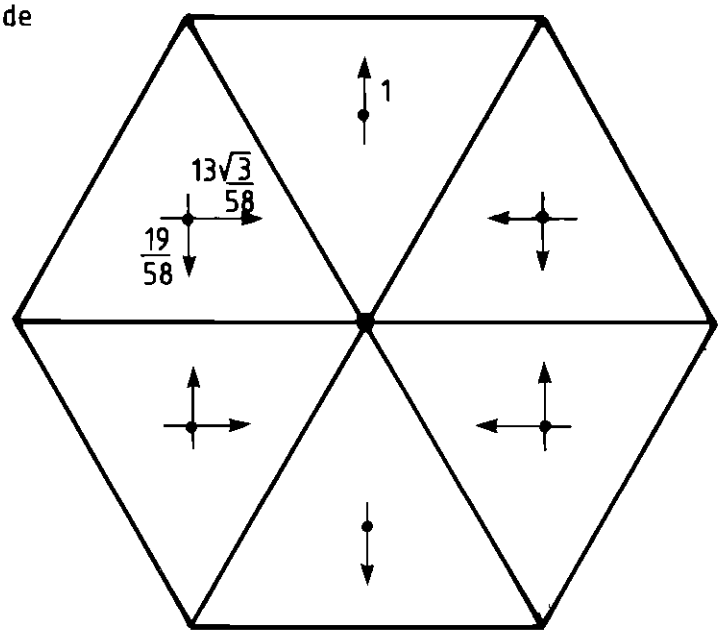

Convection magnitude

$$\propto \varepsilon\left(\frac{F^2}{g\Delta}\right)^3$$

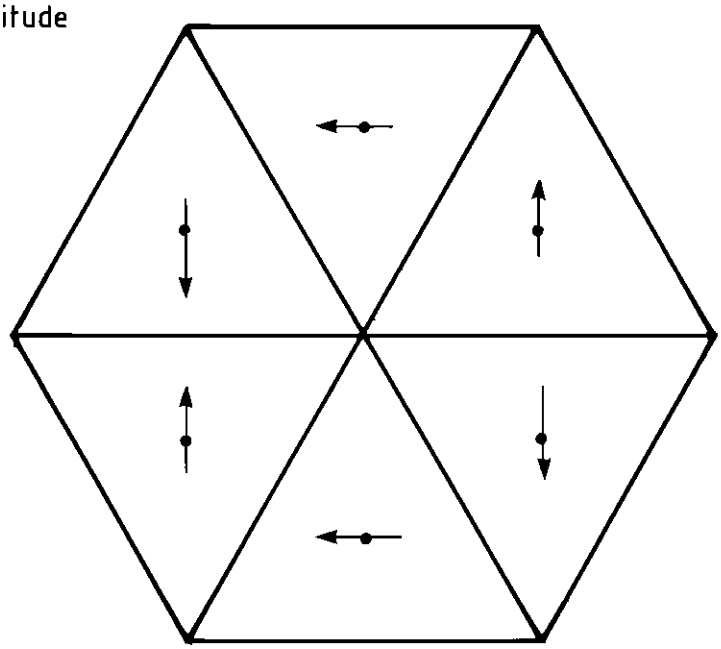

Fig 5.18 Error components for third iteration

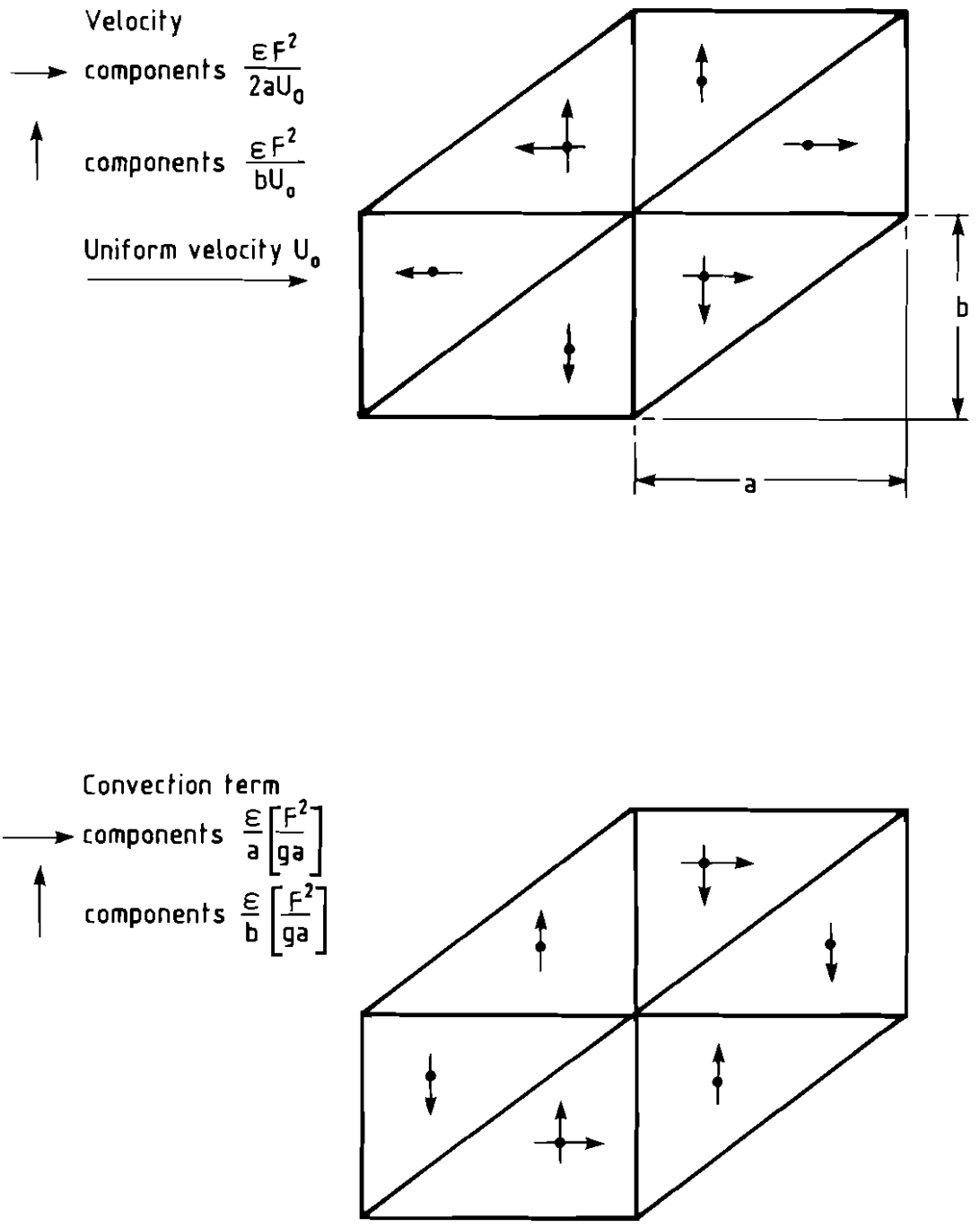

Fig 5.19 Error components for iteration 1 on right triangular mesh

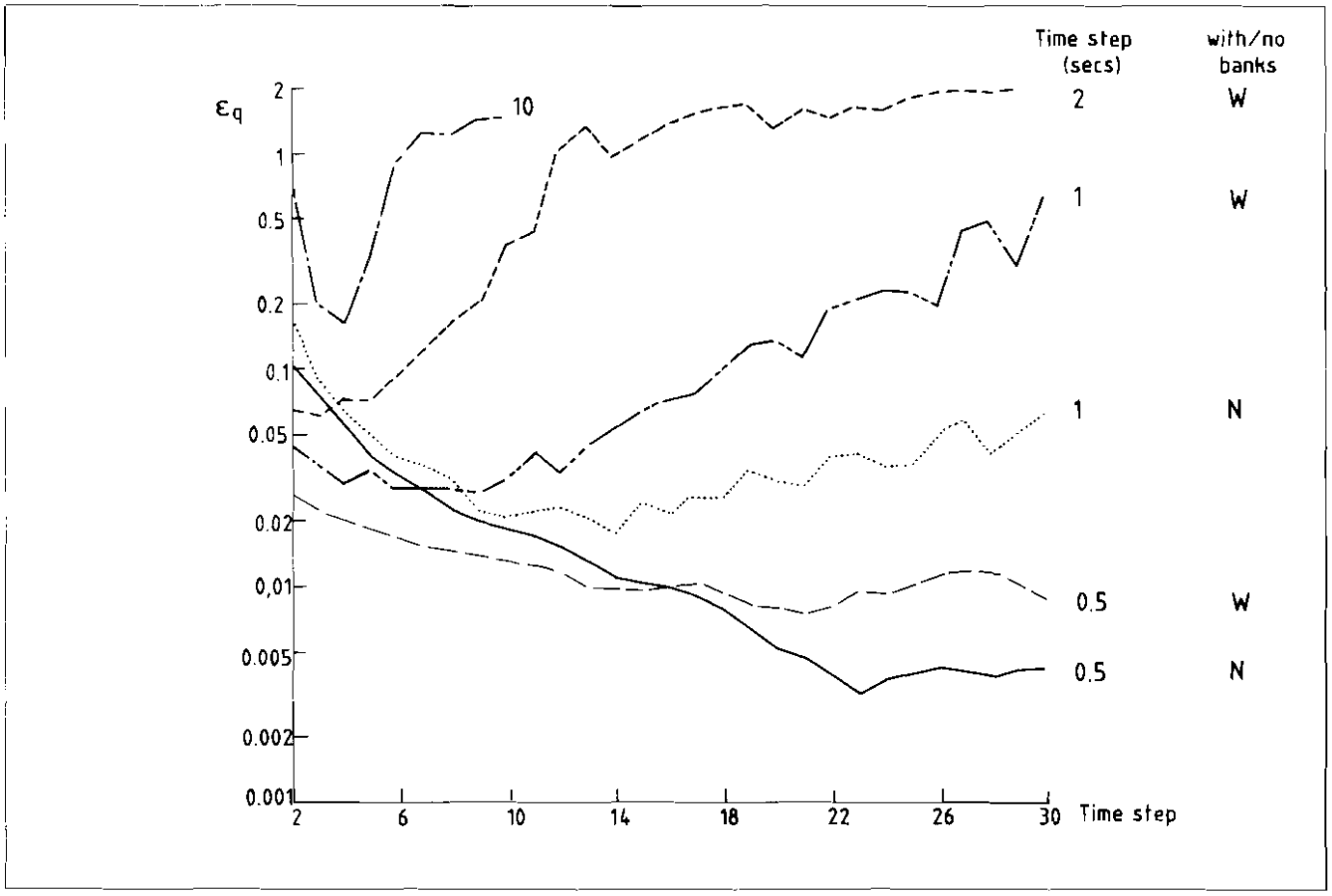

Fig 5.20 Convergence parameter for unit flow, ε_q (Mesh 2)

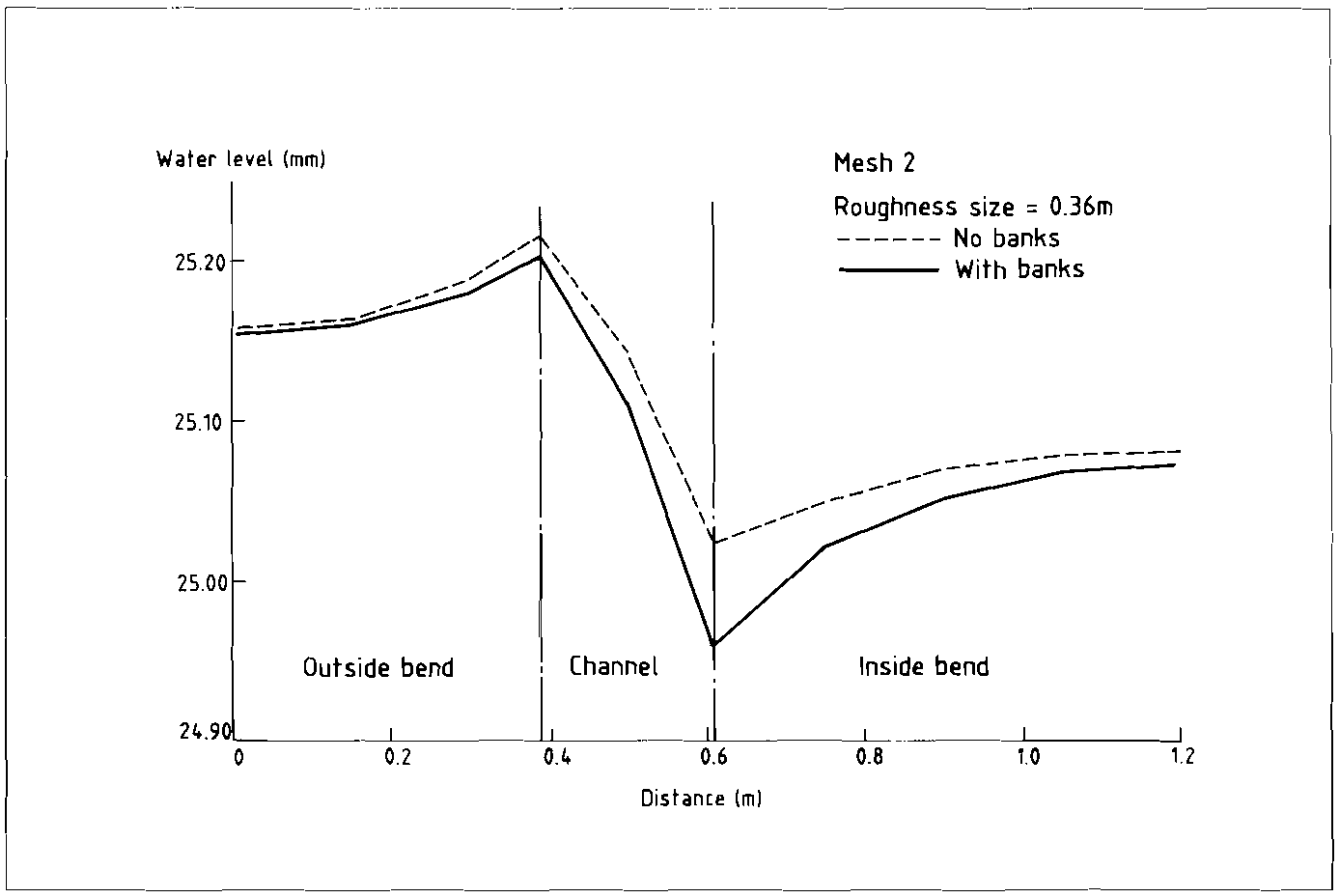

Fig 5.21 Transverse surface profiles with and without banks

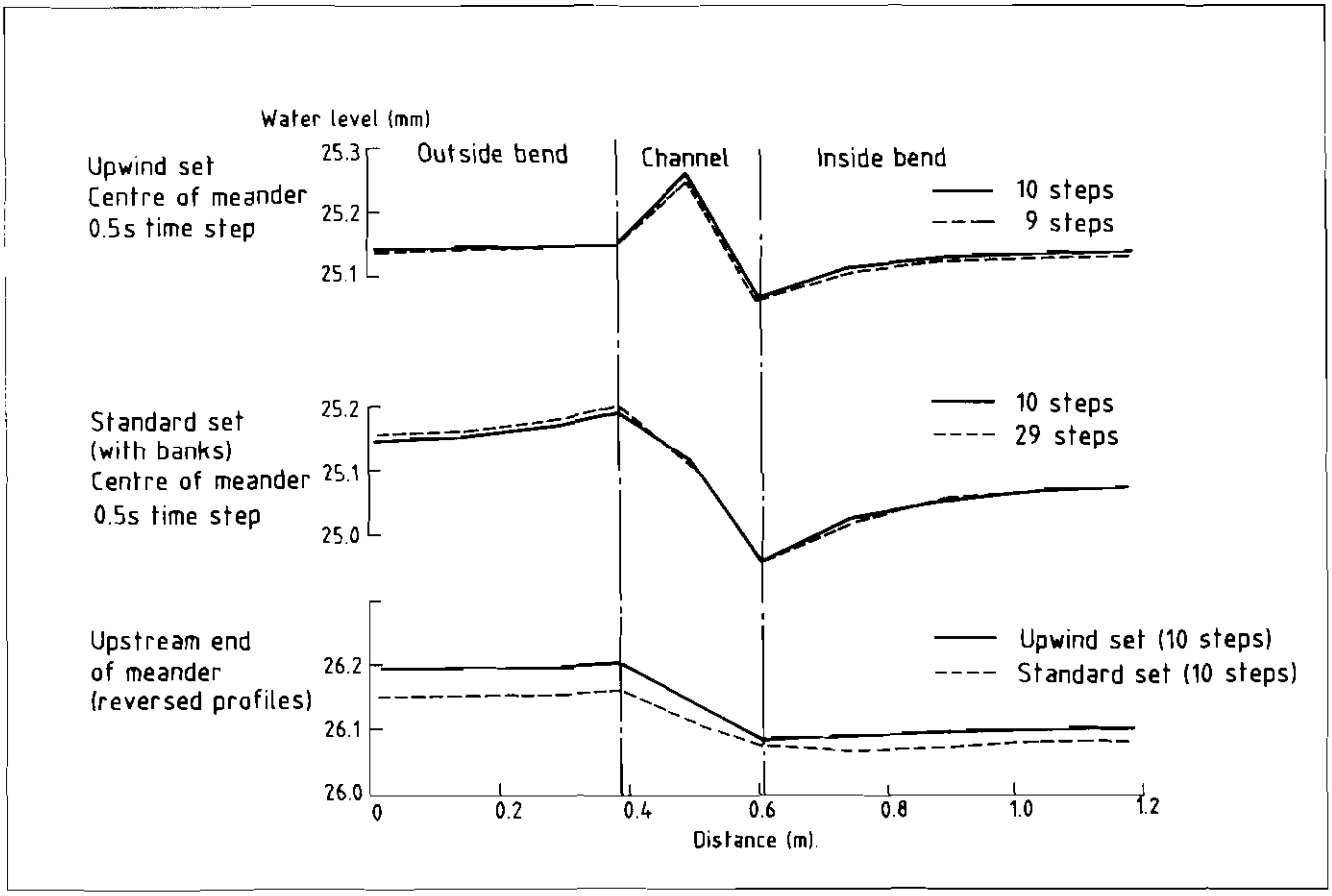

Fig 5.22 Transverse surface profiles for upwind and standard neighbour sets (Mesh 2)

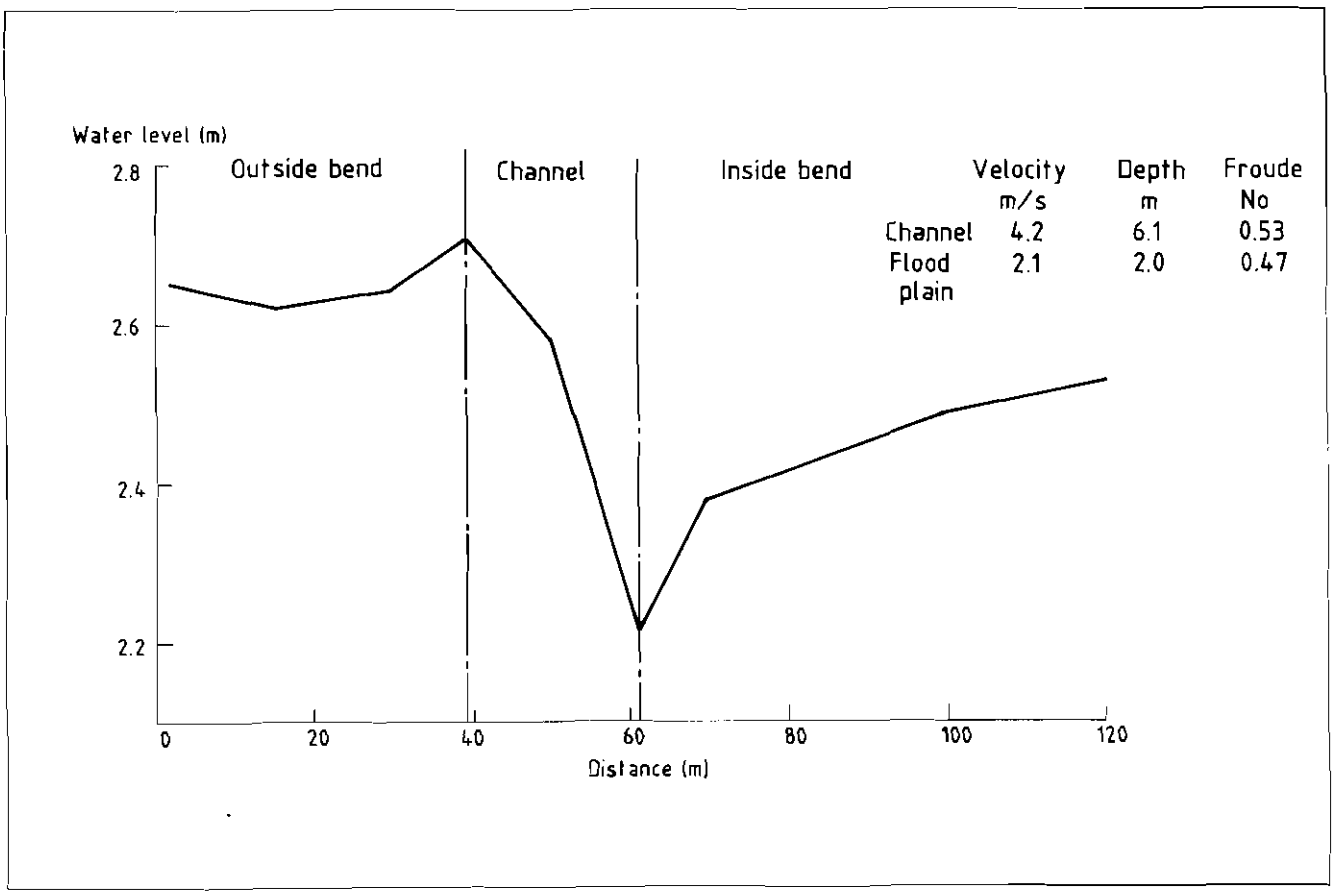

Fig 5.23 Transverse surface profile at centre of meander (Mesh 4, roughness size 0.36m)

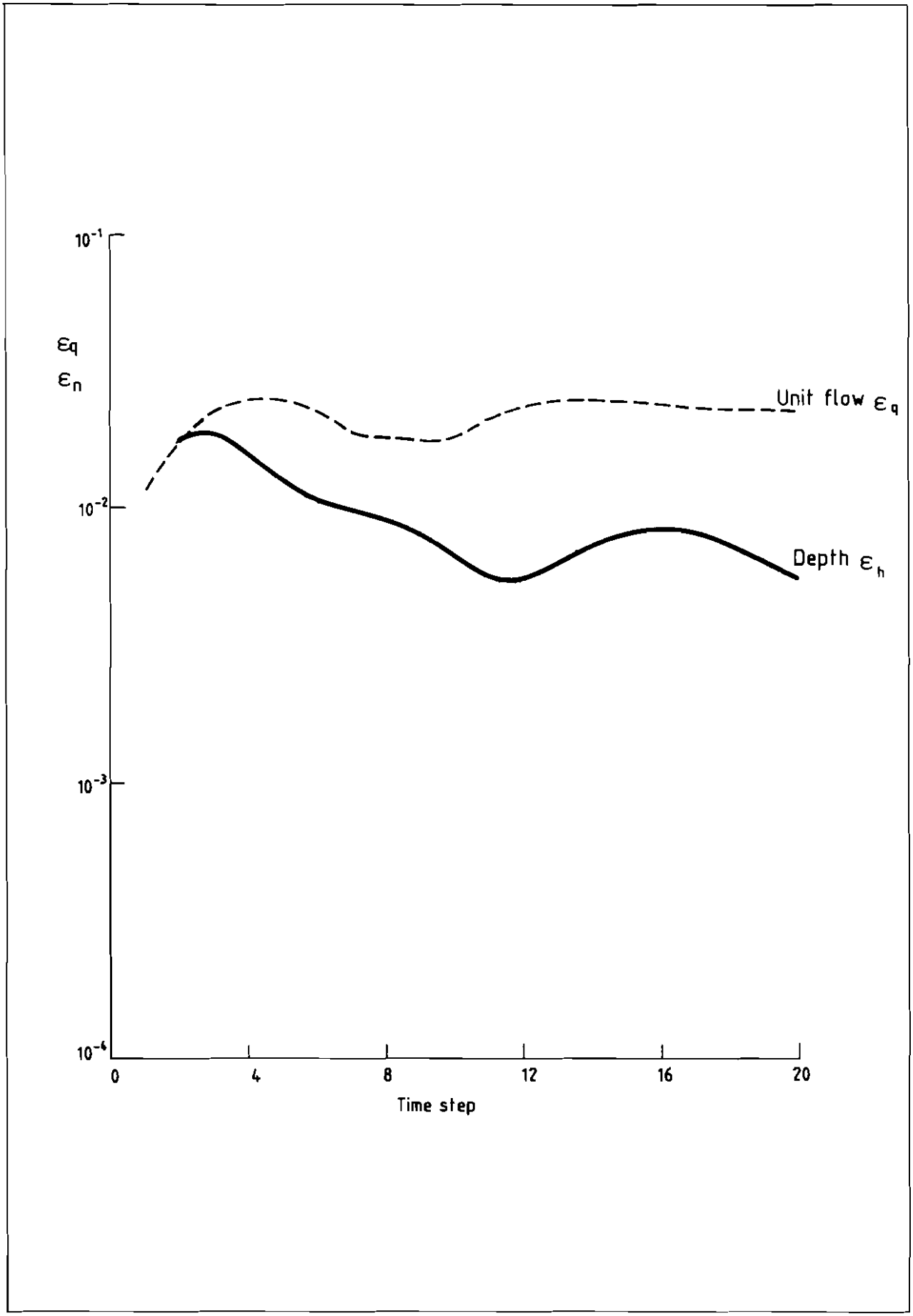

Fig 5.24 Convergence parametres for Mesh 4 roughness size 0.36m

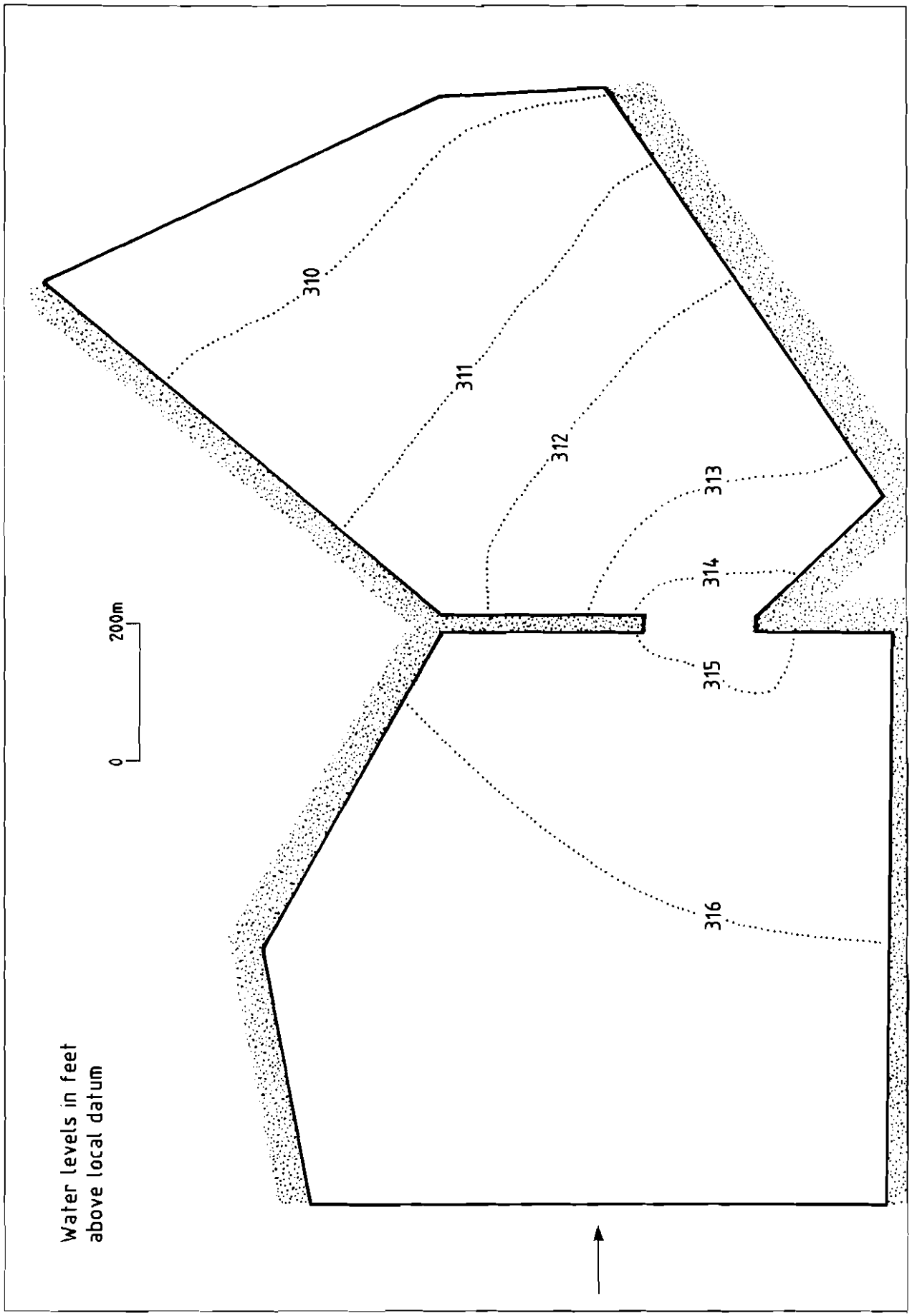

Fig 5.25 Water level contours for Tallahala Creek data (no convection term)

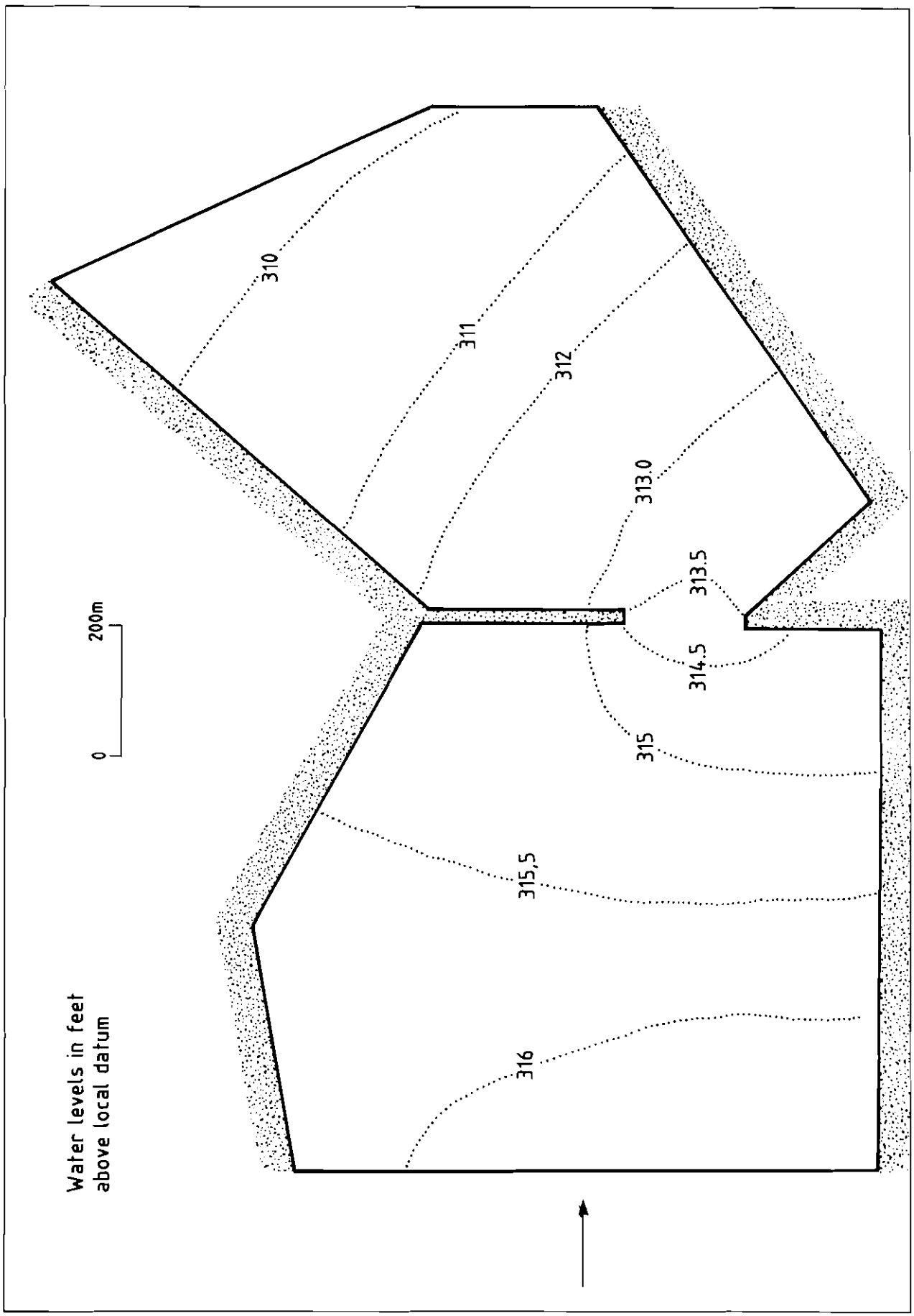

Fig 5.26 Water surface contours from Tseng (1975)

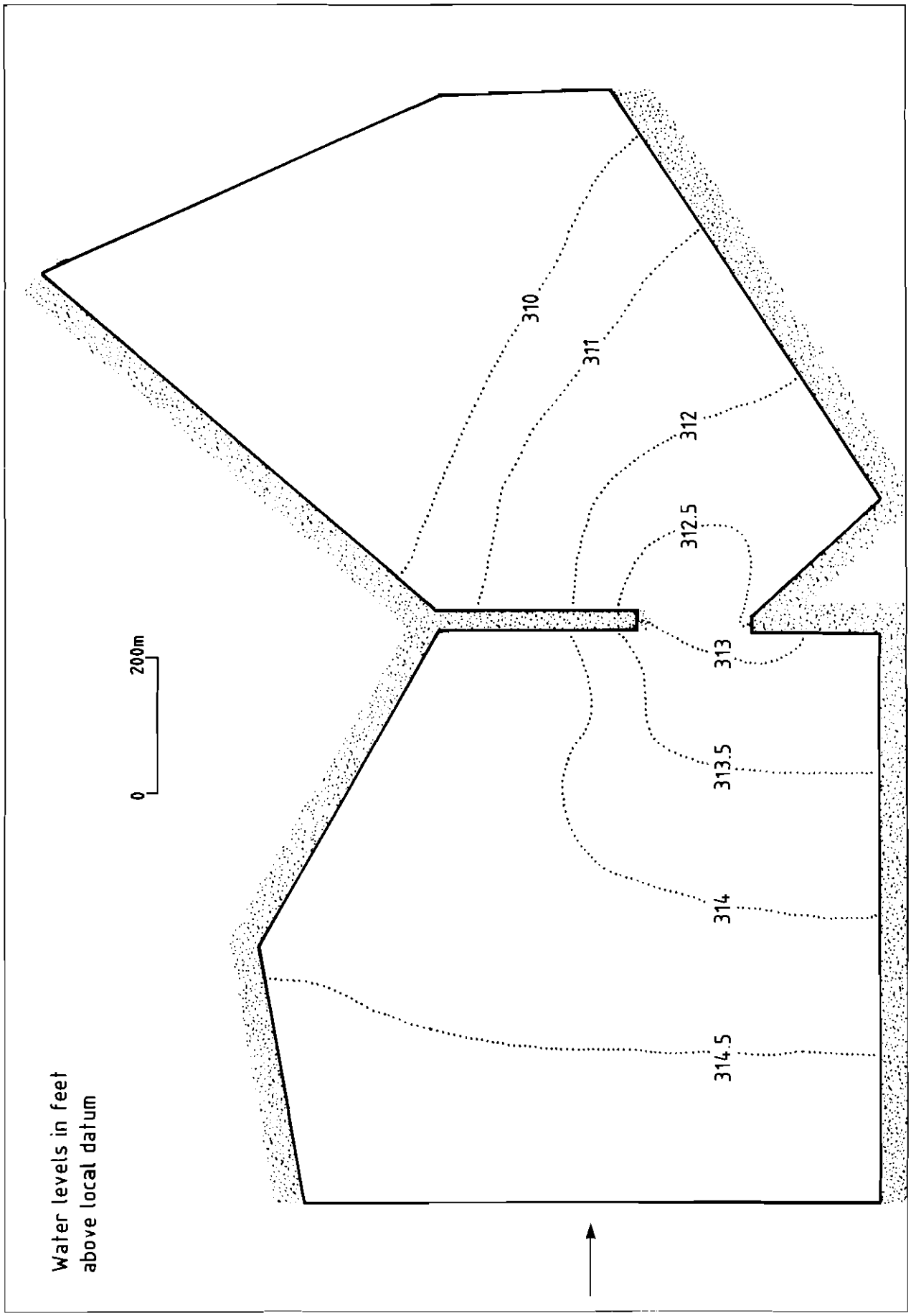

Fig 5.27 Water surface contours from Franques and Yannitell (1974)

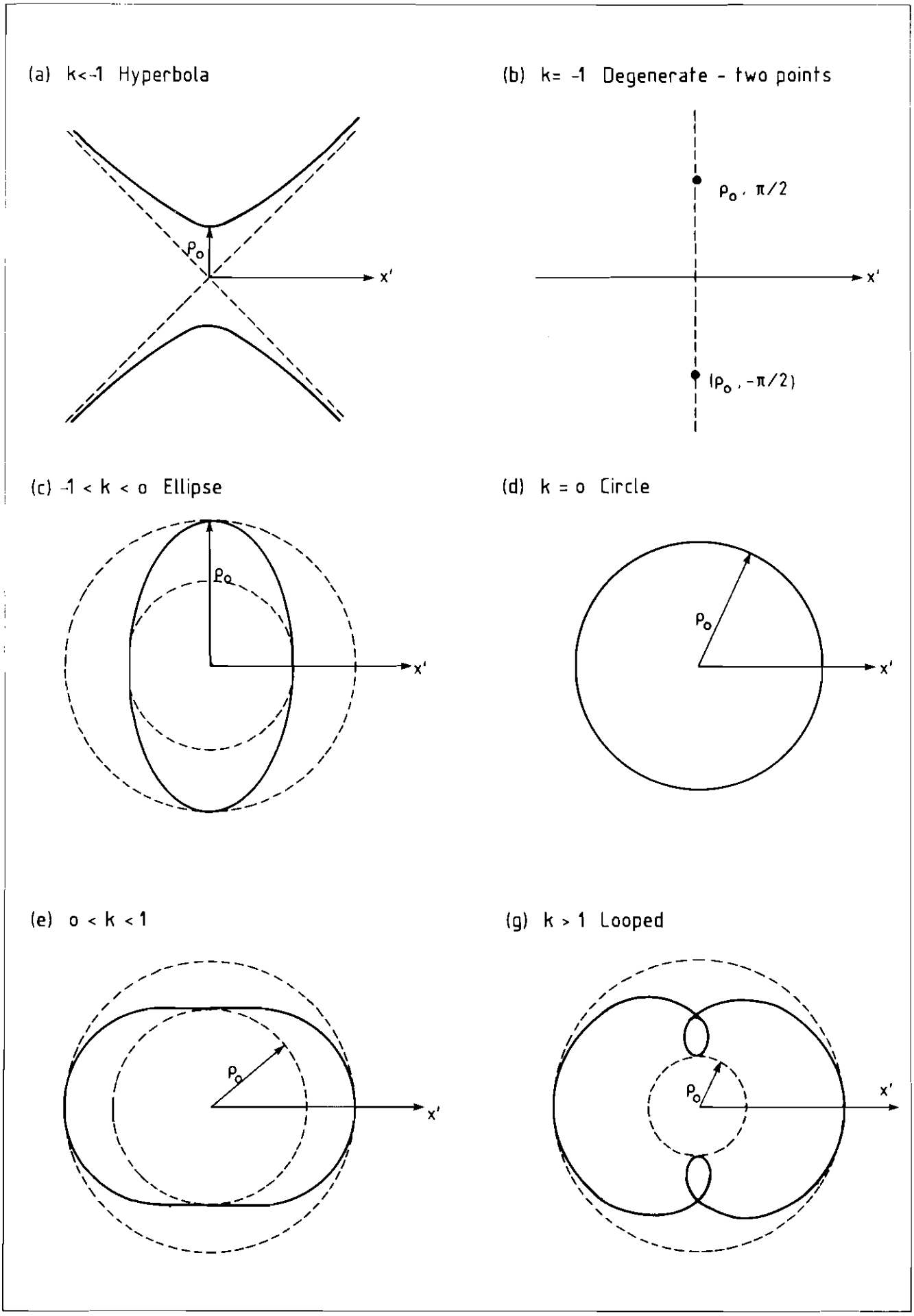

Fig A1.1 Intersections of the bicharacteristic surfaces with the plane t = to

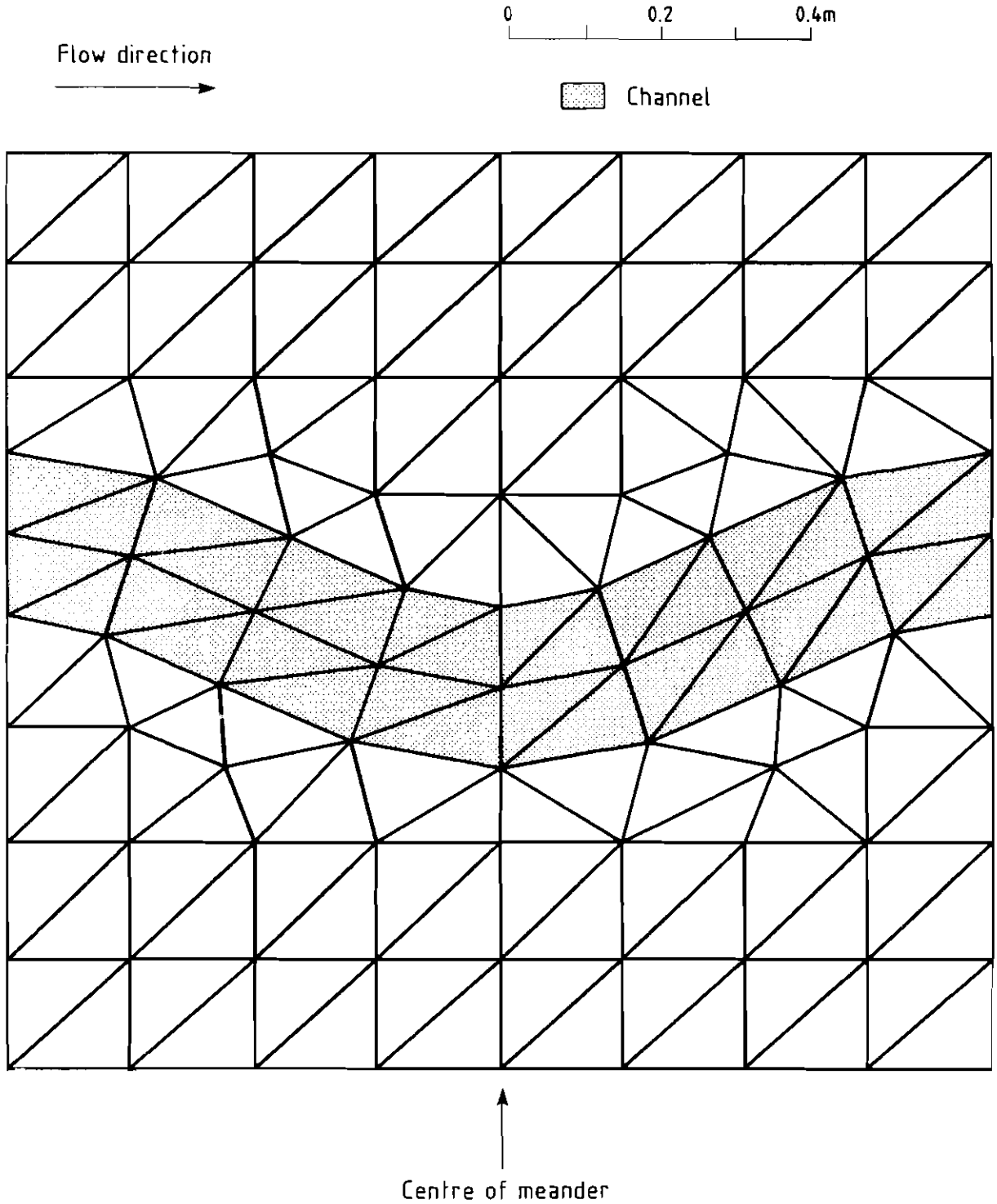

Fig A2.1 Geometry of Mesh 1

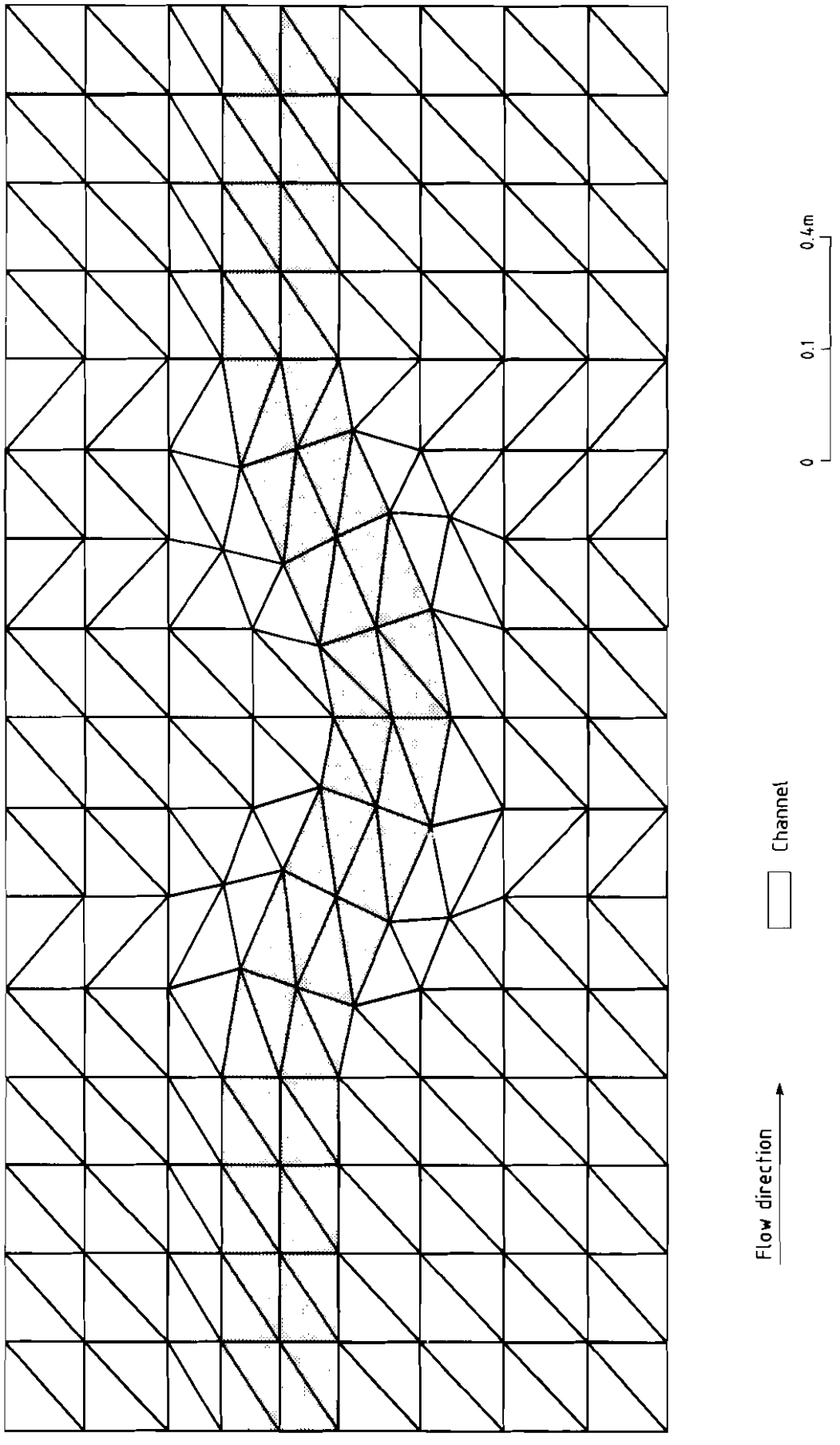

Fig A2.2 Geometry of Meshes 3 and 4

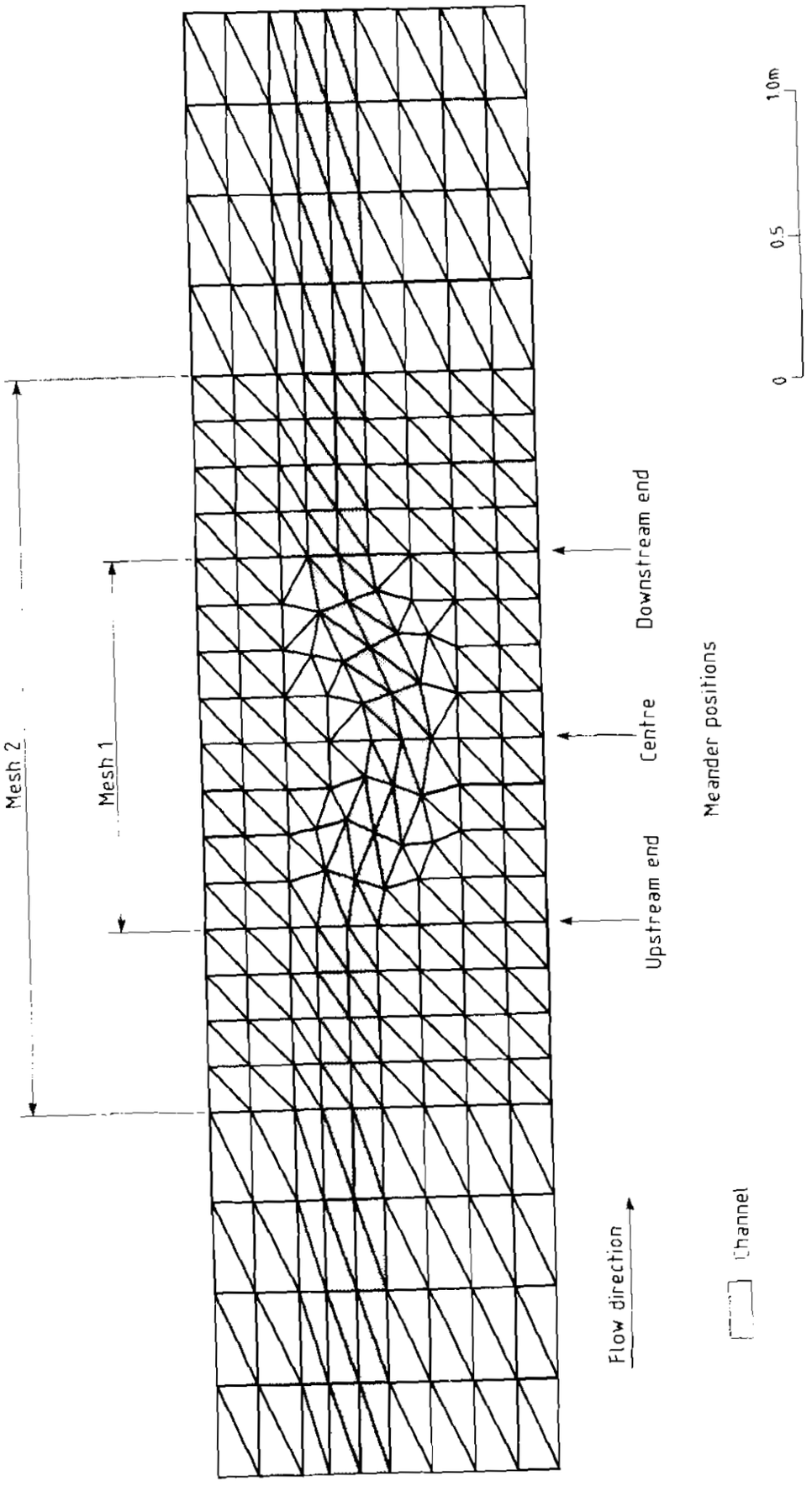

Fig A2.3 Geometry of Mesh 5 (showing Meshes 1 and 2)

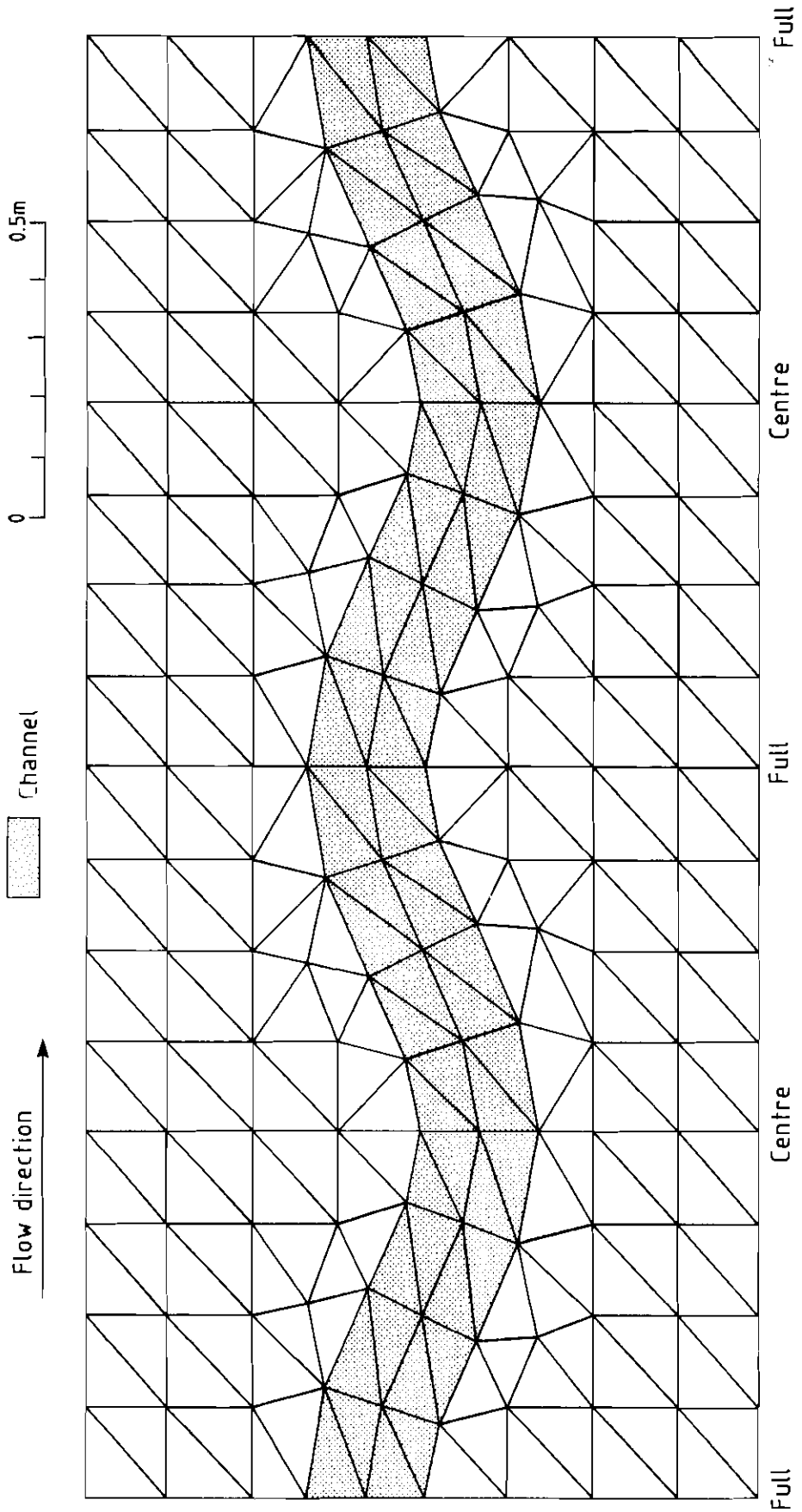

Fig A2.4 One third of Mesh 7

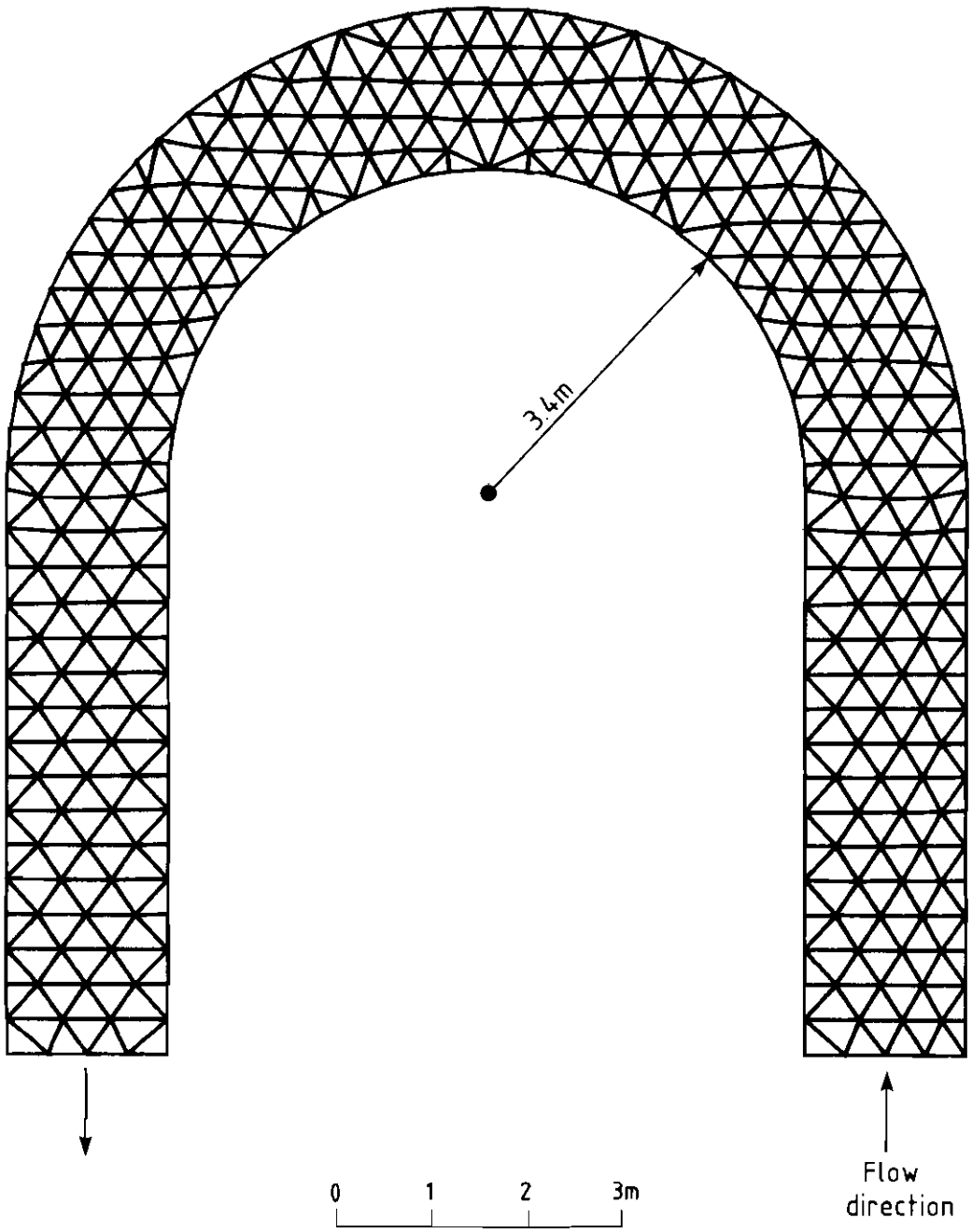

Fig A2.5 Geometry of Mesh 8

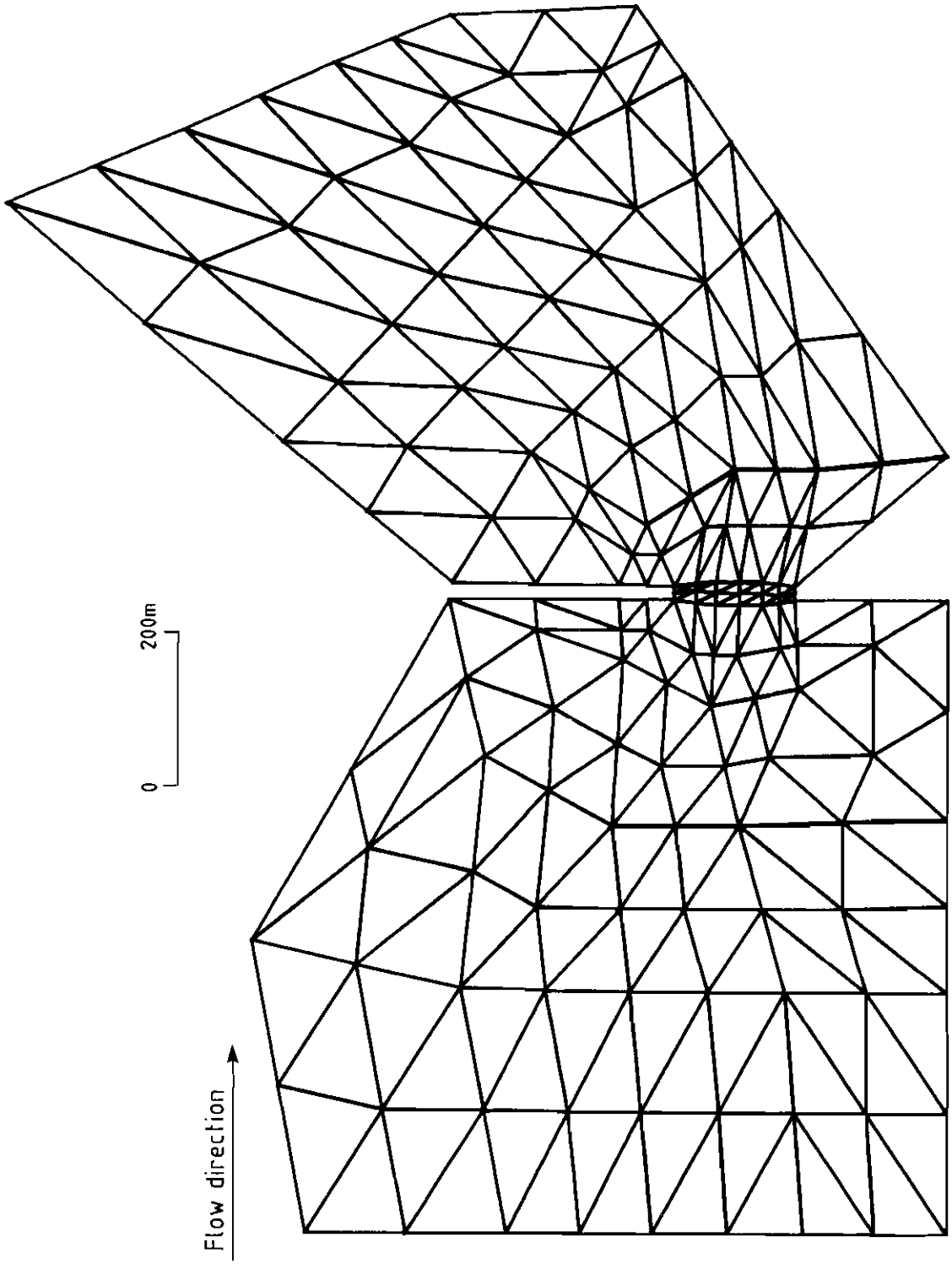

Fig A2.6 Geometry of Mesh 9 from Tseng (1975)